Catalytic Steam Reforming of Bio-Oil to Hydrogen Rich Gas

Trane-Restrup, Rasmus

Publication date:
2013

Document Version
Publisher's PDF, also known as Version of record

DTU Chemical Engineering
Department of Chemical and Biochemical Engineering

Ph.D. Thesis

Catalytic Steam Reforming of Bio-Oil to Hydrogen Rich Gas

Written by

Ph. D. student Rasmus Trane-Restrup

Under Guidance of
Professor Anker Degn Jensen
Department of Chemical and Biochemical Engineering
Technical University of Denmark
and
Professor Søren Dahl
Department of Physics
Technical University of Denmark

PREFACE

This thesis has been submitted as partial fulfillment of the requirements to obtain a Ph.D.-degree at the Technical University of Denmark. This Ph.D.-project is entitled "*Catalytic Steam Reforming of Bio-Oil to Hydrogen Rich Gas*" and the work has been carried out at the Combustion and Harmful Emissions Control (CHEC) research group at the Department of Chemical and Biochemical Engineering, Technical University of Denmark (DTU). Besides the experimental work presented in this thesis, the tasks of the project have been; supervision of students projects, work as a teaching assistant in the course "Introduction to Chemical and Biochemical Engineering", and participation in courses corresponding to 30 ECTS-points. An external research stay of 3 months at the School of Chemical, Biological, and Material Engineering at the University of Oklahoma (OU) has been included as well. The work was conducted in the biofuel research group under the supervision of Professor Daniel E. Resasco.

The Ph.D.-project is a part of Catalysis for Sustainable Energy (CASE) initiative and the European Graduate School for Sustainable Energy (EGSSE). CASE is a collaboration between several departments from DTU and industrial partners, while EGGSE is a collaboration between DTU, the Technical University of München (TUM), and Eindhoven University of Technology (TUE). Both of these organizations aim to increase collaboration between different departments at DTU and other technical universities in Europe.

There are several persons, who have helped to shape and support this project, which all deserve a big "Thank you". First I would like to thank my supervisors, Anker D. Jensen and Søren Dahl, for feedback during meetings and for discussions regarding the project. The help in daily problems and regularly project meetings with Anker D. Jensen is greatly appreciated. Then I would like to thank my colleagues at DTU Chemical Engineering for creating a good work environment. A special thanks go my colleagues working within catalysis, Peter, Martin, Jakob, and Xiao, for discussions and help regarding characterizations techniques and other problems. The workshop and the technical staff at DTU Chemical Engineering have helped a lot with the experimental equipment, both troubleshooting and design of new parts, and I appreciate their help and support.

XRD, TEM, and TPR analysis could not have been done without the help of Zoltam Imre Balogh and Thomas Willum Hansen from DTU CEN, as well Irek Sharafutdinov and Helge Kildahl Rasmussen from DTU Physics. Their help is appreciated.

I am glad that professor Daniel E. Resasco gave me the opportunity to come and work at OU for three months. It was an inspiring, interesting, and educational stay and I thank the graduate students and staff at OU for their kind and helpful nature and their help in the lab and with daily problems. I especially acknowledge graduate student Miguel Ángel Borja González for all the help he gave me during my stay at OU. Finally I acknowledge the grant from Balslev Fonden, which, in part, financed the stay at OU.

My parents help and support during my education is greatly appreciated.

Finally, a special "'Thank you"' goes to my lovely wife, Martine, who has been a great help through my education and this Ph.D.-project.

Rasmus Trane-Restrup, 13. September 2013

ABSTRACT

Bio-oil is a liquid produced by pyrolysis of biomass and its main advantage compared with biomass is an up to ten times higher energy density. This entails lower transportation costs associated with the utilization of biomass for production of energy and fuels. Nevertheless, the bio-oil has a low heating value and high content of oxygen, which makes it unsuited for direct utilization in engines. One prospective technology for upgrading of bio-oil is steam reforming (SR), which can be used to produce H_2 for upgrading of bio-oil through hydrodeoxygenation or synthesis gas for processes like the Fischer-Tropsch synthesis. In the SR of bio-oil or bio-oil model compounds high degrees of conversion and high yields of H_2 can be achieved, but stability with time-on-stream is rarely achieved. The deactivation is mainly due to carbon deposition and is one of the major hurdles in the SR of bio-oil.

There are two main pathways to minimize carbon deposition in steam reforming; either through optimization of catalyst formulation or through changes to the process parameters, like changes in temperature, steam to carbon ratio (S/C), or adding O_2 or H_2 to the feed. In this thesis both pathways have been explored.

Steam reforming of ethanol has been conducted over Ni-based catalysts in attempts to minimized carbon deposition through changes to the catalyst formulation. Furthermore the effect of temperature was investigated for Ni on $MgAl_2O_4$, $CeZrO_4/MgAl_2O_4$, CeO_2, and $Ce_{0.6}Zr_{0.4}O_2$ at a S/C-ratio of 6. The support material affected the conversion and carbon deposition while the product distributions as function of temperature were similar. The yield of CO and H_2 increased with increasing temperature while the yield of CO_2, methane, and ethene decreased with temperature. The most abundant by-products were methane and ethene but acetic acid, acetone, and acetaldehyde were also produced in minor amounts. $Ni/Ce_{0.6}Zr_{0.4}O_2$ showed the highest activity, but also suffered from severe carbon deposition as carbon whiskers. $Ni/CeZrO_4/MgAl_2O_4$ had the second highest activity and showed lower carbon deposition compared with both $Ni/Ce_{0.6}Zr_{0.4}O_2$ and $Ni/MgAl_2O_4$. The carbon deposition over $Ni/Ce_{0.6}Zr_{0.4}O_2$ and $Ni/MgAl_2O_4$ had a maximum at 500 ℃, which coincided with the maximum in the ethene formation. This, along with estimations of the affinity for carbon deposition from the gas composition, showed that ethene is the main precursor to carbon deposition.

CeO_2, ZrO_2, K, or mixtures hereof were added to $Ni/MgAl_2O_4$, and all of them lowered the carbon deposition and increased the activity. The addition of CeO_2 gave the lowest carbon deposition probably due to an increased oxidation of carbon by CeO_2. Stability tests over 24 h at 600 ℃ over $Ni\text{-}K/MgAl_2O_4$ and $Ni/K\text{-}CeO_2/MgAl_2O_4$ both showed deactivation with time-on-stream mainly due to carbon deposition as carbon whiskers.

Sulfur was added as K_2SO_4 to $Ni\text{-}CeO_2/MgAl_2O_4$ to selectively poison Ni-sites and inhibit carbon deposition. The sulfur poisoning induced a decrease in the carbon deposition and an increase in the yield of hydrocarbons indicating a lowering of the hydrocarbon SR activity. The optimal loading of sulfur was 0.03 $wt\%$ S added as K_2SO_4 and the lowest rate of carbon deposition of 1.2 $\frac{mg\ C}{g_{Cat} \cdot h}$ was achieved with this catalyst.

The results from changes in the catalyst composition indicated that carbon free operation was not possible and so operational measures were investigated next. The effect of the S/C-ratio and addition of H_2 or O_2 to the feed on the product yields and carbon deposition in the SR of ethanol over $Ni/MgAl_2O_4$, $Ni/Ce_{0.6}Zr_{0.4}O_2$, and Ni/CeO_2 at 600 ℃ was investigated. Increasing the S/C-ratio from 1.6 to 8.2 over $Ni/MgAl_2O_4$ increased ethanol conversion from 53 % to 80 % as well as the yield of H_2, while the carbon deposition and yield of hydrocarbons decreased. Oxygen addition increased conversion, decreased the yield of hydrocarbons and H_2 as well as the carbon deposition. Carbon deposition was almost eliminated at an O/C-ratio of approximately 0.8. The penalty of adding O_2 was a decrease in the yield of H_2 corresponding to loss of 1 mole of H_2 pr. mole of ethanol converted compared with SR without O_2. H_2-addition had little influence on the catalyst performance, only a slight deactivation was observed at high H_2/ethanol-ratios probably due to a high surface coverage of H-species inhibiting the reforming reactions.

A 90 h test at O/C=1.1, S/C=6, and 600 ℃ over $Ni/MgAl_2O_4$ showed stable behavior and a total carbon deposition of less than 0.1 mg (rate of carbon deposition was 7 $\frac{\mu g\ C}{g_{Cat} \cdot\ h}$). The results indicate that stable operation in the SR of ethanol is only possible under oxidative conditions.

Bio-oil contains a wide range of oxygenated species ranging from acetic acid to guaiacol and it would be of interest to obtain knowledge about their behavior in reforming. Therefore SR of ethanol, acetic acid, acetone, acetol, 1-propanol, and propanal was investigated over $Ni/MgAl_2O_4$ at temperatures between 400 and 700 ℃ and at S/C=6. The yield of H_2 and conversion increased with increasing temperature while the yield of by-products decreased with temperature in the SR of the investigated compounds. The yield of H_2 approached the thermodynamic limit at the highest temperatures investigated, where full conversion was achieved at the applied space velocity. No significant differences in conversion as function of temperature between the different model compounds were observed. However, the product distribution depended on the model compound and C_3-oxygenates produced a larger fraction of byproducts compared to C_2-oxygenates. Temperatures of 600 ℃ or above were generally needed to minimize the fraction of by-products and obtain a syngas containing mainly CO, CO_2, H_2, and H_2O with only traces of CH_4.

Significant deactivation of the catalyst was observed for all of the compounds and was mainly due to carbon deposition. The carbon formation was highest for alcohols due to a higher formation of olefins, which are potent coke precursors.

Steam reforming of 2-methylfuran, furfural, and guaiacol as function of temperature and time was investigated over one of the most promising catalysts, Ni/CeO_2-$K/MgAl_2O_4$. The major products were, at all temperatures, CO, CO_2, and H_2, but formation of by-products, such as small hydrocarbons or fragments of the parent model compounds, was observed and the yield of these compounds decreased with increasing temperature. A large formation of aromatic compounds, benzenediols and phenol, was observed in the SR of guaiacol even at 600 ℃ and temperatures as high as 780 ℃ were needed to eliminate the formation of these compounds. Temperatures of 600 ℃ were needed to eliminate the formation of by-products in the SR of 2-methylfuran and furfural.

Carbon deposition was apparent in the SR of the model compounds at 600 ℃ and S/C-ratio of 5 over Ni/CeO_2-$K/MgAl_2O_4$ and was most pronounced for guaiacol followed by furfural and 2-methylfuran. The carbon deposition could almost be eliminated by adding oxygen to feed at the expense of a lower yield of H_2. However, stable operation over 24 h could not be achieved in the SR of guaiacol and furfural even under oxidative SR conditions.

DANSK RESUMÉ

Bio-olie kan produceres ud fra biomasse gennem pyrolyse og har en energidensitet, som kan være op til ti gange højere end biomasse, hvilket kan gøre produktionen af energi eller brændsler ud fra biomasse mere favorabelt, grundet lavere udgifter til transport. Bio-olie er dog ikke uproblematisk at arbejde med, da den har et højt indhold af ilt, en lav brændværdi, og er termisk og kemisk ustabil. Olien skal derfor behandles for at øge dens stabilitet og værdi, og dette kan gøres ved dampreformering over egnede katalysatorer ved temperaturer mellem 400 og 1000 ℃, hvor olien gennem reaktion med damp omdannes til CO, CO_2, og H_2. Deaktivering af katalysatorerne er et af de største problemer i dampreformering af bio-olie, og dette skyldes i høj grad kulaflejringen på katalysatoren.

I denne afhandling er forskellige redskaber til at mindske kuldannelse blevet undersøgt i dampreformering af ethanol over Ni-baserede katalysatorer. Bærermaterialet er blevet varieret mellem $MgAl_2O_4$, $CeZrO_4/MgAl_2O_4$, CeO_2 og $Ce_{0.6}Zr_{0.4}O_2$ hvilket ikke ændrede produktfordelingen væsentlig, mens både aktivitet og dannelse af kul varierede. Omdannelsen samt udbyttet af H_2 og CO steg med stigende temperaturer, mens udbyttet af CO_2, methan og ethen faldt i damp reformeringen af ethanol ved et S/C-forhold på 6. $CeZrO_4/MgAl_2O_4$, som bærer, viste lovende resultater, da den både havde en høj og stabil aktivitet, samt en lav kuldannelse. $Ce_{0.6}Zr_{0.4}O_2$ havde den højeste aktivitet, men også den højeste kuldannelse, som whiskers. Kuldannelsen som funktion af temperaturen over $Ni/MgAl_2O_4$ and $Ni/Ce_{0.6}Zr_{0.4}O_2$ havde en maksimum ved 500 ℃, hvor den maximale produktion af ethen også blev observeret. Dette viser, sammen med termodynamiske estimeringer af kuldannelsespotentialet af produktgassen, at ethen er den væsentligste kilde til kulaflejring i dampreformeringen af ethanol over disse katalysatorer.

K, CeO_2 og ZrO_2 samt blandinger heraf blev tilsat $Ni/MgAl_2O_4$ og de bidrog alle til at mindske kuldannelsen og øge aktiviteten. Ni/CeO_2-$K/MgAl_2O_4$ viste sig, at være en interessant katalysator, da den både havde lav kuldannelse og høj aktivitet ved 600 ℃. Forsøg over længere tid viste dog kuldannelse som whiskers.

Svovl tilsætning i små mængder (0.03-0.12 $wt\%$ S) gennem imprægnering med K_2SO_4 til Ni-$CeO_2/MgAl_2O_4$ viste, at man kunne mindske kuldannelsen yderligere, men den totale aktivitet blev også svagt sænket. Den laveste kuldannelseshastighed blev opnået over Ni-$CeO_2/MgAl_2O_4$ tilsat 0.03 $wt\%$ S som K_2SO_4 og den var 1.2 $\frac{mg\ C}{g_{Cat} \cdot h}$.

Ændringer i katalysatorformuleringen var ikke nok til at eliminere kuldannelse i dampreformering af ethanol og derfor blev ændringerne af procesparametre også undersøgt. Tilsætning af mere damp eller ilt til fødestrømmen kunne mindske kuldannelse samt øge aktiviteten i dampreformeringen af ethanol. Kuldannelsen blev sænket mest ved tilsætning af ilt, hvilket dog skete på bekostning af udbyttet af H_2, som faldt fra 75 % ved O/C=0 til 50 % ved O/C=0.8. Ilttilsætning med et O/C-forhold på 0.8 eller derover kunne stort set eliminere kuldannelse, og et forsøg over 90 h ved O/C=1.1 og 600 ℃ over $Ni/MgAl_2O_4$ viste en total kuldannelse på mindre end 0.1 mg C (gennemsnitlig kulaflejringshastighed var 7 $\frac{\mu g\ C}{g_{Cat} \cdot\ h}$).

Brinttilsætningen til føden blev også undersøgt i dampreformering af ethanol, men dette gav en svag deaktivering ved høje forhold mellem H_2 og ethanol, sandsynligvis på grund af en høj dækning af H-specier på katalysatoren, hvilket inhiberede reformeringsreaktionerne.

Bio-olie indeholder en lang række forskellige forbindelser af varierende størrelse og det kunne være interessant, at undersøge hvordan de reagerer under dampreformering. Derfor blev dampreformering af ethanol, eddikesyre, acetol, acetone, propanal, og 1-propanol undersøgt som funktion af temperatur og tid over $Ni/MgAl_2O_4$. Produktfordelingen som funktion af temperaturen var tæt på ligevægtssammensætningen ved temperaturer over 500 ℃, hvilket betød at udbyttet af H_2 og CO steg med stigende temperaturer, mens udbyttet af CO_2 og biprodukter, som CH_4 og C_2H_4, faldt. Dehydrering og dehydrogenering var sidereaktion i dampreformeringen af alkoholer, mens ketonisering blev observeret i dampreformering af eddikesyre. Omdannelsen af modelkomponenterne steg med stigende temperatur, og der blev ikke observeret væsentlige forskelle i omdannelse mellem modelkomponenter. Der blev dog observeret et øget udbytte af biprodukter i dampreformering af 1-propanol kontra ethanol, hvilket indikerer, at reaktiviteten falder med øget kædelængde.

Deaktivering grundet kuldannelse blev observeret for alle komponenter og var ca. 30 % højere i dampreformeringen af ethanol, 1-propanol, og eddikesyre, sammenlignet med dampreformering af de resterende komponenter. I dampreformering af alkoholer skyldes dette en højere dannelse af olefiner, som er kilde til kulaflejring.

Dampreformering af cykliske modelkomponenter, som 2-methylfuran, furfural, og guaiacol, er blevet undersøgt som funktion af både temperatur og tid over en de mest lovende katalysatorer, Ni/CeO_2-$K/MgAl_2O_4$. Produkterne i disse reaktioner var hovedsagligt CO, CO_2, og H_2 ved alle temperaturer, men der blev også observeret mindre kulbrinter samt forskellige fragmenter af modelkomponenterne. Udbyttet af CO_2 og biprodukter faldt med stigende temperaturer, mens omdannelsen, samt udbyttet af H_2 og CO steg. I damp reformering af furfural og 2-methylfuran var udbyttet af biprodukter lavt ved temperaturer omkring 600 ℃, mens der kræves temperaturer omkring 780 ℃ i damp reformering af guaiacol for at eliminere dannelsen af biprodukter. Biprodukterne var methane, ethanol, 1-propanol og acetone i dampreformeringen af furfural og 2-methylfuran, mens aromatiske forbindelser som phenol og benzenedioler blev observeret i dampreformeringen af guaiacol.

Kuldannelsen i dampreformering af de cykliske forbindelser ved S/C=5 og 600 ℃ var højest for guaiacol, efterfulgt af furfural og 2-methylfuran, hvilket sammen med det væsentligt højere udbytte af biprodukter viser, at dampreformering af aromatiske forbindelser er vanskelig.

Tilsætning af ilt til føden i dampreformering af de cykliske forbindelser mindskede kuldannelsen og udbyttet af H_2, samtidig med at aktiviteten blev øget. Hvilket O/C-forhold, der kræves for stabil drift over 4 h afhang af modelkomponenten og var 0.4 i dampreformeringen af 2-methylfuran, mens det var 1.0 eller derover i dampreformeringen af furfural og guaiacol. Stabil dampreformering af furfural og guaiacol ved 600 ℃ over 24 h kunne dog ikke opnås selv ved tilsætning af ilt.

LIST OF PUBLICATIONS

International peer-reviewed journals

- Rasmus Trane, Søren Dahl, Martin Skov Skjøth-Rasmussen, Anker Degn Jensen: Catalytic steam reforming of bio-oil, *International Journal of Hydrogen Energy*, **366**, (2012), 29-43.

- Rasmus Trane-Restrup, Søren Dahl, Anker Degn Jensen: Steam reforming of ethanol: Effects of support and additives on Ni-based catalysts, *International Journal of Hydrogen Energy*, Accepted, (2013).

- Rasmus Trane-Restrup, Søren Dahl, Anker Degn Jensen: Steam reforming of ethanol over Ni-based catalysts: Effect of feed composition on catalyst stability, Submitted to *Applied Catalysis A: General*, (2013).

- Rasmus Trane-Restrup, Daniel E. Resasco, Anker Degn Jensen: Steam reforming of light oxygenates, Submitted to *Catalysis Science & Technology*, (2013).

- Rasmus Trane-Restrup, Anker Degn Jensen: Steam reforming of bio-oil model compounds, Planned for submission to an international peer reviewed journal, (2013).

Oral conference contributions

- Rasmus Trane, Søren Dahl, Anker Degn Jensen: Steam reforming of ethanol: A model compound of bio-oil, Presented at: ACS Fall Meeting, Denver, USA, 28th of August-1st of September 2011.

- Rasmus Trane-Restrup, Daniel E. Resasco, Anker Degn Jensen: Steam reforming of bio-oil model compounds, Presented at: Catalysis for renewable sources: fuel, energy, chemicals, Lund, Sweden, 22nd-27th of July 2013.

Poster conference contributions

- Rasmus Trane, Søren Dahl, Anker Degn Jensen: Steam reforming of bio-oil model compounds, Presented at: The International Congress of Catalysis, München, Germany, 1st-6th of July 2012.

- Rasmus Trane, Søren Dahl, Anker Degn Jensen: Minimizing carbon deposition in steam reforming of ethanol, Presented at: 23rd North American Catalysis Society Meeting, Louisville, USA, 2nd-7th of June 2013.

Non-scientific publications

- Peter Mølgård Mortensen, Rasmus Trane: Bulk Chemical Production with Bio-oil, Published online at http://www.case.dtu.dk, spring 2011.

- Peter Mølgård Mortensen, Rasmus Trane: Affald fra marken bliver til CO_2-neutrale brændstoffer, Published online at http://www.case.dtu.dk, spring 2011.

INTRODUCTION

In present years the world is experiencing rising oil prices, partly due to a lack of oil. Furthermore, the climate debate has led to an increasing request for fuels for transportation with a lower carbon foot print. Thus, there is a need for alternative liquid fuels based on biomass, which is considered a CO_2 neutral fuel.

One interesting option is to pyrolyse the biomass to obtain char and pyrolysis oil, which could in principle be used as a fuel. This is particularly attractive for the use of biomass resources from remote areas, where the pyrolysis can be performed locally to obtain the oil with an energy density which is about 10 times higher than that of the loosely packed biomass (e.g. a straw bale). The resulting biomass char could be spread on the fields to improve soil properties and return most of the nutrients.

However, pyrolysis oil is a complex mixture containing hundreds of organic oxygen containing compounds, such as acids, alcohols, aldehydes, furans, phenols and esters, in which the oxygen content can be as high as 50 %. These oxygenates leads to several problematic properties of the oil including high viscosity, thermal and chemical instability, corrosiveness, poor heating value, and immiscibility with hydrocarbon fuels. Therefore pyrolysis oils must be upgraded before use, by processes where the content of oxygen is decreased, i.e. involving de-oxygenation, hydro-deoxygenation and decarboxylation. This is most efficiently carried out by the action of suitable catalysts in the gas phase in the presence of hydrogen. The required hydrogen could be obtained by steam reforming a part of the oil. Hydrogen is also of interest in fuel cell applications and in many chemical processes such as synthesis of ammonia, synthetic natural gas etc. However, the mechanism and kinetics of steam reforming of oxygenates such as those present in pyrolysis oil is not yet well understood and so there is a lack of efficient and stable catalysts for this purpose.

The purpose of this Ph.D. project is to investigate the gas phase steam reforming (SR) of biomass pyrolysis oil. The study will be devoted to well-defined model compounds from the different classes of compounds present in pyrolysis oils, as mentioned above. The project includes a literature study of the current state-of-art for steam reforming of pyrolysis oil oxygenates. Furthermore an experimental setup as well as the necessary analytical techniques to analyze the product mixtures was established. The heterogeneous catalysts suitable for the steam reforming of selected oxygenates was identified based on literature studies. Characterization of the catalysts by different methods (BET, TEM, XRD etc.) was also conducted.

This Ph.D. theis consists of seven chapters, which describes the experimental work conducted during the course of this project along with a review of literature on the steam reforming of hydrocarbons and oxygen containing hydrocarbons. The chapters are briefly described below.

- Chapter 1 reviews the SR of oxygen containing hydrocarbons with respect to reaction mechanisms, suitable catalysts, and their stability. Furthermore alternative strategies for SR of oxygen containing compounds like fluidized bed, oxidative SR, or aqueous

phase SR is discussed. This chapter has been published as a review of steam reforming of bio-oil in International Journal of Hydrogen Energy.

- Chapter 2 describes the experimental setups used at DTU and OU, how the catalysts were prepared, and how the characterization of the catalysts was conducted.
- Chapter 3 discusses the experimental work regarding the SR of ethanol and how changes to the catalyst formulation affected activity, carbon deposition, and product distribution. The main results from this chapter have been accepted for publication in International Journal of Hydrogen Energy.
- Chapter 4 contains the results from the SR of ethanol on the effect of the level of H_2, O_2, and H_2O in the feed on carbon deposition, conversion, and product distribution. The main results from this chapter have been submitted to Applied Catalysis A: General.
- Chapter 5 shows results from the SR of light water soluble oxygenates. The product distributions as function of temperature are used to elucidate steps in the reaction paths. Furthermore reactivity and deactivation of the different model compounds are compared. The results presented in this chapter have been submitted to Catalysis Science and Technology.
- Chapter 6 contains results from the SR of three cyclic model compounds of bio-oil, 2-methyl furan, furfural, and guaiacol, where the product distribution as function of temperature as well as function of time was investigated. Furthermore oxygen addition was investigated. The main results from this chapter will be submitted to an international peer reviewed journal.
- Chapter 7 summarizes the main findings from the literature and the experimental work. Furthermore, the prospect for SR of oxygen containing compounds as a source of hydrogen or synthesis gas in the future is discussed.

Supporting information used in the different chapters are found in appendix A and B.

CONTENTS

1. Literature review . . . 17
1.1 Introduction . . . 17
1.2 Conventional steam reforming . . . 20
1.3 Steam reforming of oxygenates . . . 23
1.3.1 General considerations . . . 23
1.3.2 SR of acetic acid . . . 25
1.3.3 SR of ethanol . . . 32
1.3.4 SR of oxygenated compounds . . . 37
1.3.5 SR of bio-oil . . . 40
1.4 Sulfur poisoning . . . 41
1.5 Reactors and reforming concepts . . . 43
1.5.1 Prereforming . . . 44
1.5.2 Fluidized bed reforming . . . 44
1.5.3 Autothermal reforming . . . 45
1.5.4 Catalytic partial oxidation . . . 46
1.5.5 Other concepts . . . 46
1.5.6 Industrial plant . . . 47
1.6 Other conversion techniques . . . 48
1.6.1 Catalytic cracking . . . 48
1.6.2 Aqueous phase reforming . . . 49
1.7 Discussion . . . 50
1.8 Conclusion . . . 51

2. Experimental . . . 53
2.1 Catalyst preparation . . . 53
2.2 Experimental setup at DTU . . . 54
2.2.1 Catalytic test . . . 57
2.2.2 Determination of the amount of carbon deposited . . . 57
2.3 Experimental setup at OU . . . 58
2.3.1 Catalytic test at OU . . . 58
2.3.2 Temperature programmed oxidation at OU . . . 59
2.4 Catalyst characterization . . . 59
2.4.1 Calculations . . . 59

3. Steam reforming of ethanol: Effects of support and additives on Ni-based catalysts . . . 61
3.1 Characterization . . . 62
3.2 Effect of temperature and W/F . . . 65
3.3 Influence of carrier material . . . 68
3.3.1 Deactivation . . . 70
3.4 Effect of temperature on carbon deposition . . . 73
3.5 Effect of additives . . . 75

3.5.1 Effect of TOS . . . 78
3.6 Sulfur addition . . . 79
3.7 Conclusions . . . 83

4. Steam reforming of ethanol: Effect of feed composition on catalyst stability . . . 85
4.1 Characterization . . . 86
4.2 Effect of S/C-ratio . . . 86
4.3 Oxidative steam reforming . . . 90
4.4 Hydrogen addition . . . 93
4.5 Stability tests . . . 95
4.6 Discussion of reaction mechanism in SR of ethanol . . . 99
4.7 Conclusions . . . 102

5. Steam reforming of light water soluble oxygenates . . . 104
5.1 Characterization . . . 105
5.2 General trends . . . 105
5.3 Steam reforming of ethanol . . . 106
5.4 Steam reforming of acetic acid . . . 106
5.5 Steam reforming of acetone . . . 108
5.6 Steam reforming of propanal . . . 108
5.7 Steam reforming of 1-propanol . . . 109
5.8 Steam reforming of acetol . . . 110
5.9 Comparison . . . 110
5.9.1 Reaction pathway . . . 113
5.9.2 Deactivation . . . 114
5.10 Conclusions . . . 116

6. Steam reforming of cyclic oxygenates . . . 117
6.1 Characterization . . . 117
6.2 Steam reforming of 2-methylfuran . . . 118
6.3 Steam reforming of furfural . . . 122
6.4 Steam reforming of guaiacol . . . 126
6.5 Postreaction characterization . . . 130
6.6 Comparison of SR of different oxygenates . . . 134
6.7 Conclusions . . . 135

7. Conclusions . . . 137
7.1 Outlook . . . 138

Bibliography . . . 140

Appendices . . . 157

A. Diffusion limitations . . . 157
A.1 Mears criterion . . . 157
A.2 Weisz-Prater criterion . . . 160
A.3 Temperature gradients . . . 162
A.4 Reactor geometry . . . 164
A.5 Dispersion . . . 164
A.6 Conclusions . . . 166

B. Estimation of affinity for carbon deposition 167

NOMENCLATURE

List of abbreviations

- CSTR : Continuous stirred tank reactor
- CT : Cold trap
- DS : Desulfurization
- FID : Flame ionization detector
- GC : Gas chromatograph
- GHSV : Gas hourly space velocity
- HDO : Hydrodeoxygenation
- ICP-OES : Inductively coupled plasma optimal emission spectroscopy
- LHSV : Liquid hourly space velocity
- LHV : Lower heating value
- MAR : Mass action ratio
- MFC : Mass flow controller
- MS : Mass spectrometer
- OSR : Oxidative steam reforming
- P : Pump
- PFR : Plug flow reactor
- POX : Partial oxidation
- SP : Syringe pump
- SR : Steam reforming
- SV : Space velocity
- TCD : Thermal conductivity detector
- TEM : Transmission electron microscopy
- TPO : Temperature programmed oxidation
- TPR : Temperature programmed reduction

- WGS : Water gas shift
- WHSV : Weight hourly space velocity
- XRD : X-ray diffraction

List of symbols

- A : Area
- C_i : Concentration
- D_i : Diffusion coefficient
- D_a : Effective dispersion coefficient
- d_p : Particle diameter
- $F_{i\ ,m}$: Molar flow of i
- F_v : Volumetric flow rate
- h : Heat transfer coefficient
- H : Height
- k : Rate constant
- k_c : Mass transfer coefficient
- k_t : Thermal conductivity
- L_b : Length of bed
- M : Molar mass
- m_i : Mass of i
- n : Reaction order
- $n_{\mathrm{C}\ ,i}$: Number of carbon atoms in i
- n_i : Molar flow of i
- Nu : Nusselts number
- p : Pressure
- Pe: Peclet number
- Pr: Prandtls number
- R : Gas constant
- r_i : Reaction rate
- Re : Reynolds number

- Sc : Schmidts number
- Sh : Sherwoods number
- T : Temperature
- U : Gas velocity
- V_i : Volume of i
- X : Conversion

List of greek symbols

- β : Full width at half maximum
- ϵ : Characteristic energy
- η : Viscosity
- θ : Bragg angle
- λ : X-ray wavelength
- ν : Kinematic viscosity
- ρ_b : Density of bed
- ρ_c : Density of the catalyst
- σ : Hard-sphere diameter
- σ_c : Constriction factor
- τ : Tortuosity
- ϕ_p : Porosity

1. LITERATURE REVIEW

The purpose of this review is to present the state-of-the-art of SR of bio-oil for synthesis gas production. The main focus will be on SR of whole bio-oil and model compounds such as phenols, but results from the SR of ethanol and acetic acid will also be presented. Reaction mechanisms, kinetics, applied catalysts, and reforming concepts will be presented and suggestions to further investigations will be given.

1.1 Introduction

In the recent decades it has become evident that fossil fuels are a limited resource and that the emission of CO_2 could cause global warming with severe changes to the climate [1, 2]. To diminish the dependency on fossil fuels and to reduce CO_2 emissions much research is focused on new or alternative and sustainable fuels or energy sources. One of the possible alternative energy sources is biomass, which is a renewable and CO_2-neutral fuel and carbon source. The biomass energy potential has been estimated to be between 50 and 1100 $EJ/year$ in 2050 [3–6] while the total global energy consumption is estimated to be between 600 and 1000 $EJ/year$ in the same year [7]. Based on these numbers it appears that biomass can provide some of the energy needed in the future and hereby delay the depletion of the fossil resources.

Biomass can be converted by thermal and catalytic processes to several types of liquid or gaseous products. It can be gasified to produce synthesis gas, which subsequently can be used to produce power in gas turbines or to produce a wide range of fuels; methanol, DME, alcohols of various chain length by the higher alcohol synthesis, and high grade diesel by the Fischer-Tropsch synthesis [8–10]. Another interesting possibility is to flash pyrolyze the biomass, which produces liquids (bio-oil), gases, and solids (char) [8, 11–14]. The flash pyrolysis is conducted in an inert atmosphere at temperatures between 400 and 600 ℃ with high heating and cooling rates (1000-10.000 K/s) and low residence time in the reactor (1-2 s). Liquid yields up to 75 $wt\%$ can be achieved by a proper choice of operating conditions in the pyrolysis process [8, 11, 14, 15]. The gas and char yields typically range between 10-20 $wt\%$ and 10-15 $wt\%$, respectively [13, 14]. Bio-oil can be produced in several different reactor types ranging from entrained flow to ablative and fluidized bed systems. Demonstration and industrial pyrolysis reactors with capacities between 1 and 50 t/h have been or are in operation [13].

The bio-oil can have a volumetric energy density up to ten times higher than biomass and is therefore more suitable for transport as the transportation cost will be much lower compared with biomass [15]. One of the problems with utilizing biomass in the energy sector can therefore be partly solved by the flash pyrolysis process.

The by-products from the flash pyrolysis can be utilized as the gases can be used to dry the biomass and be combusted to provide energy for the pyrolysis process [8, 11]. The char can be combusted as well. However this might be troublesome as the char contains high amounts of inorganics, which can vaporize and condense again on the heat transfer surfaces causing corrosion and reduced heat transfer. Therefore an attractive possibility could be to spread the char on agricultural lands as fertilizer and soil improver, which also would sequest CO_2 to

Tab. 1.1: *The average composition of bio-oil produced through flash pyrolysis of two different types of biomass, a mix of pine and spruce or a softwood mixture. Results are from a round robin laboratory analysis of the same bio-oils [20]. "Others" include ketones, aldehydes, and alcohols. PAH: Poly aromatic hydrocarbons. Pine and spruce bio-oil was produced in a fluidized bed reactor at 460 °C and the bio-oil from softwood was produced in a rotating cone reactor at 500 °C.*

		85 % pine and 15 % spruce	Softwood mixture
Water	[$wt\%$]	20-23	30-35
Acids	[$wt\%$]	3-22	3-27
Others	[$wt\%$]	2-21	2-27
Sugars	[$wt\%$]	4-9	4-7
Phenols	[$wt\%$]	3-4	1-3
Lignin	[$wt\%$]	2-18	13-32
PAH	[ppm]	8	3

some extent [16, 17]. According to Lehman and Joseph [17] if 1 % of annual plant uptake is converted into char it could mitigate 10 % of the anthropogenic CO_2 emissions. The carbon in the char is believed to be released over a period of 1000 years [16]. However, the char could contain PAH's or trace metals which could cause pollution of the soil.

The bio-oil consists of many different oxygenated compounds like acids, ketones, alcohols, phenols, guaiacols etc. The bio-oil and the biomass have similar heating values per mass and the energy efficiency of the pyrolysis is therefore close to the liquid yield in the flash pyrolysis, which means that values around 60-75 % can be achieved [18, 19]. However, energy should also be supplied to dry, downsize, and pyrolyze the biomass and since the energy from the pyrolysis gases may not be sufficient the energy efficiency for the entire biomass to bio-oil process might be lower.

The distribution among the different types of oxygenates in the bio-oil varies depending on the feedstock and under which conditions the bio-oil was produced. The average oxygenate composition for two bio-oils produced in different reactors and from different feedstock is shown in table 1.1. Acids and lignin constitutes the largest organic fraction in the bio-oil, while significant amounts of water also are present. Acetic acid, hydroxyacetaldehyde, acetol, and levoglucosan constitute some of the most abundant molecules [20].

The physical properties and elemental composition of bio-oil are compared to the composition of fossil fuel oil in table 1.2. The fuel oil used for comparison is equivalent to fuel oil no. 4, which is a heavy diesel blend sometimes referred to as residual fuel oil. The most important differences between bio-oil and fuel oil are the oxygen content, sulfur content, and pH. The high oxygen content in the bio-oil induces the low heating value, high acidity, and also instability of the bio-oil as the oxygenates can polymerize under storage. The polymerization causes an increase in viscosity and average molar weight with time [20–22]. A doubling or even tripling of the viscosity of bio-oil due to ageing might occur over a year [20]. This polymerization might make upgrading of the bio-oil more difficult as complex molecules, which are more difficult to convert, could be formed. Ageing of the bio-oil can also decrease the volatility, cause phase separation, and gum formation in the bio-oil as well [21]. Thus long-term storage of the bio-oil could cause severe changes to the bio-oil and should be avoided. The acidity of bio-oil is another problem as corrosive resistant materials are needed for piping and process

equipment, which often are more expensive. The sulfur content in bio-oil is much lower than in crude oil which, in general, is advantageous, but even the low levels might be a problem for catalytic processing of the oil as sulfur might deactivate the catalysts. This is especially a problem if Ni or noble metals are used as catalysts.

Tab. 1.2: *The composition and other characteristics of an average bio-oil and fuel oil equivalent to fuel oil no. 4 [22, 23].*

		Bio-oil	Fuel oil
Moisture content	$[wt\%]$	15-30	0.02
pH		2.0-3.7	-
Density	$[kg/m^3]$	1.1-1.3	0.9
C	$[wt\%]$	32-49	85
H	$[wt\%]$	6.9-8.6	11
O	$[wt\%]$	44-60	1
N	$[wt\%]$	0-0.2	0.3
S	$[wt\%]$	0-0.05	0.2
Solids	$[wt\%]$	0.2-1	1
Lower heating value	$[MJ/kg]$	13-18	40.3

The bio-oil can be converted to different products and might therefore constitute a platform feedstock in a bio-refinery. It can be converted to a gasoline like product by partial hydrodeoxygenation (HDO) or to synthesis gas by steam reforming (SR) [8, 9, 24]. The H_2 from the SR can be used as a fuel or a reactant in either the HDO of the bio-oil or in other chemical processes like hydrotreating or ammonia synthesis which uses H_2 or in the Fischer-Tropsch or production of synthetic natural gas, which uses synthesis gas.

Steam reforming of bio-oil has the potential to be CO_2-neutral and is therefore a sustainable route to hydrogen or synthesis gas. Steam reforming of fossil fuels is used frequently in the chemical industry to produce reactants and the shift to SR of bio-oil would decrease the CO_2-emission. A lifecycle analysis has shown the SR of bio-oil is more energy demanding compared to SR of fossil fuels, which is partly due to addition of methanol as a stabilizer for the bio-oil and also a lower H/C-ratio is the feed. However, the decrease in greenhouse gas emissions would be around 50 % for the SR of bio-oil compared with SR of natural gas [25]. Another life cycle analysis based on an entire biorefinery with pyrolysis and bio-oil upgrading has shown that the concept could be economically viable and lead to decreased emissions of CO_2 [26]. In the analysis performed by Gebreslassie et al. [26] the H_2 used for hydrotreating of the bio-oil was produced by SR of CH_4 and therefore a further decrease in greenhouse gas emissions might be achievable if SR of bio-oil was used for H_2 production instead. Similar results was reported in a LCA study by Han et al. [27]. Furthermore it has been estimated that the production costs of bio-oil through flash pyrolysis enables a selling price of bio-oil at values lower than the cost of fuel oil [28]. A simple flow diagram for the process from biomass to synthesis gas can be seen in figure 1.1. Another process for converting biomass into synthesis gas or H_2 is through gasification and subsequent shift conversion. However, the yield of H_2 is lower compared with the flash pyrolysis and SR of bio-oil [12]. Furthermore, gasification will often require an air separating unit to produce pure oxygen and this is expensive and energy intensive.

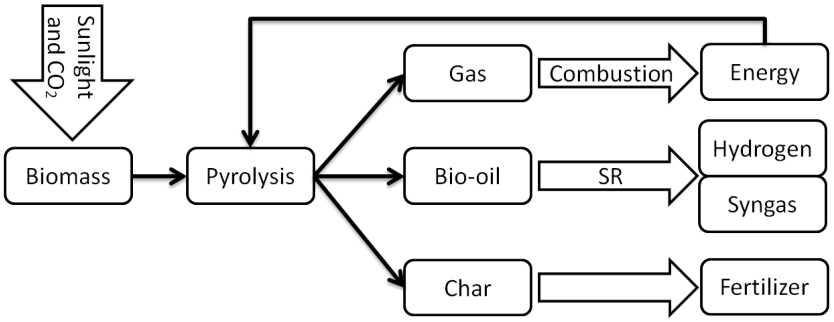

Fig. 1.1: *Simple flow diagram for the complete path from biomass to synthesis gas via bio-oil SR.*

1.2 Conventional steam reforming

Steam reforming is a process where hydrocarbons react with steam at high temperatures and are converted to carbon oxides and H_2. Steam reforming is normally accompanied by the water gas shift (WGS) and the methanation reaction, where the extents of these reactions depend on the operating conditions. The reforming, WGS, and methanation reactions are shown below [29–31].

$$\text{Reforming:} \quad C_nH_m + n\ H_2O \rightleftharpoons n\ CO + (n + m/2)\ H_2 \tag{1.1}$$

$$\text{WGS:} \quad CO + H_2O \rightleftharpoons CO_2 + H_2 \tag{1.2}$$

$$\text{Methanation:} \quad CO + 3H_2 \rightleftharpoons CH_4 + H_2O \tag{1.3}$$

The reforming reaction is endothermic reaction while the methanation and WGS are exothermic reactions. The reforming equilibrium is favored by high temperatures and low pressures, while the WGS is shifted toward CO and H_2O at high temperatures [29–31]. The reforming reaction (reaction 1.1) is not reversible over most SR catalysts at the reaction conditions usually employed.

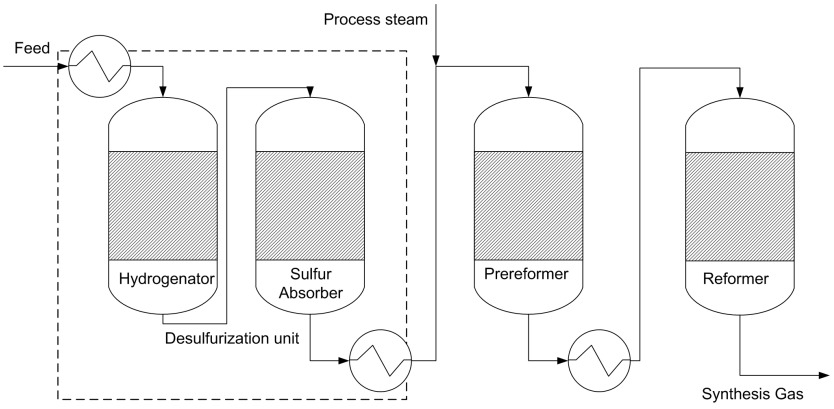

Fig. 1.2: *Simple flowsheet for an industrial steam reforming unit with a prereformer.*

The SR process has been investigated thoroughly with natural gas and other fossil fuels as reactants and is also used industrially to produce synthesis gas or hydrogen for processes like the Haber-Bosch (NH_3) or the Fischer-Tropsch (diesel) synthesis [30–33]. An industrial plant for SR of natural gas generally consist of three units as shown in figure 1.2. First a desulfurization unit with two reactors to reduce the sulfur content to *ppb*-levels by hydrogenating the sulfur compounds in the first reactor (hydrogenator) and then absorbing the formed H_2S in

the second reactor (sulfur absorber). Secondly a prereformer, which operates at temperatures between 350 and 550 ℃, converts the C_{2+} hydrocarbons to mainly methane and carbon oxides. The third unit is the primary reformer, where the methane is converted to synthesis gas at temperatures from 450 to 1050 ℃ [29–31, 34, 35]. The desulfurization is needed because the Ni-catalysts typically used in the reformers are deactivated by H_2S in trace amounts [29–31, 36]. The prereformer allows feedstock flexibility and a higher inlet temperature to the reformer, because the higher hydrocarbons, which can cause carbon deposition at high temperatures, are converted to CH_4 before they reach zones with high temperatures [35]. The synthesis gas can be shifted catalytically downstream the reformer to achieve a ratio between H_2 and CO suitable for the downstream processing [29–31]. The SR of natural gas is generally conducted at pressures around 30 *bar* as the natural gas is delivered at this pressure and the downstream processing is pressurized as well. Furthermore the equipment will be smaller when the gas is pressurized and the process is operated at elevated pressures.

The SR of hydrocarbons occurs through adsorbed species on the catalyst (adsorbed species will be denoted with $*$). The hydrocarbons dissociatively adsorb on the metal forming C_xH_y* and the steam dissociatively adsorbs on the support or on the metal particles forming OH-species. The $OH*$ and C_xH_y* can then react at the interface between the metal and the support or on the metal particles forming CO and H_2 [30, 37]. CO_2 is formed from CO and H_2O through the WGS (reaction 1.2). Bengaard et al. [38] have shown that the reaction mechanism for SR of CH_4 proceeds through the adsorbed species, as described above. The surface reactions in the SR of CH_4 are generally assumed to be [30, 38, 39]:

$$CH_4(g) + 2* \rightleftharpoons CH_3* + H* \tag{1.4}$$
$$CH_3* + * \rightleftharpoons CH_2* + H* \tag{1.5}$$
$$CH_2* + * \rightleftharpoons CH* + H* \tag{1.6}$$
$$CH* + * \rightleftharpoons C* + H* \tag{1.7}$$
$$H_2O(g) + 2* \rightleftharpoons HO* + H* \tag{1.8}$$
$$OH* + * \rightleftharpoons O* + H* \tag{1.9}$$
$$C* + O* \rightleftharpoons CO* + * \tag{1.10}$$
$$CO* \rightleftharpoons CO(g) + * \tag{1.11}$$
$$2H* \rightleftharpoons H_2(g) + 2* \tag{1.12}$$
$$\text{Overall: } CH_4 + H_2O \rightleftharpoons 3H_2 + CO \tag{1.13}$$

Carbon formation in conventional SR can occur both in the gas phase and through surface reactions. The gas phase reactions include cracking of hydrocarbons and free radical reactions, which induces condensation of tars [40–42]. On the surface of the catalyst and under SR-condtions free reactive surface carbon atoms, called C_α, can be formed and these can easily be gasified to carbon oxides. If C_α is not converted to gaseous species (carbon oxides or CH_4) it may accumulate on the surface and polymerize to the less reactive carbon type, C_β, which can lead to formation of encapsulating carbon or carbon whiskers. Accumulation and polymerization of C_α to C_β will require a larger ensemble of Ni-atoms. Therefore, small Ni-particles reduce the carbon formation tendency. Another strategy is to decorate the most active carbon forming sites by sulfur. This has been used in SPARG process from Haldor Topsoe A/S, which enables SR units to operate at low S/C-ratios and with no carbon formation [43, 44].

The deposited carbon can have three different forms; pyrolytic coke, whiskers, and gum. The formation of pyrolytic coke and whiskers occurs mainly at high temperatures while gum formation is a problem at low temperatures [30, 36, 38]. The actual limit where carbon free operation is possible depends on feedstock, pressure, and S/C-ratio. The potential for forming whiskers and pyrolytic coke can be estimated as described by Rostrup-Nielsen and Christiansen [42]. The carbon formation is generally reduced at high steam-to-carbon (S/C) ratios meaning that the temperature window between the high and low temperature carbon formation increases with S/C [30, 31]. The different carbon formation reactions are shown below [30, 32, 36]:

$$\text{Boudouard:} \quad 2CO \rightleftharpoons C_s + CO_2 \tag{1.14}$$

$$\text{CO decomposition:} \quad CO + H_2 \rightleftharpoons C_s + H_2O \tag{1.15}$$

$$\text{CH}_4\text{ decomposition:} \quad CH_4 \rightleftharpoons C_s + 2H_2 \tag{1.16}$$

$$\text{CH decomposition:} \quad C_nH_m \rightarrow nC_s + m/2H_2 \tag{1.17}$$

$$\text{Gum:} \quad C_nH_m \rightarrow (CH_2)_n \rightarrow \text{Gum} \tag{1.18}$$

$$\text{Pyrolytic coke:} \quad C_nH_m \rightarrow \text{Olefins} \rightarrow \text{Coke} \tag{1.19}$$

Reactions 1.14 to 1.18 are catalytic reactions and dependent on the type of catalyst while reaction 1.19 mainly depends on temperature. However, CO decomposition and the Boudouard reaction are mainly thermodynamical favorable at low temperature, while CH_4 decomposition or other decomposition reactions mainly will occur at high temperatures. Carbon whiskers are produced through reactions 1.14 to 1.17 and is a major problem for Ni-catalysts [30, 31].The whiskers are graphene tubes, which grow from the nickel particles and they are mainly initiated at the most active step sites on the metal (Ni) particles. The whiskers will leave most of the Ni surface free to catalyze reactions and the main problem is that they will cause disintegration of the support material [42]. Addition of small amounts of alkali metals or other metals, which can adsorb on the step sites, to the catalyst can significantly reduce the formation of whiskers [30, 38]. They block, completely or partially, the most active sites (step sites) and the nucleation of the graphene cannot occur. The addition of alkali metals, which blocks the step sites, will also decrease the activity of catalyst, because the step sites are the most active sites for the SR as well [30, 38]. Furthermore the addition of alkali can cause an increased risk of sintering. A smaller metal particle size can also decrease the whisker formation, because the formation of the graphene tubes is not energetically favorable before the carbon island exceeds a critical size. This value has been estimated by DFT calculations to be 25 $\AA$ and experimental results suggest that metal particles less than 50 $\AA$ in diameter should show low whisker formation [30].

Sintering of the catalyst can also be a problem especially at high temperatures, high metal loadings, or high steam partial pressures [30, 45]. In this process fewer and larger metal particles are formed, either by Ostwald ripening or cluster migration and coalescence. Sintering will usually occur above the Tamman temperature of metals, which is half the melting temperature in Kelvin, because the metal atoms become mobile above this point. The Tamman temperature for pure nickel is 863 K [46].

Poisoning of the SR catalysts by sulfur can also be problem, which will be discussed further in section 1.4.

The conventional SR process is usually catalyzed by group VIII metals and nickel is preferred due to its lower price and good activity, even though noble metal catalysts can be more active and less prone to coke formation [29, 30, 47]. The support material used are MgO, other basic oxides, Al_2O_3, calcium or magnesium aluminates [32].

1.3 Steam reforming of oxygenates

In this section results from SR of several different model compounds and bio-oil will be presented. The first subsection will be general considerations regarding the SR of oxygenates. The term yield of H_2 will be used in the following sections as descriptor for how well equilibrated a gas is produced. The maximum achievable production of H_2 will be determined by the temperature and the approach to equilibrium in the WGS and methanation reactions.

1.3.1 General considerations

The general reaction scheme for the SR of oxygenates is:

$$C_nH_mO_p + (n - p)\ H_2O \rightarrow\ nCO + (n - p + m/2)\ H_2 \tag{1.20}$$

Reaction 1.20 in combination with WGS (reaction 1.2) fully shifted toward the right is:

$$C_nH_mO_p + (2\ n - p)\ H_2O \rightarrow\ nCO_2 + (2\ n - p + m/2)\ H_2 \tag{1.21}$$

Steam reforming of oxygenates is often described by reaction 1.21 although at high temperatures WGS is shifted to the left and CO will also be present in significant amounts. The methanation of CO (reaction 1.3) will also influence the product distribution at equilibrium especially at low temperatures and/or high pressures as these conditions favor this reaction [30]. Thermal decomposition can also occur as the oxygenates often are thermally unstable and this reaction should be minimized due to the coke formation [48–51]. The decomposition can be described by:

$$C_nH_mO_p \rightarrow\ C_xH_yO_z + \text{gases} + \text{coke} \tag{1.22}$$

Steam reforming of oxygenates is, like the conventional SR, endothermic and therefore it is favored by high temperatures. Low pressures will also favor the SR as predicted by Le Châteliers principle. Thermodynamics predicts full conversion of oxygenates and the composition of the final product will be governed by the equilibrium prescribed by WGS and methanation. High yields of H_2 in SR requires a shift catalyst downstream the reformer operated at a lower temperature, which can convert the CO to CO_2 and H_2 by WGS [12]. If SR of oxygenates should provide synthesis gas to a process, a shift catalyst might be needed to adjust the CO/H_2-ratio. The CO/H_2-ratio depends on the temperature and S/C-ratio; high temperatures will increase the CO/H_2 while increasing the S/C will lower the CO/H_2-ratio at a given temperature.

The possible yields of H_2, both stoichiometric and at equilibrium, in the SR of different model compounds and a bio-oil, at 750 °C, S/C-ratio of 5, and atmospheric pressure, are shown in table 1.3. The stoichiometric yield is defined as the number of moles of H_2 produced pr. mole of carbon based on reaction 1.21. The equilibrium yield + WGS assumes that the CO present in the offgas can be shifted to H_2 and CO_2 in a downstream shift reactor at 200 °C [12, 51]. The WGS equilibrium is, at this temperature, shifted completely toward H_2 and CO_2. In table 1.3 it can be seen that possible equilibrium yields are around 85 % of the stoichiometric. Values close to 100 % should be possible if a shift catalyst at 200 °C is employed downstream the reformer as indicated by the last column in table 1.3 [12, 51].

The use of high temperatures in the SR process has two effects; one is that WGS is shifted toward CO and H_2O, which decreases the H_2-concentration, and the other one is that the methane is steam reformed. Therefore high temperatures are needed for full conversion of the

Tab. 1.3: *Thermodynamical equilibrium hydrogen yield from the steam reforming of different bio-oil model compounds or whole bio-oil [12, 51]. Values from Aspen Plus simulations at 750 °C , atmospheric pressure, and S/C-ratio of 5. st: stoichiometric. + WGS indicates the offgas is shifted at 200 °C.*

Feedstock	Stoichiometric $\left[\frac{mole\ H_2}{mole\ C}\right]$	Equilibrium [% of st.]	+ WGS [% of st.]
Ethanol	3.0	85.9	96.2
Phenol	2.33	84.3	96.3
Glucose	2.0	86.3	97.5
Poplar bio-oil[a]	2.14	85.2	96.9

[a] Average molar composition $C_6H_{8.82}O_{4.02}$.

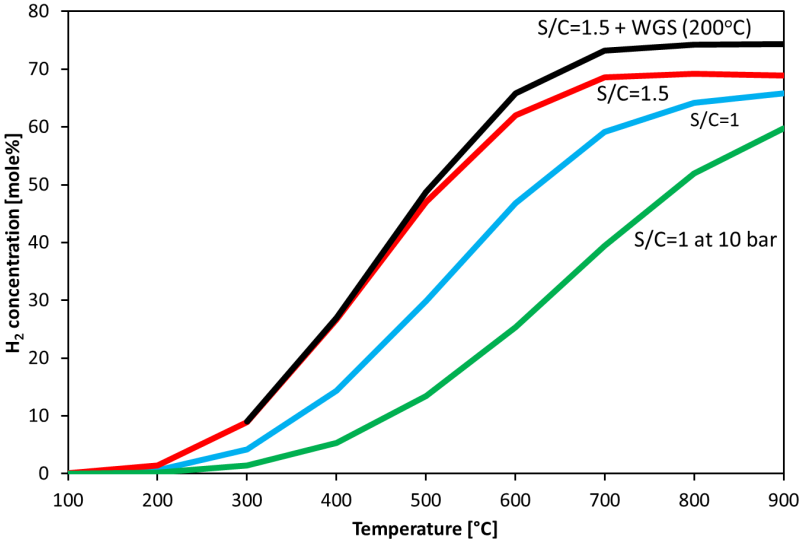

Fig. 1.3: *The equilibrium H_2 concentration on a water free basis as function of the temperature for S/C-ratios 1 and 1.5 at 1 bar and S/C-ratio of 1 at 10 bar for ethanol. + WGS indicates that the CO present is shifted to H_2 and CO_2 by a low temperature shift catalyst at 200 °C. The thermodynamic calculations are conducted in FactSage 6.0.*

hydrocarbons into CO_x and H_2 and then a lower temperature shift can be performed to shift the CO/H_2 ratio toward the desired value.

The ratio between steam and carbon is an important parameter because increasing this ratio will increase the conversion and also reduce carbon formation. This occurs because steam gasification of the deposited carbon might be possible due to a higher partial pressure of water and because the thermal decomposition of the oxygenates is suppressed [52]. The effects of the S/C-ratio and the pressure are illustrated in figure 1.3, where the equilibrium H_2 concentration as function of the temperature is shown for different S/C-ratios and pressures. In figure 1.3 it can be seen that the equilibrium H_2 concentration on a H_2O free basis increases with increasing S/C-ratio or decreasing pressure. The effect of shifting the offgas by the WGS catalyst at 200 °C can also be seen in figure 1.3.

The equilibrium offgas composition as function of the temperature in the SR of ethanol is shown in figure 1.4 to illustrate the trends in the product distribution in the SR of oxygenates. The conversion is at low temperatures, below 400 °C, mainly to CH_4 and CO_2 and as the

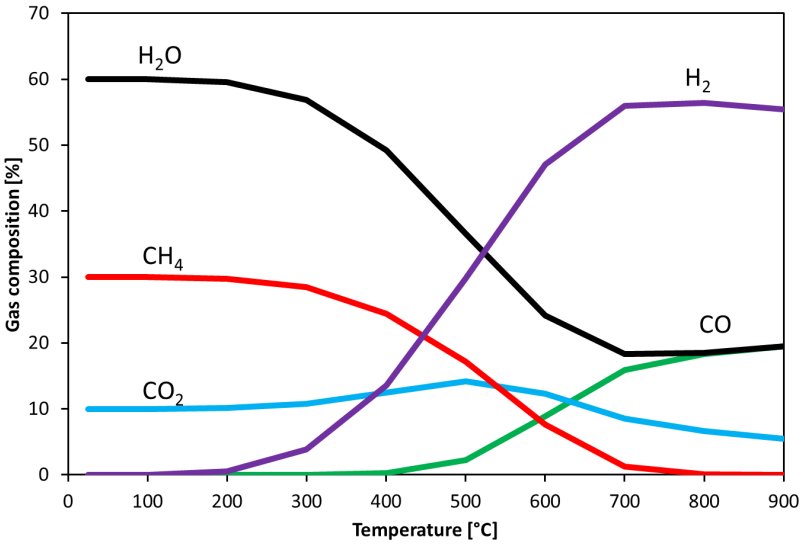

Fig. 1.4: *The equilibrium offgas composition as function of the temperature in the SR of ethanol at 1 bar and S/C-ratio of 1.5. The thermodynamic calculations are conducted in FactSage 6.0.*

temperature increases the CH_4, CO_2, and H_2O fractions decrease and the H_2 and CO fractions increase. The WGS reaction shifts toward CO and H_2O above 700 °C, which lowers the H_2 and CO_2 concentration. The effects of S/C-ratio, pressure, and temperature has been shown by thermodynamic calculations [53–56] and verified by several experimental studies [48, 57–63]. However, the conversion predicted by thermodynamics cannot be reproduced below 400 °C as full conversion rarely is achieved at low temperatures.

The deactivation mechanisms in the SR of oxygenates are similar to those encountered in the conventional SR, namely; carbon deposition, sintering, and sulfur poisoning.

The SR of oxygenates have mainly focused on the SR of ethanol, due to the general large interest in bio-ethanol, but SR of acetic acid, as model compound for bio-oil, have also been investigated. There have also been conducted studies on larger model compounds of bio-oil, like phenols, cresols, or whole bio-oil, but not to the same extent as for acetic acid and especially ethanol.

The motivation for testing model compounds instead of whole bio-oil is that it is possible to get a better understanding of the reactions, influence of experimental conditions, deactivation etc. because it is known exactly what enters the reactor. Therefore it is possible to recreate similar conditions and concentrations when testing different catalysts and hereby allow better comparison between them. Furthermore, the separation and analysis of the reactor effluent is easier due to the limited number of products.

1.3.2 SR of acetic acid

Carboxylic acids are present in large amounts in bio-oil (see table 1.1) and acetic acid is reported as the most abundant [20]. Therefore acetic acid has been used as model compound of bio-oil in many studies. The SR of acetic acid is accompanied by many possible side reactions. The most relevant of these can be seen in table 1.4. The unwanted reactions are dehydration to ketene (reaction 6 in table 1.4) and the ketonization (reaction 2 in table 1.4) to acetone. Ketene can combine to form ethene by reaction 8, which is a known coke precursor [48, 52, 64], while acetone can polymerize by aldol condensation and form coke through reactions 9 to 11

Tab. 1.4: *Possible reactions in the steam reforming of acetic acid [48, 52, 64, 67, 68].*

Reaction	Name	Reaction scheme
1	SR	$CH_3COOH + 2\ H_2O \rightarrow\ 2CO_2 + 4H_2$
2	Ketonization	$2CH_3COOH \rightarrow\ CH_3COCH_3 + CO_2 + H_2O$
3	SR acetone	$CH_3COCH_3 + 3\ H_2O \rightarrow\ 3CO + 6H_2$
4	Decomposition 1	$CH_3COOH \rightarrow\ CH_4 + CO_2$
5	Decomposition 2	$CH_3COOH \rightarrow\ 2H_2 + CO_2 + C$
6	Dehydration	$CH_3COOH \rightarrow\ CH_2CO + H_2O$
7	SR ketene	$CH_2CO + H_2O \rightarrow\ 2CO + 2H_2$
8	Ketene coupling	$2CH_2CO \rightarrow\ C_2H_4 + 2CO$
9	Acetone 1	$2CH_3COCH_3 \rightarrow\ H_2O + (CH_3)_2CCHCOCH_3$
10	Acetone 2	$(CH_3)_2CCHCOCH_3 + CH_3COCH_3 \rightarrow\ C_9H_{12} + 2H_2O$
11	Acetone 3	$C_9H_{12} \rightarrow\ Coke$

[65]. The dehydration and ketonization are mainly observed at medium conversions, or in experiments, where support materials are used without an active phase [48, 52]. Rhodium and some support materials, especially ZrO_2, catalyze the ketonization and larger amounts of acetone can be formed [48, 65]. Takanabe et al. [66] reported that ZrO_2 without metal had a conversion around 85 % mainly to acetone at weight hourly space velocity (WHSV) of 9 h^{-1} and 450 ℃. The addition of metal to the support material will generally reduce the extent of the ketonization [52, 66].

The most desired reactions in table 1.4 are the SR reactions or the decomposition to CH_4 and CO_2, which can be reformed to the desired products.

The complete conversion of acetic acid is reported to occur at temperatures between 400 and 800 ℃ depending on the catalyst and operating conditions [48, 48, 59, 60, 66, 69–74]. The conversion over support material, like Al_2O_3, without a catalytic active metal exceeds 10 % at WHSV of 36 h^{-1} and temperatures above 850 ℃ and is mainly by thermal decomposition to CH_4 and CO_2 [48]. At higher temperatures (900 ℃ or above) hydrogen production can also occur over Al_2O_3 [48]. The conversion over quartz particles is higher compared with support materials and full conversion can be achieved at 950 ℃ and WHSV of 36 h^{-1} [48, 70]. However, homogenous reactions affect the process and full conversion to CH_4, CO_2, H_2, and CO have been reported to occur in the empty reactor at 950 ℃ at the same flow rate and same reactor as used by Basagiannis and Verykios [48]. At 750-800 ℃ the conversion is 10 % or below [48, 74].

Mechanism and kinetics

Takanabe et al. [75] used IR-measurements, pulse experiments, and flow reactor experiments to arrive at a mechanism for SR of acetic acid over a Pt/ZrO_2-catalyst, where the first step is a dissociative adsorption of the acid to form acetate or acyl species on the Pt-surface by the reactions:

$$CH_3COOH + 2\ * \quad \rightleftharpoons \quad CH_3COO* + H* \tag{1.23}$$

$$CH_3COOH + 2\ * \quad \rightleftharpoons \quad CH_3CO* + OH* \tag{1.24}$$

DFT-calculations and experiments have shown that these species are formed on Pt-surfaces [76, 77]. In the DFT-calculations direct conversion of acetic acid to CH_4, CO, and CO_2 is

assumed to occur through acyl species [76, 78]. The decomposition reactions of acyl species was proposed by Gursahani et al. [76] to be:

$$CH_3CO* \rightleftharpoons CH_4 + CO* - \tfrac{1}{2}H_2 \quad (1.25)$$
$$CH_3CO* + * \rightleftharpoons CH_2CO* + H* \quad (1.26)$$
$$CH_2CO* + * \rightleftharpoons CHCO* + H* \quad (1.27)$$
$$CHCO* + * \rightleftharpoons CH* + CO* \quad (1.28)$$
$$CH* + 2H* \rightleftharpoons CH_4 + 3* - \tfrac{1}{2}H_2 \quad (1.29)$$

The acyl and acetate species formed in reactions 1.23 and 1.24 can decompose to CO, CO_2, and CH_x* where $x \leq 3$ according to Takanabe et al. [75]. However, no specific surface reactions were proposed for the decomposition reaction but it could be:

$$CH_3CO* \rightleftharpoons CH_3* + CO* \quad (1.30)$$

In combination with with reactions 1.5-1.12, which is supported by Wang et al. [78].

Takanabe et al. [75] proposed that the CH_x-species either could polymerize to form a carbon layer on the catalyst or react with OH-species from the support and form carbon oxides and H_2. The OH-species are formed by dissociative adsorption of steam, reaction 1.8. The operating conditions will probably determine whether the carbon formed in this mechanism is pyrolytic carbon, gum, or whiskers. Takanabe et al. [75] proposed that the reaction between OH-species and CH_x or graphite species occurs at the boundary between the Pt and ZrO_2 [75]. In a mechanism similar to the one described above, decomposition of the oxygenate on the metal and reaction with OH-species at the metal-surface interface, could occur for all oxygenates according to Takanabe et al. [75].

To substantiate the bifunctional mechanism it was shown that the hydrogen production from the SR of acetic acid over Pt-catalysts could be related to the number of Pt-atoms at the periphery of the metal particles rather than number of Pt-sites in total [79]. Furthermore, a study with deuterated acetic acid (CH_3COOD) on Pt-ZrO_2 by Güell et al. [77] showed that the acetic acid indeed decomposed to CH_3* and CO_2 as proposed by Takanabe et al. [75].

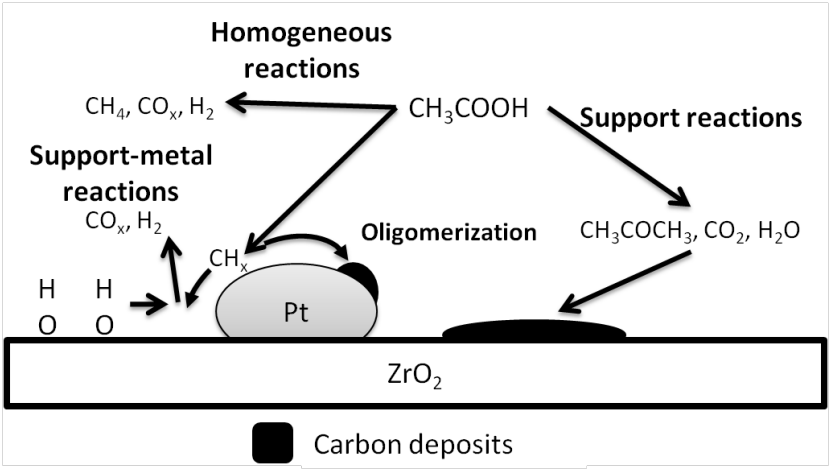

Fig. 1.5: *The bifunctional reaction mechanism proposed by Takanabe et al. [75], where possible side reactions are indicated as well. Figure adapted from ref. [75].*

A schematic of the mechanism proposed by Takanabe et al. [75] for the SR of acetic acid is shown in figure 1.5. This mechanism is, in some aspects, similar to the bifunctional mechanism

proposed for conventional SR [30, 39]. However, this mechanism is not very specific and do not describe the actual surface reactions, which might occur.

Wang et al. [51] have proposed the following surface reactions to occur in the SR of acetic acid:

$$CH_3COOH + 2* \rightleftharpoons CH_3COO* + H* \quad (1.31)$$
$$CH_3COO* \rightleftharpoons CH_3* + CO_2 \quad (1.32)$$
$$CH_3* + 3* \rightleftharpoons C* + 3H* \quad (1.33)$$
$$C* + H_2O \rightleftharpoons CO* + H_2 \quad (1.34)$$

Reactions 1.33 and 1.34 are not elementary steps and must occur through several reactions, which could be similar to steps in the mechanism for SR of methane, which is described by reactions 1.4 to 1.12. At low temperatures the reverse of reaction 1.4 will also be important as CH_4 can be formed from CH_3*. The main difference between these two mechanisms is how the CH_3*-species is formed. The above sequence of reactions corresponds well with the general mechanism proposed by Takanabe et al. [75]. It should also be noted that elemental carbon is involved in the process and gasification of this species should occur fast to minimize the carbon formation [51, 80].

A kinetic study of the SR of acetic acid has been conducted by Galdamez et al. [81], where first order kinetics were proposed and based on this assumption it was shown that the hydrogen production rate could be related to the difference between the actual and the equilibrium concentrations. The expression used by Galdamez et al. [81] was:

$$r_i = k_i \cdot \left(\left(\frac{m_i}{m_a} \right)_{Eq} - \frac{m_i}{m_a} \right) \quad (1.35)$$

where r_i is the production rate of component i, m_i is the mass flow of component i, m_a is the mass flow of acetic acid in the feed, m_i/m_a is the yield of component i in $g/(g(\text{acetic acid}))$, and the subscript Eq refers to the equilibrium. The term $\left(\frac{m_i}{m_a}\right)_{Eq}$ is zero for CH_4 and C_2-species and equation 1.35 is reduced to:

$$r_i = -k_i \cdot \left(\frac{m_i}{m_a} \right) \quad (1.36)$$

The rate constants based on eq. 1.35 and 1.36 are shown in table 1.5 along with the R^2-values which indicates a good correspondence between the experiments and eq. 1.35 and 1.36. The model by Galdamez et al. [81] might fit the data quite well, but it is highly empirical and extrapolation based on eq. 1.35 seems questionable.

Catalysts

Several different transition metals have been tested in the SR of acetic acid. These are the base metals Co, Ni, Fe, and Cu [48, 57, 59, 60, 64, 69–74, 80–83] and the noble metals Pt, Pd, Rh, and Ru [48, 52, 66, 68, 75]. The reaction rate over base metals is highest for Co and Ni, while the rate over Fe and Cu is significantly lower [70]. At 450 ℃ and LHSV of 8.3 h^{-1} full conversion can be achieved over Co or Ni while the conversion over Fe or Cu are roughly 25 $wt\%$. The order of decreasing activity for the base metals is [70]:

Tab. 1.5: *The rate constant based on the kinetic expression proposed by Galdamez et al. [81] and shown in eq. 1.35. C_2 includes C_2H_2, C_2H_4, and C_2H_6.*

Gas	Rate constant $\left[\frac{g_{\text{Acetic acid}}}{g_{\text{Cat}} \cdot min}\right]$	R^2
H_2	0.3802	0.9985
CO_2	0.5655	0.9816
CH_4	0.1705	0.9687
C_2	0.4534	0.9809

$$\text{Ni} > \text{Co} > \text{Fe} > \text{Cu}$$

The metals were all supported on alumina and had a metal loading of 20 $wt\%$.

The Co and Ni-catalysts have the ability to both break C-C and C-H-bonds, which is needed for converting acetic acid, and this explains the better performance of these metals compared to Fe, which mainly can break C-C bonds and Cu which mainly can break C-H bonds [70]. The long-term stability is higher for Ni compared with Co and in some cases also the activity [70, 84]. This is due to an increased carbon formation on the Co catalysts. Another drawback of Co is that it cannot be kept reduced under industrial conditions, where there is plug flow [85]. In laboratory scale experiments back mixing and diffusion of H_2 can keep Co reduced.

A mixture of Ni and Co in a molar ratio of 1 to 4 without any support have shown better performances compared to pure Ni or Co [69]. Full conversion and no CO formation could be achieved at temperatures down to 400 ℃ and LHSV of 5.1 h^{-1}.

A study by Basagiannis and Verykios [48] has shown that the most active noble metals were Rh and Ru, while Pd and Pt showed much lower activity. In this study it was reported that Ni catalysts were even more active compared with the noble metals [48]. The order of activity in terms of conversion and TOF, with 1 $wt\%$ metal content for all the noble metals except for Rh with 0.5 wt%, was [48]:

$$\text{Ni} > \text{Rh} > \text{Ru} > \text{Pd} > \text{Pt}$$

The Ni catalysts used in the comparison above had a metal loading of 17 $wt\%$ and was like the other metals supported on Al_2O_3. In general it is reported that Ni catalysts can obtain activities similar to the noble metals, but the noble metals are less prone to carbon formation and therefore more stable over time [48, 86].

A study by Hu and Lu [82] investigated the influence of different promoter metals on the performance of a Ni/Al_2O_3-catalyst in the SR of acetic acid. They tested Li, Na, K, Mg, Fe, Co, Zn, Zr, La, and Ce and found that the addition of K gave the largest improvement in the catalytic performance both in the terms of activity and stability. The addition of Co, Fe, or Zn decreased the conversion over the catalyst, while the addition of the other promoters increased the conversion, but only K, Li, and Na decreased the yield of CH_4 as well [82]. The performances of some of the promoted Ni-catalysts are listed in table 1.6, where the aforementioned trends can be seen. Y_{CH_4} describes how many moles of carbon CH_4 constitutes compared with the total moles of carbon in carbon containing products and similar Y_{H_2} describes how many moles of H_2 is produced compared with total number of moles of H_2 in the H_2 containing products.

Tab. 1.6: *The conversion and yield of CH_4 and H_2 for different promoted Ni-catalysts in the SR of acetic acid [82]. T: 400 ℃, p: 1 bar, S/C: 7.5, LHSV: 12.1 h^{-1}.*

Catalyst	X_{AA} [%]	Y_{CH_4} [%]	Y_{H_2} [%]
Ni/Al_2O_3	67.8	14.7	66.2
$Ni\text{-}Na/Al_2O_3$	93.8	4.0	89.6
$Ni\text{-}K/Al_2O_3$	100	1.4	93.5
$Ni\text{-}Mg/Al_2O_3$	47.8	12.3	57.6

The optimal amount of promoter was 8 $wt\%$ for K, which could increase activity, decrease the yield ofCH_4, and increase the long-term stability. These effects were ascribed to a decrease in the activity for methanation, because CO dissociation, which is most likely to occur at step sites, was inhibited by K. The addition of K decreased the reduction temperature, resulting in more metallic Ni-particles on the catalyst at the applied reduction temperature of 600 ℃, which also could be responsible for the improved performance [82]. It was also suggested that K-promotion decreased sintering of Ni on the catalysts [82]. The addition of K is known from the SR of hydrocarbons to decrease the carbon whisker formation because the active step sites are covered by K [38, 87], and it is also reported to increase the steam adsorption [32, 37]. This could explain the increased long-term stability for the K promoted Ni-catalysts.

The promoting effect of K, increased activity and stability, and perhaps also decreased sintering, in the SR of oxygenates is contrary to what is observed in the SR of CH_4 where K promotion decreases the overall activity of the catalyst and increase the risk of sintering [30, 42].

The support material in the catalyst is important and can be optimized to induce a more stable and active catalyst. Al_2O_3 is an acidic support and is known to catalyze cracking reactions and hereby form coke on the catalyst [88]. The coke formation can be suppressed and the catalytic activity improved, if the Al_2O_3 is mixed with a basic oxide like MgO, CeO_2, or La_2O_3 [48, 52, 89]. The structure of the mixed oxides is probably a spinel type structure, at least for the mixture of MgO and Al_2O_3 [52]. Of the basic oxides it seems that MgO is the best promoter [48, 52]. The increased activity by the addition of basic oxides can be ascribed to a higher amount of OH-species from water dissociation on the support, which can diffuse onto the metal particles and participate in reactions and also a smaller size of the metal particles [48, 52]. The improved stability is due to less coke deposition, because less cracking occurs as the number of acid sites is decreased and also because steam gasification of the coke might be facilitated by spillover of O- or OH-species from the support to the metal particles [52].

Apparent activation energies for the SR of acetic acid over different active metals on different support materials have shown that surface reactions on the support or at the support metal interface are important as the activation energies changes most with a change in support and not with a change in the type of active metal [48].

Support materials, like ZrO_2 and CeO_2, have also been tested with Ni as the active material; severe coking occurs on the acidic ZrO_2-catalyst and much less on CeO_2-catalyst [68]. ZrO_2 is an acidic support, which leads to significant cracking and also coke deposition, and furthermore it catalyzes the formation of acetone which can condense and form coke [65, 68]. CeO_2 showed a better performance compared with ZrO_2 which was ascribed to a higher activity in the SR of acetone or lower production of acetone [90]. It was also suggested that Ce has the ability to supply oxygen to oxidize the coke on the catalyst and being reoxidized by steam, which

Tab. 1.7: *The conversion, yield of H_2, and carbon deposition at 750 °C for five different catalysts in the steam reforming of acetic acid [48]. Carbon deposition was estimated based on 4 h experiment and defined as the percentage of carbon fed to reactor, which deposits on the catalyst. Atmospheric pressure, S/C-ratio=1.5, GHSV= 13050 $cm^3/(g \cdot h)$.*

Catalyst	Conversion [%]	Y_{H_2} [%]	Carbon deposition [% of carbon feed]
Al_2O_3	5	0	4.65
1 *wt*% Pt/Al_2O_3	8	20	0.37
0.5 *wt*% Rh/Al_2O_3	55	95	0.39
17 *wt*% Ni/Al_2O_3	80	99	0.24
17 *wt*% $Ni/(MgO/Al_2O_3)$	100	100	0.10

also was shown by TPR experiments [68]. Another explanation could be that the CeO_2 can activate H_2O through dissociative adsorption and the formed $OH*$ or $O*$ can diffuse on to the metal particles and react with the carbon.

Mixtures of CeO_2 and ZrO_2 have also been used as support and better performance than with Al_2O_3 or $MgAl_2O_4$ could be achieved [67, 91]. Ni or Rh supported on $Ce_{0.63}Zr_{0.37}O_2$ had a higher yield of H_2 compared with Ni or Rh on CeO_2 in the SR of ethanol [92]. $Pt/Ce_xZr_{1-x}O_4$ catalysts with a ratio between Ce and Zr of 1:3, on the other hand, showed a lower conversion and yield of H_2 compared with Pt/CeO_2 [90].

The influence of the carrier and active metal in the catalyst for SR of acetic acid is illustrated in table 1.7, where the conversion, yield of H_2, and carbon deposition for four different catalysts and two support materials are shown. When adding metal to the support material conversion increases and the carbon deposition decreases, and when the metal changes from Pt to Rh to Ni the conversion and yield of H_2 increases and the carbon deposition decreases. However, the much higher metal loading on the Ni catalyst will contribute to the increased conversion. Finally table 1.7 shows that adding MgO to an acidic support like Al_2O_3 increases the conversion and yield of H_2 and diminishes the carbon deposition even further [48].

The metal content in the Ni catalysts is generally around 5-30 *wt*% [49, 60, 61, 74, 89, 93] and for the noble metals it is often around 1 *wt*%, although values up to 10 *wt*% have been reported [48, 58, 63, 84, 94, 95]. The conversion generally increases with increasing metal content [48, 84, 95] and for a Ni-Al co-precipitated catalyst it was found that the optimal Ni loading was 28 *wt*% [60, 61]. However a Ni content between 10 and 20 *wt*% is more common as higher loading can cause severe problems with sintering [45]. A recent study by An et al. [80] have shown that the optimal Ni loading on γ-Al_2O_3 was 12 *wt*% as the highest conversion and H_2-yield in combination with lower carbon deposition could be achieved with this catalyst. The different values for Ni loading indicate that the optimal loading depends on the carrier material.

Some of the most promising catalysts for the SR of acetic acid are highlighted in table 1.8 along with their performances. The stability is the time taken for the conversion to decrease 10 % from its initial value. If the conversion has not decreased 10 % within the time shown in the article the stability is indicated as larger than that time. This definition of stability will be used throughout this review. However, the stability of the catalyst is difficult to tabulate

Tab. 1.8: *Selected catalysts and their performance in the SR of acetic acid.*

Metal	Support	T [°C]	S/C $[\frac{mole}{mole}]$	LHSV[a] $[h^{-1}]$	X [%]	$Y_{st,\ H_2}$[b] [%]	Stability[c] $[h]$	Ref.
17 *wt*% Ni	MgO/Al_2O_3	650	1.5	36 (W)	95	-	>45 (1 %)	[48]
5 *wt*% Ru	MgO/Al_2O_3	650	1.5	36 (W)[d]	99	-	75	[48]
30 *wt*% Ni with 8 *wt*% K	Al_2O_3	600	1.5	12.1	95	75	>30 (6 %)	[82]
18 *wt*% Ni	Al_2O_3	600	5.8	16	82	74	-	[96]
18 *wt*% Co	La/Al_2O_3	400	1	10.1	85	75	>20 (2 %)	[83]
0.5 *wt*% Rh	$CeZrO_4$	650	3	47	90	80	15	[86]

[a] (W) indicates that the SV is stated as WHSV.
[b] Yield of hydrogen defined as moles produced divided by the maximum theoretical yield.
[c] Time for the conversion or Y_{H_2} to decrease 10 % from its initial value. > X indicates that data in the article are shown for X hours, but the conversion have not decreased 10 %. The number in parenthesis is the decrease in conversion in percent.
[d] WHSV increased to 58 after 40 *h*.

as it might depend on the space velocity (SV). If the catalyst bed is much larger than required for full conversion then a deactivation front would move down the bed and full conversion might be possible despite that a large part of the catalyst bed has been deactivated. Ideally stability experiments should be conducted at experimental conditions which do not provide full conversion in order to make a good estimate of the deactivation rate and stability. A problem with this might be that under these conditions the carbon deposition potential might be larger as well and therefore not give a suitable estimate of the possible time of operation.

It can be seen that none of the catalysts in table 1.8 have stability over longer periods of time, which is primarily due to carbon formation. It is possible to achieve full conversion and high yields of H_2, but the catalysts are not stable over time, which is the main concern if the SR of bio-oil should have industrial potential.

1.3.3 SR of ethanol

The equilibrium composition in the SR of ethanol is shown in fig. 1.4, but in practice a number of by-products can be formed through the reactions shown in table 1.9. The most common ones are acetaldehyde, acetic acid, acetone, ethene, and methane [49, 50, 57, 93, 97–99]. Reaction 1 and 1a are the overall SR reactions with and without WGS, while reactions 2-9 in table 1.9 constitutes the possible side reactions for the SR of ethanol. Acetone can be converted to coke by the same reactions as in the SR of acetic acid (reactions 9-11 in table 1.4). The dehydration reaction (reaction 3 in table 1.9) should be minimized as ethene is as precursor for carbon formation as indicated by reaction 3a in table 1.9, which is the decomposition of ethene. Ethene has the highest potential for carbon formation of all hydrocarbons [32, 100].

Barattini et al. [57] reported that the main products from the SR of ethanol over an inert material like quartz at temperatures between 400 and 800 °C were acetic acid from oxidation (reaction 5 in table 1.9) and ethene from dehydration (reaction 3 in table 1.9). In the presence of a catalyst and at low degrees of conversion, oxidation to acetic acid and the formation of acetaldehyde were the dominating reactions [57]. At higher conversions the products were CO_2, CO, H_2, and CH_4, which can be formed by combinations of many of the reactions shown in table 1.9. Barattini et al. [57] also reported that acetate or acetic acid were the

Tab. 1.9: *Possible reactions in the steam reforming of ethanol [49, 50, 57, 93, 97].*

Reaction	Name	Reaction scheme
1	SR ethanol	$CH_3CH_2OH + 3\ H_2O \rightarrow\ 2CO_2 + 6H_2$
1a	SR ethanol without WGS	$CH_3CH_2OH + H_2O \rightarrow\ 2CO + 4H_2$
2	Dehydrogenation	$CH_3CH_2OH \rightarrow\ CH_3CHO + H_2$
3	Dehydration	$CH_3CH_2OH \rightarrow\ CH_2CH_2 + H_2O$
3a	Ethene decomposition	$CH_2CH_2 \rightarrow\ 2C_s + 2H_2$
4	Decarbonylation	$CH_3CHO \rightarrow\ CH_4 + CO$
5	Oxidation	$CH_3CH_2OH + H_2O \rightarrow\ CH_3COOH + H_2$
6	Decomposition	$CH_3CH_2OH \rightarrow\ CH_4 + CO + H_2$
7	Recombination	$2CH_3CHO \rightarrow\ CH_3COCH_3 + CO + H_2$
8	SR acetone	$CH_3COCH_3 + 3\ H_2O \rightarrow\ 3CO + 6H_2$
9	SR acetic acid	$CH_3COOH + 2\ H_2O \rightarrow\ 2CO_2 + 4H_2$

key intermediates in the SR of ethanol over NiZnAl-catalysts. These intermediates would correspond well to the mechanism proposed by Takanabe et al. [75], where acetate species participated in surface reactions in the SR of acetic acid.

Acetone and acetaldehyde were reported as the main by-products at low conversions and temperatures below 500 ℃ over Ni, Ir, and Co supported on ceria by Zhang et al. [93]. Benito et al. [101] concluded, based on a temperature-programmed desorption (TPD) study, that the SR of ethanol proceeded through acetaldehyde species adsorbed on the surface. The surface species could either decompose, be steam reformed, or react with surface species like CH_3* and form acetone, which could undergo SR as well.

Fatsikostas and Verykios [89] and others [95, 102] found acetaldehyde as a by-product along with CH_4 and C_2H_4. It therefore seems that the main by-products in the SR of ethanol are acetaldehyde and small hydrocarbons. Acetaldehyde might be an intermediate in the process as it is present in most studies of SR of ethanol. The formation of by-products is generally low at high conversion and the main problem is not the yield of desired products nor activity, but rather catalyst deactivation due to carbon deposition [89, 95].

Based on the literature regarding SR of hydrocarbons and ethanol it seems likely that the most important reactions are the SR of ethanol combined with WGS and SR of methane as these will determine the product distribution. Thermal decomposition is probably also an important reaction, especially at high temperatures. The main deactivation path would probably be through dehydration and subsequent ethene decomposition due the high carbon formation potential of this compound. A reaction network similar to the reactions described above have been proposed by Subramani and Song [99] and can be seen in figure 1.6. In this network it is indicated the acetaldehyde is one of the intermediates, which is in accordance with the literature.

Experimental studies on the SR of ethanol are generally conducted at temperatures between 300 and 800 ℃ and full conversion can be achieved at 400 ℃ although mainly to CH_4. At higher temperatures the yield of CH_4 decreases, because the methanation equilibrium is shifted toward CO and H_2, and the yield of H_2 increases [57, 93, 97]. This is in accordance with the thermodynamic equilibrium shown in figure 1.4.

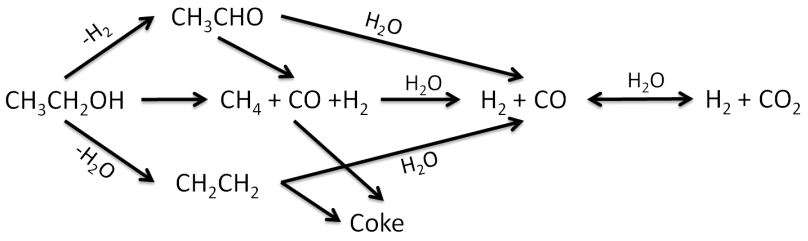

Fig. 1.6: *Reaction pathway for the SR of ethanol proposed by Subramani and Song [99]. Figure adapted from ref. [99].*

Mechanism and kinetics

The reaction mechanism for SR of ethanol is not completely clear and no general consensus has been reached. However, similarities between the mechanisms proposed for the SR of acetic acid and ethanol do exist.

The surface species involved in the SR of ethanol has been reported as ethoxy, acetate, acetaldehyde, and formic acid [103–105]. One of the mechanisms that have been proposed is based on three main reactions, namely SR of ethanol (reaction 1 in table 1.9), WGS (reaction 1.2), and ethanol decomposition (reaction 6 in table 1.9) [104]. It involves both formic acid and acetaldehyde as intermediates and was proposed by Sahoo et al. [104]. Both the SR and decomposition might occur through acetaldehyde intermediates. In the SR mechanism, the ethanol adsorbs on the surface and undergoes dehydrogenation to acetaldehyde and the steam undergoes dissociative adsorption to OH- and H-species. Acetaldehyde will then decompose to methyl and formaldehyde and both of them are transformed into formic acid, which decomposes to CO_2 and H. The reactions involved in this mechanism for the SR of ethanol are [104]:

$$CH_3CH_2OH(g) + 2* \rightleftharpoons CH_3CH_2O* + H* \quad (1.37)$$
$$CH_3CH_2O* + * \rightleftharpoons CH_3CHO* + H* \quad (1.38)$$
$$2* + H_2O(g) \rightleftharpoons OH* + H* \quad (1.39)$$
$$CH_3CHO* + H* \rightleftharpoons CH_3* + HCHO* \quad (1.40)$$
$$CH_3* + OH* \rightleftharpoons CH_3OH* + * \quad (1.41)$$
$$CH_3OH* + * \rightleftharpoons CH_3O* + H* \quad (1.42)$$
$$CH_3O* + * \rightleftharpoons HCHO* + H* \quad (1.43)$$
$$HCHO* + OH* \rightleftharpoons HCOOH* + H* \quad (1.44)$$
$$HCOOH* + 2* \rightleftharpoons CO_2* + 2H* \quad (1.45)$$
$$CO_2* + \rightleftharpoons CO_2(g) + * \quad (1.46)$$
$$2H* \rightleftharpoons H_2(g) + 2* \quad (1.47)$$

The ethanol decomposition is suggested to occur through reactions 1.37 and 1.38 combined with the two following reactions [104]:

$$CH_3CHO* + * \rightleftharpoons CH_4* + CO* \quad (1.48)$$
$$CH_4* \rightleftharpoons CH_4(g) + * \quad (1.49)$$

where the CO* can desorb as shown in reaction 1.52.

In reaction 1.40 there is formed CH_3*, which also is an intermediate in the SR of hydrocarbons, and an alternative or parallel path could therefore be reactions 1.5 to 1.12. The path

might be more probable as it is energetically favorable in the SR of methane. DFT-calculations by Mavrikakis et al. [106] have shown that the C-C bond breaking in reaction 1.40 could be energetically favorable, but the study also indicated that CH_2CO* might be an important intermediate in C-C bond breaking.

The WGS was included in the mechanism by Sahoo et al. [104] and it was assumed to occur through formate species. Usually the WGS is assumed to proceed through CO*, CO_2*, H*, and O* [107]. Sahoo et al. [104] described the WGS by the following reactions along with the dissociative adsorption of water (reaction 1.39), dissociation of formic acid (reaction 1.45), and dissociative adsorption of H_2 (reaction 1.47) [104]:

$$HCOOH* + * \rightleftharpoons HCOO* + H* \quad (1.50)$$

$$HCOO* + * \rightleftharpoons CO* + OH* \quad (1.51)$$

$$CO* \rightleftharpoons CO(g) + * \quad (1.52)$$

$$HCOO* + * \rightleftharpoons CO_2* + H* \quad (1.53)$$

CO_2 and H_2 can desorb from the catalyst through reactions 1.46 and 1.47, respectively. The rate determining steps were proposed to be reactions 1.38, 1.48, and 1.51 for the ethanol SR, ethanol decomposition, and the WGS, respectively, but no reason for this choice was given [104]. A further refinement of this mechanism could be to include the carbon formation, e.g. by reaction 3 and 3a in table 1.9 and also an alternative reaction path for the dissociation of CH_3*.

Rate expressions was deduced based on the three rate determining steps mentioned above and a Langmuir-Hinshelwood approach and showed good agreement with experimental data [104].

The mechanism proposed by Sahoo et al. [104] is more detailed compared to the mechanism proposed by Takanabe et al. [75] for the SR of acetic acid as detailed surface reactions are included. The overall scheme in both mechanisms have similarities: adsorption through the oxygen functionality followed by decomposition to CH_x and CO_x. However, the mechanism proposed by Sahoo et al. [104] does not use two different adsorption sites for steam and ethanol as proposed by Takanabe et al. [75]. Mechanisms similar to one described above have also been proposed in refs. [101, 108–110].

Another mechanism has been proposed by Busca et al. [105], where the acetaldehyde reacts with O^{2-}-species from the surface and forms acetate. Acetate can then react with OH^- forming CH_4, CO, and O^{2-} and the CH_4 can then be reformed. Another proposal is that the acetate can decompose to CH_4 and CO_2 [111]. Similar mechanisms have been reported by others [103, 112, 113].

The kinetics of the SR of ethanol have been investigated by Akande et al. [114], who proposed four different models, with different rate limiting steps. The models were based on three basic steps. Step one is the adsorption of ethanol (reaction 1.54); step two is the dissociation of adsorbed ethanol (reaction 1.55); step three is the reaction between gaseous steam and the absorbed species (an Eley-Rideal mechanism as shown in reactions 1.56 and 1.57):

$$CH_3CH_2OH + * \rightleftharpoons CH_3CH_2OH* \quad (1.54)$$

$$CH_3CH_2OH* + * \rightleftharpoons CH_3OH* + CH_2* \quad (1.55)$$

$$CH_3OH* + H_2O \rightleftharpoons CO_2 + 3H_2 + * \quad (1.56)$$

$$CH_2* + 2H_2O \rightleftharpoons CO_2 + 3H_2 + * \quad (1.57)$$

Akande et al. [114] concluded that the dissociation of ethanol on the catalyst surface (reaction 1.55) was the rate determining step.

The assumption of an Eley-Rideal type mechanism (reaction 1.56 and 1.57) is questionable as steam-species on the surface of the catalyst is reported to participate in the SR reactions [30, 38, 75, 104]. Furthermore, reactions 1.55 and 1.57 appear unlikely as they would require breaking and rearrangement of several bonds in one step. Therefore this mechanism and derived kinetics seems questionable.

Kinetic models based on simple power law expressions have also shown good agreement with experimental results [114–116]. The reaction order of water has been reported to be slightly negative or zero, while the reaction order of ethanol has been reported to be between 0.43 and 1 [114–116]. The dependence of total pressure has not been investigated.

Catalysts

The SR of ethanol is, like the SR of acetic acid, catalyzed by both base and noble metals. Within the group of noble metals there is disagreement on which metal is most active. Liguras et al. [95] have found that the order of activity for 1 *wt*% metal on Al_2O_3 was:

$$\mathrm{Rh} > \mathrm{Pt} > \mathrm{Pd} > \mathrm{Ru}$$

A similar order was reported by Aupretre et al. [92], with the small difference that Pd and Pt switched places. The metal loadings were approx. 1 *wt*% in this study as well. Basagiannis et al. [97] on the other hand reported that the activity based on conversion decreased in the following order:

$$\mathrm{Pd} > \mathrm{Pt} > \mathrm{Ru} > \mathrm{Rh}$$

The support was also Al_2O_3 in this study, but the metal loadings were 1 *wt*%, 0.5 *wt*%, 5 *wt*%, and 2 *wt*%, respectively. Based on TOF, Pt shown a higher activity compared with Pd. The metal crystallites size and dispersion were similar in the studies by Basagiannis et al. [97] and Liguras et al. [95]. The exact reason for the differences in activity is not known, but it might be ascribed to differences in the examined temperature interval, as Basagiannis et al. [97] investigated temperatures between 300 and 400 ℃ while Liguras et al. [95] investigated the SR of ethanol at temperatures between 600 and 850 ℃. Both of the orders of activity for the noble metals in the SR of ethanol are different from what is observed in the SR of acetic acid. This might indicate that different reaction steps are important in the conversion of the two compounds.

Ni is the most used base metal and shows better performance compared with Co [49, 117]. The typical Ni-catalysts used in the SR of ethanol can achieve full conversion at temperatures between 300 and 800 ℃ depending on the type of support, S/C-ratio, and space velocity [89, 102, 118, 119], while noble metal catalysts showed full conversion at temperatures between 500 and 800 ℃ [94, 95, 97, 118, 120]. High yields of H_2 were achieved at full conversion for both types of catalysts. Similar temperature ranges were employed in the SR of acetic acid and similar performances have been achieved [48, 58, 59].

The activity of the noble metals and Ni are comparable, while the carbon formation is reported to be lower for noble metal catalysts, similar to what is observed in conventional SR and in the SR of acetic acid [30, 92, 121, 122].

Mixtures of different metals were tested by Le Valant et al. [123] in the SR of ethanol. It was shown that Rh-Ni/Al_2O_3 had an increased stability, conversion, and yield of H_2 compared to the Rh/Al_2O_3 catalyst [123]. The Rh-Ni had 10 *wt*% Ni and 1 *wt*% Rh and was compared to a catalyst with 1 *wt*% Rh so the increased conversion and yield of H_2 is expected as more metal sites are available for catalysis. The improved performance was ascribed to an increased activity for SR of CH_4 and the WGS due to the presence of Ni on the catalyst [123].

The addition of K to the catalyst in the SR of ethanol has been reported to lower the carbon formation, like in the SR of acetic acid [121, 122].

The influence of the support material is similar to the influence in the SR of acetic acid, namely that the addition of basic oxides to Al_2O_3 improves the performance and stability of the catalyst [89, 124, 125]. Other supports have been tested for SR of ethanol compared with the SR of acetic acid and these are MgO, TiO_2, ZnO, and Y_2O_3. MgO and TiO_2 have been used as support materials for Ru-catalysts. They showed lower activity compared with Al_2O_3, which probably can be ascribed to the much lower surface areas and poorer metal dispersion on the MgO and TiO_2-supported catalysts compared to the Al_2O_3-catalysts [95]. Y_2O_3 has been used as support for Ni catalysts where high conversion and yield of H_2 could be achieved at low temperatures [124]. Y_2O_3 was also found to be the best support for Ru in the SR of glycerin [126].

ZnO as a support material for Ni have shown high activity and good long term stability [127, 128].

Some of the promising catalysts for the SR of ethanol are shown in table 1.10 along with their performances. The yield of H_2 is based on equation 1 in table 1.9 thus 100 % yield corresponds to 6 moles of H_2 pr. mole of ethanol converted. In table 1.10 it can be seen that deactivation is a general problem in the SR of ethanol and the main source for this is carbon deposition.

Tab. 1.10: *Selected catalysts and their performance in the SR of ethanol.*

Metal	Support	T [°C]	S/C $[\frac{mole}{mole}]$	$WHSV$ $[h^{-1}]$	X [%]	Y_{H_2} [%]	Stability[a] $[h]$	Ref.
0.5 *wt*% Pt	γ-Al_2O_3	340	1.5	17	98	40	55	[97]
1 *wt*% Rh + 10 *wt*% Ni	γ-Al_2O_3	675	2	18.5	99	63	24	[123]
2 *wt*% Ir	CeO_2	650	1.5	12.6	99	75	300	[93]
15 *wt*% Co	CeO_2	700	1.5	12.6	99	75	70	[93]
15.3 *wt*% Ni	La_2O_3	320	1.5	0.6	99	60	60	[124]

[a] Time for the conversion or Y_{H_2} to decrease 10 % from its initial value.

1.3.4 SR of oxygenated compounds

Several other oxygenated compounds than ethanol and acetic acid have also been tested in SR as model compounds for bio-oil. These include aromatic compounds like phenol and *m*-cresol, or smaller compounds, like ethyl acetate and butanol. The temperature needed for full conversion of oxygenates depends on the size and type of compound. The larger and more aromatic compounds require higher temperatures to reach full conversion [59], as is shown in table 1.11.

The carbon formation in the SR of fossil oil derived products is largest for olefins and aromatics and also larger for large molecules compared with smaller ones [32]. Therefore benzene will deposit more coke than cyclohexane, which would deposit more than butane [32]. A similar pattern seems to fit the SR of oxygenates as carbon deposition from aromatic molecules, like *m*-cresol, or large molecules, like sugars, is hard to avoid [59, 129, 130]. The carbon deposition in the SR of *m*-xylene and glucose has also been reported to be larger than

Tab. 1.11: *The temperature needed for full conversion of different model compounds using a fixed bed reactor and a Ni/Al_2O_3-catalyst [59]. Operating conditions: LHSV: 10.1 h^{-1}, S/C: 6, pressure: 1 atm.*

Compound	Formula	Temperature [°C]
Acetic acid	CH_3COOH	450
Ethylene glycol	$HOCH_2CH_2OH$	500
Acetone	CH_3COCH_3	500
Ethyl acetate	$C_2H_5COOCH_3$	550
m-xylene	$C_6H_4(CH_3)_2$	650
Glucose	$C_6H_{12}O_6$	750

from SR of acetone and acetic acid under similar conditions and using the same catalyst [59]. It has also been shown that the carbon deposition increases with the chain length of both alcohols and ketones over Ni-catalysts [131]. The order of carbon deposition on same catalyst and under similar condition for several oxygenates is [59]:

Glucose > *m*-xylene > Ethyl acetate > Acetone > Ethylene glycol > Acetic acid

One type of compound that has proved difficult to reform is sugars, which can be present in amounts up to 10 *wt*% of the bio-oil. Sugars are non-volatile and thermal decomposition before the reactor bed is therefore possible. This can form char in the freeboard of the reactor which will deposit on the catalyst particles and in the reactor, thus high S/C-ratios (above 10) are needed if char formation should be diminished [132]. The steam is used to gasify the char, which otherwise would deposit on the catalyst causing deactivation. The char deposition is larger for disaccharides compared with monosaccharides, as char deposition is unavoidable in the SR of sucrose even at very high S/C-ratios (>30) [132]. SR of glucose and xylose with low carbon deposition could be achieved at high S/C-ratios (>10). The temperatures used in the SR of sugars are around 800 °C and H_2-yields between 70 and 90 % at full conversion has been achieved [59, 132]. Due to the issues with volatility of sugars it has been proposed to process them in aqueous phase reforming (APR), which will be described in section 1.6.2.

Another compound, which has been reported to be present in large amounts in bio-oil is *m*-cresol (C_7H_8O). This compound has also proven difficult to reform over Ni-catalysts. High temperatures (up to 900 °C) and S/C-ratios (up to 6) were needed for full conversion [129, 130, 132]. At these conditions there was still some carbon formation. This problem could be solved by recycling the liquid effluent from the reactor and hereby significantly increase the S/C, which caused the carbon formation to decrease to an acceptable level [129].

Some of the side reactions, which are reported to occur in the SR of *m*-cresol, are demethylation, isomerization, methylation, and polymerization [129, 130].

Steam reforming of ethylene glycol is proposed to occur through dioxy adsorbed species [133]. This compound will decompose mainly by breaking of C-H and C-C bonds forming CO and H_2. The breaking of the C-O bond could result in carbon deposition [133]. The mechanism is similar to ones proposed for ethanol with the difference that ethanol only have one oxy-bond to the surface.

Tab. 1.12: *Catalysts and operating conditions used for the steam reforming of different oxygenated compounds at atmospheric pressure.*

Feed	Metal	Content $[wt\%]$	Support	Temp. [°C]	S/C $[\frac{mole}{mole}]$	GHSV[a] $[h^{-1}]$	Y_{H_2} [% of st.]	Stability[b] $[h]$	Ref
m-Cresol	Ni	>6	$MgO\text{-}Al_2O_3$	800-900	2.5-5	0.5 (W)	82	6	[129]
m-Cresol	Ni		UC G-90C	625-875	3-6	8650	77		[132]
Dibenzyl Ether	Ni	-	UC G-90C	625-875	3-6	11790	85		[132]
Glucose	Ni		UC G-90C	-	7-47	538-717	89	2	[132]
Sucrose	Ni		UC G-90C	-	34	562	72	2	[132]
Phenol	Rh	0.5	MgO	575-725	13	32,400	92		[134]
Phenol	Rh	0.5	CeO_2	575-725	13	32,400	78		[134]
Phenol	Rh	0.5	ZrO_2	575-725	13	32,400	78		[134]
Phenol	Rh	0.5	$MgZrCeO_2$	575-725	13	32,400	71		[134]
Phenol	Rh	0.5	$MgZrO_2$	575-725	13	32,400	84		[134]
Phenol	Rh	1.5	$CeZrO_2$	575-725	7-13	80,000	80	24	[135]
Phenol	-		Calcite	650-800	11-13	22,000	15[c]		[136]
Phenol	-		Dolomite	650-800	11	22,000	17[c]		[137]
Phenol	Pt	1	$CeZrO_2$	686-778	17	43	93		[67]
Phenol	Rh	1	$CeZrO_2$	675-771	17	43	97		[67]
Phenol	Pd	1	Al_2O_3	672-766	17	43	58		[67]
Phenol	Pd	1	$CeZrO_2$	687-781	17	43	99		[67]
Glucose	Ni	30	Al_2O_3	300-800	1-9	10.1(W)	87	3	[59]
Ethylene Glycol	Ni	30	Al_2O_3	300-800	1-9	10.1(W)	90	11	[59]
Ethyl acetate	Ni	30	Al_2O_3	300-800	1-9	10.1(W)	92.5	15	[59]
Acetol	Ni	23-33	Al_2O_3	550-750	5.6	30,000-60,000			[61]
n-butanol	Ni	23-33	Al_2O_3	550-750	14.7	30,000-60,000			[61]

[a] (W) indicates that the SV is stated as WHSV.

[b] Time for the conversion or Y_{H_2} to decrease 10 % from its initial value. > X indicates that data in the article are shown for X hours, but the conversion have not decreased 10 %.

[c] At conversion around 30 %

Steam reforming of phenol has also been investigated with various metals and support materials [67, 134–138]. In these studies high S/C-ratios are often employed and despite this full conversion is rarely achieved. One of exception is catalysts with Rh supported on mixed metal oxides consisting of Ce, Mg, and Zr, which have been tested in the SR of phenol at temperatures between 350 and 550 ℃ and showed high degrees of conversion and high yields of H_2 [139]. Reaction mechanisms have not been proposed for the SR of phenol but studies have indicated phenol needs two different adsorption sites adjacent to each other for bonding to the surface and that some of the involved surfaces species are carbonates and formates [136, 139]. Based on a study by Rioche et al. [67] it appears that the Rh followed by Pt and Pd is the most active metal for the SR of phenol (see table 1.12).

Suggested reaction mechanisms for compounds larger than ethanol and acetic acid are few and not very specific as indicated above. This is probably due to the large number of possible products and surfaces species, which can react in many different ways. This is similar to what is observed in the SR of hydrocarbons, where an exact mechanism only has been elucidated for methane and paraffins.

The catalyst and operational conditions used in the SR of other model compounds than acetic acid and ethanol are shown in table 1.12 along with the performance of the catalysts. Specifically the SR of phenol requires very high S/C-ratios and despite the high S/C and use of noble metals, the catalyst is not stable for more than 24 h [135].

An interesting point observed in the SR of phenol is that $CeZrO_2$ appears to be a more interesting support as the hydrogen yield, in two of the cases, is improved when shifting from Al_2O_3 to $CeZrO_2$ [67]. This in accordance with results from SR of ethanol and acetic acid.

From table 1.12 it can be seen that high yields of H_2 is possible, but also that most of the catalysts suffer from rapid deactivation, despite high S/C-ratios.

1.3.5 SR of bio-oil

The SR of whole bio-oil and the aqueous fraction of the bio-oil (formed by fractionation due to water addition) has been tested over different catalysts and using different experimental set-ups. The aqueous phase contains water soluble oxygenates, like acetic acid, hydroxyacetone, furans, and phenols [140]. The organic fraction contains lignin-like compounds and other oxygenated compounds, like sugars, and can be a substitute for phenol in the production of phenol-formaldehyde resins after extraction with ethyl acetate [12, 141]. The aqueous fraction has a S/C ratio around 4 on weight basis or 6 to 8 on a molar basis, which corresponds well to the desired composition for SR and additional water is not needed (see table 1.13) [12, 141–144]. A slurry of bio-oil and char has also been processed in a fluidized bed reactor, but the char content only enhanced the problems with coke and ash formation, which entailed a lowered overall conversion and a shorter lifetime of the catalyst [145].

The reactions, which occur in the SR of bio-oil, are a combination of all the reactions, mentioned in section 1.3.2 and 1.3.3, and the reaction network is therefore large and complicated. The thermal decomposition and SR are, like for the model compounds, probably the most important reactions. Due to the large number of compounds in the bio-oil it might be hard to develop a detailed kinetic model for SR of bio-oil and it has not been attempted so far. However, a lumped kinetic model based on the different functional groups, chain length, or other subdivisions might be used to describe the reaction.

The metals used as catalysts in SR of bio-oil are similar to the ones used in the studies of model compounds and ranges from base to noble metal catalysts, although Ni catalysts are

favored [58, 144, 146–148]. The order of activity for the different metals might be similar to what is observed with model compounds and in the SR of hydrocarbons.

Garcìa et al. [148] showed that the adding Cr or Co to a Ni catalyst could increase H_2 and decrease the yield of methane and benzene. Adding La_2O_3 or MgO to alumina had a similar effect on the product distribution, which was ascribed to an increased steam gasification [148].

Sorbents for CO_2, like dolomite or CaO, have also been tested as catalysts in SR of bio-oil and simultaneous CO_2 capture [149]. The degree of conversion is not stated but high yields of H_2 and a low production of CO_2 initially can be achieved at 600 ℃. However, the sorbents deactivate fast and loose activity when regenerated [149].

The catalysts used to convert bio-oil might be deactivated by sintering and carbon formation, like for the model compounds. However, there is another problem when processing biomass derived products, which is the content of inorganics. Alkali or phosphor containing salts from the biomass might be present in the bio-oil and deposit on the catalysts during SR and may also cause deactivation [22, 23]. Sulfur containing hydrocarbons might be present in the bio-oil as well and these are known poisons to Ni and noble metal catalysts [29–31, 36]. A more thorough discussion of this problem is presented in section 1.4.

Conversion of bio-oil around 100 % and H_2-yields between 60 and 100 % can be achieved [12, 58, 141]. The temperature needed for full conversion is between 600 and 800 ℃ depending on the other operating conditions. The type of reactors used in the SR of bio-oil ranges from fixed bed with trickle flow or liquid spray injection to fluidized beds. These configurations will be discussed further in section 1.5. The catalysts examined in SR of bio-oil and the operation conditions are shown in table 1.13. The stability of the catalyst is also shown and it can be seen that in most cases the catalyst deactivates rather fast, typically within 10 h mainly due to be carbon deposition by formation of gum or pyrolytic coke.

Based on table 1.13 it might be concluded that fluidized beds are more suited for the SR of bio-oil as the stability is higher for these reactors probably because the catalyst particles experience changing conditions as they move around in the bed, including those where coke can be gasified. However, the time of stable of operation is still far from what would be required for an industrial process at least for single stage operation with no regeneration of the catalyst.

In table 1.13 it can be seen that the temperature interval investigated is similar to the temperatures used in the SR of acetic acid and ethanol. The S/C-ratios are higher compared to SR of acetic acid and ethanol, but lower compared with SR of phenol.

1.4 Sulfur poisoning

Sulfur containing hydrocarbons and especially H_2S are known poisons to both Ni and noble metals. The deactivation occurs because the sulfur binds strongly to the metal and so even very small amounts lead to severe deactivation [29–31, 36]. The sulfur blocks the active sites and reduces the activity of the catalysts. The S-bonding is reversible by treatment with H_2, but the driving force for the sulfur desorption is small [30]. The sulfur poisoning can be used beneficially as in the SPARG-process from Haldor Topsoe A/S, where H_2S in *ppm* levels is used to block the most active step sites on a Ni-catalyst [43, 44]. This decreases the coke formation, as step sites are very active in the whisker formation, which allows for operation at low S/C-ratios [30, 31].

Tab. 1.13: *Catalysts and operating conditions used for SR of bio-oils. Pressure is atmospheric, Aq indicates SR of the aqueous fraction of bio-oil.*

Type of oil	Metal	Content [$wt\%$]	Support	Temp. [°C]	S/C [$\frac{mole}{mole}$]	$G_{C_1}HSV$[a] [h^{-1}]	Y_{H_2} [% of st.]	Bed type	Stability[b] [h]	Ref
Aq. poplar	Ni	15	Al_2O_3	825-875	5-11	62,300-126,000	87	Fixed	0.5	[148]
Aq. pine	Ni		C11-NK	800-850	7-9	770-1000	89	Fluid	90	[150]
Hemicellose	Ni		C11-NK	850	7-14.1	800-1000	77	Fluid	2.5	[150]
Glycerin	Ni		C11-NK	850	2.1-2.7	1400	74	Fluid	-	[150]
Grease	Ni		C11-NK	600-850	2.7-5	950-1100	82	Fluid	16	[150]
Hardwood	Ni		C11-NK	850	5.8		80	Fluid	16	[146]
Hardwood	Ni		NREL catalyst	850	5.8	-	90	Fluid	4	[146]
Aq. saw dust	Ni	20	Dolomite	600-800	6.5	1.5 (W)	74	Fluid	5	[142]
Aq. beech wood	Ni		NREL catalyst	300-1000	8.2	300-600	90	Fixed	5	[143]
Aq. pine wood	Ni	28.5	Ca/MgAl	650	7.6	5,400-11,800	-	Fluid	2	[144]
Saw dust	Ni	7.2	MgO	700-900	1-16	1.5 (W)	80	Fixed[c]		[147]
Saw dust	Ni	15	γ-Al_2O_3	350-550	6.1	12,000	50	Fixed		[151]
Saw dust	Ni	15	CNT	350-550	2-6.1	12,000	92.5	Fixed	6	[151]
Beech wood	Pt	1	$Ce_{0.5}Zr_{0.5}O_2$	700-780	2.5-10	0.6-2.5 (W)	70	Monolith		[152]
Beech wood	Rh	1	$Ce_{0.5}Zr_{0.5}O_2$	700-780	2.5-10		52	Monolith		[152]
Aq. beech wood	Ru	5	$MgAl_2O_4$	550-800	7.2	3000-17000	60	Fixed	> 45	[58]
Beech wood	Pt	1	$CeZrO_2$	740-860	10.8	3090	70	Fixed	> 9[d]	[67]
Beech wood	Rh	1	$CeZrO_2$	860	10.8	3090	75	Fixed		[67]
Model oil 1 [e]	Ni	7.2	MgO	450-850	1-10	0.8 (W)	85	Fixed	8	[147]
Model oil 2[f]	Ni	7.2	MgO	450-850	1-10	0.8 (W)	85	Fixed	10	[147]
Aq. rice hull	Ni	5-12	CeO-ZrO	450-800	3.2-5.8	-	70	Fixed	0.5	[91]

[a] (W) indicates that the SV is WHSV

[b] Time for the conversion or Y_{H_2} to decrease 10 % from its initial value. $>$ X indicates that data in the article are shown for X hours, but the conversion have not decreased 10 %.

[c] 2-stage reactor with a guard bed

[d] Autothermal conditions

[e] Consisting of equal amounts of methanol, ethanol, acetic acid, and acetone on a weight basis

[f] Consisting of equal amounts of furfural, phenol, catechol, and m-cresol on a weight basis

The sulfur content in bio-oil can be up to 500 *ppmw* and for the aqueous fraction sulfur contents up to 370 *ppmw* have been reported [13, 23, 91], which is significant amounts as the H_2S to the conventional steam reformers are kept in the *ppb*-range [29]. Thus, this might be a problem for the metal catalysts shown in table 1.13, although it has not been addressed in the literature.

In the literature on the SR of hydrocarbons some information on sulfur resistant catalytic systems can be found [153–156]. One of the techniques used to avoid sulfur poisoning is to add a compound which binds sulfur stronger than the active metal, e.g. adding CuO to noble metal based catalysts [153, 154]. The binding of sulfur to the CuO is more thermodynamically stable and will act as a sacrificial barrier until a certain sulfur level is reached [153, 154]. A NiW catalyst on dolomite has also shown good performance for reforming of naphthalene with sulfur present as H_2S in concentrations up to 500 *ppmv* [155]. The sulfur tolerance was ascribed to an increased sulfur dissociation because of WO_3, which accelerates the sulfur release as H_2S from the catalyst [155]. Another possibility is to use a support material like $Ce_{0.8}Gd_{0.2}O_{1.9}$ where a redox reaction can occur and hereby remove the sulfur on the catalyst as H_2S [156]. However, both explanations for the S-resistance may be debated as H_2S released from the catalyst would be expected to bind to the Ni or the noble metal again forming adsorbed sulfide species. Further investigations of the mechanisms for the sulfur resistance are therefore needed.

1.5 Reactors and reforming concepts

The most widely used type of reactor in the literature is a fixed bed reactor with both liquid and gas feeds. Light model compounds like acetic acid and ethanol are typically vaporized upstream the reactor and transported to the reactor through heated lines. The bio-oil or larger model compounds cannot be vaporized without leaving a significant amount of residue and vaporization prior to the reactor is therefore not suitable. Furthermore rapid heating can cause thermal decomposition and coke formation. In studies where heavier compounds, like sugars or bio-oil, are converted other feeding techniques have been used to avoid or minimize these problems. One of them is to spray the liquid on to the catalyst through a spray nozzle in order to minimize the thermal decomposition and char formation before the reactor bed [141, 146, 150, 157, 158]. Other techniques like using droplets, where the bio-oil is encapsulated in a water droplet and dropped onto the catalyst bed [67], or only adding bio-oil dropwise [147], have also been used to minimize the thermal decomposition prior to the catalyst bed. Apart from the spray nozzle these techniques are mainly suitable for laboratory scale experiments.

In order to minimize the carbon deposition, related with the SR of bio-oil, different experimental setups have been investigated. These are two bed setups, in analogy to the prereformer concept, and a fluidized bed reactor [82, 124, 147, 150, 159, 160] as discussed below. Changes to the reaction conditions like co-feeding with O_2 has also been investigated and will be discussed along with other variations to the SR process.

Relatively high S/C-ratios are used in the SR of oxygenates as indicated in tables 1.12 and 1.13. From an industrial point-of-view this is a problem as high S/C-ratios are expensive, because more steam is needed. This will lead to high expenses for superheating of water and the size of piping and reactors will have to be increased [30]. Therefore it is important to optimize the catalyst and reactor conditions to achieve low carbon deposition at low S/C-ratios.

1.5.1 Prereforming

A two reactor plant is an analogy to a conventional SR plant, with a prereformer and a reformer (see figure 1.2). The first reactor is used to convert the reactants into CH_4, CO, CO_2, and H_2, while the second reactor is used to reform the CH_4 at higher temperatures [147]. The first reactor in a two reactor plant could be an inexpensive material like dolomite, which can be replaced when it is deactivated by carbon deposition. Vaporization, decomposition, and carbon deposition will mainly occur in the first reactor. The second bed would consist of a metal catalyst, which only process gaseous compounds and therefore the coke formation should be much smaller and the catalysts life time longer [147].

Another two-bed setup has been proposed for the SR of ethanol. Here the first bed was a Cu-catalyst operated at 370 ℃, which converted the ethanol into acetaldehyde by dehydrogenation (see reaction 2 in table 1.9). The second bed was a Ni-catalyst operated at 650 ℃, which could steam reform acetaldehyde and avoid the formation of coke and only have a small production of other by-products [159].

A similar setup with two Ni-catalysts operated at different temperature, like in the conventional SR process, could also be used. For this concept it is mainly interesting to examine the low temperature SR of oxygenates as commercial catalysts for CH_4 conversion exist. Experiments have been conducted on the low temperature SR of both acetic acid and ethanol and full conversion could be achieved between 350 and 450 ℃ [82, 97, 124]. The products mainly consisted of CH_4, H_2, CO_2, and CO and the major part was CH_4. The yield of CH_4 decreases with increasing temperature because the SR of CH_4 is favored at higher temperatures. The operating temperatures of 350-450 ℃ correspond well to the conventional prereformer conditions. Carbon formation might still be a problem at low temperatures as the carbon formation in the SR of oxygenates is found to decrease with increasing temperature [53, 54, 74]. However, a study by Rabenstein and Hacker [161] have shown that the carbon formation in the SR of ethanol have a maximum around 500-600 ℃ and thermodynamic calculations on the SR of acetic acid, acetone, and ethylene glycol indicate that if a S/C ratio of 3 or above is used then the carbon formation should be minimal [53]. However thermodynamics is perhaps not the most suitable way to evaluate carbon formation as it is mainly controlled by kinetics. The carbon formation might be avoided in the low temperature range (300-500 ℃) and the prereformer concept could be beneficial. This is also seen in the low temperature experiments where stable operation over 50 to 60 h could be achieved [97, 124]. The yield of CH_4 is high at low temperatures and an additional reforming step is needed if high amounts of H_2 should be produced. A beneficial feature of the prereformer concept could be that the initial coke formation from heating the bio-oil could be decreased as the reactor inlet temperature would be much lower compared with a single step reformer, where temperatures between 600 and 800 ℃ are needed for full conversion of bio-oil to synthesis gas.

1.5.2 Fluidized bed reforming

Fluidized beds have also been examined as reactors for the SR of oxygenates [144, 145, 150, 160, 162], as it is believed that the thermal decomposition can be controlled better in this type of reactor [150]. This might be substantiated by table 1.13 where it can be seen that the stability is generally higher for the fluidized beds. Thermal decomposition can cause coke deposition which in a fixed bed reactor would form a layer of coke in the top and freeboard of the reactor. When using a fluidized bed reactor all of the catalyst particles are in contact with the fresh bio-oil, the carbon deposition on each particle will be smaller and because of the circulation of particles there is also a larger chance of gasifying the carbon on the particles. The time of stable operation has been shown to increase when using a fluidized bed and

the regeneration time by steam gasification for the catalyst was also decreased [150]. This might substantiate less carbon deposition as the lifetime is longer and the regeneration time is shorter. A study by Lan et al. [163] have also shown that the coke deposition at similar conditions and with the same catalyst is lower in a fluidized bed compared to a fixed bed.

The fluidized bed could also be made as a dual bed, where the catalyst circulates between the beds. It is used as a SR catalyst in one of the beds and regenerated by gasification or carbon oxidation in the other bed. However, the catalyst might need to be reduced again after the oxidation process which would require a third bed. This concept has, to the authorÂ´s knowledge, not been tested for this process although it is well known from catalytic cracking.

High yields of H_2 and full conversion could achieved in fluidized beds, but deactivation by carbon deposition and also attrition of the catalyst is still a problem [145, 150, 162]. The conventional support materials, like Al_2O_3 used in the SR are rather soft and unsuited for fluidization due to attrition [160]. Therefore more durable support materials are needed and mixing Al with Ca or Mg have improved the mechanical strength of the support making it more suitable for fluidization [144, 160]. Mixing of Mg and Al resulted in the best catalyst with a high conversion and yield of H_2 similar to what is observed when using mixed MgO and Al_2O_3 supports in fixed bed reactors. A recent study by Xu et al. [164] indicates that the main source of deactivation is sintering of catalyst and not carbon deposition. Therefore there might be three significant deactivation mechanisms, namely sintering, attrition, and carbon deposition, associated with utilizing fluidized bed reactors.

A fluidized bed can be combined with a fixed bed reactor in a staged reactor concept where the bio-oil is first passed through a fluidized bed of low activity materials, like sand, and then through a fixed bed consisting of a SR catalyst [162, 165]. The idea is that the evaporation of bio-oil occurs in a fluidized bed and the resulting vapors are steam reformed in a catalytic fixed bed [162, 165]. The temperatures in the two bed can be varied, but generally a high temperature (above 700 ℃) is needed for complete conversion of the hydrocarbons in the fixed bed. The fraction of CH_4 and other small hydrocarbons are minimized resulting in an easy reformable off-gas from the fluidized bed. High yields of H_2 could achieved, but the carbon yield was below 100 % indicating that carbon deposition still occurred [165].

1.5.3 Autothermal reforming

The formation of carbon deposition is, as mentioned earlier, a major problem with the SR of oxygenates, as up to 15 % of the carbon might be deposited in the reactor [132, 150]. This might be reduced by co-feeding O_2 to the system, which could gasify or combust some of the deposited carbon and also provide energy for the endothermic reforming reactions. Experiments and also thermodynamics have shown that the H_2-yield decreases and the CO_2-yield increases compared with SR without O_2, while the coke formation is suppressed [54, 67, 166–168]. Laosiripojana et al. [169], on the other hand, investigated the oxidative SR of ethanol at S/C of 1.5 over Ni/CeO_2 and found that the addition of 0.4-0.6 mole of oxygen pr. mole of carbon (O/C-ratio) increased the yield of H_2 and lowered the carbon deposition. Over a Ni/Al_2O_3-catalyst at S/C-ratio of 1.5 oxygen addition, in general, increased the H_2-yield [169]. Medrano et al. [168] reported that an O/C-ratio of 0.04 increased the stability of the catalyst in the SR of acetic acid at 650 ℃, WHSV of 9.3 h^{-1}, and S/C-ratio of 5.6 with only a minor influence on the H_2 yield. Similar results were found in the SR of bio-oil where the addition of oxygen in an O/C ratio of 0.04 decreased the carbon deposition by 50 % in a fluidized bed [144]. The above described effects are functions of the amount of O_2 fed to the reactor as increasing amounts of oxygen will decrease the carbon deposition and H_2-yield [124]. The amount of O_2 needed for autothermal conditions is dependent on the type

of biomass that is converted. It will increase with temperature and does not change much with increasing S/C-ratios [54]. An increased risk of catalyst sintering has been reported with oxygen present which might counterbalance the advantage of the decrease in carbon deposition [67, 166]. It should be noted that the process equipment for producing pure O_2 is expensive and is only economically viable for large industrial autothermal reformers [31].

In the autothermal reforming heat for the endothermic reforming reactions is supplied by combustion of some of the bio-oil. Thus, no external heat must be supplied to the reactor at autothermal conditions. However, heat should be supplied to preheat the reactants, because the H_2 yield would decrease significantly when heat supplied by the oxidation of bio-oil should preheat the feed as well [54]. The oxygen could also be supplied in amounts less than needed for autothermal conditions, which could decrease the coke formation and only affect the H_2-yield slightly. A hybrid reactor with both external (furnace) and internal heat supply (oxygen) could be used for this purpose.

1.5.4 Catalytic partial oxidation

Oxygen can be supplied as a reactant without H_2O, which is referred to as catalytic partial oxidation (CPO), because the amount of air supplied is substoichiometric for combustion. Schmidt et al. [158] has tested the CPO and autothermal SR (reaction with both H_2O and O_2) in two different types of setups. A staged system with a large freeboard over a catalytic bed of Rh-Ce-Al_2O_3, where the bio-oil is introduced as a mist through a spray nozzle, and a similar setup where the spray is just above the catalyst bed. The staged setup provides better protection of the catalyst and a higher yield of H_2, which could be due to a more efficient mixing of the gases prior to the reactor [158]. The two setups were tested both in the CPO and autothermal SR with bio-oil as feed. Both of these systems showed relatively high yields of H_2 and almost full conversion of carbon to gas, but deactivation was still a problem. The highest yield of H_2 was achieved with autothermal SR [158]. The staged setup was tested in the autothermal reforming of ethanol, where homogeneous decomposition of ethanol occurred prior to the catalysts bed. Promising results, with relatively long catalyst lifetime and short residence times (below 10 ms) were achieved with the configuration [157].

A thermodynamic analysis by Rabenstein and Hacker [161] of SR, CPO, and autothermal reforming of ethanol have shown that SR is the least energy demanding process at temperatures above 600 ℃ while below 600 ℃ autothermal reforming is favorable. CPO is less favorable at all the temperatures investigated. The CPO/SR has not been investigated thoroughly, but as mentioned above it might be a way to achieve relatively long catalytic lifetimes and relatively high hydrogen yield.

1.5.5 Other concepts

Current assisted SR, membrane reactors, and other alterations to the SR process have also been tested in the SR of different oxygenated compounds. Results from these studies are discussed below.

In the current assisted SR a wire runs through the catalytic bed and when current is passed through the wire it becomes hot and delivers energy to the bed and thermal electrons may also be formed [96]. The thermal electrons can reduce the metal species in the catalyst and also cause dissociation of water or oxygenate. The current assisted SR of acetic acid decreases the temperature needed for full conversion and increases the yield of H_2 [96]. These effects are functions of applied current and increases with increasing current. Similar results have been obtained by Hou et al. [151] in the SR of bio-oil and around 90 $wt\%$ conversion could

be achieved at 400 ℃. Another feature of the current assisted SR is that the energy efficiency is higher due to a more efficient heating by the wires inside the catalyst bed [96]. However on an industrial scale heating by use of electricity might be more expensive compared to heat generated at the plant and this method could therefore be less feasible in large scale.

The current assisted SR has been tested in a dual reactor with bio-oil as a feed as well. In this setup the bio-oil is first passed through a bed of inert materials and then through a catalytic bed where current could be applied [170]. Similar effects as described above were found in this study and Kan et al. [170] claims that the highest H_2 yield from biomass can be achieved through this process. However, full conversion was not achieved and deactivation still a problem.

The motivation for using a membrane reactor instead of the conventional fixed bed setup is that SR and gas separation can be combined into one unit, and produce high purity H_2 in a one-step process [171, 172]. This process is only suitable for H_2 production as H_2 permeable membranes are used. The membrane SR of acetic acid can at relatively low temperature of 400 ℃ be used with none or little carbon formation. The H_2 yield and CO-free H_2 recovery was low, around 50 % and 70 %, respectively [171, 172]. This indicates that the process is not efficient as the overall yield of CO free H_2 is only 35 %.

The co-feeding of H_2 and H_2O has been tested, because it might hydrogenate coke precursors and decrease the coke formation. On an industrial scale H_2-addition might be done by recycling some of the reactor effluent. A study by Laosiripojana et al. [169] on the SR of ethanol have shown that the formation of hydrocarbons and coke was decreased by H_2 co-feeding. At high ratios between ethanol and H_2 (above 3) these effects became less pronounced and the CH_4 formation increased [169]. Jacobs et al. [111] tested the addition of H_2 to low temperature SR of ethanol, and found increased conversion and yield of CH_4.

A Y-shaped reactor with two catalytic beds has also been tested as possible reactor configuration. The idea behind this concept is that bio-oil can be fed both to the first and the second bed and the CO_2 produced in the first bed can used to reform the bio-oil in the second bed and hereby produce a gas which mainly consists of CO and H_2 [173]. The concept has been tested in SR, CPO, and oxidative SR coupled with CO_2 reforming and full conversion and a product gas of mainly H_2 and CO can be produced in all the cases at temperatures above 700 ℃ [173]. The main problem with the dry reforming is that the coke formation is larger compared to both SR, CPO, and oxidative SR alone and higher temperatures are also needed for full conversion [173].

1.5.6 Industrial plant

In the industry the reactor for the SR of bio-oil would probably be a fixed bed reactor as conventional SR is conducted in this type of reactor and knowledge from process design of conventional steam reformers can be used. This would require a catalyst with a low deactivation rate because regeneration or catalyst reloading is expensive. Large scale fixed bed reactors are easier to design and operate than fluidized beds; therefore fixed bed might be chosen despite a higher carbon deposition and shorter catalyst lifetime. If a coke resistant SR catalyst is found, it would also drive the reactor choice toward the fixed bed.

The steam reformer unit for converting bio-oil could have one or two reactors. However the two-reactor setup probably would be better suited as it has a lower potential for carbon formation, is better suited for variations in the feed, and have a better energy efficiency [174].

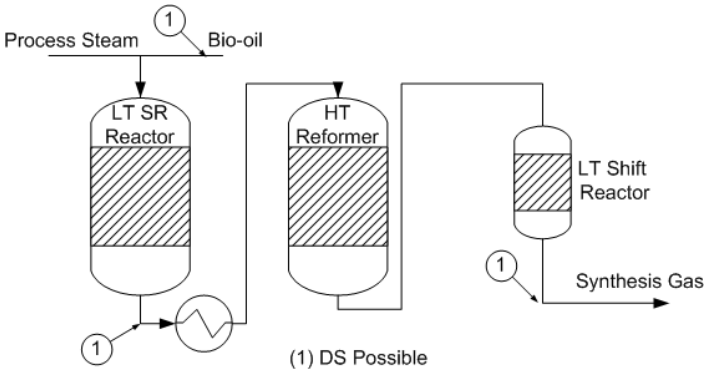

Fig. 1.7: *Simple flowsheet for a two-reactor industrial plant for the SR of bio-oil. (1) indicates possible location for the desulfurization of bio-oil or product gasses.*

The size of the main reformer would be smaller which could be favorable for an economic point-of-view. This is the case for the conventional SR-units [42, 174]. However, it would require a catalyst that could fully convert the bio-oil to C_1-species at temperatures around 500 °C and be resistant toward carbon formation and catalyst poisons in the bio-oil. Downstream the reformer there would probably be a low temperature shift reactor to increase the H_2-yield or achieve a specific H_2/CO-ratio. A simple flow diagram for an industrial two reactor setup is shown in figure 1.7.

A desulfurization (DS) unit might be included prior to the reforming section as sulfur poisoning could be a problem as indicated in section 1.4. However, this might be difficult as carbon deposition could be a problem due to the thermally unstable oxygenates in the bio-oil. If the prereformer principle is used, the DS could be conducted after the prereformer to avoid coke formation in the DS-unit, if a sulfur resistant catalyst is used in the prereformer. DS is needed at some point in the process as the downstream processes require virtually sulfur-free gas. The DS between the reformers would probably entail lowering the temperature for the DS and then increasing it again after the DS unit, which is uneconomical but necessary if traditional SR catalysts are used in the reformer.

1.6 Other conversion techniques

In the following subsections alternative methods, like cracking of bio-oil or aqueous phase reforming of oxygenates, for converting the bio-oil to synthesis gas or hydrogen will be reviewed to provide a full picture of the possibilities.

1.6.1 Catalytic cracking

Catalytic cracking is to pass the bio-oil through a reactor with a catalytic bed and hereby crack or decompose the bio-oil to gaseous products. The theoretical H_2-yield will be lower compared to SR because extra H_2 from H_2O cannot be incorporated into the product gas. Catalytic cracking of the bio-oil has been investigated, because it does not require steam and therefore no energy for superheating the water is needed. The drawbacks of the process are a low H_2-yield and increased formation of coke, because the carbonaceous residues cannot be gasified by steam. The catalyst will therefore have to be regenerated frequently by combustion using oxygen [87, 175]. The catalysts tested for cracking of bio-oil are monoliths with Pt or Rh on CeO_2-ZrO_2 [175], Ni/Al_2O_3 or Ni-K on La_2O_3-Al_2O_3 [87].

Davidian et al. [87] proposed that the bio-oil is thermally decomposed in the gas phase to small hydrocarbons, carbon oxides and steam. The formed hydrocarbons can react with steam or CO_2 on the catalyst and form CO and H_2, but the carbon formation would be rather large due to the low steam content [87].

Cracking of acetic acid has also been investigated using a Ni-K/La_2O_3-Al_2O_3 catalyst, where full conversion and yield of H_2 close to the thermodynamic equilibrium could be achieved from 550 ℃ at LHSV of 4.1 h^{-1} [176]. It should be noted that despite high yield of H_2, the production of H_2 will still be lower compared to SR. A dual reactor setup was also tested, where the feed or oxygen could be directed to the catalyst beds. Regeneration of the catalyst occurred under O_2-flow and was conducted in one of the beds, while the other one was used for hydrogen production. Using this configuration stable operation over 48 h could be achieved [176, 177].

1.6.2 Aqueous phase reforming

Aqueous phase reforming is, as the name implies, reforming of oxygenates in an aqueous solution by the use of a heterogeneous catalyst. The benefits of this process are the low temperatures, which reduces the thermal decomposition and ensures that the WGS (reaction 1.2) is shifted toward H_2 and CO_2. Furthermore, vaporization of feed and water is not needed, which reduces the energy consumption [178]. Aqueous phase reforming have been can be conducted at temperatures up to 265 ℃ and pressures up to 60 *bar* with WHSV between 3 and 30 h^{-1} [179–182]. It has mainly been examined as a way to produce H_2 from sugars produced by acid or enzymatic hydrolysis of biomass [178, 179]. Ethylene glycol, other biomass related components like cellulose, and ethanol have also been tested as feed in APR [180, 181, 183–185], but not other model compounds of bio-oil. However, it could be an interesting way to process the aqueous phase of the bio-oil due to the lower energy requirements.

The main products in APR are CO, CO_2, H_2, or small hydrocarbons and it has been shown that the yield of H_2 decreases with increasing size of the feed molecule, while the hydrocarbon yield increases [178]. Furthermore feed molecules can undergo homogeneous reactions to produce other smaller oxygenated compounds e.g. in the APR of sorbitol the products included acids, ketones, alcohols, and paraffins of various length [186]. A problem with the process is that low concentrations of oxygenates is used (typically less than 10 $wt\%$) and full conversion to gaseous compounds is rarely achieved [180–182]. The production rate of H_2 in APR of ethylene glycol is roughly 100-1000 times less than what can be achieved in SR of ethanol [57, 81, 187]. Shabaker et al. [187] reports a production rate of 188 $\mu g/(g_{Cat} \cdot min)$ in the APR of ethylene glycol while Galdamez et al. [81] and Barattini et al. [57] reports values between 0.06 and 0.19 $g/(g_{Cat} \cdot min)$ in the SR of acetic acid and ethanol, respectively. Another problem with APR is that low temperatures are used, which entails that the methanation equilibrium is shifted toward CH_4, and methane must therefore be converted in another step along with other gaseous hydrocarbons. The low degrees of conversion and low production rate for APR will entail large reactors and large recycle loops. Deactivation can also be a problem in APR, when processing heavier compounds, but stable operation over 250 h with ethylene glycol as feed has been achieved [187].

The reaction mechanism suggested for APR of ethylene glycol consists of two pathways, either C-O and C-C bond breaking and these pathways are shown in figure 1.8.The desired pathways is C-C-bond breaking leading to the formation of CH_xO-species on the catalyst, which can decompose to CO and H_2. The CO reacts with either water by the WGS or H_2 through the methanation forming CO_2 or CH_4, respectively. The C-O bond can also be

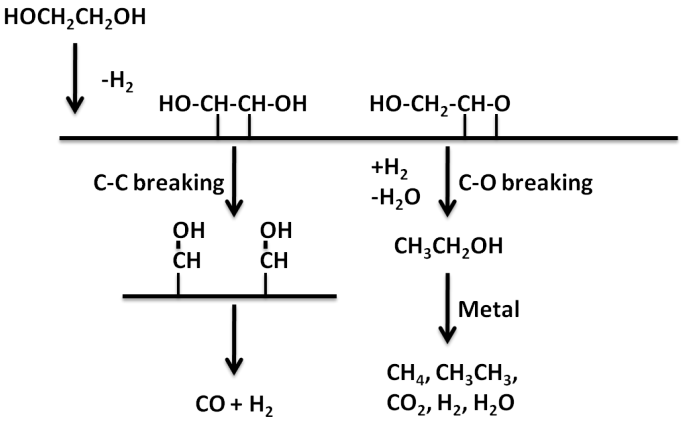

Fig. 1.8: *The reaction mechanism for C-C and C-O breaking in the APR of ethylene glycol over a metal catalyst. The horizontal lines represent a metal surface. Figure adapted from [178].*

cleaved, which would lead to the formation of small hydrocarbons like CH_4 or C_2H_6. A suitable catalyst should have a high activity in the WGS and the C-C-bond breaking and a low activity for the C-O cleaving to ensure that the products are mainly CO, CO_2, and H_2.

In ethylene glycol and sugars all the C-atoms are bound to O-atoms and CO-species can be formed almost exclusively, corresponding to the desired reaction path (C-C-bond breaking) and leading to high yields of H_2. Breaking of the C-C-bond in acetic acid or ethanol would lead to CO and CH_x-species on the catalyst. These species cannot be converted by the APR reforming and would lead to the formation of CH_4, other small hydrocarbons, or coke. The APR could be used as a prereforming step with subsequent SR of the small hydrocarbons, if it should be used to fully convert the bio-oil into H_2 and carbon oxides. A problem with processing bio-oil in an aqueous solution might be phase separation, which could cause transport problems and poor contact between reactants and catalyst as bio-oil is known to phase separate when mixed with water. A more drastic pretreatment step could be gasification in supercritical water without a catalyst to break down the molecules and possibly get a product which is more readily steam reformed.

The catalytic metals used in the APR are similar to the ones used in the SR of bio-oil and ranges from Ni to different noble metals. The order of decreasing activity based on TOF for CO_2-production over the different metals tested in the APR of ethylene glycol is [178, 183]:

$$\mathrm{Pt} \approx \mathrm{Ni} > \mathrm{Ru} > \mathrm{Rh} \approx \mathrm{Pd} > \mathrm{Ir}$$

The Pt-catalyst can be improved by alloying with Ni, Fe, or Co, which could be due to a lowering of the d-band center, which would cause a lowering of the heat of adsorption for H_2 and CO [179]. This would lead to more free surface sites on the catalyst and a higher probability for reaction.

The best support materials for the APR of ethylene glycol is TiO_2, carbon, or Al_2O_3 [178].

1.7 Discussion

In the previous sections different reactors and concepts, which can or have been used for SR of bio-oil, have been presented. It has been shown that SR of bio-oil is thermodynamically favorable and that highly active catalysts do exist, but carbon formation is a major concern

as it causes fast deactivation. This problem can be attacked from two different angles either by changing the catalyst or by changing the reactor type and operating conditions. Another major concern is the sulfur content of the bio-oil as it can cause deactivation as well and it should either be removed prior to the reactor(s) or a sulfur resistant catalyst should be used and the sulfur could be removed downstream the reactor. The process gas should be virtually free of H_2S (sub *ppb*-level) if it should be used for Fischer-Tropsch or in fuel cells so sulfur removal must be employed at some point.

Sulfur resistant catalytic systems are known from the literature on SR of hydrocarbons and might be suited in SR of oxygenates, but these systems still need testing. Other changes to both support and metal in the catalyst might also enhance the performance of the catalyst. Alloying of different metals, new support materials, or new promoters could be possible changes to the SR catalysts.

Most of the conversion techniques, discussed above, have drawbacks and are far from industrial application. A one-step SR will have problems with carbon formation both in fixed and fluidized bed reactors with the current catalysts. However, slightly autothermal conditions might significantly improve the performance at the expense of lower H_2-yield. A two step process will probably improve the process both for fluidized and fixed beds. A prereformer-reformer concept therefore seems promising. These have not been investigated thoroughly, yet, and proof of concepts is still missing. The prereformer-reformer concept is known from the conventional SR, and the coke formation can probably be reduced because of a lower reactor inlet temperature and therefore also lower degree of thermal decomposition in the prereformer. Another possibility could be an APR reactor as a prereformer, but the APR still need further development as the products for the process ranges from C_1 to C_6-molecules and these might still be soluble in water. Therefore a separation and two additional steam reforming steps might be needed to produce synthesis gas or hydrogen from bio-oil through APR.

1.8 Conclusion

The SR of bio-oil is an environmentally friendly route to produce H_2 or synthesis gas and therefore could become an important process in the future. Many different catalytic systems have been investigated and the most promising metals seem to be Ni, Rh, or Ru. Ni is preferred if the catalyst should be used industrially as it is the cheapest and most abundant of the metals. The most promising support materials are mixtures of basic oxides and Al_2O_3 as these show higher activity and lower carbon formation compared to alumina. Potassium can be used as a promoter as it can increase the activity and reduce the coke formation. Nevertheless, one of the main concerns with the tested catalysts is the low stability with typical operating hours for acceptable rates being less than 100 h.

The SR of bio-oil is still in an early phase of its development. Some aspects of the SR of bio-oil which need further investigation and optimization if the SR should be used industrially are:

- Kinetics and reaction mechanisms for other compounds than ethanol are scarce but bio-oil consists of many other compounds. It could be interesting to test additional model compounds as well as whole bio-oil in order to gain further insights into the SR reactions.

- The influence of sulfur should be investigated as it is a known poison for the conventional SR process. Development of sulfur resistant catalysts could be interesting as desulfurization of the bio-oil might be troublesome.

- Proof of concept for the prereformer concept with a two step reactor, where the bio-oil is first converted to C_1-species at low temperature followed by a high temperature reformer, which converts the CH_4 into H_2, CO, and CO_2.
- Further studies of different catalysts or operating conditions to allow extended periods of operation.

2. EXPERIMENTAL

This chapter describes the production of catalysts, the used experimental setups, and the different characterization techniques. Two different experimental setups have been used, one at the Technical University of Denmark (DTU) and one at the University of Oklahoma (OU), and furthermore the setup at DTU has been modified during the course of the Ph.D.-project to accommodate feeding of the different model compounds.

2.1 Catalyst preparation

The catalysts investigated in this project were prepared by incipient wetness impregnation. Five different carriers for NiO were impregnated with a $Ni(NO_3)_2$-solution; CeO_2 (AMR Ltd., 141 m^2/g), $Ce_{0.6}Zr_{0.4}O_2$ (AMR Ltd., 137 m^2/g), $MgAl_2O_4$ (Puralox MG30/150, SASOL Germany, 143 m^2/g), $MgAl_2O_4$, and $CeZrO_4/MgAl_2O_4$. The two latter supports were prepared in-house according to the procedure described below. Ni was added to the supports by dissolving $Ni(NO_3)_2 \cdot 6\ H_2O$ (Sigma-Aldrich, $>$ 97 % pure) in a volume of water corresponding to the pore volume of the dry support material. The solution was mixed with the dry carrier material and stirred. The wet particles were dried at 110 ℃ overnight and calcined at 800 ℃ (heating rate 10 ℃/min) for 2 h.

Magnesium aluminate was prepared by incipient wetness impregnation of a high surface area alumina (Puralox TH 150, SASOL Germany, 150 m^2/g) with $Mg(NO_3)_2$ as precursor for MgO. The alumina was mixed with a solution containing stoichiometric amounts of $Mg(NO_3)_2$ (Fluka, 99 % pure) followed by drying at 110 ℃ and calcination at 900 ℃ (heating rate 10 ℃/min) for 8 h.

The synthesized $MgAl_2O_4$ was co-impregnated with Ni, K, CeO_2, ZrO_2. Maximum two species were impregnated at a time, so when naming the catalysts / denotes separate impregnation steps while - denotes co-impregnation. After each impregnation step the catalyst was dried and after the final impregnation it was calcined at 800 ℃ (heating rate 10 ℃/min) for 2 h. $Ce(NO_3)_3 \cdot 6\ H_2O$, $ZrO(NO_3)_2 \cdot H_2O$, and KNO_3 were used as precursors for CeO_2, ZrO_2, and K, respectively. The precursors were acquired from Sigma-Aldrich Ltd. and were $\geq$ 99 % pure.

Sulfur addition to the catalysts was done by impregnating the calcined catalyst with a solution of K_2SO_4 or H_2SO_4 followed by drying at 110 ℃ overnight. The impregnation liquids had concentrations corresponding to a nominal sulfur coverage of roughly 6, 13, and 26 %, which corresponded to a sulfur content of 0.03-0.12 $wt\%$. Sulfur coverage was calculated by assuming that all the sulfur from the liquid adsorbs on the Ni-particles. The number of Ni surface sites was estimated based on the particle size determined by XRD and assuming spherical particles and a Ni-atom area of $6.2 \cdot 10^{-20}\ m^2$ (calculated based on a face-centered cubic nickel atom in the (100) plane).

$MgAl_2O_4$ prepared in-house was used for the experiments presented in chapter 3, while the commercial $MgAl_2O_4$ from SASOL was used as support in the remaining experiments described in the chapters 4-6.

2.2 Experimental setup at DTU

The flowsheets for the different configurations of the experimental setup at DTU can be seen in fig. 2.1. The setup used for SR of ethanol, fig. 2.1(a), consisted of a gas supply section where up to eight different gases could be connected, a liquid supply section where two bubble columns were used to supply water and ethanol. Nitrogen flows were saturated with ethanol or water at 60 ℃ and 79 ℃, respectively, in the bubble columns and led to the reactor. The gases and liquids were mixed in lines heated to 110 ℃ prior to entering a quartz reactor placed in a three zone furnace. After the reactor there was a condenser operated at 6-7 ℃, which collected liquid samples. After the condenser the gases passed the analysis section, which consisted of a Varian MicroGC CP-4900 and a 5-channel Rosemount NGA 2000 on-line gas analyzer. The MicroGC had two parallel lines; a molecular sieve 5A column and a PoraPlot Q column connected to a thermal conductivity detector (TCD). The GC measured the concentrations of CO, CO_2, H_2, CH_4, C_2H_4, and C_2H_6 in the dry gas. Samples were injected to the GC every 10 *min*. The on-line gas analyzer measured the CO, CO_2, and O_2 concentrations continuously and data points were collected every 30-60 *s*. Data from the GC was used to determine the product distribution and representative measurements every approx. 30-60 *min* were used to show trends and deactivation.

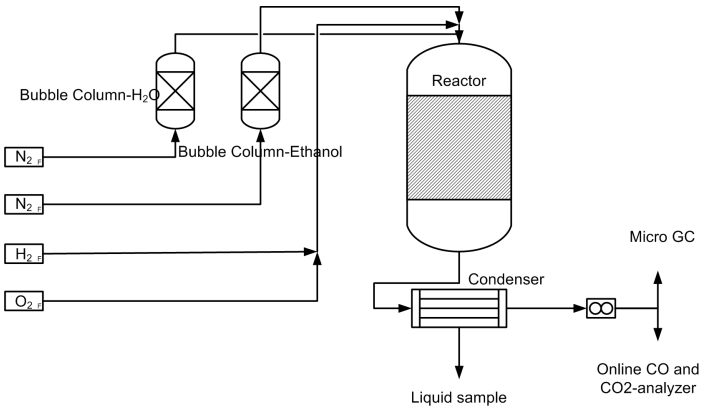

(a) Evaporator for H_2O and ethanol

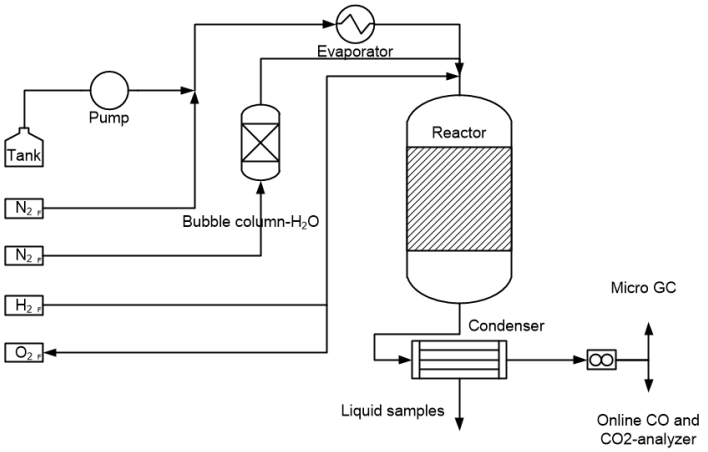

(b) Evaporator and pump

Fig. 2.1: *Flowsheets of the experimental setups used at the Technical University of Denmark.*

The feeding system was altered for long term experiments ($\geq$ 24 *h*) with ethanol as well as experiments with 2-methylfuran, furfural, and guaiacol, as shown in fig. 2.1(b). The desired

Tab. 2.1: *Comparison of conversion and yield of H_2, CO, CO_2, CH_4, and C_2H_4 with the feed delivered by a pump or evaporators over Ni/CeO_2-$K/MgAl_2O_4$. Experimental conditions: S/C: 5.5-6.0; Temp.: 586 ℃; m_{Cat} = 0.50 g, Ni loading: 8.2 wt%, F_T = 1600 NmL/min, y_{Eth} = 3.1 − 3.3 vol%, y_{H_2O} = 36.3 − 37.2 vol%, N_2 as balance.*

Feed system	X [%]	Y_{H_2} [%]	Y_{CO_2} [%]	Y_{CO} [%]	Y_{CH_4} [%]	$Y_{C_2H_4}$ [%]
Pump	99.5	76.3	82.5	14.4	3.0	0
Evaporator	99.6	78.2	82.9	12.4	4.8	0

mixture of water and ethanol was pumped through an evaporator operated at 250 ℃ and then fed to the reactor through the feeding tube along with N_2 for dilution in the long term SR of ethanol experiments. The pump was a Knauer Smartline 100 pump and the evaporator was 3.175 *mm* stainless steel tube wrapped around a copper core heated by a heating cartridge. Similar results were obtained with the two feeding systems as shown table 2.1.

2-methylfuran, furfural, and guaiacol are immiscible with water and a third option was used for feeding oxygenate and water. Water was fed to the reactor by saturating a flow of nitrogen in a bubble column, while the oxygenate was pumped and mixed with a flow of nitrogen then sent to the top of the reactor and mixed with the steam/N_2-stream before entering the reactor. Plugging of the evaporator occurred, when heating the 2-methyl furan and furfural in N_2, and therefore it was chosen to pump the oxygenate directly to the reactor without preheating to avoid polymerization of the oxygenates and subsequent plugging of the evaporator. The flow rate used in the SR of the different model compounds, as well as flow of nitrogen and steam can be seen in table 2.2.

Analysis of the liquid from the condenser was conducted by a Shimadzu GCMS/FID-QP2010 UltraEi fitted with a Supelco Equity-5 column. Identification was made on the mass spectrometer (MS) and quantification was done on the flame ionization detector (FID).

Tab. 2.2: *Flow of oxygenate, steam, and water in the SR of the different model compounds.*

Compound		Ethanol	2-methyl furan	Furfural	Guaiacol
F_{N_2}	$\left[\frac{NmL}{min}\right]$	960	1016	1015	1022
$F_{\text{Model compound}}$	$\left[\frac{g}{min}\right]$	0.1	0.082	0.097	0.089
$F_{\text{Model compound}}$	$\left[\frac{NmL}{min}\right]$	49	22.5	22.5	16.1
F_{H_2O}	$\left[\frac{NmL}{min}\right]$	588	562	562	563
S/C	$\left[\frac{mole\ H_2O}{mole\ C}\right]$	6	5	5	5

In all the different experiments the catalyst was placed between two pieces of quartz wool resting on a quartz frit inside a quartz tube with an inner diameter of 17 *mm* placed in the furnace. The steam and oxygenate mixture was fed from the top of the reactor through an inlet tube with an outer diameter of 6 *mm* and perforated with 12 holes in the end to distribute the gas over catalyst bed. The outlet of the inlet/feeding tube was approx. 50 *mm* above

the catalyst bed allowing time for mixing while minimizing homogeneous gas phase reactions before reaching the catalyst. The temperature was measured by a thermocouple placed in a pocket just below the quartz frit. The schematics of the quartz reactor system, which consists of a main tube, reactor top and bottom as well as a sample tube, where the catalyst is placed, can be seen in fig. 2.2. Furthermore the assembled reactor is shown in this figure.

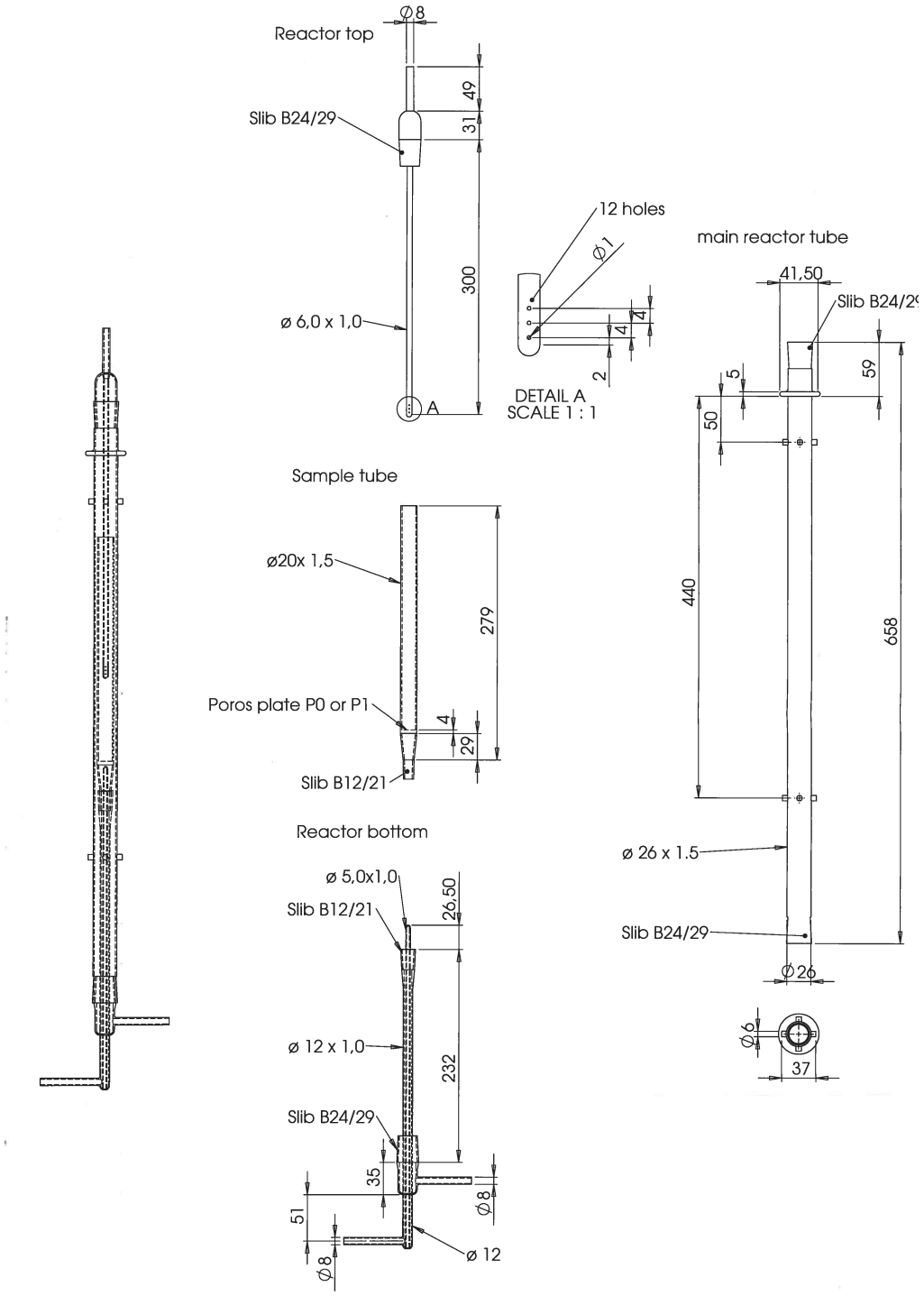

Fig. 2.2: *Quartz reactor system developed at the Technical University of Denmark.*

Tab. 2.3: *General reaction conditions in the SR of ethanol. N_2 as balance gas in all experiments.*

Flow $[NmL/min]$	Ethanol [vol%]	H_2O [vol%]	O_2 [vol%]	H_2 [vol%]
1500-1600	3.0-3.5	10-50	0-6.3	0-3.6

2.2.1 Catalytic test

0.5 g of catalyst with $d_p = 410 - 725\ \mu m$ or $d_p = 250 - 410\ \mu m$ was loaded into the reactor and then heated to 600 ℃ in a flow of N_2. At 600 ℃ the flow was changed to a 50/50 flow of N_2 and H_2 of roughly 500 NmL/min for 1 hour to reduce the NiO to Ni. After reduction the reactor was purged with N_2 for 10 min and then the reactants were directed to the reactor. The general flow rates and gas composition investigated in the SR of ethanol can be seen in table 2.3. The overall flow rates were similar in the SR of cyclic compounds, but the feed gas consisted of 1.0-1.5 $vol\%$ of oxygenate, roughly 35 $vol\%$ H_2O, various amounts of O_2 (0-4.8 $vol\%$), and N_2 as balance. The pressure was in all cases atmospheric and temperatures between 400 and 800 ℃ were investigated. The number of carbon atoms fed to the system was similar in the SR of 2-methylfuran, furfural, guaiacol, and ethanol.

Estimations based on Weisz-Prater and Mears criteria for internal and external diffusion showed that diffusion was not limiting for the overall reaction with the applied particle sizes and experimental conditions. Furthermore experiments with $d_p = 410-725\ \mu m$ and $d_p = 250-410\ \mu m$ showed similar results with respect to conversion and carbon deposition. Estimation of diffusion and other aspects of the reactor design are evaluated in Appendix A. The main conclusions are that external diffusion is not limiting and neither is internal diffusion as least for particles below 425 μm. Furthermore, a criterion for achieving plug flow is not met, but it appears that modeling as plug flow reactor gives the best description of conversion. There should not be large temperature gradients between catalyst particles and the surrounding gas, based on a criterion by Mear and a simple energy balance over a particle.

2.2.2 Determination of the amount of carbon deposited

The amount of carbon deposited during an experiment was determined by temperature programmed oxidation (TPO) of the entire catalyst bed and sample tube. The procedure was, cooling of the reactor to 200 ℃ followed by heating to 700 ℃ (10 ℃/min) in a 1 NL/min flow of 2-3 $vol\%$ O_2 in N_2. The evolution of CO and CO_2 was monitored by the online gas analyzer (data points every 5 s) and the amount of carbon was determined by integration of these signals.

Temperature programmed oxidation was also performed in another flow reactor setup, when the spent catalyst should be characterized by others techniques as well. The setup used only 10-15 mg of spent catalysts. The samples were oxidized in 1000 NmL/min flow of 10 % O_2 in N_2 between room temperature and 700 ℃, with an average heating rate of 12 ℃/min. The offgas composition was monitored by an ABB AO2000 gas analyzer with two channels and concentration of CO and CO_2 were logged every 15 s. No significant differences in the temperature of oxidation, CO and CO_2 release, or the amount of carbon deposited were observed between the two options for determination of the amount of carbon deposited.

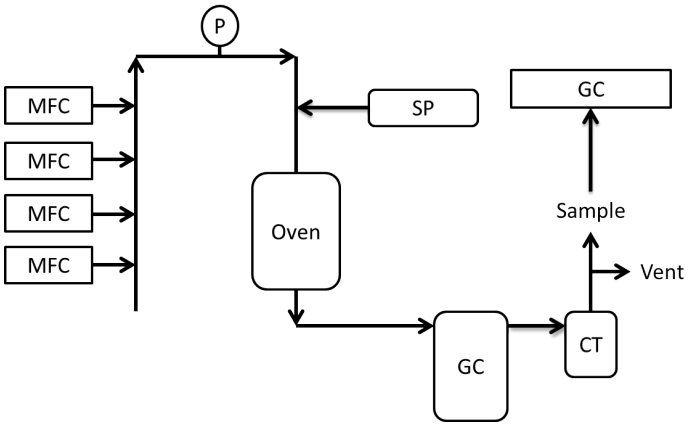

Fig. 2.3: *Flowsheet of the experimental setup used at the University of Oklahoma. CT: Cold trap, GC: Gas chromatograph, MFC: Mass flow controller, P: Pressure gauge, SP: Syringe pump.*

2.3 Experimental setup at OU

The schematics of the setup used at OU are shown in fig. 2.3. The setup consisted of four gas lines with corresponding mass flow controller (MFC) connected to a vaporizer where injection of a liquid was possible. The vaporizer was a 6.35 mm stainless steel tube heated to 300 ℃ by heating tape and the feed mixture of water and oxygenate was delivered by a syringe pump and injected into the vaporizer through a septum. In the vaporizer the feed was mixed with the carrier gas. The reactant mixture then entered a quartz reactor placed in a furnace. The temperature was measured by a thermocouple on the outside of the reactor tube. The reactor effluent was connected to a Varian 3800 gas chromatograph (GC) equipped with a Restek Rxi-5Sil mass spectrometry (MS) column, a flame ionization detector (FID), and a thermal conductivity detector (TCD) by a heated line kept at 300 ℃. This GC was used to determine the concentrations of oxygenates and C_3-hydrocarbons. After the GC, there was a cold-trap with ice, to condense water, products, and unconverted oxygenates. The gases from the cold trap were collected in a gas bag and analyzed by a GC/TCD (Carle AGC 400) to determine the concentration of CO, CO_2, H_2, CH_4, C_2H_4, C_2H_6, and N_2. The online GC did measurements every 25 min, while gas samples were taken to the GC/TCD every 30 to 45 min.

2.3.1 Catalytic test at OU

The catalyst with a particle size of $d_p = 250 - 425\ \mu m$ was loaded in a quartz tube with an outer diameter of 6.35 mm and a length of 343 mm. The catalyst was placed on a constriction in the middle of the quartz tube between two layers of quartz wool. The catalyst was heated to 600 ℃ in a flow of N_2 of 40 NmL/min. At 600 ℃ the flow was changed to 50/50 mixture of N_2 and H_2 for 1 h to reduce the NiO on the catalyst to Ni. After the reduction the catalyst was flushed with N_2 for 5 min. The experiment was started hereafter by adjusting the N_2 flow, starting the syringe pump, and inserting the needle through the septum in the vaporizer. The feed gas had a S/C-ratio of 6 and the mole fractions of oxygenates and H_2O were 2-3 % and 36 %, respectively, with N_2 as balance.

2.3.2 Temperature programmed oxidation at OU

The amount of carbon on the spent catalysts was determined by TPO. 2-5 mg of spent catalyst was placed between two layers of quartz wool in a quartz reactor with outer diameter of 6.35 mm and a length of 394 mm. The sample was heated from room temperature to 800 ℃ (heating rate of 10 ℃/min) in a flow of 5 % O_2 in He. The released carbon oxides were converted to CH_4 over a methanation catalyst operated at 400 ℃ and the amount of CH_4 formed was measured by FID.

2.4 Catalyst characterization

The BET surface area of all the prepared catalysts was measured by N_2 adsorption at its boiling point using multipoint BET theory with seven points in the $p/p_0 = 0.05 - 0.3$ range using a Quantachrome iQ2.

XRD-patterns were recorded for spent and fresh catalyst powders by a PANalytical X'Pert PRO Diffractometer, which had a rotating sample holder, a rotating copper anode X-ray source, nickel filter, and automatic anti-scatter and divergence slits. The particle size of Ni, NiO, and CeO_2 were determined from the XRD patterns and the line broadening of peaks using the Scherrer equation, eq. 2.1, [188]:

$$d_p = \frac{K \cdot \lambda}{\beta \cdot \cos(\theta)} \tag{2.1}$$

Where K is shape factor set to 0.9 [188], λ is the X-ray wavelength, β is full width at half maximum corrected for the instrumental line broadening, while θ is the Bragg angle.

Temperature programmed reduction (TPR) of the catalysts were conducted in a flow of 10 % H_2 in He and the temperature was raised from room temperature to 900 ℃ with a temperature ramp of 5 K/min. The concentrations of H_2O, H_2, and He were followed by a mass spectrometer.

Bright field transmission electron microscopy of fresh and spent catalysts were conducted on a Tecnai T20 G2 microscope with a thermionic-lanthanum hexaboride, LaB_6, as electron source. The fresh catalysts were reduced, cooled down, and removed from the reactor and then transported to TEM investigations. The TEM samples were crushed, slurried with ethanol and deposited on a copper grid covered with a lacey carbon film.

Elemental analysis of the catalysts was conducted by dissolving the catalyst and then using inductively coupled plasma optimal emission spectroscopy (ICP-OES).

2.4.1 Calculations

W/F is defined as mass of catalyst pr. molar flow of oxygenates, $F_{Oxy,\ m}$:

$$\mathrm{W/F} = \frac{m_{Cat}}{F_{Eth,\ m}} \quad \left[\frac{g \cdot h}{mole}\right] \tag{2.2}$$

WHSV is defined as mass flow of ethanol, $F_{Eth,\ m}$ pr. mass of catalyst:

$$\mathrm{WHSV} = \frac{F_{Eth,\ m}}{m_{Cat}} \quad [h^{-1}] \tag{2.3}$$

Conversion, X, is calculated on a carbon basis as:

$$X = \frac{\sum n_{C,\ i} \cdot n_i}{n_{C,\ i} \cdot n_{\mathrm{Oxy},\ in}} \cdot 100\% \tag{2.4}$$

Tab. 2.4: *$n_{H_2,\ Max}$ used in calculations of the yield of H_2.*

Model compound	$n_{H_2,\ Max}$
Acetic acid	4
Acetol	7
Acetone	8
Ethanol	6
Furfural	10
Guaiacol	16
2-methylfuran	12
Propanal	8
1-propanol	9

Where $n_{C,\ i}$ is the number of carbon atom in component i and n_i is the number of moles of compound i produced.

The yield of products, Y_i, is based on the definition by Fogler [189] and calculated as:

$$Y_i = \frac{n_{C,\ i} \cdot n_i}{\sum n_{C,\ i} \cdot n_i} \cdot 100\% \tag{2.5}$$

The yield of H_2 is defined as:

$$Y_{H_2} = \frac{n_{H_2}}{n_{H_2,\ Max} \cdot X \cdot n_{Oxy,\ in}} \cdot 100\% \tag{2.6}$$

The factor of $n_{H_2,\ Max}$ is the maximum number of H_2 moles, which can be produced from 1 mole of oxygenates including full shift of CO to CO_2 and H_2 (reaction 1.21). $n_{H_2,\ Max}$ for all the investigated compounds is shown table 2.4.

Carbon deposition is reported as the amount of carbon deposited pr. amount carbon in the feed, $\frac{mole\ C}{mole\ C_{Feed}}$, and in mass of carbon deposited pr. mass of catalyst and time, $\frac{mg\ C}{g_{Cat} \cdot h}$.

3. STEAM REFORMING OF ETHANOL: EFFECTS OF SUPPORT AND ADDITIVES ON NI-BASED CATALYSTS

High degrees of conversion and high yield of H_2 can be achieved in the SR of bio-oil and other oxygenates, but deactivation due to carbon deposition is also observed and is one of the major hurdles for industrial application. In the following it is attempted to minimize the carbon deposition in the SR of ethanol over Ni-based catalysts. Ethanol was chosen as model compound of bio-oil because it has a functionality which is found in bio-oil and is prone to carbon deposition as shown by several studies [49, 50, 63, 122, 190]. Furthermore SR of ethanol is interesting on its own as it can be used to provide H_2 for fuel cells in mobile applications [49].

Steam reforming of ethanol can be described by the following reactions:

$$C_2H_6O + H_2O \rightleftharpoons 2\ CO + 4\ H_2 \tag{3.1}$$

$$C_2H_6O + 3\ H_2O \rightleftharpoons 2\ CO_2 + 6\ H_2 \tag{3.2}$$

Reaction 3.1 is the general SR-reaction, while reaction 3.2 assumes full shift of CO to CO_2 by reaction with H_2O (reaction 1.2), which yields two additional moles of H_2. Beside the water-gas shift (WGS), reaction 1.2, methanation, reaction 3.4, might also influence the product distribution:

$$CO + H_2O \rightleftharpoons CO_2 + H_2 \tag{3.3}$$

$$CO + 3H_2 \rightleftharpoons CH_4 + H_2O \tag{3.4}$$

The offgas composition in the SR of ethanol is governed by the equilibrium between the reactions shown above e.g. reactions 3.1, 3.3, and 3.4. High temperatures will favor the reforming reactions and produce H_2 and CO as reaction 3.1 is shifted toward the right, while reaction 3.4 will be shifted to the left. The WGS, reaction 3.3, will be shifted toward CO and H_2O at temperatures above 800 ℃ and therefore the maximum H_2 production is achieved at intermediate temperatures, 600-800 ℃ [85].

Side reactions observed in SR of ethanol are dehydration, reaction 3.5, or dehydrogenation, reaction 3.6, yielding ethene and acetaldehyde, respectively [49, 50, 89, 99, 191].

$$C_2H_6O \rightarrow C_2H_4 + H_2O \tag{3.5}$$

$$C_2H_6O \rightarrow C_2H_4O + H_2 \tag{3.6}$$

Especially, formation of ethene is troublesome as it has a high potential for forming carbon deposits [32, 99, 100, 192]. Carbon formation from ethene could occur through decomposition followed by accumulation and polymerization [100, 191, 192]:

$$C_2H_4 \rightarrow 2C + 2H_2 \rightarrow \text{Carbon} \tag{3.7}$$

Alternatively, carbon deposits can be formed through direct polymerization of ethene [49, 50, 89]:

$$nC_2H_4 \rightarrow \text{Carbon} \tag{3.8}$$

There are two routes to minimize carbon deposition, either the catalyst formulation can be optimized or the reaction conditions can be changed, e.g. changing the temperature, the water content, or adding oxygen to feed. In this chapter a systematic investigation of different options for lowering the rate of carbon deposition in SR of ethanol and hereby enhancing catalyst lifetime through changes in the catalyst formulation is carried out, including changing support material, adding promoters, and doping with sulfur. Furthermore the effect of temperature on conversion, product distribution, and carbon deposition will be investigated.

Several catalysts have been investigated in the SR of ethanol including Ni, Cu, Co, Ir, Au, Pt, Pd, Ru, and Rh on Al_2O_3 [63, 89, 95, 97, 131, 166, 193, 194]; Ni, Ag, Rh, and Ru on $MgAl_2O_4$ [121–123, 195]; Pt, Rh, Co, Pt, and Ir on $Ce_xZr_{1-x}O_2$ [62, 90, 93, 94, 119, 120, 196–199], and several other systems like perovskites or hydrotalcites based catalysts [57, 200]. For a complete overview the reader is referred to the following reviews [49, 50, 98, 99]. As indicated above, many metals can be used in SR but Ni is one of few active metals used in conventional SR catalysts, due to the low price and good activity compared with the more expensive noble metals [42].

Magnesium or calcium aluminates are used as supports for industrial SR catalysts and have a low number of acid sites, which reduces the risk of decomposition of the oxygenates and therefore also the risk of carbon deposition [52]. Furthermore a more stable and higher activity for $MgAl_2O_4$ compared with Al_2O_3 has been reported [48, 52, 58]. The increased activity has been ascribed to an increased water dissociation on the support and formation of smaller metal particles [48, 52]. Furthermore steam gasification of the coke might be facilitated by spillover of O- or OH-species from the support to the metal particles [52]. CeO_2 and $Ce_xZr_{1-x}O_2$ have been reported to facilitate water dissociation and thereby supply O for oxidation of carbon on the surface due to their redox properties [68, 90, 94, 201, 202].

Potassium is known from conventional SR to bind to step sites on Ni-particles and hereby reduce the rate of reaction but also the risk of carbon formation as carbon islands cannot grow large enough to nucleate carbon whiskers [30, 42]. Results from the SR of acetic acid over K-promoted Ni/Al_2O_3 catalysts showed reduced CH_4 formation, increased activity, and lower carbon deposition [82]. An optimal loading of K was reported to be 8 $wt\%$ [82]. Results from the SR of ethanol over $Ni/MgAl_2O_4$ showed a decrease in the carbon deposition by a factor of 3 when doping with 1 $wt\%$ of K [122].

Based on the results presented above it is chosen to investigate four support materials for Ni; $MgAl_2O_4$, $CeZrO_4/MgAl_2O_4$, CeO_2, and $Ce_{0.6}Zr_{0.4}O_2$. Furthermore addition of K, CeO_2, ZrO_2, or mixtures hereof to $Ni/MgAl_2O_4$ to promote stable activity will be investigated.

3.1 Characterization

The nickel particle size based on XRD measurements and surface area of all the tested catalysts are shown in table 3.1. The surface areas and nickel particle sizes are in the same range for all the $MgAl_2O_4$ based catalyst with values of 52-69 m^2/g and 6-9 nm, respectively. Ni/CeO_2 and $Ni/Ce_{0.6}Zr_{0.4}O_2$ both have higher surface areas and larger Ni particles with values around 90-113 m^2/g and 10-20 nm, respectively. Therefore Ni seems to be better dispersed on $MgAl_2O_4$ and $CeZrO_4/MgAl_2O_4$ compared with CeO_2 and $Ce_{0.6}Zr_{0.4}O_2$.

TEM-images of reduced $Ni/MgAl_2O_4$ and $Ni/Ce_{0.6}Zr_{0.4}O_2$ as well as the particle size distribution determined from TEM-images can be seen in fig. 3.1. For $Ni/Ce_{0.6}Zr_{0.4}O_2$ (fig. 3.1(a)) it is difficult to distinguish between Ni and the support, but it can be seen that the particles in general had a size of 13 nm ± 3 nm, which is slightly below the results obtained with XRD.

Tab. 3.1: *Nominal metal loading, surface area, and NiO particle size of the fresh catalysts prior to reduction. XRD reflection peak from NiO peak at $2\theta = 62.8°$ used for determination of particle size.*

Catalyst	Promoter	Metal loading $[wt\%]$	Surface area $[m^2/g]$	$d_{p,\ \mathrm{NiO}}$ $[nm]$
$Ni/Ce_{0.6}Zr_{0.4}O_2$	-	8.2	90	15-20
Ni/CeO_2	-	8.2	113	10
$Ni/MgAl_2O_4$	-	8.1	69	7
$Ni/CeZrO_4/MgAl_2O_4$	10 $wt\%$ CeO_2 and ZrO_2	8.0	63	6
$Ni\text{-}K/CeZrO_4/MgAl_2O_4$	9 $wt\%$ CeO_2 and ZrO_2, 5 $wt\%$ K	8.2	47	8
$Ni\text{-}K/MgAl_2O_4$	5 $wt\%$	8.2	55	7
$Ni\text{-}CeO_2/MgAl_2O_4$	11 $wt\%$ CeO_2	8.3	59	9
$Ni/CeO_2\text{-}K/MgAl_2O_4$	5 $wt\%$ CeO_2 and K	8.2	54	6

The size distribution from the TEM-images is used to calculate the mean volume diameter, which is used for comparison. XRD was conducted on unreduced samples while the TEM was conducted on reduced samples, which could explain the difference in particle size. For $Ni/MgAl_2O_4$ (fig. 3.1(b)) Ni and the support can be distinguished as the Ni particles are the dark/black particles. The particle size determined from the TEM analysis was $8\ nm \pm 2\ nm$, which is similar to the XRD results. The trends in Ni particle sizes obtained by XRD are confirmed by TEM.

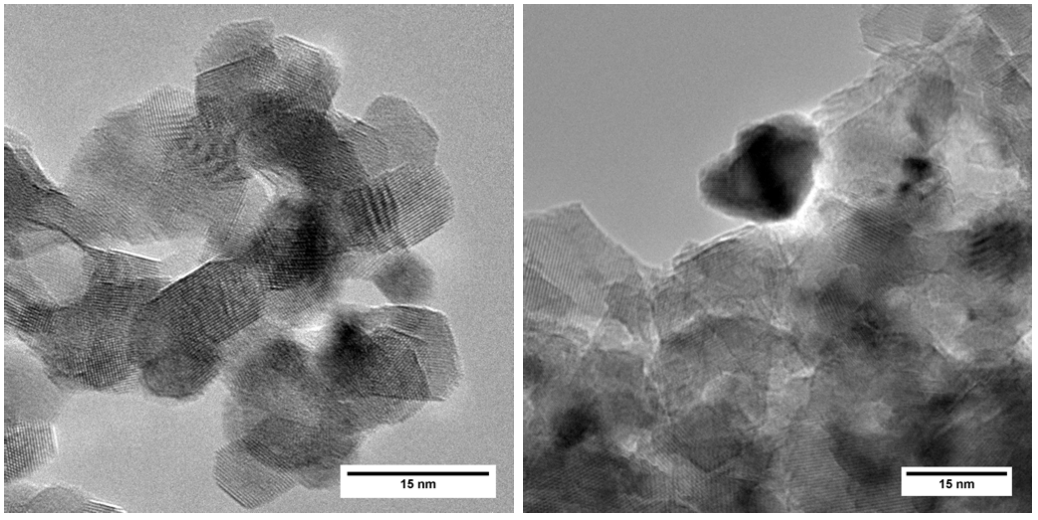

(a) $Ni/Ce_{0.6}Zr_{0.4}O_2$ (b) $Ni/MgAl_2O_4$

Fig. 3.1: *TEM images of reduced catalysts prior to SR experiments.*

The XRD-patterns for NiO on CeO_2, $Ce_{0.6}Zr_{0.4}O_2$, $MgAl_2O_4$, and $CeZrO_4/MgAl_2O_4$ can be seen in fig. 3.2(a), 3.2(b), 3.2(c), and 3.2(d), respectively. XRD-analysis of the different catalysts confirmed that the mixed oxide of Ce and Zr was $Ce_{0.6}Zr_{0.4}O_2$ and that the $MgAl_2O_4$ indeed had spinel structure and was not a mixture of MgO and Al_2O_3. On the

$Ni/MgAl_2O_4$-catalysts, some formation of $NiAl_2O_4$ phase was observed. Addition of K and CeO_2 to $Ni/MgAl_2O_4$ could not be detected by the XRD-analysis, probably due to a small particle size or because they were present as layers or amorphous species. The loading of CeO_2 corresponded to roughly one monolayer, while the potassium loading was chosen based on the optimal value of 8 $wt\%$ K found by Hu and Lu [82]. Their catalyst however had a surface area of 125 m^2/g, roughly twice the value of our catalyst, and thus we used about 4 $wt\%$ K to provide the same surface coverage of K. It corresponded to about two monolayers of K.

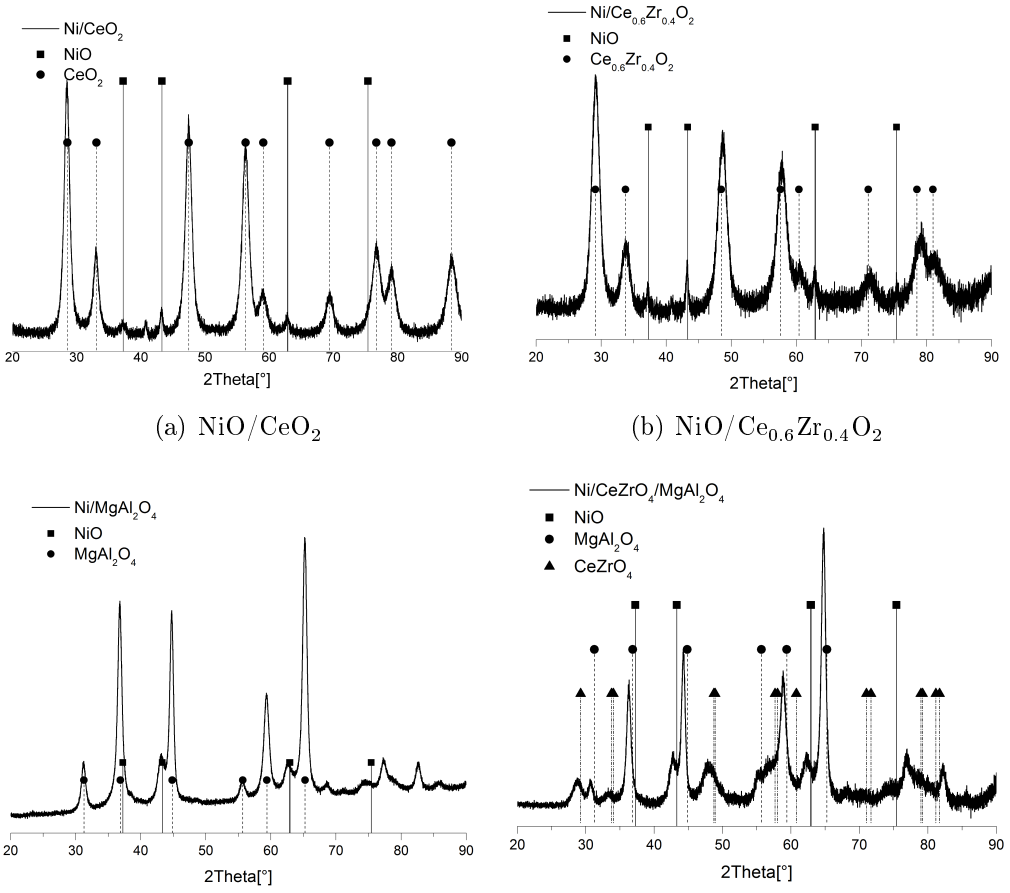

(a) NiO/CeO_2 (b) $NiO/Ce_{0.6}Zr_{0.4}O_2$

(c) $NiO/MgAl_2O_4$ (d) $NiO/CeZrO_4/MgAl_2O_4$

Fig. 3.2: *XRD patterns of the fresh catalysts; NiO/CeO_2, $NiO/Ce_{0.6}Zr_{0.4}O_2$, $NiO/MgAl_2O_4$, and $NiO/CeZrO_4/MgAl_2O_4$.*

The addition of $CeZrO_4$ to $Ni/MgAl_2O_4$ was detected by XRD and confirmed the presence of $CeZrO_4$ and not single oxides like CeO_2 and ZrO_2. No formation of mixed oxides with Ce or Zr incorporated in to the $MgAl_2O_4$-phase was observed showing that these species were present as true promoters on the surface of $MgAl_2O_4$.

The H_2O evolution as function of temperature for TPR of Ni on CeO_2, $Ce_{0.6}Zr_{0.4}O_2$, $MgAl_2O_4$, and $CeZrO_4/MgAl_2O_4$ can be seen in fig. 3.3. All the supports had reduction peaks around 200-400 ℃, which could correspond to the reduction of NiO with low interaction with the support. For $Ni/MgAl_2O_4$ and $Ni/CeZrO_4/MgAl_2O_4$, there is an additional broad reduction peak between 500 and 900 ℃. This could correspond to reduction of NiO closely bound to the support material as high dispersion and strong interaction are known to shift the reduction peaks toward higher temperature [203–205]. However, the high temperature reduction

peak could also arise from the reduction of $NiAl_2O_4$ [204, 205]. An increased reducibility for $Ni/CeZrO_4/MgAl_2O_4$ compared with $Ni/MgAl_2O_4$ have been reported by Eltejaei et al. [204]. This could also be the case here as the water evolution was higher for $Ni/CeZrO_4/MgAl_2O_4$ compared with $Ni/MgAl_2O_4$.

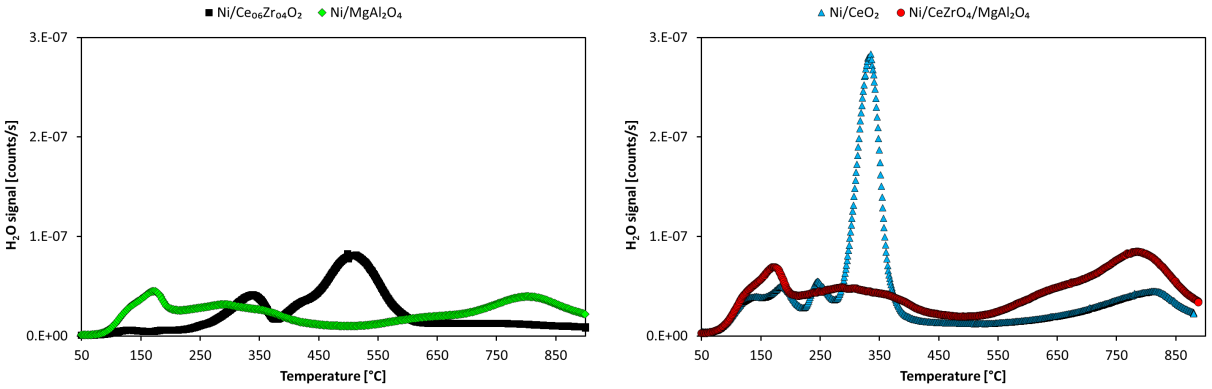

(a) $Ni/Ce_{0.6}Zr_{0.4}O_2$ and $Ni/MgAl_2O_4$ (b) Ni/CeO_2 and $Ni/CeZrO_4/MgAl_2O_4$

Fig. 3.3: *Water evolution during TPR of for $Ni/MgAl_2O_4$, Ni/CeO_2, $Ni/Ce_{0.6}Zr_{0.4}O_2$, and $Ni/CeZrO_4/MgAl_2O_4$. Gas: 10 % H_2 in He, heating rate 10 °C/min.*

In the TPR of Ni/CeO_2 there are a couple of small reduction peaks at 100-275 °C, which can be ascribed to reduction of oxygen in the CeO_2-lattice [206]. At 330 °C there is large reduction peak partly from the reduction of NiO [207, 208]. The significantly larger size of this peak could be explained by reduction of CeO_2 to Ce_2O_3 by spillover of H_2 from the metal particles, which has been observed for noble metal catalysts [208]. At 800 °C there is a reduction peak which could correspond to reduction of bulk CeO_2 to Ce_2O_3 [206, 209].

Temperature programmed reduction of $Ni/Ce_{0.6}Zr_{0.4}O_2$ showed two reduction peaks, one at 330 °C and one at 500 °C. The peak at 330 °C is probably due to the reduction of NiO, while the peak at 500 °C could be reduction of Ce^{4+} to Ce^{3+} or reduction of NiO with strong interaction with $Ce_{0.6}Zr_{0.4}O_2$ [207].

Reductions, which occurs higher than 600 °C, might still occur at 600 °C if exposed to H_2 in a much higher concentration [203]. Therefore, full reduction of at least the active Ni should be possible in the activity tests even though the catalysts are reduced at 600 °C.

3.2 Effect of temperature and W/F

The effect of temperature on conversion and product distribution in the SR of ethanol was investigated for several Ni-based catalysts at temperatures between 400-700 °C and a S/C-ratio of 6. The conversion of ethanol over all of the catalysts at each temperature level initially decreased with time and then reached a relatively stable conversion after approximately 1.5 *h*. The decrease in conversion was largest at 400 °C and 500 °C, which shows that severe deactivation due to carbon deposition or oxidation of Ni occurred at the lowest temperatures. The conversion as function of time at the four temperature levels during SR of ethanol over $Ni/CeZrO_4/MgAl_2O_4$ can be seen in fig. 3.4, while the initial and pseudo steady state conversion for the other catalysts can be seen in table 3.3. The conversion reported in the following is the pseudo steady state conversion, unless otherwise stated.

The temperature dependence experiments were conducted from high to low temperatures to minimize the influence of carbon deposition and subsequent deactivation of catalysts which

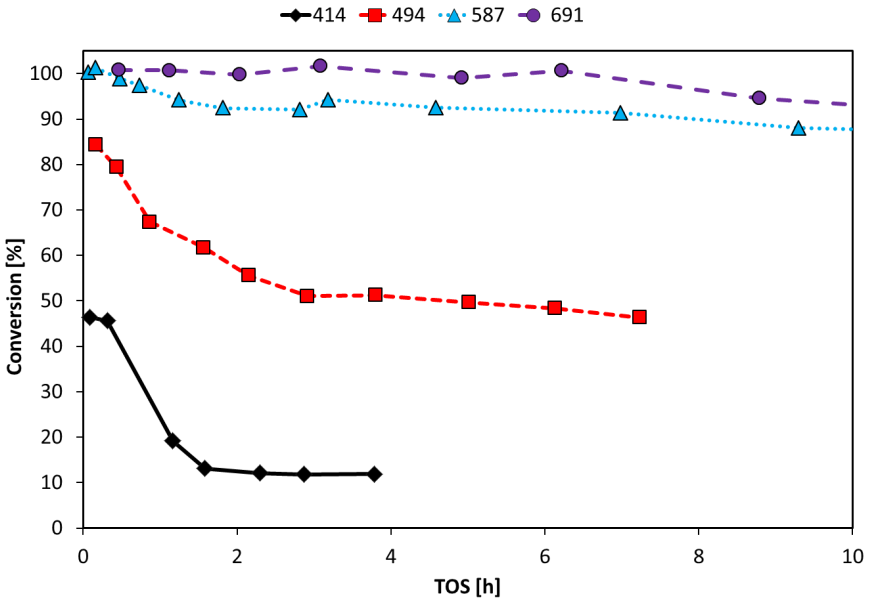

Fig. 3.4: *The conversion as function of time during SR of ethanol at different temperatures over* $Ni/CeZrO_4/MgAl_2O_4$. *Experimental conditions: S/C: 5.8,* $m_{Cat} = 0.50$ *g, Ni loading: 8.2 wt%,* $F_T = 1.6$ NL/min, $y_{Eth} = 3.4$ *vol%,* $y_{H_2O} = 38.8$ *vol%,* N_2 *as balance.*

is reported to occur at a larger extent at temperatures between 400 and 550 ℃ [210]. To check for deactivation, the experiment at 600 ℃ over $Ni/MgAl_2O_4$ was repeated after operation at 500 ℃ and 400 ℃. The conversion and yield of CH_4 and C_2H_4 from the last point at 600 ℃ during the first cycle and first point of the second cycle can be seen in table 3.2. There was a slight decrease in conversion after being at 400 ℃ and 500 ℃ , which could be due to carbon deposition.

Tab. 3.2: *Comparison of conversion and yield of* CH_4 *and* C_2H_4 *after SR at 600 and 700 ℃ and after SR at 700, 600, 500, 400 ℃.*

Cycle	Conversion [%]	Y_{CH_4} [%]	$Y_{C_2H_4}$ [%]
1	84	3.3	2.4
2	82	3.8	1.8

The trends in product distribution as function of temperature were similar over all of tested catalysts and the results from SR of ethanol over $Ni/CeZrO_4/MgAl_2O_4$ are used to highlight these trends. The offgas concentrations on H_2O and N_2-free basis as function of the temperature over $Ni/CeZrO_4/MgAl_2O_4$ at S/C=6 can be seen in fig. 3.5. The fractions of CH_4 and CO_2 in the offgas decreased with increasing temperature, while the fractions of H_2 and CO increased. This corresponds to an increase in the activity for the SR reactions and a shift in the WGS toward CO and H_2 with temperature as predicted by thermodynamics. The fraction of ethene, decreased with temperature and approached zero at 600 ℃ and above.

A comparison between the thermodynamic equilibrium and the actual product distribution over $Ni/CeZrO_4/MgAl_2O_4$ can be seen in figure 3.6. The figure shows that the product distribution approached equilibrium with increasing temperature. At the highest temperature the actual offgas composition and thermodynamic equilibrium were quite close.

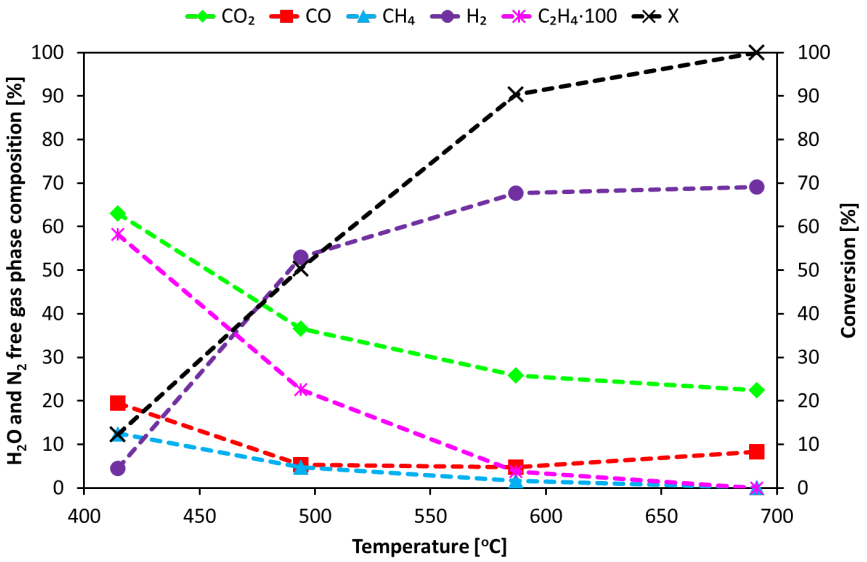

Fig. 3.5: *The offgas composition on H_2O and N_2-free basis and conversion as functions of temperature over $Ni/CeZrO_4/MgAl_2O_4$. Ethene fraction multiplied by 10. Experimental conditions: S/C: 5.8, m_{Cat} = 0.50 g, Ni loading: 8.2 wt%, F_T = 1.6 NL/min, y_{Eth} = 3.4 vol%, y_{H_2O} = 38.8 vol%, N_2 as balance.*

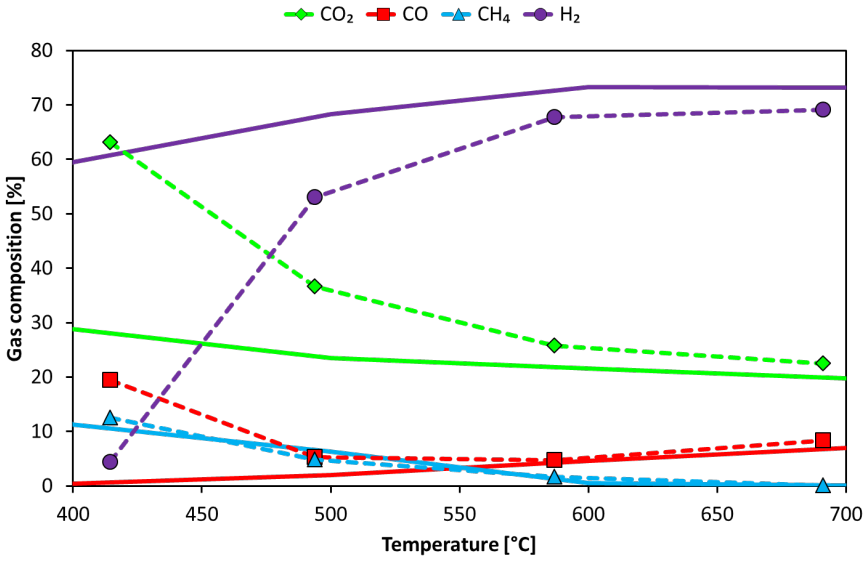

Fig. 3.6: *The offgas composition as function of temperature over $Ni/CeZrO_4/MgAl_2O_4$ compared with the thermodynamic equilibrium predicted by FactSage 6.0. Dashed lines: Experimental data; Full line: Thermodynamic equilibrium. Experimental conditions: S/C: 5.8, m_{Cat} = 0.50 g, Ni loading: 8.2 wt%, F_T = 1.6 NL/min, y_{Eth} = 3.4 vol%, y_{H_2O} = 38.8 vol%, N_2 as balance.*

The yield of H_2 was 3 % at 400 °C over $Ni/CeZrO_4/MgAl_2O_4$ and then increased with temperature to 75 % or 4.5 moles of H_2 produced pr. mole of ethanol converted at 700 °C. There was no significant difference in maximum yield of H_2 between the different catalysts, which was achieved at 700 °C and varied between 72 % and 75 %.

The liquid effluent from the condenser contained mainly ethanol and water, but small amounts of acetaldehyde, acetic acid, and acetone were also identified. In addition condensation at dry ice temperature revealed di-ethyl ether as well. The conversions to these species decreased with increasing temperatures and were below 1 % at 400 °C. The reactions responsible for formation of these compounds are dehydrogenation, oxidation, recombination, and dehydration as shown in reactions 3.9 to 3.12. Similar by-products have been reported by others [52, 57, 89].

$$CH_3CH_2OH \rightleftharpoons CH_3CHO + H_2 \tag{3.9}$$
$$CH_3CH_2OH + H_2O \rightleftharpoons CH_3COOH + H_2 \tag{3.10}$$
$$2CH_3CHO \rightleftharpoons CH_3COCH_3 + CO + H_2 \tag{3.11}$$
$$2CH_3CH_2OH \rightleftharpoons C_2H_5OC_2H_5 + H_2O \tag{3.12}$$

The effect of W/F over $Ni/MgAl_2O_4$ at 600 °C and a S/C-ratio of 6 is shown in fig. 3.7. The conversion and yield of H_2 decreased with decreasing W/F, while the yield of CH_4 and C_2H_4 increased. This showed that as W/F became smaller the offgas composition moved away from the thermodynamical equilibrium as expected.

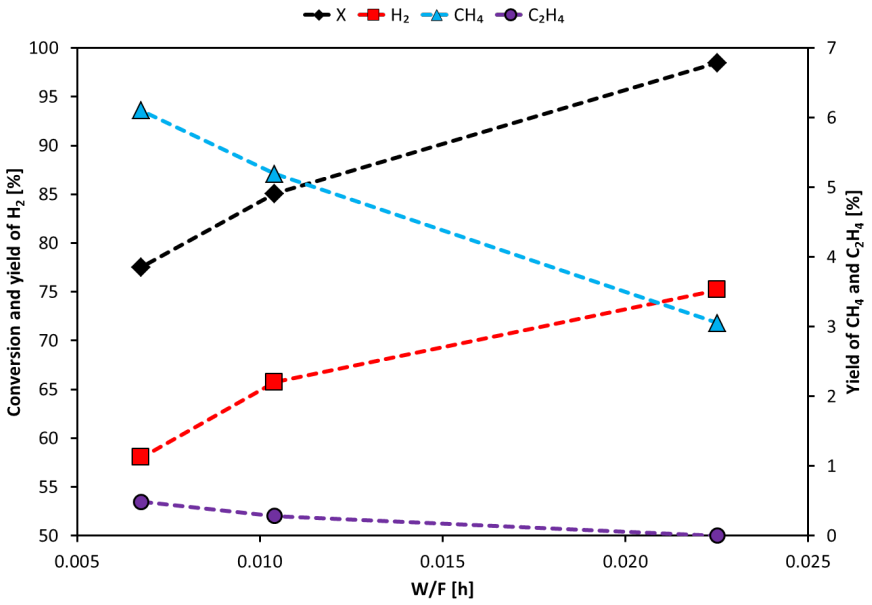

Fig. 3.7: *Conversion, yield of hydrocarbons, and yield of H_2 as function of space velocity in the SR of ethanol over $Ni/MgAl_2O_4$ at 600 °C. Experimental conditions: S/C: 6, Temp.: 563-583 °C, $m_{Cat} = 0.50$ g, Ni loading: 8.2 wt%, $F_T = 0.8 - 2.8$ NL/min, x_{Eth}=3.9 %, $x_{H_2O} = 47\%$, N_2 as balance.*

3.3 Influence of carrier material

The conversion as function of temperature over four different Ni-based catalysts is shown in fig. 3.8. The conversion was highest for $Ni/Ce_{0.6}Zr_{0.4}O_2$ and $Ni/CeZrO_4/MgAl_2O_4$ while $Ni/MgAl_2O_4$ and Ni/CeO_2 had lower degrees of conversion. Similar differences were observed in initial activities (see table 3.3).

The nickel particle size for the different catalysts ranged from 6 to 15 *nm* and it is generally assumed that smaller particles will be more active due to the higher dispersion and a higher

Tab. 3.3: *Comparison of initial (Ini) and pseudo steady state (PSE) conversion as function of temperature over the tested Ni-based catalysts. TOS: 50-70 h. Experimental conditions: S/C: 5.3-6.0, $m_{Cat} = 0.50\ g$, Ni loading: 8.0-8.2 wt%, $F_T = 1.5-1.6\ NL/min$, $y_{Eth} = 3.2 - 3.5\ vol\%$, $y_{H_2O} = 38.6 - 39.2\ vol\%$, N_2 as balance.*

Temp. [°C]	$Ni/Ce_{0.6}Zr_{0.4}O_2$		Ni/CeO_2		$Ni/MgAl_2O_4$		$Ni/CeZrO_4/MgAl_2O_4$	
	Ini	PSS	Ini	PSS	Ini	PSS	Ini	PSS
400	49	17	32	9	28	9	37	12
500	79	66	59	43	56	36	77	52
600	96	95	76	65	94	84	99	90
700	100	100	97	89	100	95	100	100

number of active step sites [38]. However, the nickel particle size did not seem to be determining for the conversion as the $Ni/CeZrO_4/MgAl_2O_4$ and $Ni/MgAl_2O_4$, which had similar d_p (see table 3.1), gave different conversions. Furthermore, $Ni/Ce_{0.6}Zr_{0.4}O_2$ with the largest nickel particles showed the highest conversion. Therefore it seems that the type of support is more important than the size of the nickel particles at least as long as the Ni particles do not differ much in size.

The high activity of $Ni/Ce_{0.6}Zr_{0.4}O_2$ could be ascribed to increased water dissociation for this support [66, 67]. This will lead to more OH-species on the surface of the catalysts, which can react with C-species forming carbon oxides and H_2. Reactions with lattice oxygen on these types of support have also been proposed and might contribute as well [68]. It can be seen from fig. 3.8 that the addition of CeO_2 and ZrO_2 to $MgAl_2O_4$ increased the conversion, which could be ascribed to a similar effect.

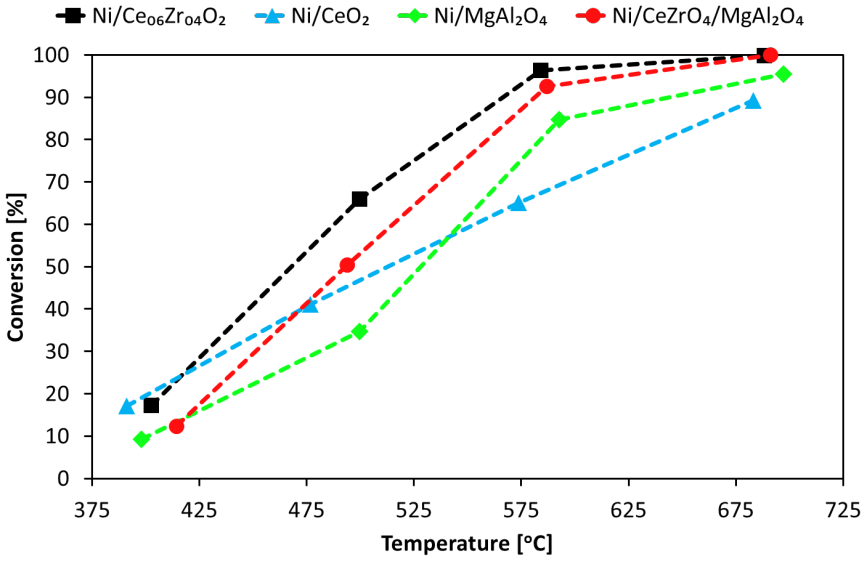

Fig. 3.8: *Comparison of conversion as function of temperature over the tested Ni-based catalysts. TOS: 50-70 h. Experimental conditions: S/C: 5.3-6.0, $m_{Cat} = 0.50\ g$, Ni loading: 8.0-8.2 wt%, $F_T = 1.5 - 1.6\ NL/min$, $y_{Eth} = 3.2 - 3.5\ vol\%$, $y_{H_2O} = 38.6 - 39.2\ vol\%$, N_2 as balance.*

3.3.1 Deactivation

It was chosen to test the different catalysts at 600 ℃ for 4 h in order to determine differences in carbon deposition and activity during SR of ethanol. At this temperature full conversion was not achieved, which leads to higher potential for forming carbon deposits and therefore it is easier to distinguish differences in catalytic performances.

The conversion as function of time over four different catalysts tested at 600 ℃ can be seen in fig. 3.9. All the tested catalysts showed a more or less pronounced decrease in conversion with time. The deactivation was most pronounced for Ni/CeO_2 and $Ni/MgAl_2O_4$ while especially $Ni/Ce_{0.6}Zr_{0.4}O_2$ had a low drop in conversion with time.

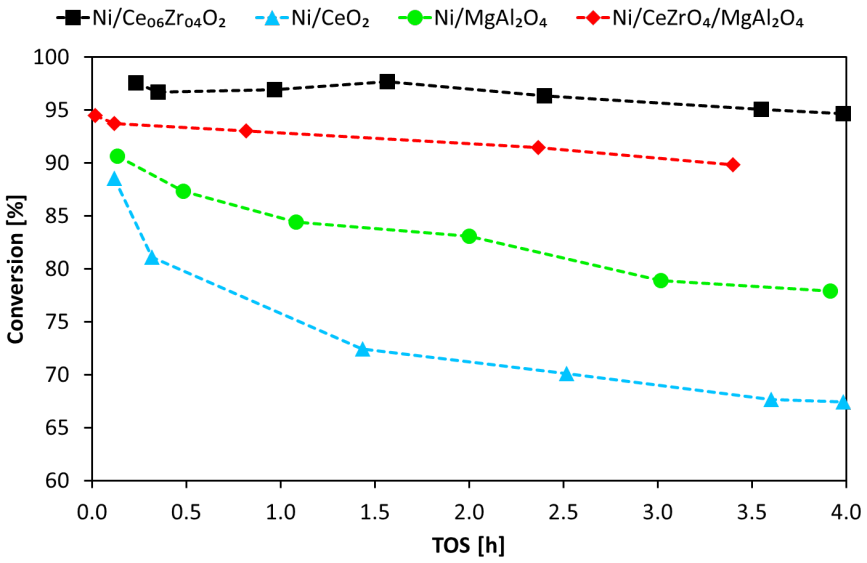

Fig. 3.9: *Conversion as function of time at 580 ℃ for Ni on four different supports. Experimental conditions: S/C: 5.3-6.0, Temp.: 579-585 ℃, $m_{Cat} = 0.50\ g$, Ni loading: 8.0-8.2 wt%, $F_T = 1.5 - 1.6\ NL/min$, $x_{Eth} = 3.2 - 3.5\ vol\%$, $y_{H_2O} = 38.6 - 39.2 vol\%$, N_2 as balance.*

Deactivation in the SR can be ascribed to sintering and carbon deposition [49, 50]. Temperature programmed oxidation of the spent catalysts as well as measurement of surface area and nickel particle size of the spent catalysts were performed to elucidate what caused the deactivation.

The release of carbon oxides during TPO of the spent catalysts is shown in fig. 3.10. It can be seen that the carbon oxides release occurred at different temperatures depending on the support material. $Ni/Ce_{0.6}Zr_{0.4}O_2$ showed carbon oxide release in a broad peak at temperatures between 350 and 580 ℃ while $Ni/MgAl_2O_4$ had a single broad peak with a maximum at 560 ℃. Ni/CeO_2 had two peaks; one around 475 ℃ and a broad one from 550 ℃ to 650 ℃. $Ni/CeZrO_4/MgAl_2O_4$ showed carbon release at three different peak temperatures, 475 ℃, 515 ℃, and 545 ℃. The first coincide with the first peak from Ni/CeO_2, while the last peak coincide with the oxidation from $Ni/MgAl_2O_4$. The results indicate that the carbon was oxidized at different temperatures depending on whether it is located on a redox-active support or on the Ni particles. CeO_2 and $CeZrO_4$ are known as soot oxidation catalysts [202] and therefore these might catalyze the oxidation of carbon at lower temperature compared with $MgAl_2O_4$ or Ni and be responsible for the carbon release at temperatures below 550 ℃.

The results from the TPO experiments can give an indication of which type of carbon was deposited on the catalysts. It has been reported that carbon oxides released below 500

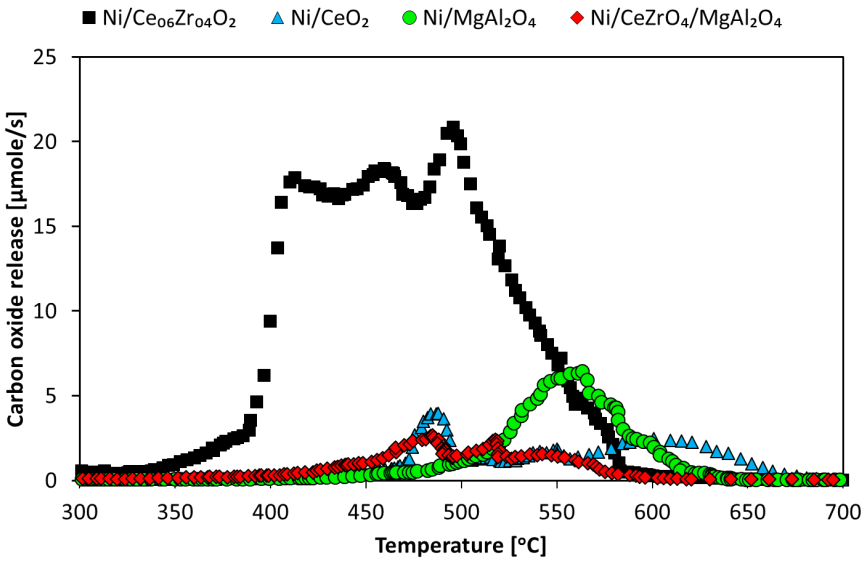

Fig. 3.10: *Carbon oxides release as function of temperature over Ni-based catalysts after 4 h on stream. Experimental conditions: F_T= 0.9-1 NL/min, O_2= 2-3 %, N_2 as balance, heating rate: 10 K/min.*

℃ arises from monoatomic carbon or filamentous carbon like single walled carbon nanotubes, while carbon oxides released above 500 ℃ arises from amorphous carbon with different degrees of graphitization or bulkier forms of carbon nanotubes [119, 211, 212]. The oxidation agent in these studies was O_2. This could indicate that carbon formed on $Ni/Ce_{0.6}Zr_{0.4}O_2$ mainly was monoatomic carbon or single walled nanotubes, while the carbon formed on $Ni/MgAl_2O_4$ was amorphous carbon. On Ni/CeO_2 it appears that both types of carbon are formed as two peaks are observed. However due to the catalytic properties of CeO_2 and $CeZrO_4$ in carbon oxidation the above limits might not apply.

TEM-images of the spent catalysts were acquired to investigate this further. Figure 3.11(a) and 3.11(b) shows TEM images of spent $Ni/Ce_{0.6}Zr_{0.4}O_2$ particles and carbon whiskers can clearly be observed. This can, to some extent, explain the stable activity of this catalyst as the Ni particles will be able to catalyze the SR reactions despite carbon deposition [40, 41]. A TEM image of a spent $Ni/MgAl_2O_4$ catalyst can be seen in fig. 3.11(c). Analysis of this image and other images did not reveal carbon whiskers, which could indicate that the carbon was mainly present as amorphous or encapsulating carbon.

Tab. 3.4: *Conversion and carbon deposition during a 4 h experiment at approx. 600 ℃ over $Ni/Ce_{0.6}Zr_{0.4}O_2$ and $Ni/MgAl_2O_4$. Experimental conditions: S/C: 5.3-6.0, Temp.: 579-585 ℃, m_{Cat} = 0.50 g, Ni loading: 8.0-8.2 wt%, F_T = 1.5 − 1.6 NL/min, x_{Eth}=3.2-3.5 %, x_{H_2O}=38.6-39.2 %, N_2 as balance.*

Catalyst	Conversion		Carbon deposition	
	Initial	After 4 *h*	$\left[\frac{mmole\ C}{mole\ C_{Feed}}\right]$	$\left[\frac{mg\ C}{g_{Cat} \cdot h}\right]$
$Ni/Ce_{0.6}Zr_{0.4}O_2$	98	95	15.2	96
Ni/CeO_2	89	67	2.9	19
$Ni/MgAl_2O_4$	89	78	4.1	26
$Ni/CeZrO_4/MgAl_2O_4$	95	90	2.2	15

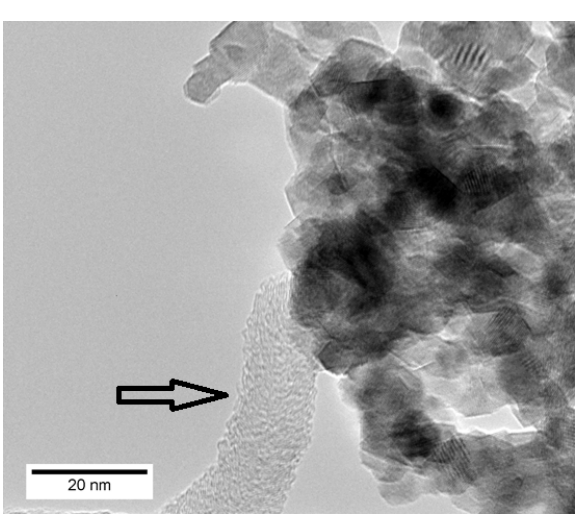

(a) $Ni/Ce_{0.6}Zr_{0.4}O_2$

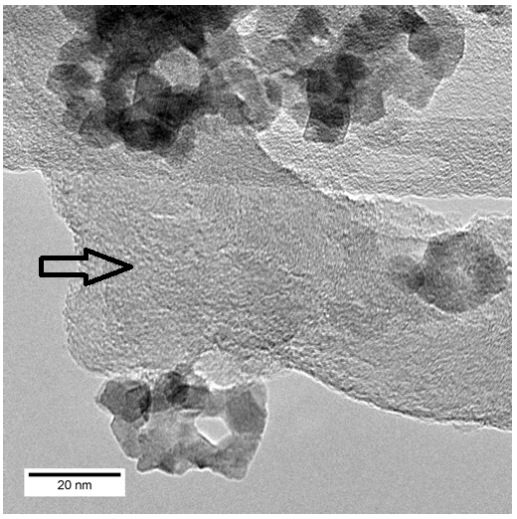

(b) $Ni/Ce_{0.6}Zr_{0.4}O_2$

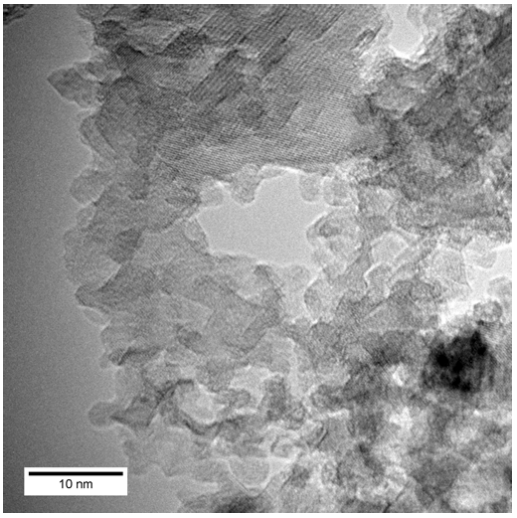

(c) $Ni/MgAl_2O_4$

Fig. 3.11: *TEM images of spent catalysts. Carbon whiskers in fig. (a) and (b) are indicated by an arrow.*

The amount of carbon deposited on each of the catalysts is shown in table 3.4. The highest carbon deposition was observed over $Ni/Ce_{0.6}Zr_{0.4}O_2$, 15.2 $\frac{mmole\ C}{mole\ C_{Feed}}$ or 96 $\frac{mg\ C}{g_{Cat} \cdot h}$, which may seem contradictory to the fact that it remained stable and active over time. However, as discussed above carbon was present as whiskers on this catalyst, which is known not to decrease the catalytic activity [40, 41]. The other catalysts had much lower levels of carbon deposition in the range of 2-4 $\frac{mmole\ C}{mole\ C_{Feed}}$ or 15-26 $\frac{mg\ C}{g_{Cat} \cdot h}$. The results show that adding to $CeZrO_4$ to $Ni/MgAl_2O_4$ decreased carbon deposition from 26 to 15 $\frac{mg\ C}{g_{Cat} \cdot h}$. This decrease could be due to reaction of coke with lattice oxygen from $CeZrO_4$ [202] or due to an increased amount of OH-species on the support. The carbon on $Ni/CeZrO_4/MgAl_2O_4$ was oxidized at a lower temperature compared with $Ni/MgAl_2O_4$, see fig. 3.10, which shows that $CeZrO_4$ catalyzes carbon oxidation in the TPO experiments and will probably also do this under reaction conditions.

Ni/CeO_2, $Ni/MgAl_2O_4$, and $Ni/CeZrO_4/MgAl_2O_4$ had nickel particles with a size of 6-10

nm while $Ni/Ce_{0.6}Zr_{0.4}O_2$ had nickel particles with d_p of 15-20 *nm* (see table 3.1). Therefore the lower amount of carbon on Ni/CeO_2, $Ni/MgAl_2O_4$, and $Ni/CeZrO_4/MgAl_2O_4$ compared with $Ni/Ce_{0.6}Zr_{0.4}O_2$ could be due to smaller Ni particles, which lowers the risk of formation of carbon whiskers [30].

The surface area and NiO-particle size before and after a temperature dependence experiment are shown in table 3.4. The surface area for Ni/CeO_2 and $Ni/Ce_{0.6}Zr_{0.4}O_2$ decreased by a factor of roughly 3 and 2, respectively, and the Ni particle size increased by similar factors. For $Ni/MgAl_2O_4$ and $Ni/CeZrO_4/MgAl_2O_4$ the surface area did not decrease significantly, while the Ni particle size increased by a factor of 1.5 for both catalysts. The change in Ni particle size for all the catalysts showed that sintering did occur. However, the two spinel based catalysts seemed more stable as the BET surface areas and Ni particle size did not change much over a 60-70 *h* experiment.

The results show that all the tested Ni-based catalysts suffer from sintering and carbon deposition to some extent, which led to deactivation. Therefore other changes to the catalyst formulation orprocess based optimization is needed in order to minimize these problems.

Tab. 3.5: *Comparison between BET surface area and XRD Ni particle size before and after a temperature dependence experiment with 60-70 h on stream.*

Catalyst	Surface area		NiO particle size	
	Fresh $[m^2/g]$	Spent $[m^2/g]$	Fresh $[nm]$	Spent $[nm]$
$Ni/Ce_{0.6}Zr_{0.4}O_2$	90	42	15-20	20-28
Ni/CeO_2	113	35	10	27
$Ni/MgAl_2O_4$	69	66	7	11
$Ni/CeZrO_4/MgAl_2O_4$	63	53	6	9

3.4 Effect of temperature on carbon deposition

The carbon deposition and ethene formation as function of temperature in the SR of ethanol at S/C=6 for experiments with 4 *h* on stream over $Ni/MgAl_2O_4$ and $Ni/Ce_{0.6}Zr_{0.4}O_2$ can be seen in fig. 3.12. The experiments for $Ni/Ce_{0.6}Zr_{0.4}O_2$ at 400 ℃ and 500 ℃ were stopped after 2 *h* on stream due to excessive carbon build up causing a large pressure drop over the reactor.

The carbon deposition on both $Ni/MgAl_2O_4$ and $Ni/Ce_{0.6}Zr_{0.4}O_2$ had a maximum at 500 ℃. For $Ni/MgAl_2O_4$ it decreased with temperature from 15 $\frac{mmole\ C}{mole\ C_{Feed}}$ to 0.03 $\frac{mmole\ C}{mole\ C_{Feed}}$ (94 to 0.2 $\frac{mg\ C}{g_{Cat} \cdot h}$) when increasing the temperature from 506 to 741 ℃. For $Ni/Ce_{0.6}Zr_{0.4}O_2$ a decrease from 88 $\frac{mmole\ C}{mole\ C_{Feed}}$ to 0.06 $\frac{mmole\ C}{mole\ C_{Feed}}$ (552 to 0.4 $\frac{mg\ C}{g_{Cat} \cdot h}$) in carbon deposition was observed when increasing the temperature from 495 to 755 ℃. The peak release of carbon oxides over $Ni/MgAl_2O_4$ during TPO occurred at 520 ℃ after operating at 400 ℃ while carbon oxides release after operating at 700 ℃ occurred at 600 ℃. For $Ni/Ce_{0.6}Zr_{0.4}O_2$ an additional carbon oxides release peak at 630 ℃ was observed after operation at 700 ℃ and 750 ℃. The shift in carbon oxide release toward higher temperatures during TPO indicated that the carbon deposited at low temperatures had a lower degree of graphitization and was more reactive. Furthermore, other routes to carbon deposition like thermal decomposition of ethanol may become important with increasing temperatures and led to other types of carbon deposition causing the observed shift.

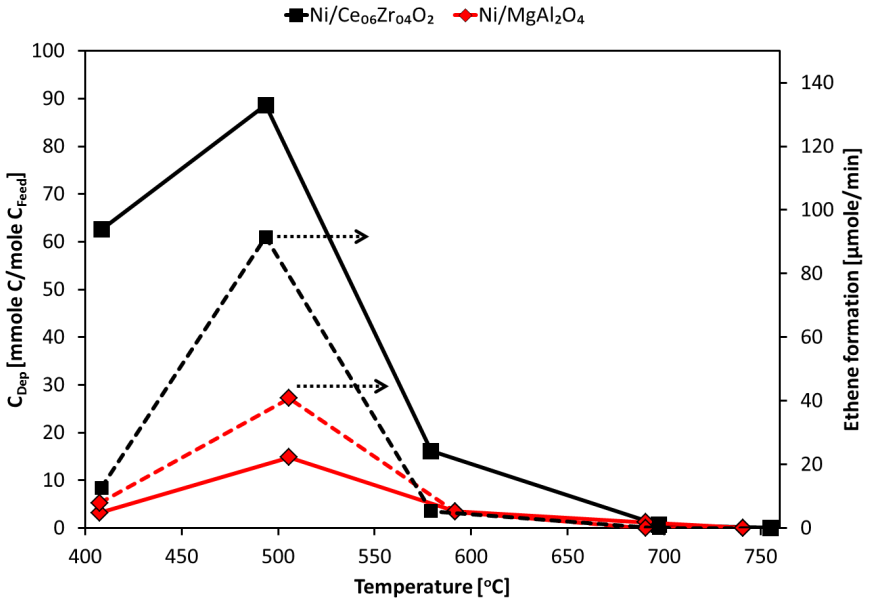

Fig. 3.12: *Carbon deposition and ethene formation after 4 h on stream as function of temperature over $Ni/MgAl_2O_4$ and $Ni/Ce_{0.6}Zr_{0.4}O_2$. Full lines: Carbon deposition; Dashed lines: Ethene formation. The experiments at 400 and 500 ℃ for $Ni/Ce_{0.6}Zr_{0.4}O_2$ were stopped after 2 h due to risk of blockage. Experimental conditions: S/C: 5.5-6.2, Temp: 408-755 ℃, $m_{Cat} = 0.50$ g, Ni loading: 8.1-8.2 wt%, $F_T = 1.5$ NL/min, $y_{Eth} = 3.2 - 3.6$ vol%, $y_{H_2O} = 38.8 - 39.0$ vol%, N_2 as balance.*

The formation of ethene as function of temperature had a maximum at 500 ℃ and at low temperatures were significantly higher for $Ni/Ce_{0.6}Zr_{0.4}O_2$ compared to $Ni/MgAl_2O_4$, see fig. 3.12. The maximum in carbon deposition over both catalysts coincide with the maximum of formation of ethene, which is a very potent coke precursor [43, 192]. This could explain the high deposition of carbon at 500 ℃. Thermodynamic analysis using the measured and thermodynamic equilibrium offgas composition (Rostrup-Nielsen and Christiansen [42]) did not show potential for carbon formation from methane decomposition, Boudouard reaction, or CO decomposition at 500 ℃. However, at 400 ℃ there is affinity for carbon formation through methane decomposition. The affinity for carbon formation through the different reactions as function of temperature is described in Appendix B.

The decrease in carbon deposition with increasing temperature could also be explained by an increased reaction rate for the SR reactions leading to fewer carbon-species on the surface of the catalysts. Furthermore the gasification of deposited carbon by either steam or CO_2 will increase with temperature as well. At the lowest temperature of 400 ℃ ethanol may not be activated and therefore conversion and carbon deposition are lower. In fig. 3.4, there was observed a large drop in conversion at 400 ℃ over time, even larger than at 500 ℃, where carbon deposition was more severe. An explanation could be partial oxidation of the catalyst at 400 ℃ caused by the high concentration of steam and low concentration of H_2.

Results from thermodynamic and experimental studies of the SR of ethanol predict a decrease in carbon deposition with temperature [53, 64, 74, 213, 214]. Similar to this study, Wang et al. [210] found a maximum in carbon deposition at 500 ℃ for SR of ethanol over a Co/CeO_2 catalyst. Wang et al. [210] ascribed the high carbon formation to disproportionation of CO and CH_4 and a slow reaction rate for steam and dry reforming. Another and perhaps more likely explanation could be a formation of carbon from ethene, as indicated in fig. 3.12.

An interesting difference between $Ni/MgAl_2O_4$ and $Ni/Ce_{0.6}Zr_{0.4}O_2$ was found in the product distribution at 750 ℃ where $Ni/MgAl_2O_4$ completely converted ethanol to carbon oxides while $Ni/Ce_{0.6}Zr_{0.4}O_2$ still had small amounts of methane in the offgas. Furthermore, a slight loss in both methane SR and WGS activity with time over $Ni/Ce_{0.6}Zr_{0.4}O_2$ was observed at 755 ℃, whereas $Ni/MgAl_2O_4$ was stable over time (the experiment had a run time of 4 h).

A drawback of running at high temperatures is that sintering is more likely to occur. Therefore the surface area of the spent catalysts was measured to investigate how severe the sintering was and the results are shown in table 3.6. It can be seen that no sintering of the catalysts took place at temperatures between 500 ℃ and 700 ℃, while at roughly 750 ℃ sintering increased and the surface area decreased.

Tab. 3.6: *Surface area of $Ni/Ce_{0.6}Zr_{0.4}O_2$ and $Ni/MgAl_2O_4$ after 4 h on stream at different temperatures. Experimental conditions: S/C: 5.5-6.2, Temp: 408-755 ℃, m_{Cat} = 0.50 g, Ni loading: 8.1-8.2 wt%, $F_T = 1.5\ NL/min$, $y_{Eth} = 3.2 - 3.6$ vol%, $y_{H_2O} = 38.8 - 39.0$ vol%, N_2 as balance.*

Catalyst	Fresh	400 ℃	500 ℃	600 ℃	700 ℃	750℃
$Ni/Ce_{0.6}Zr_{0.4}O_2$	88	-	-	67	67	53
$Ni/MgAl_2O_4$	69	66	61	61	60	53

3.5 Effect of additives

Steam reforming of ethanol at 600 ℃ and S/C-ratio of 6 for 4 h and subsequent determination of carbon deposition was conducted for $Ni/MgAl_2O_4$ promoted with K, CeO_2, ZrO_2, or mixtures hereof to evaluate whether these additives could have a beneficial effect on the catalyst performance. The surface area, NiO particle size, additive- and Ni-loading for the promoted catalysts can be seen in table 3.1. The additives did not significantly influence Ni-particle size or surface area and therefore the changes in catalytic performance can be ascribed to the properties of the additives.

The conversion as function of time for the different $Ni/MgAl_2O_4$ catalysts can be seen in fig. 3.13. The conversion was high and relatively stable for the catalysts promoted with K, CeO_2-K, $CeZrO_4$, and $K/CeZrO_4$. The base catalyst, $Ni/MgAl_2O_4$, behaved as shown previously with a decrease in conversion over the entire 4 h while the catalyst with CeO_2 had an induction period of 1 h before reaching a stable conversion in the range of 85 %. In conclusion adding CeO_2, K, or $CeZrO_4$ seem to promote a more stable performance of the catalyst.

The product distributions were similar for the base and promoted $Ni/MgAl_2O_4$ and above 95 % of converted ethanol was converted to carbon oxides and H_2, and less than 5 % to methane and ethene. However, a slight increase in the yield of CH_4 was observed for the promoted catalysts compared with $Ni/MgAl_2O_4$. The yield of ethene can be seen in fig. 3.14 and was similar for the base case and most of the promoted catalysts. Two exceptions were for $Ni/K\text{-}CeO_2/MgAl_2O_4$, which had no ethene in the offgas, and $Ni/CeO_2/MgAl_2O_4$, which had a higher yield of ethene.

The effect of tested additives on conversion, yield of ethene, and carbon deposition are shown in fig. 3.14. All of the additives improved the catalyst performance either with respect to conversion, carbon deposition, or in most of the cases both. Promotion with CeO_2 led to the lowest carbon deposition of 0.9 $\frac{mmole\ C}{mole\ C_{Feed}}$ or 6 $\frac{mg\ C}{g_{Cat} \cdot h}$ while the conversion was similar

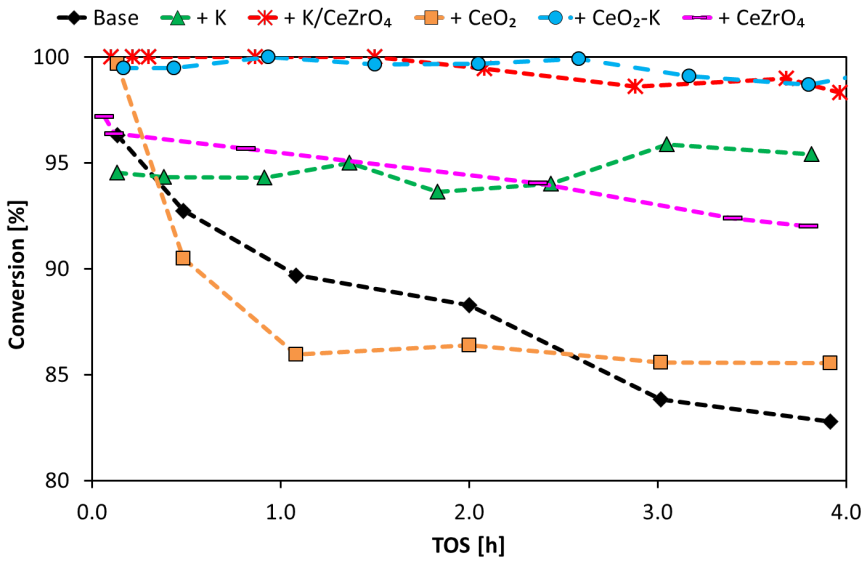

Fig. 3.13: *Conversion as function of time on stream for $Ni/MgAl_2O_4$ and $Ni/MgAl_2O_4$ promoted with CeO_2, CeO_2-K, $CeZrO_4$, K, and K-$CeZrO_4$. Experimental conditions: S/C: 5.6-6.1, Temp.: 579-592 °C, $m_{Cat} = 0.50\ g$, Ni loading: 8.0-8.3 wt%, $F_T = 1.5\ NL/min$, $y_{Eth} = 3.2 - 3.6\ vol\%$, $y_{H_2O}y = 38.8 - 39.0\ vol\%$, N_2 as balance.*

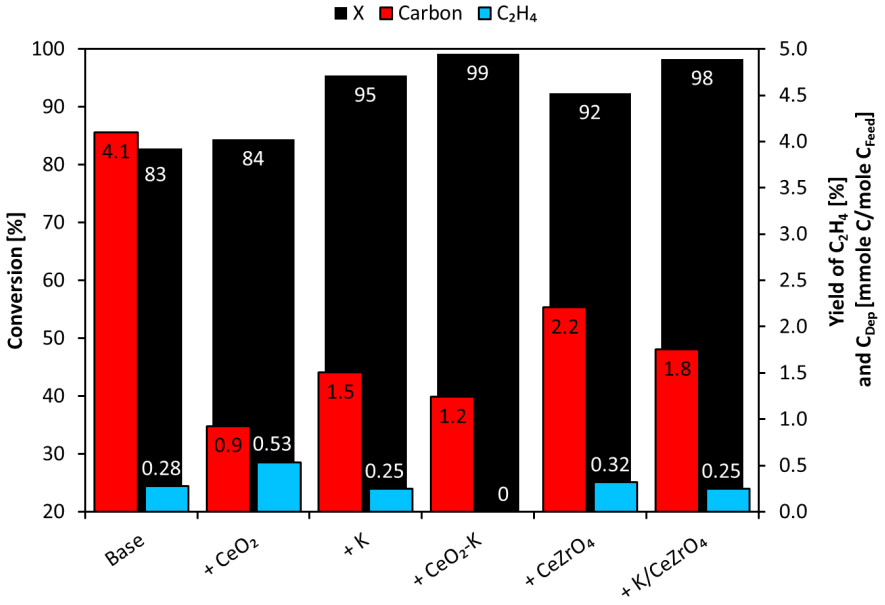

Fig. 3.14: *Comparison of conversion, carbon deposition, and yield of ethene after 4 h on stream for $Ni/MgAl_2O_4$-catalysts with different additives. Experimental conditions: S/C: 5.6-6.1, Temp.: 579-592 °C, $m_{Cat} = 0.50\ g$, Ni loading: 8.0-8.3 wt%, $F_T = 1.5\ NL/min$, $y_{Eth} = 3.2 - 3.6\ vol\%$, $y_{H_2O} = 38.8 - 39.0\ vol\%$, N_2 as balance.*

to the base case. Ni/CeO_2 had the lowest activity of the four tested support materials and sintered quite significantly, however it did show low carbon deposition. The higher conversion of ethanol over Ni-$CeO_2/MgAl_2O_4$ compared to Ni/CeO_2, as well as an improved stability could be explained by a stabilization of the CeO_2 on $MgAl_2O_4$ so sintering decreased (see fig.

3.9 and 3.13). The decrease in carbon deposition might be explained by ceria monomers or small CeO_2 particles on $MgAl_2O_4$, which facilitated oxidation of surface carbon during SR.

Ni-K/$MgAl_2O_4$ also showed a decrease in carbon deposition and as well as an increased conversion compared with the base case. Therefore K and CeO_2 both seem to influence the catalyst by enhancing oxidation/gasification or decreasing deposition of solid carbon while K also induces a higher activity. Similar trends have been reported by others [82, 122]. Adding both CeO_2 and K to the base catalyst improved the conversion while carbon deposition was on a level between adding either only K or only CeO_2. The promotion with $CeZrO_4$ also increased conversion, but carbon deposition was the highest among the promoted catalysts, albeit still significantly lower than the base Ni/$MgAl_2O_4$ catalyst. The increase in conversion when adding $CeZrO_4$ could be due to increased water dissociation or spill-over effects, as mentioned earlier. The Ni/K-CeO_2/$MgAl_2O_4$ seems to be the most interesting catalyst as it combined a high conversion with a low rate of carbon deposition.

The decrease in carbon deposition was not due to changes in ethene formation and therefore it appears the role of the additives is to increase the rate of SR reactions and hereby minimize the carbon deposition.

Tab. 3.7: *Conversion and carbon deposition in SR of ethanol after 4 h on stream over Ni/K-CeO_2/$MgAl_2O_4$ and Ni-K/$CeZrO_4$/$MgAl_2O_4$ at different space velocities. Experimental conditions: S/C: 5.6-6.1, Temp.: 579-592 °C, $m_{Cat} = 0.264 - 0.50$ g, Ni loading: 8.2 wt%, $F_T = 1.5$ NL/min, $y_{Eth} = 3.2 - 3.5$ vol%, $y_{H_2O} = 38.8 - 39.0$ vol%, N_2 as balance.*

Catalyst	WHSV $[h^{-1}]$	Conversion [%]	Carbon deposition $\left[\frac{mmole\ C}{mole\ C_{Feed}}\right]$	Carbon deposition $\left[\frac{mg\ C}{h}\right]$	$Y_{C_2H_4}$ [%]
Ni/K-CeO_2	13	98	1.2	4	0.00
Ni/K-CeO_2	25	81	1.3	4	0.28
Ni-K/$CeZrO_4$	12	100	1.8	5	0.24
Ni-K/$CeZrO_4$	25	81	1.5	5	0.59

Ni/K-CeO_2/$MgAl_2O_4$ and Ni-K/$CeZrO_4$/$MgAl_2O_4$ both showed almost full conversion and to ensure that the low carbon deposition was due to the additives and not full conversion the experiments were repeated at a higher space velocity. The results from the experiments at different space velocities are shown in table 3.7. The results show interestingly that the same amount of carbon was deposited at the higher space velocity with conversion around 80 % and this shows that the additives do decrease the carbon deposition in the case of Ni/K-CeO_2/$MgAl_2O_4$ and Ni-K/$CeZrO_4$/$MgAl_2O_4$ also under more demanding conditions. The yield of ethene increased slightly with increasing space velocity, however it did not seem to influence the carbon deposition significantly. The carbon deposition seemed to be more dependent on temperature compared to space velocity as the increasing the space velocity did not influence the total amount of carbon deposition.

Carbon burn-off experiments were also carried for the Ni/$MgAl_2O_4$ catalysts with the different additives. The carbon oxides release as function of temperature over the promoted catalysts are shown in fig. 3.15. The carbon oxides release for the promoted catalysts shifted toward lower temperatures, which indicates that combustion and also gasification is catalyzed by K as well as ZrO_2 and CeO_2. However, the difference could also be due to different types

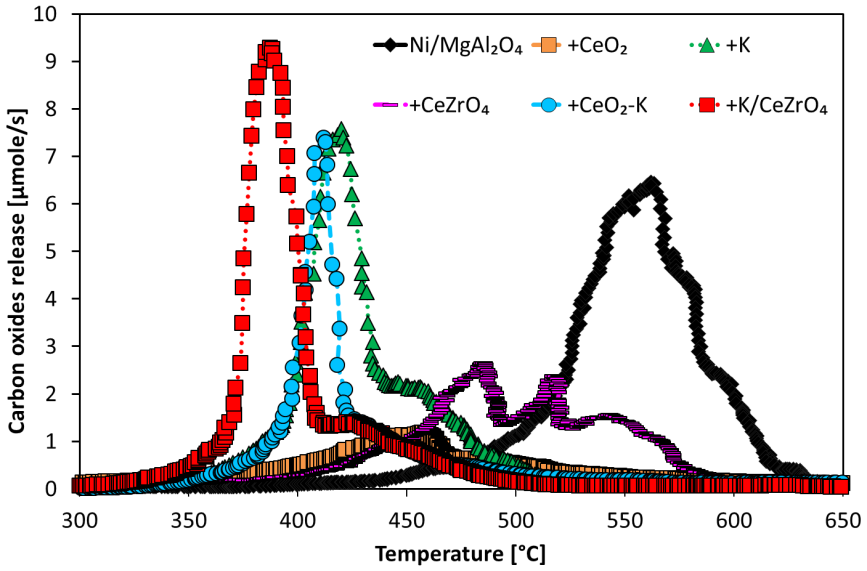

Fig. 3.15: *Release of carbon oxides as function of temperature over promoted $Ni/MgAl_2O_4$ catalysts after 4 h on stream. Experimental conditions: F_T= 0.9-1 NL/min, O_2= 2-3 %, N_2 as balance, heating rate: 10 K/min.*

of carbon on the catalysts. The catalyzing effects of K, CeO_2, and ZrO_2 on combustion and gasification is known from the combustion and gasification literature [202, 215, 216]. This is also a contributing factor to the lowering of carbon deposition as well as the increase in activity observed in this study.

3.5.1 Effect of TOS

Two of the catalysts with additives, Ni-K/$MgAl_2O_4$ and Ni/CeO_2-K/$MgAl_2O_4$, which showed a rather stable conversion with time and a low rate of carbon deposition, were tested for an extended period of time (24 *h*) to further investigate stability and carbon deposition. The conversion and yield of hydrocarbons as function of time for Ni-K/$MgAl_2O_4$ and Ni/CeO_2-K/$MgAl_2O_4$ can be seen in fig. 3.16. The conversion over both catalysts decreased slowly with time with a rate of roughly 0.1 %-point pr. *h*. Furthermore the yield of hydrocarbons increased with time and a more pronounced increase was observed after 20 *h* on stream. No ethene was detected in the effluent from SR of ethanol over Ni/CeO_2-K/$MgAl_2O_4$, while the yield of ethene increased from 0.10 % to 0.16 % over Ni-K/$MgAl_2O_4$. Therefore deactivation was apparent even though the first four *h* on stream appeared stable. However the decrease in conversion with time was more pronounced for Ni/$MgAl_2O_4$ and therefore the additives still provided a marked improvement.

The amount of carbon formed after 24 *h* on stream was determined and the total carbon deposition and the average rate of carbon formation at different times can be seen in table 3.8. The carbon deposition over Ni-K/$MgAl_2O_4$ and Ni/CeO_2-K/$MgAl_2O_4$ was quite similar after 4 *h*, however the buildup of carbon after 24 *h* was lower for Ni/CeO_2-K/$MgAl_2O_4$. This could indicate that CeO_2 has a positive effect on the carbon deposition even during longer periods of operation. The TPO profiles moved towards higher temperatures after 24 *h* on stream and for Ni/CeO_2-K/$MgAl_2O_4$ a shoulder at 475 °C increased with time, which could indicate that the type of carbon deposition changes with time

TEM-images of spent Ni-K/$MgAl_2O_4$ and Ni/CeO_2-K/$MgAl_2O_4$ can be seen in fig. 3.17. These images show that carbon whiskers were formed on both catalysts. Carbon whiskers can,

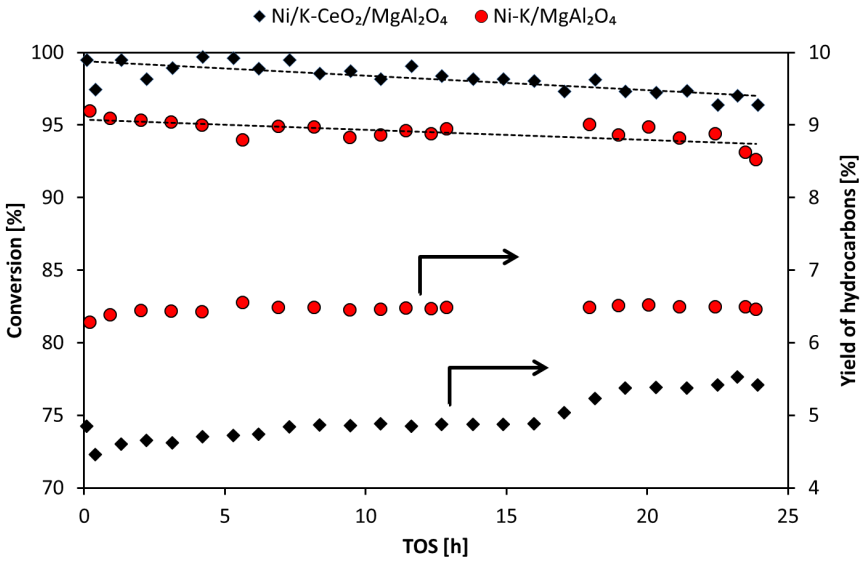

Fig. 3.16: *Conversion and yield of hydrocarbons as function of time for Ni-K/$MgAl_2O_4$ and Ni/CeO_2-K/$MgAl_2O_4$. Experimental conditions: S/C: 6, Temp.: 576 ℃, m_{Cat} = 0.50 g, Ni loading: 8.0-8.3 wt%, F_T = 1.5 NL/min, y_{Eth} = 3.3 vol%, y_{H_2O} = 40.1 vol%, N_2 as balance.*

Tab. 3.8: *Total carbon deposition and average rate of formation on Ni-K/$MgAl_2O_4$ and Ni/CeO_2-K/$MgAl_2O_4$ as function of time at 600 ℃. Average values are from intervals from 0-4 h and 4-24 h. Experimental conditions: S/C: 6.0, Temp: 579-586 ℃, $m_{Cat} = 0.50$ g, Ni loading: 8.2 wt%, $F_T = 1.5-1.6$ NL/min, $y_{Eth} = 3.7-3.9$ vol%, $y_{H_2O} = 38.9$ vol%, N_2 as balance.*

Catalyst	Time $[h]$	Total C_{Dep} $[mg\ C]$	Carbon deposition $\left[\frac{mg\ C}{g_{Cat} \cdot h}\right]$	$\left[\frac{mmole\ C}{mole\ C_{Feed}}\right]$
Ni-K/$MgAl_2O_4$	4	20	8.4	1.2
Ni-K/$MgAl_2O_4$	24	44	2.7	0.4
Ni/CeO_2-K/$MgAl_2O_4$	4	17	9.8	1.5
Ni/CeO_2-K/$MgAl_2O_4$	24	33	3.7	0.6

with time, break the catalyst pellets causing pressure drop over the catalyst bed, which can be detrimental for industrial units, due to mal distribution of the gas causing local hot spots [42].

The surface area and nickel particle size before and after a 24 h experiment at 600 ℃ can be seen in table 3.9. The surface area of the catalysts did not change during 24 h operation at 600 ℃. However, the NiO particle size increased from 7 to 12 nm for Ni-K/$MgAl_2O_4$ and from 6 to 9 nm for Ni/CeO_2-K/$MgAl_2O_4$, which indicate sintering of the Ni-particles for both of the catalysts. Sintering due to the TPO might also account for some of the observed sintering as O_2 is known to promote sintering [217].

3.6 Sulfur addition

Sulfur addition was investigated on Ni-CeO_2/$MgAl_2O_4$ to test if coverage of part of the Ni particles by sulfur could decrease the carbon deposition. Sulfur might lower the carbon depo-

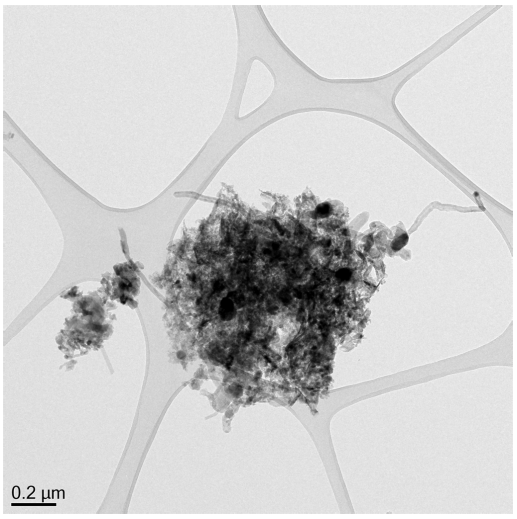

(a) Ni-K/$MgAl_2O_4$ at 9900 times magnification

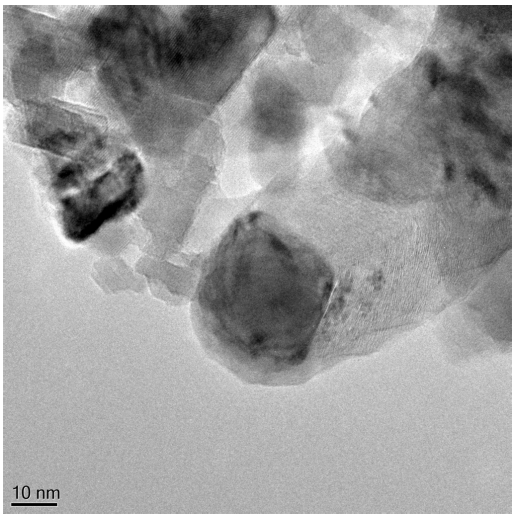

(b) Ni-K/$MgAl_2O_4$ at 95000 times magnification

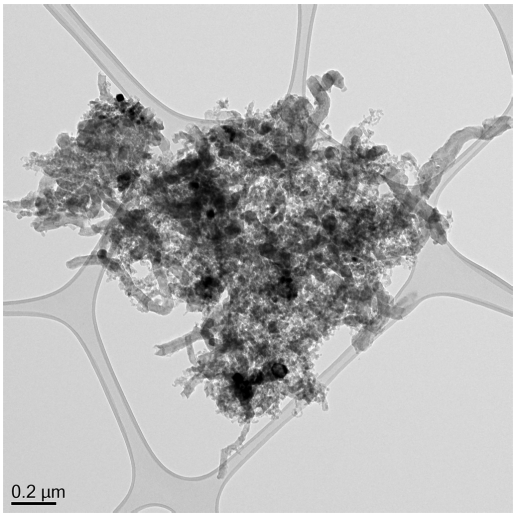

(c) Ni/CeO_2-K/$MgAl_2O_4$ at 9900 times magnification

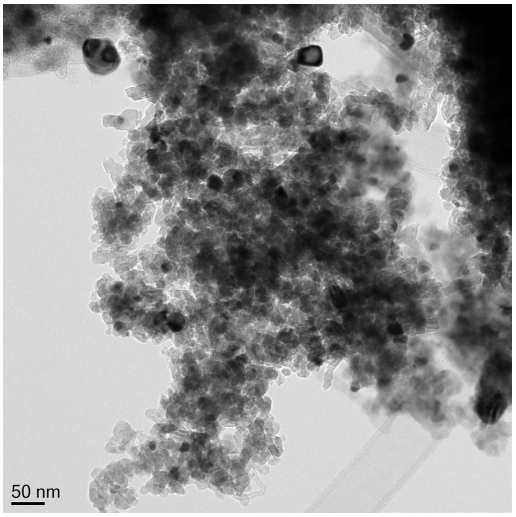

(d) Ni/CeO_2-K/$MgAl_2O_4$ at 29000 times magnification

Fig. 3.17: *TEM images of spent Ni-K/$MgAl_2O_4$ and Ni/CeO_2-K/$MgAl_2O_4$ after 24 h on stream in the SR of ethanol at 600 °C and a S/C-ratio of roughly 6.*

Tab. 3.9: *Comparison between BET surface area and XRD Ni particle size for Ni-K/$MgAl_2O_4$ and Ni/CeO_2-K/$MgAl_2O_4$ before and after a stability experiment with 24 h on stream at 600 °C.*

Catalyst	Surface area		NiO particle size	
	Fresh $[m^2/g]$	Spent $[m^2/g]$	Fresh $[nm]$	Spent $[nm]$
Ni-K/$MgAl_2O_4$	55	55	7	12
Ni/CeO_2-K/$MgAl_2O_4$	54	54	6	9

sition by covering the step sites which are active in carbon deposition and hereby decrease the formation of solid carbon or the presence of sulfur might limit the size of carbon islands and

inhibit the formation of carbon whiskers [41, 42]. A sulfur coverage of roughly 13 % (0.06 *wt*% S) on Ni-$CeO_2/MgAl_2O_4$ was achieved by impregnation with an aqueous solution of K_2SO_4 or H_2SO_4 to test if a decrease in carbon deposition could be achieved and how the conversion and product distribution would be influenced by sulfur, or sulfur and potassium. The sulfur and potassium content of fresh and spent catalysts was determined by ICP-OES. The sulfur content of a $Ni/MgAl_2O_4$-catalyst impregnated with K_2SO_4, nominal content: 0.03 *wt*% S (300 *ppmw* S), before and after an experiment was 245 *ppmw* S before and 260 *ppmw* S after an experiment. Therefore the sulfur impregnated on catalysts remained there after heating, reduction, steam reforming, and oxidation.

The sulfur content was determined for a spent catalyst impregnated with H_2SO_4 and it was 690 *ppmw* S, compared with the calculated amount of 600 *ppmw* S. The sulfur and potassium content of the spent catalyst with 300 *ppmw* and and 700 *ppmw* K was determined to be 530 *ppmw* S and 920 *ppmw* K, so a bit higher than expected. Thus neither sulfur nor potassium were lost from the catalyst during calcination or reduction.

Tab. 3.10: *Conversion, yield of hydrocarbons, and carbon deposition for $Ni/CeO_2/MgAl_2O_4$ with different S-sources and without sulfur addition. The nominal sulfur coverage was 13 % or 0.06 wt% S. TOS: 4 h. Experimental conditions: S/C: 5.7-6.0, Temp: 586-588 °C, m_{Cat} = 0.50 g, Ni loading: 8.2 wt%, F_T = 1.5 NL/min, y_{Eth} = 3.3 − 3.4 vol%, y_{H_2O} = 38.8 − 39.0 vol%, N_2 as balance.*

Catalyst	Type	Conversion [%]	$Y_{C_yH_x}$ [%]	Carbon deposition $\left[\frac{mg\ C}{g_{Cat}\cdot h}\right]$	Carbon deposition $\left[\frac{mmole\ C}{mole\ C_{Feed}}\right]$
$Ni/CeO_2/MgAl_2O_4$		85	2.9	6.0	9.3
$Ni/CeO_2/MgAl_2O_4$	K_2SO_4	89	9.5	2.2	3.4
$Ni/CeO_2/MgAl_2O_4$	H_2SO_4	85	11.6	3.3	5.1

The conversion, yield of hydrocarbons, and carbon deposition with and without sulfur are presented in table 3.11. An increase in conversion and yield of hydrocarbons, and a decrease in carbon deposition upon sulfur addition by K_2SO_4 was observed. The increase in conversion was unexpected as sulfur is known to inhibit SR due to blockage of surface sites on the Ni particles. Therefore the effect of K was investigated by adding the sulfur in the form of H_2SO_4. Potassium can influence the catalytic performance and increase conversion as shown in section 3.5 as well as by others [82, 122]. Table 3.11 shows that impregnation with H_2SO_4 induced a decrease in carbon deposition and a larger increase in yield of hydrocarbons compared with K_2SO_4, but the conversion was similar to the base case. Therefore, the increased conversion might be ascribed to the presence of potassium and it also appears that K induces a lower yield of hydrocarbon. This was also reported by Hu and Lu [82], who investigated the effect of potassium on Ni/Al_2O_3 in the SR of acetic acid. The increase in the yield of hydrocarbons compared with the base catalyst can be interpreted as a decrease in activity as the hydrocarbons were not converted to the same extent. The hydrocarbons were 95 % CH_4 and 5 % C_2H_4. Interestingly, the amount of ethene formed was highest with sulfur present so the decrease in carbon deposition cannot be ascribed to a decrease in the ethene formation.

The product yields and conversion as function of time over Ni-$CeO_2/MgAl_2O_4$ impregnated with 0.06 *wt*% S by either H_2SO_4 or K_2SO_4 as impregnation agent can be seen in fig. 3.18(a) and 3.18(b). The catalysts impregnated with either H_2SO_4 or K_2SO_4 showed quite stable conversion and product distribution with time on stream. A slight increase in the yield of ethene with time was observed Ni-$CeO_2/MgAl_2O_4$ impregnated with H_2SO_4.

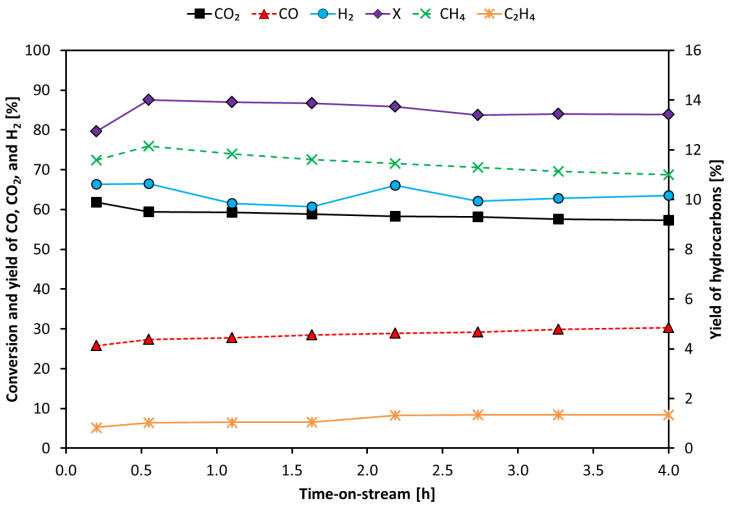

(a) $Ni/CeO_2/MgAl_2O_4$ impregnated with H_2SO_4

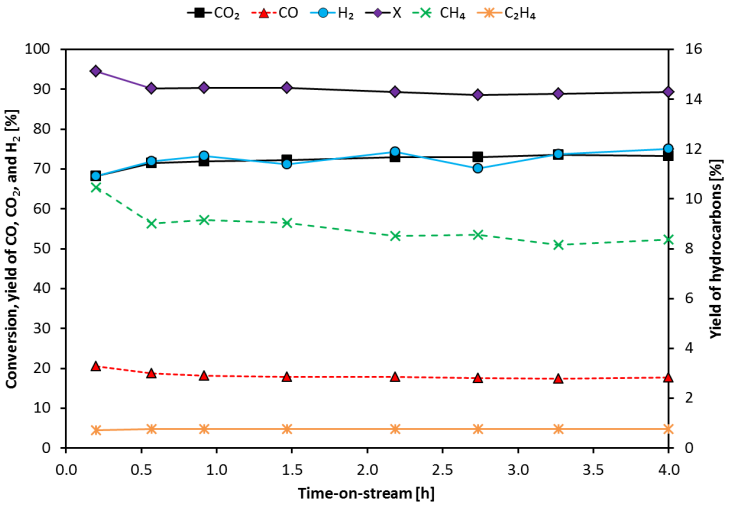

(b) $Ni/CeO_2/MgAl_2O_4$ impregnated with K_2SO_4

Fig. 3.18: *Yield of CO, CO_2, CH_4, C_2H_4, and H_2 and conversion as function of time-on-stream in the SR of ethanol at 600 ℃ for sulfur impregnated catalysts. Experimental conditions: S/C: 5.7-6.0, Temp: 586-588 ℃, m_{Cat} = 0.50 g, Ni loading: 8.1-8.2 wt%, S loading: 0.06 wt%, F_T = 1.5 NL/min, y_{Eth} = 3.3 − 3.4 vol%, y_{H_2O} = 38.8 − 39.0 vol%, N_2 as balance.*

Catalysts with a sulfur loading of 0.03 *wt%*, 0.06 *wt%*, and 0.12 *wt%* were synthesized by impregnation with K_2SO_4 to investigate the influence of the amount of sulfur on the catalytic performance and the results of these tests are shown in table 3.11. It was found that the yield of hydrocarbons increased while the yield of H_2 decreased with increasing amounts of sulfur on the catalysts. All of the sulfur treated catalysts showed a relatively stable conversion during the 4-hour experiments. This shows that sulfur does inhibit especially conversion of methane and ethene to carbon oxides and H_2. The carbon deposition is lower with sulfur than without in the three cases investigated with a minimum at 0.03 *wt%* S. These results indicate that addition of small amounts of sulfur can be used to block sites on the catalyst and hereby inhibit carbon deposition. The loss in activity due to sulfur can mainly be seen

as an increase in the yield of hydrocarbons. Bengaard et al. [38] have shown that the SR of CH_4 has a lower energy barrier on step sites and blockage of these sites will lead to a lower conversion of methane. This entails a lower amount of carbon species on the surface and a lower risk of carbon deposition due to slower nucleation of carbon whiskers or agglomeration of carbon deposits. Similar to the observations in this study.

Tab. 3.11: *Conversion, yield of H_2, yield of hydrocarbons, and carbon deposition in SR of ethanol over $Ni/CeO_2/MgAl_2O_4$ with different degrees of sulfur coverage. Sulfur added as K_2SO_4. TOS: 4 h. Experimental conditions: S/C: 5.7-6.0, Temp: 586-588 °C, m_{Cat} = 0.50 g, Ni loading: 8.1-8.2 wt%, F_T = 1.5 NL/min, y_{Eth} = 3.3 − 3.4 vol%, y_{H_2O} = 38.8 − 39.0 vol%, N_2 as balance.*

Sulfur [$wt\%$ S]	S-coverage [%]	Conversion [%]	Carbon deposition $\left[\frac{mg\ C}{g_{Cat} \cdot h}\right]$	Carbon deposition $\left[\frac{mmole\ C}{mole\ C_{Feed}}\right]$	Y_{H_2} [%]	$Y_{C_yH_x}$ [%]
0	0	85	6.0	9.3	80	3.5
0.03	6	90	1.2	1.5	74	6.2
0.06	13	89	2.2	3.4	73	9.5
0.12	26	89	2.4	3.4	64	12.7

3.7 Conclusions

In this work the SR of ethanol was investigated over Ni-based catalysts and several strategies for minimizing carbon deposition by changing the catalyst formulation were explored. The main conclusions are:

- Carbon deposition and sintering leading to loss af activity was apparent in SR of ethanol for Ni supported on different carriers including CeO_2, $Ce_{0.6}Zr_{0.4}O_2$, $MgAl_2O_4$, and $CeZrO_4/MgAl_2O_4$.
- Carbon deposition was most severe at 500 °C most likely due to a high fraction of ethene in the product gas which is a known as a severe carbon precursor. Increasing the temperature to 700 °C or above significantly decreased the carbon deposition.
- Promotion of $Ni/MgAl_2O_4$ with K, CeO_2, and ZrO_2 increased the conversion and lowered the carbon deposition by factors of 2-4. These catalysts appeared very stable over 4 hours of operation. Potassium most likely partly blocks the sites of carbon formation, while the redox-active promoters increase the OH availability on the catalyst and/or provide lattice oxygen for reaction with carbon precursors.
- Experiment over 24 h with Ni/CeO_2-$K/MgAl_2O_4$ and Ni-$K/MgAl_2O_4$ catalysts, however, did showed a slow decrease in activity with time accompanied with carbon deposition with a rate of 0.8-1.2 mg C/h. The carbon formed after 24 h was partly as carbon whiskers, which can be detrimental for SR reactors.
- Selective poisoning with sulfur in the form of SO_4 to Ni-$CeO_2/MgAl_2O_4$ led to a decrease in carbon deposition as well as the overall activity of the catalyst, probably due to blockage of step sites on the Ni-particles. The lowest carbon deposition rate over 4 hours of operation of all the tested catalysts was obtained for the Ni-$CeO_2/MgAl_2O_4$ catalyst with 0.03 $wt\%$ S added in the form of K_2SO_4.

The results show that it is possible to improve the stability and activity of Ni-based catalysts in steam reforming of oxygenated species by suitable promoters. Nevertheless carbon formation still takes place which indicates that other, process related means are needed as well for long term operation.

4. STEAM REFORMING OF ETHANOL: EFFECT OF FEED COMPOSITION ON CATALYST STABILITY

Carbon deposition, leading to catalyst deactivation, is major hurdle for the SR of bio-oil and oxygenates, as mentioned above. The previous chapter dealt with optimization of catalyst formulation in order to minimize the carbon deposition, but this could not completely eliminate carbon deposition. Therefore other options for minimizing carbon deposition and inducing a stable performance of the catalyst, like changing the feed composition, is investigated. In this chapter, the addition of H_2, O_2, and H_2O to the feed gas in SR of ethanol has been tested systematically to elucidate the effects on carbon deposition, conversion, and product yields.

Oxidative SR can be used to decrease carbon deposition as oxygen may react with carbon or carbon precursors on the surface of the catalysts. However, oxidative conditions will increase the formation of CO_2 and decrease the H_2-production [54, 67, 157, 158, 166–168, 197, 200, 218]. Among others Cavallaro et al. [63] reported a decrease in carbon deposition from 0.28 $mg/(g_{Cat} \cdot h)$ to 0.01 $mg/(g_{Cat} \cdot h)$ at 650 ℃ and S/C-ratio of 4.2 over Rh/Al_2O_3 when adding O_2 to the feed gas at a O/C-ratio of 0.4. No carbon was deposited on a $La_{0.9}Ce_{0.1}NiO_3$-perovskite catalyst operated at 300-800 ℃, S/C=1.5, and O/C=0.5 [200]. Furthermore it was shown that O/C-levels lower than 0.5 led to carbon deposition over $La_{0.9}Ce_{0.1}NiO_3$ at S/C=1.5 and 500 ℃ [200]. The yield of H_2 depends on both S/C-ratio and O/C-ratio and Salge et al. [218] reported a maximum yield of H_2 in SR of ethanol under oxidative conditions of 57.5 %, according to the definition of yield used in this work, at 600 ℃, S/C=4.5, and O/C=0.66 over a Rh-Ce monolith catalyst [218]. Peela et al. [197] reported a drop in the yield of H_2 at 550 ℃ and S/C=3 from 65 % at O/C=0 to 43 % at O/C=1.5. These results show that addition of oxygen to the feed may solve the carbon deposition problem, but at the cost of a lower yield of H_2.

An other strategy to minimize the carbon deposition problem would be to add hydrogen to the feed. Hydrogen might hydrogenate unsaturated compounds like ethene and therefore decrease the deposition of carbon. Furthermore the additional H_2 will ensure that the catalyst is reduced under the reaction conditions. Laosiripojana et al. [169] investigated addition of H_2 at H/C-ratios between 0 and 5 at S/C-ratio of 1.5 and found a decrease in the yield of hydrocarbons and carbon deposition on Ni/CeO_2 and Ni/Al_2O_3 at 900 ℃ in the SR of ethanol. The yield of CH_4 decreased from 10.6 % at H/C=0 to 7.1 % at H/C=5, while the carbon deposition decreased from 1.08 monolayers at H/C=0 to 0.13 monolayers at H/C=5 over Ni/CeO_2. Jacobs et al. [111] reported an increased conversion and methane formation over Pt/CeO_2 at 300 ℃, S/C-ratio of 16.7, and H/C-ratio between 0-26.7 in SR of acetic acid. The conversion increased from 5.4 % at H/C=0 to 35.6 % at H/C=26.7, while the yield of CH_4 increased from 28 % at H/C=0 to 49.4 % at H/C=26.7. The opposite effect of H_2 on the methane formation between Laosiripojana et al. [169] and Jacobs et al. [111] might be ascribed to the effect of temperature on the equilibrium. At temperatures below 500 ℃ methanation of CO and CO_2 is thermodynamically favorable while at temperatures above 500 ℃ the equilibrium will be shifted toward carbon oxides. Therefore the effect of H_2 might be

Tab. 4.1: *Nominal metal loading, surface area, and NiO particle size of the fresh catalysts prior to reduction. XRD reflection peak from NiO peak at $2\theta = 62.8°$ used for determination of particle size.*

Catalyst	Metal loading $[wt\%]$	Surface area $[m^2/g]$	NiO particle size $[nm]$
$Ni/Ce_{0.6}Zr_{0.4}O_2$	8.2	90	28
Ni/CeO_2	8.2	113	10
$Ni/MgAl_2O_4$	8.2	98	4

an increased rate of reaction, which brings the product gas closer to equilibrium i.e. methane at temperatures below 500 ℃ and carbon oxides above 600 ℃.

$Ni/MgAl_2O_4$ has been used as test catalyst in most of the experiments presented in this work. It was chosen as the main catalyst, because it is a thermally very stable catalyst, which has proven effective in SR of hydrocarbons. It is often the choice for industrial SR units due to a good compromise between price and activity [30, 42]. Results from SR over $Ni/Ce_{0.6}Zr_{0.4}O_2$ and Ni/CeO_2 catalysts are presented to show that the trends observed in the SR over $Ni/MgAl_2O_4$ can be transferred to other catalytic systems.

4.1 Characterization

The surface area, metal loading, and NiO particle size for the investigated catalysts are shown in table 4.1. The three support materials, CeO_2, $Ce_{0.6}Zr_{0.4}O_2$, and $MgAl_2O_4$, all yielded catalysts with surface areas in the range of 90-113 m^2/g, while the NiO particles were between 4 and 28 nm in diameter. The quite large difference in particle size might influence catalyst performance as well as carbon deposition [196, 200]. Generally, smaller particles increase activity and decrease carbon deposition. The XRD patterns for the three catalysts in table 3.1 can be seen in fig. 4.1(a)-4.1(c) and confirmed that the structure of both of the mixed oxides were $Ce_{0.6}Zr_{0.4}O_2$ and $MgAl_2O_4$.

4.2 Effect of S/C-ratio

The effect of temperature and space velocity (W/F) on the SR of ethanol over different Ni-based catalysts were investigated in the previous chapter. Based on these results the temperature 600 ℃ was chosen to investigate the effect of H_2, O_2, H_2O. The conversion was around 75 % over $Ni/MgAl_2O_4$ at this temperature, a S/C-ratio of 6, and the applied space velocity, which allows evaluation of changes in activity and product distribution with time on stream. In addition the propensity to carbon deposition of the reaction mixture is more clearly revealed when the conversion is kept well below 1. The products obtained in the SR of ethanol over $Ni/Ce_{0.6}Zr_{0.4}O_2$, $Ni/MgAl_2O_4$, and Ni/CeO_2 were CO, CO_2, CH_4, C_2H_4 as well as acetone, acetic acid and acetaldehyde. The three latter compounds were only formed in minor amounts at 600 ℃ with a combined yield of 0.1 %.

The S/C-ratio is important in SR as it can influence product distribution, conversion, and deactivation. The conversion as function of time at 600 ℃ over $Ni/MgAl_2O_4$ at four different S/C-ratios ranging from 1.6 to 8.2 is shown in fig. 4.2. Deactivation was apparent in all the

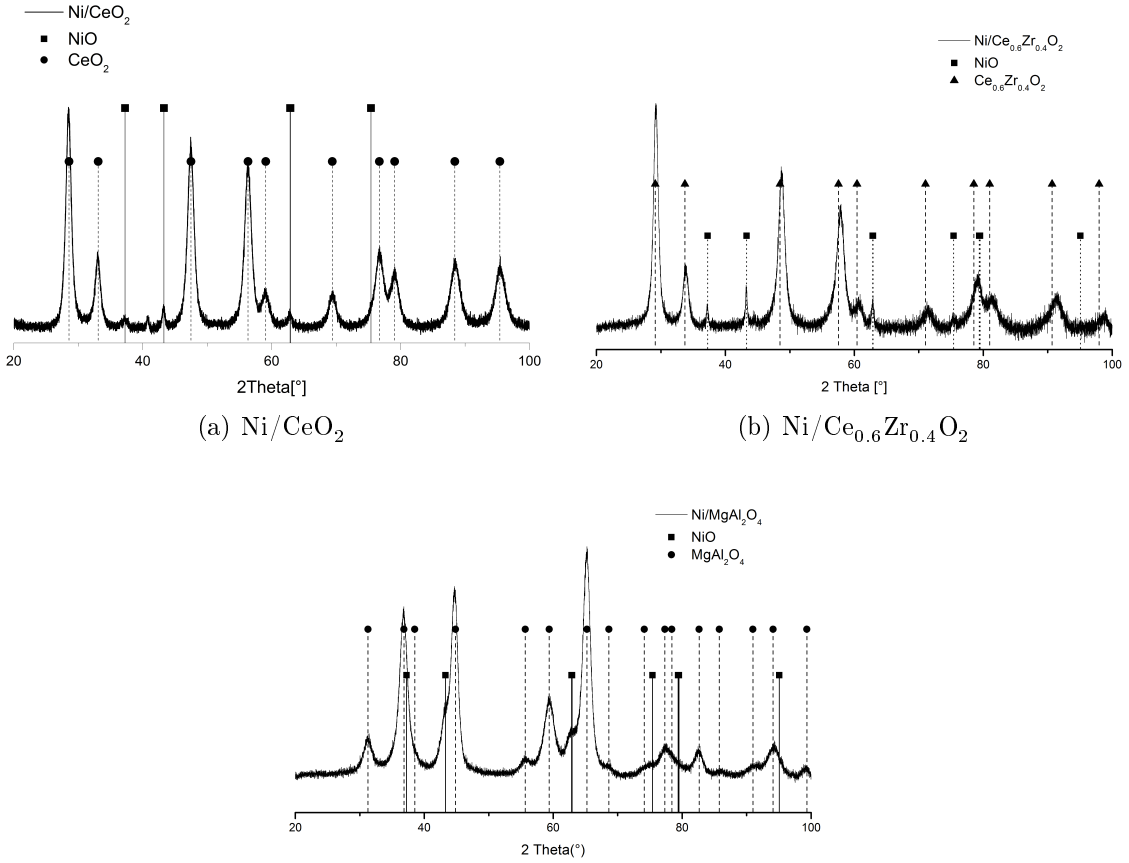

(a) Ni/CeO_2 (b) $Ni/Ce_{0.6}Zr_{0.4}O_2$

(c) $Ni/MgAl_2O_4$

Fig. 4.1: *XRD patterns for the tested catalysts.*

cases and was most pronounced at the lowest S/C-ratios. A decrease in conversion of 4-5 %-point over 4 h operation was observed for S/C-ratios between 1.6 and 6.0. At an S/C-ratio of 8.2 the decrease in conversion was significantly smaller, roughly 1 %-point.

The conversion and carbon deposition after 4 h on stream as function of S/C-ratio is shown in fig. 4.3. The conversion increased from 53 % to 80 % when the S/C ratio increased from 1.6 to 8.2. The effect of increasing the S/C-ratio was most pronounced at low values, where an increase in conversion from 53 % to 69 % was observed when increasing S/C-ratio from 1.6 to 2.9. The carbon deposition decreased almost linearly with increasing S/C-ratio from 10.5 $\frac{mmole\ C}{mole\ C_{Feed}}$ or 70 $\frac{mg\ C}{g_{Cat} \cdot h}$ at S/C=1.6 to 1.8 $\frac{mmole\ C}{mole\ C_{Feed}}$ or 11 $\frac{mg\ C}{g_{Cat} \cdot h}$ at S/C=8.2. Both of these trends could be due to increased rate of steam gasification/reforming due to increased amount of oxygen containing species on the catalyst.

The almost linearly decreasing carbon deposition suggests that further increments of the S/C-ratio could decrease the carbon deposition further. Linear extrapolation of the carbon deposition as function of S/C-ratio indicates that a S/C-ratio of 9.7 is required for carbon free operation at the applied reaction conditions.

The yield of H_2, CH_4, and C_2H_4 as function of S/C-ratio can be seen in fig. 4.5. The yield of H_2 increased with S/C-ratio from 45 % at S/C=1.6 to 76 % at S/C=8.2. Furthermore, the approach to equilibrium became closer with increasing S/C-ratio and the yield of H_2 in % of equilibrium increased from 64 to 90 % when increasing the S/C-ratio from 1.6 to 8.2. Increasing the amount of steam was expected to increase the yield of H_2 as the WGS will

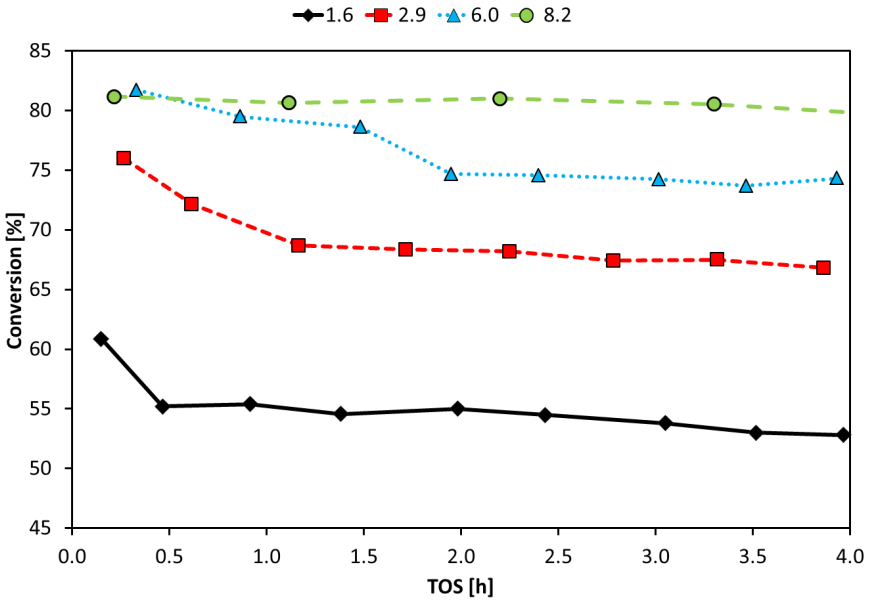

Fig. 4.2: *Conversion as function of time over $Ni/MgAl_2O_4$ during SR of ethanol at different S/C-ratios. Experimental conditions: Temp.: 585-590 ℃; $m_{Cat} = 0.50$ g, Ni loading: 8.2 wt%, $F_T = 1.6$ NL/min, $y_{Eth} = 3.0 - 3.3$ vol%, $y_{H_2O} = 10.2 - 50.4$ vol%, N_2 as balance.*

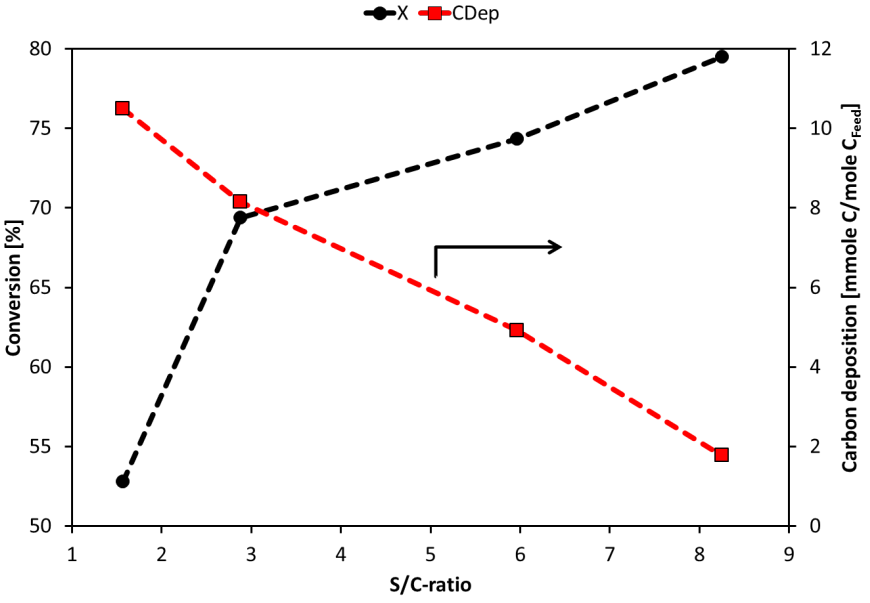

Fig. 4.3: *Conversion and rate of carbon deposition after 4 h on stream as function of S/C-ratio over $Ni/MgAl_2O_4$. Experimental conditions: Temp.: 585-590 ℃; $m_{Cat} = 0.50$ g, Ni loading: 8.2 wt%, $F_T = 1.6$ NL/min, $y_{Eth} = 3.0-3.3$ vol%, $y_{H_2O} = 10.2-50.4$ vol%, N_2 as balance.*

shift toward CO_2 and H_2. This was also seen on the CO_2/CO-ratio, which increased from about 1 at S/C=1.6 to 4.7 at S/C=8.2. The mass action ratio (MAR) for the WGS and methanation reactions as functions of S/C-ratio can be seen in fig. 4.4. The MAR for WGS increased with increasing S/C-ratio showing that the product gas approached equilibrium for WGS with increasing S/C-ratio. Similar trends were observed in ref. [57, 63, 169, 219]. The

MAR for methanation varied slightly with S/C-ratio and no clear trend was observed.

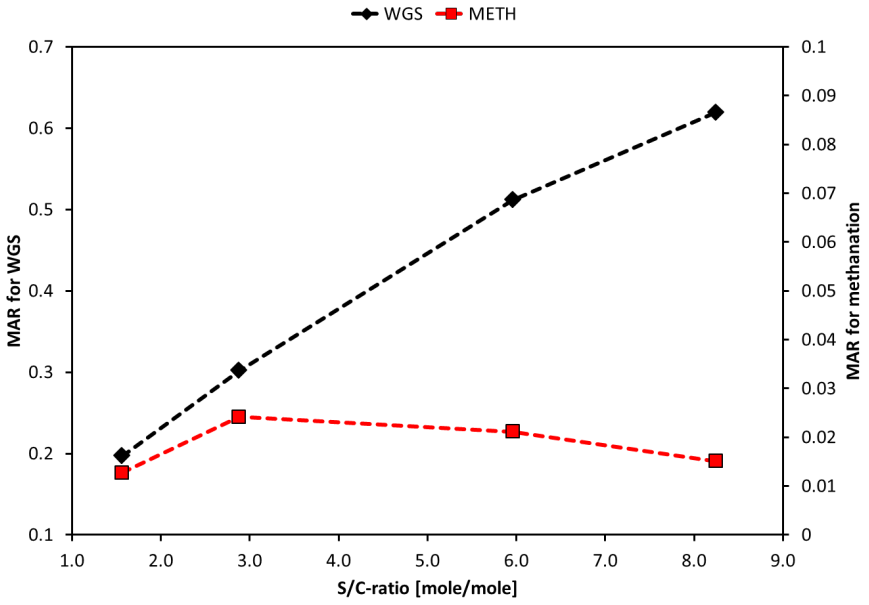

Fig. 4.4: *Mass action ratios for water gas shift and methanation as function of S/C-ratio over* $Ni/MgAl_2O_4$. *Experimental conditions: Temp.: 585-590 ℃;* $m_{Cat} = 0.50$ *g, Nickel loading: 8.2 wt%,* $F_T = 1.6$ NL/min, $y_{Eth} = 3.0 - 3.3$ *vol%,* $y_{H_2O} = 10.2 - 50.4$ *vol%,* N_2 *as balance.*

The yield of C_2H_4 was 26 % at S/C=1.6 and decreased to 3.1 % at S/C=8.2 and combined with the increase in conversion with S/C-ratio this could indicate that the first step in the SR of ethanol over $Ni/MgAl_2O_4$ is dehydration. This indicates that the effect of increasing the S/C-ratio was to increase the overall rate of reaction, which increases the total conversion and decreases the yield of intermediates. The decrease in carbon deposition correlated well with the C_2H_4 in the offgas (see fig. 4.3 and 4.5) and therefore a contributing factor to the decrease in carbon deposition could be a faster SR of C_2H_4, converting it before it is turned into solid carbon. Thermodynamical equilibrium calculations for the dehydration of ethanol shows that it should be shifted toward ethene and water regardless of the water content at 600 ℃. This indicates that the formation of C_2H_4 should not be limited by the higher water concentration at increasing S/C-ratios and the lower C_2H_4 concentration is therefore likely due to faster conversion.

The yield of CH_4 was stable at S/C-ratios from 1.6 to 8.2, indicating little influence of steam concentration on the conversion of CH_4 at 600 ℃. A decrease in the yield of hydrocarbons with increasing S/C-ratios was observed in refs. [169, 219]. The MAR for methanation (see fig. 4.4) varied slightly with S/C-ratio and a very small decrease in the MAR was observed. This again shows that the S/C-ratio have little influence on the methanation equilibrium at 600 ℃ in the SR of ethanol.

The effect of S/C-ratio on the product yields was highest, when increasing from 3 to 6, which indicates that relatively high S/C-ratios are needed to suppress carbon deposition and increase conversion of ethanol over $Ni/MgAl_2O_4$.

The principle of equilibrated and actual gas is described in Appendix B and was used to estimate the potential for carbon formation through methane decomposition, the Boudouard reaction, and CO decomposition [42]. There was no potential for forming carbon from an equilibrated gas, but affinity to form carbon deposits was found for the actual product gas through methane decomposition at a S/C-ratio of 1.6. This shows that carbon formation is

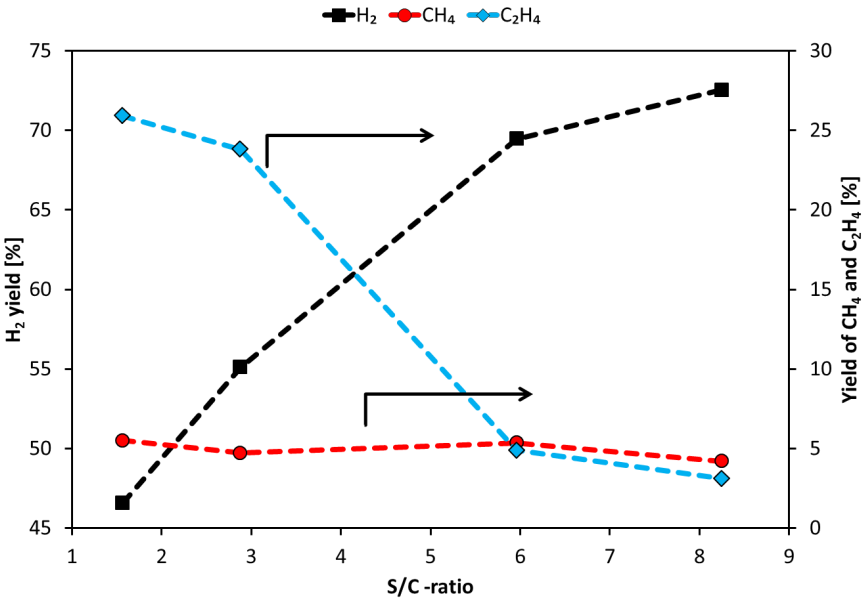

Fig. 4.5: *Yield of H2, CH_4, and C_2H_4 as function of S/C-ratio over $Ni/MgAl_2O_4$ over a 4 h experiment. Experimental conditions: Temp.: 585-590 °C; $m_{Cat} = 0.50$ g, Ni loading: 8.2 wt%, $F_T = 1.6$ NL/min, $y_{Eth} = 3.0 - 3.3$ vol%, $y_{H_2O} = 10.2 - 50.4$ vol%, N_2 as balance.*

mainly from ethene, although there might be positions in the catalyst bed with a gas composition, which could have the potential to form carbon deposits through methane decomposition especially at low S/C-ratios.

Overall, the results show that increasing the S/C-ratio increased the conversion of ethanol and yield of H_2 while decreasing the yield of hydrocarbons and carbon deposition. Operation at high S/C-ratios seems beneficial from a stability point-of-view, but it might be uneconomical in industrial units due to a high cost for superheating the steam. Furthermore it would lead to a larger reactor, pipelines, and general equipment as the gas flow rate would be high.

4.3 Oxidative steam reforming

An alternative to increasing the S/C-ratio is to co-feed oxygen, so called oxidative SR (OSR) in order to minimize the carbon deposition during SR of ethanol. The O_2 might influence the homogeneous reactions and therefore the effect of O_2 was investigated at 600 °C, S/C=6, O/C=0.26, and $y_{O_2} = 0.8$ vol% in an empty reactor. The results can be seen in table 4.2. At 600 °C and without O_2 equal amounts of CO, CH_4, and C_2H_4 were produced and the conversion was 3 %. Therefore the most important homogenous reactions were dehydration, reaction 3.5, and decomposition of ethanol, reaction 4.1:

$$CH_3CH_2OH \rightarrow CH_4 + CO + H_2 \tag{4.1}$$

With O_2 present the product distribution was similar but the conversion was 15 %. This indicates that the presence of O_2 increased the rate of homogenous dehydration and decomposition of ethanol.

The conversion of O_2 was 81 % in the blank experiment with O_2 in the feed, which indicated that O_2 would reach and react on the catalysts as no O_2 was detected in the product gas in OSR experiments regardless of the inlet concentration of O_2.

Tab. 4.2: *Conversion and offgas concentration from blank experiment with and without O_2 present. Experimental conditions: S/C: 6.1; O/C: 0.26; Temp.: 600-611 ℃; F_T=1450 NmL/min, y_{Eth} = 3.3 vol%, y_{H_2O} = 39.6 vol%, y_{O_2} = 0.1 vol%, N_2 as balance.*

Type	Conversion [%]	CO [vol%]	CO_2 [vol%]	CH_4 [vol%]	C_2H_4 [vol%]
SR	3	0.07	0	0.06	0.08
OSR	15	0.31	0.01	0.45	0.40

Oxygen co-feeding at an O/C ratio of 0.2-0.3 was tested over three different catalysts; $Ni/Ce_{0.6}Zr_{0.4}O_2$, $Ni/MgAl_2O_4$, and Ni/CeO_2. The O/C-ratios in these experiments were below what is needed for autothermal conditions which would require an O/C-ratio about 0.36 or above. Autothermal conditions are obtained when the energy from combustion of part of the ethanol equals the energy required for SR of the remaining part of the ethanol. The calculations are based on the assumption that all the energy from combustion is used for steam reforming, not heating of gas to 600 ℃.

A comparison of conversion, carbon deposition, and yield of H_2 after 4 h on stream for $Ni/Ce_{0.6}Zr_{0.4}O_2$, $Ni/MgAl_2O_4$, and Ni/CeO_2 at SR and OSR conditions can be seen in table 4.3. The conversion increased for all the catalysts when adding O_2 to the feed and full conversion was achieved for Ni/CeO_2. The increase in conversion could partly be due to an increase in homogeneous reactions as an increased conversion was observed with O_2 present in an empty reactor. More importantly, O_2 might facilitate surface reactions and increase conversion hereby. The conversion was stable with time at OSR conditions over all the catalysts.

The carbon deposition was lower at OSR conditions for all the catalysts indicating that the O_2 present under OSR will react with carbon on the catalyst and hereby remove it and/or limit its formation by oxidizing precursor species.

In table 4.3 it can also be seen that the yield of H_2 decreased at OSR-conditions with 3 to 12 %-point, which is due to oxidation to CO_2 and H_2O instead SR to H_2 and CO.

Tab. 4.3: *Conversion, carbon deposition, and yield of H_2 at SR and OSR conditions after 4 h on stream over $Ni/Ce_{0.6}Zr_{0.4}O_2$, $Ni/MgAl_2O_4$, and Ni/CeO_2. Experimental conditions: S/C: 5.8-6.0; O/C: 0.19-0.28; Temp.: 579-592 ℃; m_{Cat} = 0.50 g, Ni loading: 8.2 wt%, F_T = 1.6 NL/min, y_{Eth} = 3.2 − 3.5 vol%, y_{H_2O} = 38.4 − 38.6 vol%, y_{O_2} = 0.6 − 1.0 vol%, N_2 as balance.*

Catalyst	O/C	S/C	Conversion [%]	Carbon deposition $\left[\frac{mmole\ C}{mole\ C_{Feed}}\right]$	Carbon deposition $\left[\frac{mg\ C}{g_{Cat} \cdot h}\right]$	Y_{H_2} [%]
$Ni/Ce_{0.6}Zr_{0.4}O_2$	-	6.0	84	8.6	54.9	75
$Ni/Ce_{0.6}Zr_{0.4}O_2$	0.19	5.8	87	1.4	9.3	65
$Ni/MgAl_2O_4$	-	6.2	73	4.4	28.0	70
$Ni/MgAl_2O_4$	0.25	6.0	95	1.7	11.0	67
Ni/CeO_2	-	5.8	67	2.7	18.8	68
Ni/CeO_2	0.28	5.9	99	1.6	10.7	66

The effect of the O/C-ratio on conversion, carbon deposition, and product distribution was investigated over $Ni/MgAl_2O_4$ and $Ni/Ce_{0.6}Zr_{0.4}O_2$. The conversion and carbon deposition

after 4 h on stream as function of O/C-ratio over these catalysts are shown in fig. 4.6. For $Ni/Ce_{0.6}Zr_{0.4}O_2$ the conversion increased with increasing O/C-ratio and reached nearly full conversion at an O/C-ratio of 0.5. A similar trend was observed with $Ni/MgAl_2O_4$, however the conversion increased more rapidly with addition of low amounts of oxygen and reached full conversion at O/C-ratio of 0.84.

The carbon deposition on $Ni/Ce_{0.6}Zr_{0.4}O_2$ decreased significantly with increasing O/C-ratio and at an O/C-ratio of 0.5 around 0.2 $\frac{mmole\ C}{mole\ C_{Feed}}$ or 1.5 $\frac{mg\ C}{g_{Cat} \cdot h}$ ended up on the catalyst. Increasing the O/C-ratio to 1 decreased the carbon deposition further by approximately a factor of 10 to 0.02 $\frac{mmole\ C}{mole\ C_{Feed}}$ or 0.16 $\frac{mg\ C}{g_{Cat} \cdot h}$. A large decrease in carbon deposition with increasing O/C-ratio was also observed over $Ni/MgAl_2O_4$. The carbon deposition at an O/C-ratio of 0.84 was 0.03 $\frac{mmole\ C}{mole\ C_{Feed}}$ or 0.20 $\frac{mg\ C}{g_{Cat} \cdot h}$, which was similar to the results from OSR over $Ni/Ce_{0.6}Zr_{0.4}O_2$ at a similar O/C-ratio. The results indicate that O/C-ratios of roughly 1 is needed for almost carbon free operation at 600 ℃ over both $Ni/Ce_{0.6}Zr_{0.4}O_2$ and $Ni/MgAl_2O_4$.

When adding oxygen to the system the overall reaction changed from being endothermic at an O/C-ratio below 0.36 to exothermic at O/C-ratios above this value. This was also observed during the experiments as the reactor was almost isothermal at an O/C-ratio of 0.5, while the temperature decreased by 10 ℃ or increased by 10-15 ℃ over the reactor at O/C-ratios of 0.2 and 0.8-1.0, respectively.

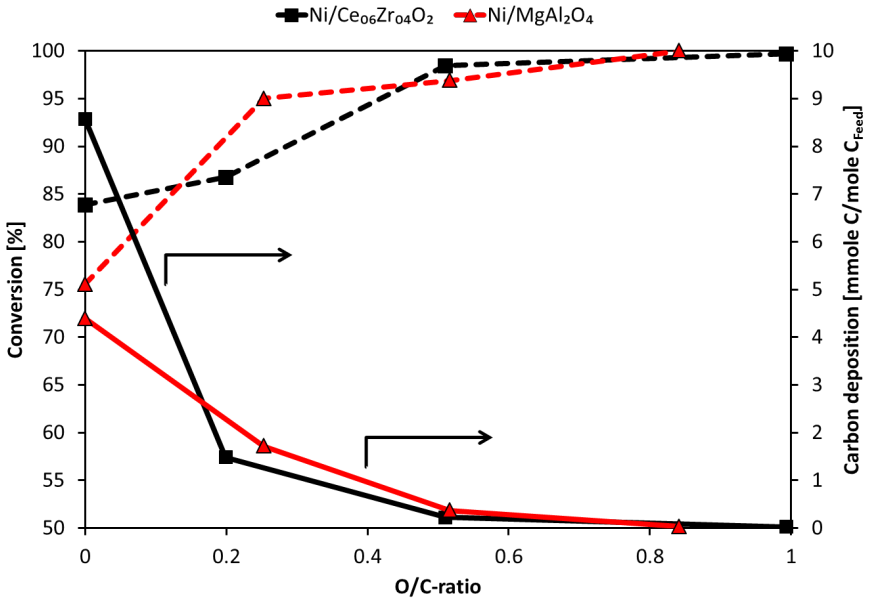

Fig. 4.6: *Conversion and carbon deposition after 4 h on stream as function of O/C-ratio over $Ni/MgAl_2O_4$ and $Ni/Ce_{0.6}Zr_{0.4}O_2$. Full lines are carbon deposition and dashed lines are conversion. Experimental conditions: S/C: 5.5-6.0; Temp.: 586-615 ℃; m_{Cat} = 0.50 g, Ni loading: 8.2 wt%, F_T = 1.6 NL/min, y_{Eth} = 3.1 − 3.3 vol%, y_{H_2O} = 36.3 − 37.2 vol%, y_{O_2} = 0 − 3.2 vol%, N_2 as balance.*

The yield of H_2, CH_4, and C_2H_4 as functions of the O/C-ratio over $Ni/Ce_{0.6}Zr_{0.4}O_2$ and $Ni/MgAl_2O_4$ can be seen in fig. 4.8. The yield of H_2 dropped from 77 % to 50 % for $Ni/Ce_{0.6}Zr_{0.4}O_2$ and from 70 % to 51 % for $Ni/MgAl_2O_4$ by increasing the O/C-ratio from 0 to 1. This corresponds to a loss of 1 mole of H_2 pr. mole of ethanol converted. A low temperature shift catalyst bed downstream the reactor might recover part of the H_2 as CO is present in the off gas. Furthermore additional H_2 can be obtained by converting the remaining hydrocarbons to carbon oxides.

The MAR for WGS and methanation as function of O/C-ratio over $Ni/Ce_{0.6}Zr_{0.4}O_2$ and $Ni/MgAl_2O_4$ can be seen in fig. 4.7. The MAR for WGS decreased slightly with increasing O/C-ratio, while the MAR for methanation increased with increasing O/C-ratio over both catalysts. This shows that oxygen is capable of converting methane under the applied conditions.

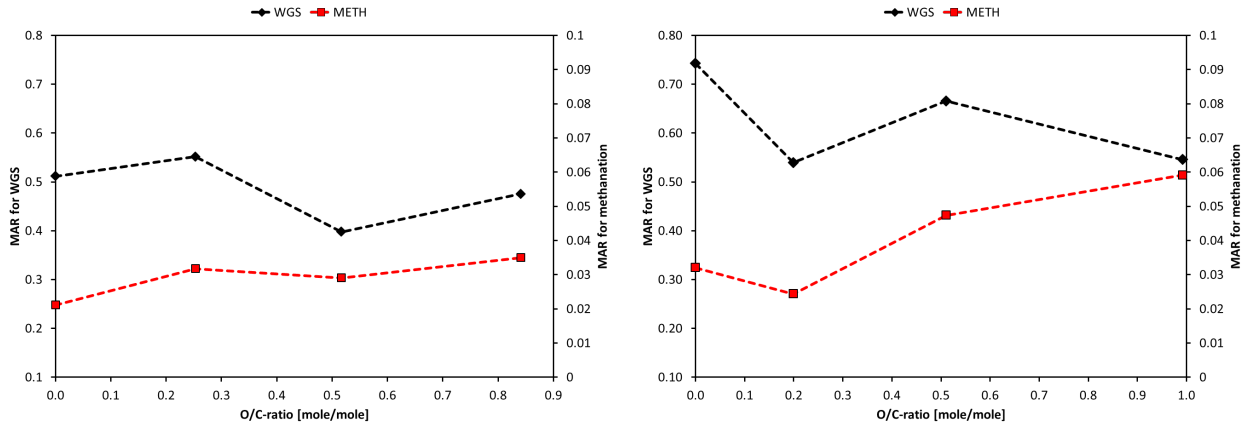

(a) $Ni/MgAl_2O_4$ (b) $Ni/Ce_{0.6}Zr_{0.4}O_2$

Fig. 4.7: *Mass action ratios for water gas shift and methanation as function of O/C-ratio over* $Ni/MgAl_2O_4$ *and* $Ni/Ce_{0.6}Zr_{0.4}O_2$*. Experimental conditions: S/C: 5.5-6.0; Temp.: 586-615 ℃;* $m_{Cat} = 0.50$ *g, Ni loading: 8.2 wt%,* $F_T = 1.6$ NL/min*,* $y_{Eth} = 3.1 - 3.3$ *vol%,* $y_{H_2O} = 36.3 - 37.2$ *vol%,* $y_{O_2} = 0 - 3.2$ *vol%,* N_2 *as balance.*

The yield of hydrocarbons over both catalysts decreased with increasing O/C-ratio. The yield of C_2H_4 decreased from 3-5 % at O/C=0 to zero at O/C-ratios above 0.8 for both catalysts indicating a higher rate of conversion of ethene with increasing concentration of O_2. Similarly the methane yield decreased from 5 % at O/C=0 to 1-2 % at O/C-ratios above 0.8.

Carbon deposition in OSR is also mainly from ethene as the principle of equilibrated and actual gas do not predict carbon formation through methane decomposition, the Boudouard reaction, and CO decomposition.

The results show that oxidative SR is an efficient way of limiting carbon deposition but at a cost of decreasing the yield of H_2.

4.4 Hydrogen addition

Hydrogen addition to the feed was tested during SR of ethanol over a $Ni/MgAl_2O_4$ catalyst at 600 ℃, S/C-ratio of roughly 6, and H_2/EtOH-ratio (H/C-ratio) between 0 and 2.5 (on molar basis). The conversion and carbon deposition as function of the H/C-ratio can be seen in fig. 4.9. The conversion increased from 73 % at H/C=0 to 81 % at H/C=1.1 and then decreased to 62 % at H/C=2.4. This indicated that additional H_2 in the feed improved the performance of the catalysts when adding H_2 in a H/C-ratio of 1 and below. However, adding higher amounts of H_2 decreased conversion probably due to a shift in the WGS, reaction 1.2, leading to fewer oxygen-species to oxidize the carbon intermediates. This is discussed further in section 4.6.

The carbon deposition as function of H/C-ratio can be seen in fig. 4.9. There was a slight decrease in carbon deposition with increasing H/C-ratio. The decrease in carbon deposition might be due to increasing hydrogenation of C or CH_x-species or due to competitive adsorption between H_2 and ethanol derivatives leading to lower amounts of C on the surface.

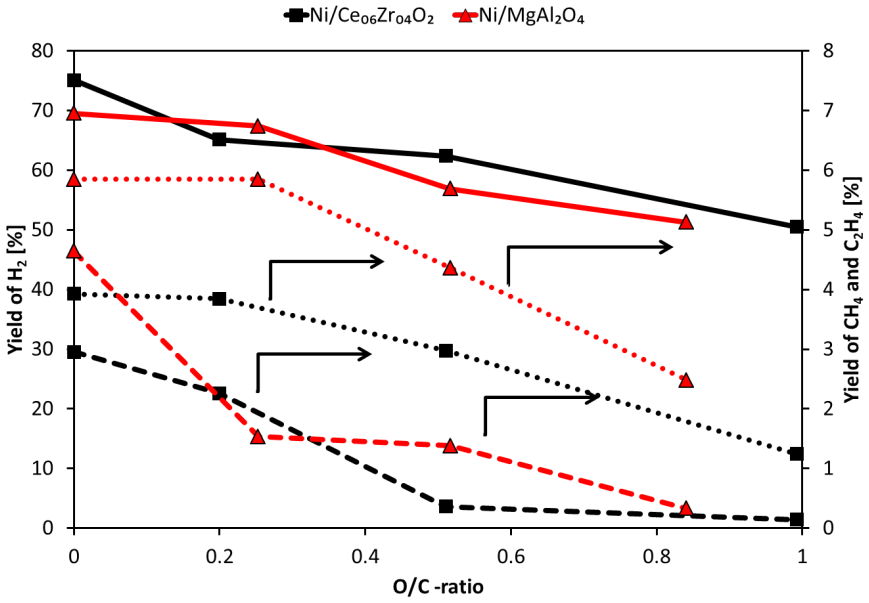

Fig. 4.8: *Yield of H_2, CH_4, and C_2H_4 as function of O/C-ratio over $Ni/MgAl_2O_4$ and $Ni/Ce_{0.6}Zr_{0.4}O_2$. Full lines are H_2 yield, dashed lines are C_2H_4 yield, and dotted lines are CH_4 yield. Experimental conditions: S/C: 5.5-6.0; Temp.: 586-615 °C; $m_{Cat} = 0.50$ g, Ni loading: 8.2 wt%, $F_T = 1.6$ NL/min, $y_{Eth} = 3.1 - 3.3$ vol%, $y_{H_2O} = 36.3 - 37.2$ vol%, $y_{O_2} = 0 - 3.2$ vol%, N_2 as balance.*

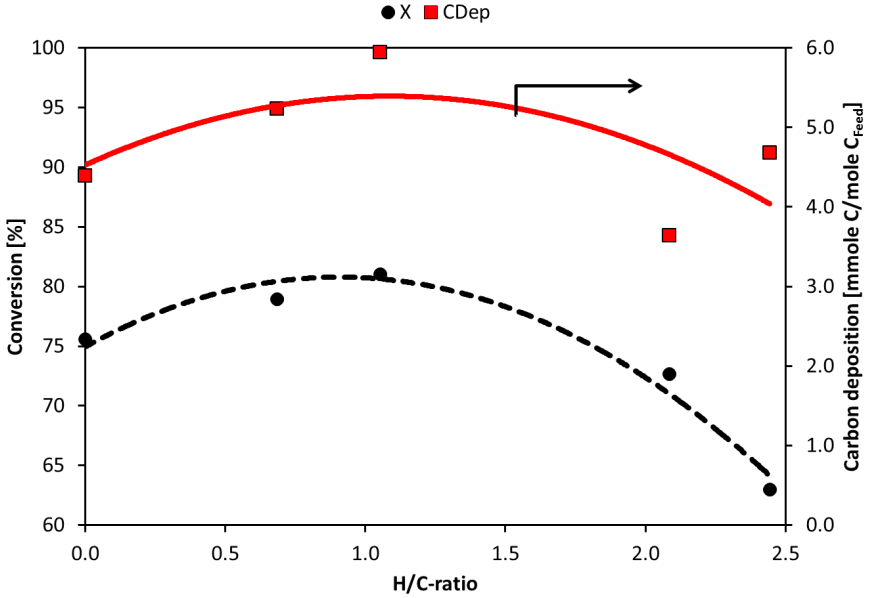

Fig. 4.9: *Conversion and carbon deposition after 4 h on stream as function of O/C-ratio over $Ni/MgAl_2O_4$. Full lines are carbon deposition and dashed lines are conversion. Experimental conditions: S/C: 5.9-6.0; Temp.: 586-592 °C; $m_{Cat} = 0.50$ g,Ni loading: 8.2 wt%, $F_T = 1.6$ NL/min, $y_{Eth} = 3.0 - 3.3$ vol%, $y_{H_2O} = 36.0 - 37.2$ %, $y_{H_2} = 0 - 7.4$ vol%, N_2 as balance.*

The yield of H_2, CH_4, C_2H_4, and C_2H_6 as function of H/C-ratio is shown in fig. 4.11. The yield of H_2 was not influenced at H/C-ratios between 0 and 1.1, but decreased at H/C-ratios higher than 1.1. This is expected as a higher concentration of H_2 will shift the WGS toward CO and H_2O (see reaction 1.2). This can also be seen on the CO_2/CO-ratio, which decreased

from 4.1 at H/C=0 to 2.5 at H/C=2.4.

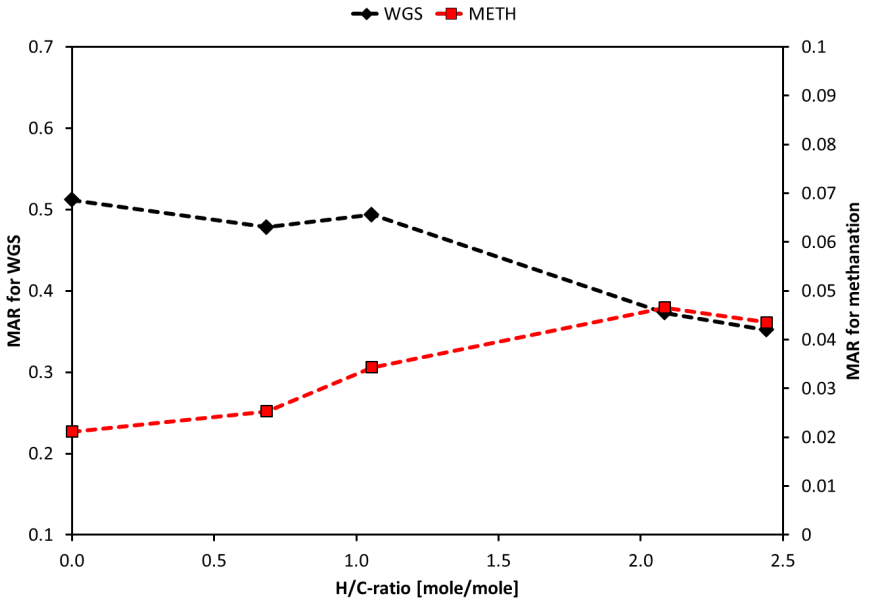

Fig. 4.10: *Mass action ratios for water gas shift and methanation as function of H/C-ratio over* $Ni/MgAl_2O_4$. *Experimental conditions: S/C: 5.9-6.0; Temp.: 586-592 ℃;* $m_{Cat} = 0.50\ g$, *Ni loading: 8.2 wt%,* $F_T = 1.6\ NL/min$, $y_{Eth} = 3.0 - 3.3\ vol\%$, $y_{H_2O} = 36.0 - 37.2\ \%$, $y_{H_2} = 0 - 7.4\ vol\%$, N_2 *as balance.*

The yield of methane increased from 5.9 % at H/C=0 to 6.7 % at H/C=2.4, which corresponded to an increase of 15 %. The increase was expected as an increase in the concentration of H_2 will shift the methanation reaction toward CH_4.

The MAR for WGS and methanation as function of H/C-ratio can be seen in fig. 4.10. The MAR for methanation increased with H/C-ratio indicating that the equilibrium was approached with increasing H/C-ratio. The MAR for WGS decreased with increasing H/C-ratio, showing that the WGS moves further away from equilibrium with increasing H/C-ratio. The coverage of catalysts with H-species with increasing H/C-ratio could account for the decrease in the WGS activity.

The yield of ethene was 4.9 % at H/C=0 then decreased to a minimum of 2.6 % at H/C=1.1 and increased to 6.2 at H/C=2.4. The decrease in yield of ethene at between H/C-ratios of 0 to 1.1 was probably due to increased rate of SR reactions as the conversion of ethanol also increased at H/C-ratios between 0 and 1.1. The increase in yield of ethene at H/C above 1.1 indicate a lower conversion of ethene, which could be due to a high coverage of hydrogen species on surface of the catalysts, $H*$, which limits the adsorption of ethene.

The yield of ethane increased from 0.52 % at H/C=0 to 1.9 % at H/C=2.4. This shows that the hydrogenation of ethene to ethane increased with increasing H/C-ratio as expected. Thermodynamics of the hydrogenation of ethene to ethane predicts full hydrogenation, so this reaction, like the methanation approaches equilibrium with increasing H/C-ratio.

The principle of equilibrated and actual gas did not show potential for carbon formation, again indicating ethene as the primary source of carbon deposition.

4.5 Stability tests

Oxidative SR and SR at a high S/C-ratio both seemed interesting as they showed low carbon deposition and stable performance for 4 *h* during SR of ethanol at 600 ℃. Therefore it was

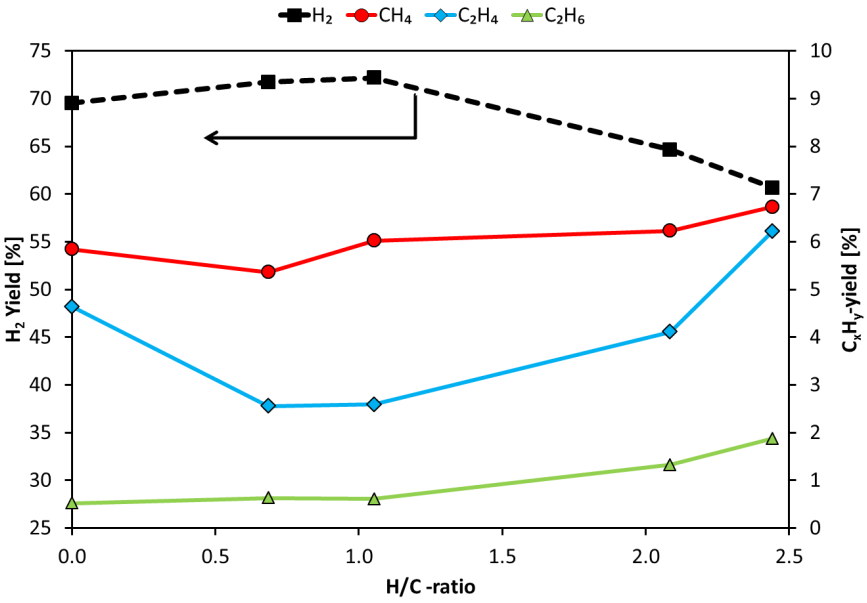

Fig. 4.11: *Yield of H_2, CH_4, C_2H_4, and C_2H_6 as function of H/C-ratio over $Ni/MgAl_2O_4$. Full lines are hydrocarbon yields and dashed lines are hydrogen yield. Experimental conditions: S/C: 5.9-6.0; Temp.: 586-592 ℃; $m_{Cat} = 0.50$ g, Ni loading: 8.2 wt%, $F_T = 1.6$ NL/min, $y_{Eth} = 3.0-3.3$ $vol\%$, $y_{H_2O} = 36.0-37.2$ %, $y_{H_2} = 0-7.4$ $vol\%$, N_2 as balance.*

chosen to conduct SR of ethanol at these reaction conditions for 24 hours to get a deeper understanding of the stability and rate of carbon deposition. The conversion and yield of hydrocarbons as function of time on stream for SR of ethanol at S/C-ratio of 6, 8, and at S/C=6 and O/C=0.8 can be seen in fig. 4.12. The yield of hydrocarbons is the combined yield of CH_4 and C_2H_4. The conversion remained stable around 100 % during the entire experiment for SR with oxygen present, while the two conditions without O_2 present showed deactivation. It was most pronounced for SR at S/C=6, where the conversion decreased from 80% to 72 % over 24 *h*, while the conversion at S/C=8 decreased from 81 % to 78 %.

The total yield of hydrocarbons under OSR was stable around 3.5-4 %, however an increase in the yield of C_2H_4 with time on stream from 0.2 % after 1 *h* to 0.7 % after 24 *h* was observed. The total yield of hydrocarbons was stable around 7 % at S/C=8 and the yield of C_2H_4 increased from 1.9 % to 3.5 % during the experiment. The yield of hydrocarbons in the SR of ethanol at S/C=6 increased from 10% to 12 % over 24 *h*, mainly due to an increase in the yield of C_2H_4 from 4.4 % to 7.7 %. Both conversion and yield of hydrocarbons as functions of time showed that more stable behavior was achieved by adding either additional water or O_2.

The conversion with oxygen present was 100 % for the entire 24 *h* experiment and therefore the experiment was repeated with a lower mass of catalyst to attempt to obtain less than full conversion. A comparison of conversion, yield of C_2H_4, CH_4, and H_2 both initially and after 24 *h* at the two different space velocities (SV) can be seen in table 4.4. As expected the conversion decreased while the yield of hydrocarbons increased with increasing SV. A slight deactivation at the higher SV over 24 *h* could be observed as conversion and yield of H_2 decreased with time, while the yield of both CH_4 and C_2H_4 increased with time.

The carbon deposition after 4 *h* and 24 *h* during SR at S/C=6, SR at S/C=6 with O/C=0.8, and SR at S/C=8 can be seen in table 4.5. In general, the rate of carbon deposition decreased with time for the three cases. At S/C=6 the total amount of carbon on the catalyst decreased from 4 to 24 *h* on stream, which could indicate that the carbon deposition had reached a

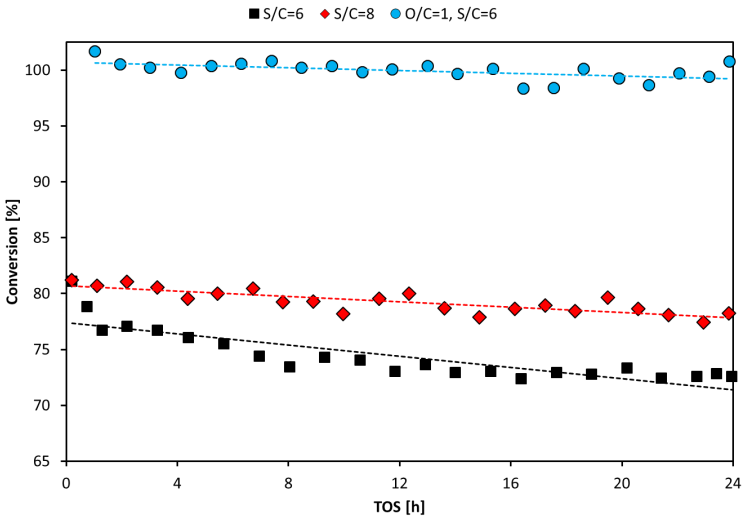

(a) Conversion as function of time on stream.

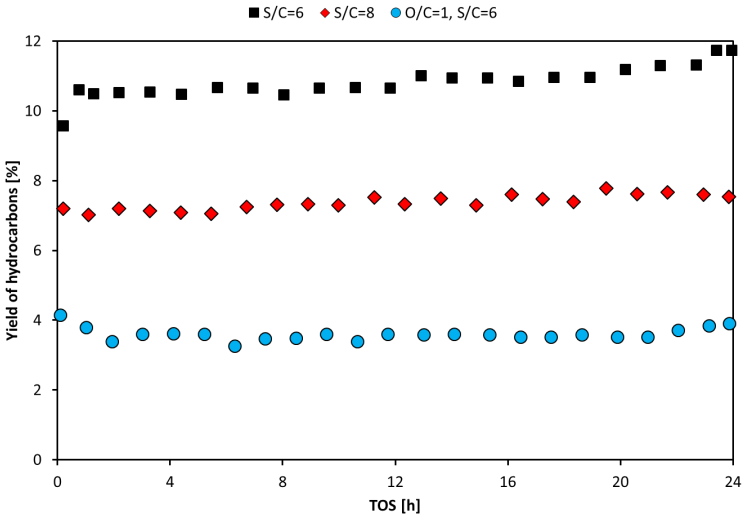

(b) Yield of hydrocarbons as function of time on stream.

Fig. 4.12: *Conversion and yield of hydrocarbons as function of time of OSR at O/C=1 and S/C=6, SR at S/C=8, and SR at S/C=6. Experimental conditions: Temp.: 590-606 °C, $m_{Cat} = 0.50\ g$, Ni loading: 8.2 wt%, $F_T = 1.6\ NL/min$, $y_{Eth} = 3.2$ %, $y_{H_2O} = 40.1 - 51.5\ vol\%$, $y_{O_2} = 0 - 2.5\ vol\%$, N_2 as balance. Hydrocarbons are CH_4 and C_2H_4.*

steady state and would remain at this level. However, an additional experiment with 100 h on stream had a total carbon deposition of 106 mg compared 54 mg after 24 h, so the carbon deposition did still increase with time on stream. The conversion also decreased with time on stream during the entire 100 h. The conversion, yield of hydrocarbons, and yield of H_2 as function of time on stream for the 100 h experiment can be seen in fig. 4.13.

Steam reforming with oxygen present seems to be most promising as the lowest carbon deposition and highest conversion can be achieved with this feed. Furthermore, at the more severe conditions (higher SV), where the ethene fraction in the offgas was higher, the carbon deposition was still low.

Tab. 4.4: *Conversion, yield of H_2, CH_4, and C_2H_4 in oxidative SR at S/C of 6 and O/C of 0.7-0.8 after 1 and 24 h on stream at different space velocities. Y: yield. Experimental conditions: Temp.: 606-608 °C, $m_{Cat} = 0.27 - 0.50$ g, Ni loading: 8.2 wt%, $F_T = 1.6$ NL/min, $y_{Eth} = 3.2 - 3.8$ %, $y_{H_2O} = 38.7 - 38.9$ vol%, $y_{O_2} = 2.5 - 2.8$ vol%, N_2 as balance.*

WHSV	Conversion		Y_{H_2}		Y_{CH_4}		$Y_{C_2H_4}$	
$[h^{-1}]$	1 h	24 h	1 h	24 h	1 h	24 h	1 h	24 h
12.6	100	100	56	54	3.4	3.1	0.2	0.7
28.3	99	97	50	48	6.3	6.8	2.7	3.2

Tab. 4.5: *Carbon deposition after 4 and 24 h for SR at S/C=6, SR at S/C=6 with O/C=0.7-0.8, and SR at S/C=8. Experimental conditions: Temp.: 576 °C, $m_{Cat} = 0.50$ g, Ni loading: 8.2 wt%, $F_T = 1.6$ NL/min, WHSV= 12.9-28.3 h^{-1}, $y_{Eth} = 3.3$ %, $y_{H_2O} = 39.5 - 51.5$ vol%, $y_{O_2} = 0 - 3.2$ vol%, N_2 as balance.*

Type	TOS	Carbon deposition		
	[h]	$\left[\frac{mmole\ C}{mole\ C_{Feed}}\right]$	$\left[\frac{mg\ C}{g_{Cat} \cdot\ h}\right]$	[mg]
SR at S/C=6	4	4.4	28.0	56
SR at S/C=6	24	0.7	4.5	54
SR at S/C=8	4	1.8	11.4	23
SR at S/C=8	24	0.7	4.7	56
SR at O/C=0.8	4	0.03	0.2	0.4
SR at O/C=0.8	24	0.02	0.1	1.4
SR at O/C=0.7 and WHSV = 28.3 h^{-1}	24	0.01	0.2	1.0

The surface area and NiO particle size for fresh and spent $Ni/MgAl_2O_4$ after 24 h on stream in the SR of ethanol at S/C=6, S/C=8, and O/C=0.8 and after oxidation of the carbon deposits can be seen in table 4.6. The NiO particle size increased and surface area decreased with time-on-stream indicating that sintering of the Ni particles and support material occurred at all of the conditions investigated. The sintering was most pronounced with oxygen present and could account for the deactivation seen in OSR despite the low carbon deposition.

Tab. 4.6: *BET surface area and Ni particle size for $Ni/MgAl_2O_4$ before and after operation at S/C=6, S/C=8, and O/C=1 and 600 °C for 24 h. XRD analysis were used to determine the particle size and the NiO reflection peak at $2\theta = 62.8°$ were used.*

	Surface area $[m^2/g]$	NiO particle size [nm]
Fresh	98	4
SR at S/C=6	84	6
SR at S/C=8	79	7
SR at O/C=0.8	69	9

Carbon deposition was not completely inhibited during SR at O/C below 1 and therefore a long term stability test was conducted at an even higher O/C-ratio. The yield of hydrocarbons

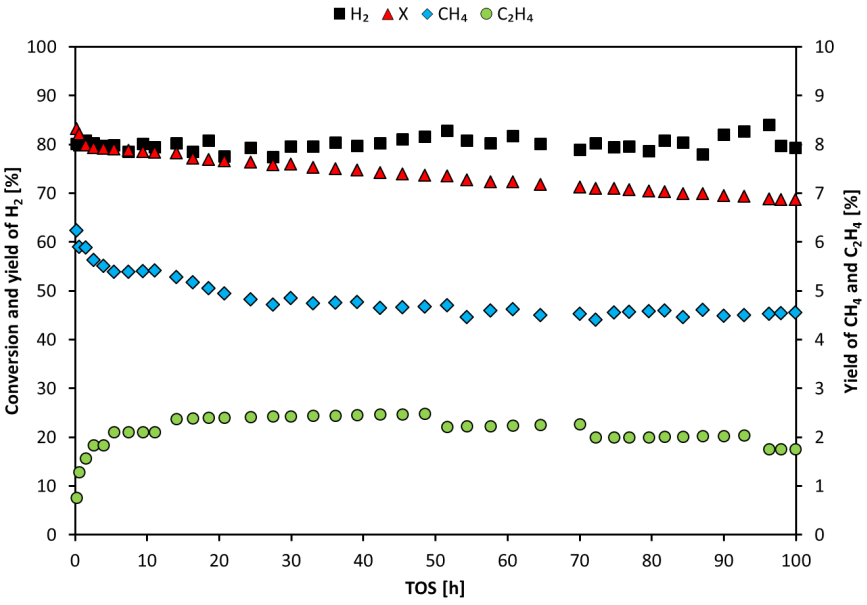

Fig. 4.13: *Conversion and yield of hydrocarbons and H_2 as function of time at S/C=6. Experimental conditions: Temp.: 590 ℃, m_{Cat} = 0.50 g, Ni loading: 8.2 wt%, $F_T = 1.6$ NL/min, $y_{Eth} = 3.2$ %, $y_{H_2O} = 40.1$ vol%, N_2 as balance.*

and H_2 as well as conversion and CO_2/CO-ratio as function time on stream during SR at O/C=1.1 can be seen in fig. 4.14. The CO_2/CO-ratio decreased while the yield of methane and ethene both increased during the first 30 hours on stream and hereafter remained stable for the next 60 *h*. The increase in yield of hydrocarbons and drop in yield of H_2 after 24 *h* on stream was due to a short malfunction of the feeding system, which the caused the feed of H_2O and ethanol to stop for a short period of time (5-10 *s*). A slight oxidation of the catalyst might have occurred at this point.

The total carbon deposition after 90 hours on stream was 0.1 *mg*, corresponding to 0.2 $\frac{\mu mole\ C}{mole\ C_{Feed}}$. The stable behavior with time-on-stream and low amount of carbon on catalyst shows that oxidative SR of ethanol at O/C-ratio above 1 are needed for stable operation with very low rate of carbon deposition (7 $\frac{\mu g\ C}{g_{Cat} \cdot h}$) over $Ni/MgAl_2O_4$. Due to the high content of O_2 in the feed it might be possible to lower the S/C-ratio as the main purpose of the steam might be to shift the gas and not to keep the catalysts free of coke.

The penalty of the more stable performance of the catalysts is a loss in the H_2 production of respectively 1 or 2 mole of H_2 pr. mole ethanol converted at O/C=0.8 and at O/C=1.1 compared with SR at S/C=6 without O_2 addition. As mentioned above additional H_2 may be obtained by a low temperature shift of the remaining CO and conversion of hydrocarbons. In this way a total hydrogen yield of 59 % or 3.6 moles of H_2 pr. mole of ethanol (shift at 300 ℃) may optimally be obtained at O/C-ratio of 1.1.

That oxidative SR of ethanol is required for stable operation was also concluded by the work of Deluga et al. [157] and others [194, 196, 197, 218] using noble metal catalysts.

4.6 Discussion of reaction mechanism in SR of ethanol

Reactions 3.1-3.6 are the overall reactions for the SR of ethanol and based on results from the literature the overall mechanism for SR of ethanol appears to be: adsorption of ethanol followed by removal of hydrogen, breaking of the C-C-bonds, and subsequent breaking of C-

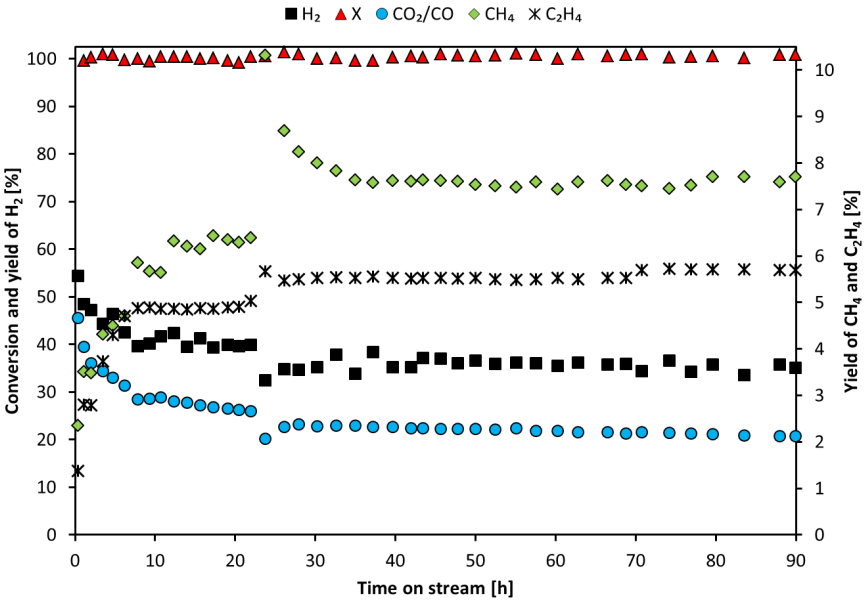

Fig. 4.14: *Conversion, CO_2/CO-ratio, yield of hydrocarbons, and yield of H_2 as function of time at O/C=1.1 and S/C=6 over $Ni/MgAl_2O_4$. Experimental conditions: Temp.: 617 °C, m_{Cat} = 0.36 g, Ni loading: 8.2 wt%, F_T = 1.6 NL/min, y_{Eth} = 3.6 %, y_{H_2O} = 37.8 vol%, y_{O_2} = 4 vol%, N_2 as balance.*

H and C-O-bonds [101, 104, 108–110, 114]. Carbon deposition in the SR of ethanol can be caused by slow removal of reactive carbon species, C_α, which causes it to polymerize and form the less active carbon species C_β [40–42]. Carbon deposits may also be formed from thermal decomposition in the gas phase above the catalysts. However, no carbon deposition was visible on the reactor tube indicating that at this temperature thermal decomposition is not significant. A third pathway to carbon deposition is through ethene as shown in reactions 3.7 and 3.8. Based on the results presented above this path appears to dominate in the carbon formation, at least with the catalysts and at the conditions applied in this study. The surface reactions for WGS, SR of ethanol, and possible carbon depositing reactions can be seen below [101, 104, 108–110, 114]. $*$ denotes a surface species or a vacant surface site.

Water gas shift [101, 104, 108–110, 114]:

$$\mathrm{H_2O(g)} + 2* \rightleftharpoons \mathrm{OH*} + \mathrm{H*} \tag{4.2}$$
$$\mathrm{OH*} + * \rightleftharpoons \mathrm{O*} + \mathrm{H*} \tag{4.3}$$
$$\mathrm{CO*} \rightleftharpoons \mathrm{CO(g)} + * \tag{4.4}$$
$$\mathrm{CO*} + \mathrm{O*} \rightleftharpoons \mathrm{CO_2*} + * \tag{4.5}$$
$$\mathrm{CO_2*} \rightleftharpoons \mathrm{CO_2(g)} + * \tag{4.6}$$
$$2\mathrm{H*} \rightleftharpoons \mathrm{H_2(g)} + 2* \tag{4.7}$$

Steam reforming of ethanol [101, 104, 108–110, 114]:

$$\mathrm{CH_3CH_2OH(g)} + 2\ * \rightleftharpoons \mathrm{CH_3CH_2O*} + \mathrm{H*} \tag{4.8}$$
$$\mathrm{CH_3CH_2O*} + * \rightleftharpoons \mathrm{CH_3CHO*} + \mathrm{H*} \tag{4.9}$$
$$\mathrm{CH_3CHO*} + * \rightleftharpoons \mathrm{CH_2CH_2*} + \mathrm{O*} \tag{4.10}$$

$$CH_2CH_2* \rightleftharpoons CH_2CH_2(g) + * \quad (4.11)$$
$$CH_2CH_2* + * \rightleftharpoons 2CH_2* \quad (4.12)$$
$$CH_3CHO* \rightleftharpoons CH_3CHO(g) + * \quad (4.13)$$
$$CH_3CHO* + * \rightleftharpoons CH_3* + CHO* \quad (4.14)$$
$$CH_3CHO* + * \rightleftharpoons CH_3CO* + H* \quad (4.15)$$
$$CH_3CO* + * \rightleftharpoons CH_3* + CO* \quad (4.16)$$
$$CH_3* + H* \rightleftharpoons CH_4* \quad (4.17)$$
$$CH_4* \rightleftharpoons CH_4(g) + * \quad (4.18)$$
$$CH_3* + * \rightleftharpoons CH_2* + H* \quad (4.19)$$
$$CH_2* + * \rightleftharpoons CH* + H* \quad (4.20)$$
$$CH* + * \rightleftharpoons C* + H* \quad (4.21)$$
$$CHO* + * \rightleftharpoons CO* + H* \quad (4.22)$$
$$C* + O* \rightleftharpoons CO* + * \quad (4.23)$$

Carbon deposition:

$$C* \rightarrow C_\alpha* \rightarrow C_\beta* \rightarrow \text{Carbon deposits} \quad (4.24)$$
$$CH_2CH_2* \rightarrow \text{Carbon deposits} \quad (4.25)$$

An alternative mechanism for SR of ethanol over Pt/Al_2O_3 at 300-400 ℃ was presented by Sutton et al. [110]. In this mechanism, the initial step was dehydrogenation of α-C-H in ethanol followed by dehydrogenation to ketenyl ($CHCO*$) and C-C bond scission of ketenyl. However, ethoxy species has been observed by diffuse infrared Fourier transform spectroscopy on $Ni/MgAl_2O_4$ catalyst in SR of ethanol [220], which indicates that the presented mechanism could be valid. The differences in the mechanisms could be due to the active metal as well as temperature interval investigated.

Acetaldehyde has been reported as an intermediate in several studies and is therefore included in the mechanisms [89, 97, 110, 200]. However, the results from this study suggest that the ethene is a more significant intermediate.

Increasing the amount of steam in the SR of ethanol over $Ni/MgAl_2O_4$ increased the conversion and yield of H_2 and decreased the carbon deposition and yield of hydrocarbons. These effects are consistent with the mechanism shown in reactions 4.2-4.25. Reaction 4.2 and subsequent reaction 4.3 will shift toward the right with increasing steam concentration leading to higher amounts of $H*$ and $O*$. The O-species will increase the partial and full oxidation of $C*$, reactions 4.5, 4.6, and 4.23, which in turn will decrease the accumulation of carbon on the surface. The increased amount of $H*$ on the surface will shift reaction 4.7 toward the right leading to a higher production of H_2.

Addition of O_2 to the feed increased conversion and decreased yield of H_2 as well as the carbon deposition. This can be understood because addition of O_2 increased the amount of $O*$ on the surface of the catalyst through dissociative adsorption of O_2:

$$O_2(g) + 2* \rightleftharpoons 2O* \quad (4.26)$$

This will, like for the addition of steam, lead to increased oxidation of $C*$ to carbon oxides. Furthermore it will inhibit the dissociation of $OH*$, reaction 4.3, and of H_2O, reaction 4.2, leading to lower amounts of $H*$ and subsequently lower yields of H_2.

Addition of H_2 to the feed in high concentration led to a decrease in conversion and increase in the yield of CH_4. The amount of $H*$ will increase with increasing concentration of H_2 in the feed through reaction 4.7, which will shift reactions 4.19-4.21 toward the left and lead to a higher formation of CH_4 in reaction 4.18. Furthermore the presence of $H*$ might inhibit the WGS leading to less $O*$ and lower degree of oxidation of carbon.

The proposed rate determining step in SR of ethanol differs between different studies of SR of ethanol. Sahoo et al. [104] used dehydrogenation of adsorbed ethoxy, reaction 4.9, in the development of a microkinetic model for SR of ethanol over Co/Al_2O_3. Sutton et al. [110] found by kinetic analysis and DFT calculations for SR of ethanol on Pt/Al_2O_3 that either dehydrogenation of α-C-H or C-C bond scission of ketenyl. Graschinsky et al. [109] reported that the surface reactions of C_1-species, reactions 4.19-4.23, were rate limiting in the SR of ethanol over $Rh(1\%)MgAl_2O_4/Al_2O_3$. Furthermore a parallel can be drawn to SR of CH_4, where Jones et al. [221] concluded that either C-oxidation, reaction 4.23, or CH_4 activation was the rate limiting step in SR of CH_4 depending on the applied temperature. CH_4 activation is less relevant in SR of ethanol and therefore the assumption of reaction 4.23 being rate limiting could be valid. This is supported by the experimental observation that increasing S/C- or O/C-ratio increased the conversion. In that case, increasing the amount of $O*$ on the catalyst leads to higher rates of reactions 4.8-4.22 and a higher degree of conversion and lower yield of hydrocarbons. This is in line with observations by Graschinsky et al. [109] and Llerca et al. [108].

4.7 Conclusions

The influence of feed gas composition in terms of O_2, H_2 and H_2O concentrations on SR of ethanol over Ni-based catalysts has been investigated in this chapter. Most experiments were made using a $Ni/MgAl_2O_4$ catalyst but also Ni/CeO_2 and $Ni/Ce_{0.6}Zr_{0.4}O_2$ were investigated. Increasing the S/C-ratio from the stoichiometric value of 1.5 to 8.2 improved the performance of the catalyst significantly as the conversion of ethanol and yield of H_2 increased while the yield of hydrocarbons and carbon deposition decreased. At S/C-ratio of 8.2 and 600 ℃ the conversion was 80 %, the yield of H_2 was 73 %, and the rate of carbon deposition was 1.8 $\frac{mmole\ C}{mole\ C_{Feed}}$ or 11.4 $\frac{mg\ C}{g_{Cat} \cdot h}$ in a 4 h experiment at the applied space velocity. The decrease in carbon deposition with increasing S/C-ratio was mainly ascribed to a faster conversion of ethene, which is a main intermediate species in the conversion of ethanol, and a severe coke precursor.

The addition of O_2 was particularly beneficial as conversion of ethanol increased while the yield of hydrocarbons and carbon deposition decreased with increasing O/C-ratio. Oxygen addition at an O/C-ratio of 0.8 to 1.0 decreased the carbon deposition to less than 0.02 $\frac{mmole\ C}{mole\ C_{Feed}}$ or 0.2 $\frac{mg\ C}{g_{Cat} \cdot h}$ over both $Ni/MgAl_2O_4$ and $Ni/Ce_{0.6}Zr_{0.4}O_2$. The penalty of adding oxygen was a loss in the yield of H_2 from 70 % to 50 % when increasing the O/C-ratio from 0 to 0.8-1.0. The decrease in carbon deposition was probably due to oxidation of carbon, while the lower yield of H_2 was due to oxidation of H_2, CO and hydrocarbons to CO_2 and H_2O. The beneficial effects of adding O_2 to the feed over $Ni/MgAl_2O_4$ catalysts, decreased carbon deposition and increased conversion, was also found on Ni/CeO_2 and $Ni/Ce_{0.6}Zr_{0.4}O_2$ catalysts.

Addition of H_2 to the feed did not improve the SR of ethanol significantly with respect to conversion, carbon deposition, or yield of hydrocarbons. High amounts of H_2 in the feed led

to lower conversion of ethanol, probably due to a high coverage of H_2 preventing ethanol to react or a decrease in surface O-species on the catalysts.

A long term test over 90 h showed that stable operation and high conversion with very low rate of carbon deposition, 7 $\frac{\mu g\ C}{g_{Cat} \cdot\ h}$, could be achieved over $Ni/MgAl_2O_4$ with O_2 in the feed at an O/C-ratio of 1.1. The results showed that oxidative SR of ethanol is the most promising method for enhancing the performance of Ni-based catalysts in the SR of ethanol.

5. STEAM REFORMING OF LIGHT WATER SOLUBLE OXYGENATES

Steam reforming of oxygen containing hydrocarbons other than acetic acid and ethanol has not been investigated to a great extent and little is known of reaction mechanisms and how they depend on the oxygen functionality and chain length. Therefore this chapter will investigate the SR of different light oxygenates, ethanol, acetic acid, acetone, acetol, 1-propanol, and propanal to elucidate differences in reactivity, reaction mechanisms, and side reactions. Furthermore will deactivation and carbon deposition during SR of these light oxygenates be investigated. Acetic acid and acetol were chosen because they are present in bio-oil and the aqueous fraction of bio-oil [19, 20], while the remaining model compounds were chosen to elucidate general trends in the SR of oxygenates.

Studies of SR of bio-oil have been conducted with the entire oil fraction, the aqueous fraction, or with single model compounds like ethanol or acetic acid [66, 67, 74, 104, 122, 141–144, 200, 222]. Other model compounds, which have been investigated to a lesser extent compared with bio-oil, ethanol, and acetic acid are; acetol [61, 131, 223, 224], propanol [131, 224–226], butanol [61, 131], ethylene glycol [59, 143, 182, 183, 187], acetone [59, 64, 75, 131, 224], ethyl acetate [59, 224], phenol [134, 136–138, 201], and sugars like glucose and sorbitol [59, 186, 227].

In the SR of hydrocarbons the main products are CH_4, CO_2, CO, and H_2, but small amounts of hydrocarbons larger than C_1 can also be formed [219, 228–232]. The suggested reaction mechanism is that the hydrocarbon adsorbs on surface followed by sequential cleaving of the C-C-bonds [219, 229]. This leads to C_1-fragments which can desorb as CH_4 or react further forming CO, CO_2, and H_2 by breaking the C-H bonds and reacting with O-species on the surface of the catalyst. The conversion at a given temperature is lowest for CH_4 and in the same range for hydrocarbons with longer chains [228].

Reaction mechanisms for ethanol and acetic acid suggest that the first step is adsorption through the oxygen followed by breaking of the C-C-bonds, which mainly produces C_1-species [75, 78, 104, 109, 110, 233].

The main products reported in the SR of oxygen containing hydrocarbons are carbon oxides, hydrogen, and hydrocarbons of equal or shorter chain length than the original compounds [61, 64, 131, 234]. Side reactions like dehydrogenation, condensation, and ketonization, which lead to oxygen containing products, have also been observed [226].

One of the few studies comparing the SR of different oxygenates at similar conditions was conducted by Palmeri et al. [131]. A similar conversion was observed in the SR of C_2-C_4 alcohols while a decrease in conversion with increasing carbon number was observed in the SR of C_2-C_4 ketones and aldehydes in this study [131]. Furthermore it was found that the CH_4 selectivity increased with increasing chain length while the H_2 selectivity decreased for both alcohols, ketones, and aldehydes [131]. A decrease in reactivity and an increase in carbon deposition with increasing chain length has also been reported by Hu and Lu [224] in the SR of both ketones and alcohols.

$Ni/MgAl_2O_4$ was chosen as catalyst in this study, as it was mainly focused on differences in reactivity, reaction pathways, and deactivation between the different model compounds

and these trends should be similar for more active catalyst with less carbon deposition like Ni/CeO_2-$K/MgAl_2O_4$.

5.1 Characterization

The surface area and NiO particle size were determined for the $Ni/MgAl_2O_4$ catalyst used for these experiments. The characteristics of the support and catalyst can be seen in table 5.1.

Tab. 5.1: *Characterization results of the fresh catalysts prepared by calcination in stagnant air at 800 ℃. The NiO peak at $2\theta = 62.8°$ was used for determination of particle size.*

Catalyst	Ni loading $[wt\%]$	Surface area $[m^2/g]$	$d_{p,\mathrm{NiO}}$ $[nm]$
$MgAl_2O_4$	-	143	-
$Ni/MgAl_2O_4$	8.2	115	5

The catalyst, $Ni/MgAl_2O_4$, had a surface area of roughly 115 m^2/g, which was lower compared to the support, indicating sintering during the calcination of the catalysts. The NiO particles were quite and roughly 5 nm in diameter. XRD analysis of the catalyst showed a $MgAl_2O_4$ and NiO phase and did not indicate that Ni was incorporated into the spinel structure, see fig. 5.1.

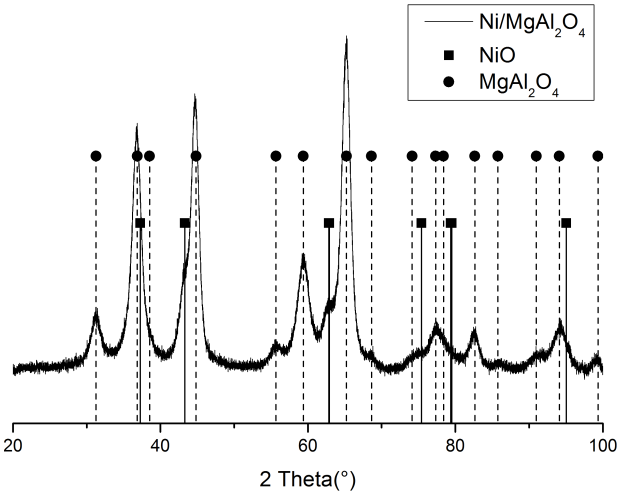

Fig. 5.1: *XRD pattern for fresh $Ni/MgAl_2O_4$.*

5.2 General trends

The effect of temperature and time-on-stream in the SR of several light oxygenates has been investigated at S/C of 6 and a mole fraction of oxygenates and H_2O of 2-3 % and 36 %, respectively. The total flow rate and molar flow of C were similar in each experiment.

In the SR of different model compounds it was found that the trends in the yield of CO and CO_2 with temperature were in accordance with the equilibrium of the WGS at temperatures of 500 ℃ or above. This means that the yield of CO increased with temperature while the yield of CO_2 decreased. The yield of H_2 increased with temperature in all the cases and a

maximum yield of H_2 of roughly 70-80 % was observed at 700 ℃, showing that H_2-production was not significant at 400 and 500 ℃. The conversion of the model compounds increased with temperature from roughly 10 % at 400 ℃ to full conversion at 700 ℃.

Blank experiments in the SR of ethanol showed conversion of less than 15 % at 700 ℃ and less than 2 % at 500 ℃, so the contribution from homogeneous reactions is considered to be insignificant. Similar degrees of conversion have been reported in the SR of ethanol [57, 61, 89, 235] and SR of acetic acid [48, 68] in a blank reactor. Higher degrees of conversion have been reported in blank experiments in the literature [81, 125, 236] but it is usually over quartz or SiC particles and therefore not comparable to our experiments as we do not dilute our catalyst.

The effect of the support material, $MgAl_2O_4$, has been tested in the SR of ethanol at 600 ℃ and only showed dehydration activity with a conversion of 30 %, so the production of carbon oxides and H_2 is mainly related to metal particles. A conversion of 40 % has been reported in the SR of acetic acid over $CaAl_2O_4$ at 750 ℃ mainly to decomposition products, CH_4 and CO_2, and similar products were reported in the SR of acetone over the same support material, although the conversion was 80 % [64]. Basagiannis and Verykios [48] reported almost zero % conversion of acetic acid over Al_2O_3 and La_2O_3 at 700 ℃. Therefore $MgAl_2O_4$ may induce dehydration but formation of CH_4 as well as CO, CO_2, and H_2 is mainly related to Ni and interactions between Ni and $MgAl_2O_4$. Ketonization and other coupling reaction may also be catalyzed by MgAl2O4 as oxides have shown activity for these reactions [237–239].

5.3 Steam reforming of ethanol

The conversion of ethanol and the product yields of CO, CO_2, H_2, CH_4, and C_2H_4 as functions of temperature in the SR of ethanol are summarized in fig. 5.2. The yield of CO_2 had a maximum at 600 ℃, while the yield of CO increased with temperature from 500 to 700 ℃. This is consistent with an increased activity for the SR reactions and shift in the WGS with temperature as predicted by thermodynamic equilibrium. The yield of H_2 increased with temperature from 6 % at 400 ℃ to 74 % at 700 ℃. The yield of methane was high at low temperatures (29 % at 400 ℃), but decreased with temperature and ended at 0 % at 700 ℃, while the yield of C_2H_4 had a maximum of 3 % at 500 ℃, although only slightly higher compared with yield at 400 ℃, and decreased to 0 % at 600 ℃. Ethene is most likely formed through dehydration of ethanol and is known as a severe carbon precursor [32, 100]. Note that with the chosen definition of yield it is possible to have a high yield even if the conversion is low.

These results suggest that ethanol adsorbs on the surface and then either dehydrate to ethene or break the C-C-bond leading to the formation of two C_1-species, which can, depending on the temperature, react and form either CH_4 or CO_x. Ethene migth also react further to CH_2* by breaking the C-C-bond. Further information on the SR of ethanol can be found in chapters 1, 3, and 4 and in refs. [49, 50, 99, 104, 240].

5.4 Steam reforming of acetic acid

The conversion of acetic acid and the product yields of CO, CO_2, H_2, CH_4, and acetone as functions of temperature in the SR of acetic acid is summarized in fig. 5.3. Here it can be seen that the main products were CO_2 and CO at all temperatures, while at low temperatures CH_4 and acetone were formed as well. From 500 to 700 ℃ the yield of CO_2 slightly decreased

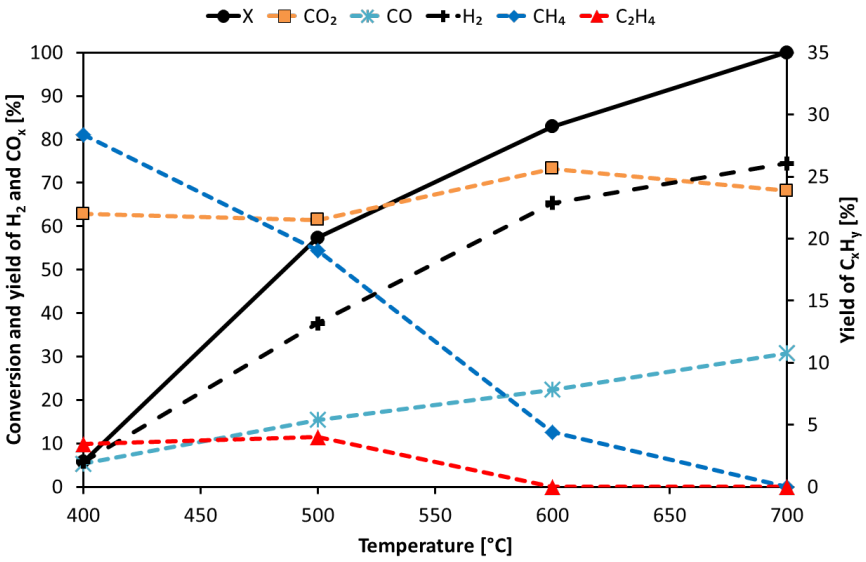

Fig. 5.2: *Conversion and yield of CO, CO_2, H_2, CH_4, and C_2H_4 as functions of temperature in SR of ethanol. 8.0 wt% $Ni/MgAl_2O_4$, S/C= 6.0, m_{Cat} = 50 mg, Flow= 230 NmL/min, x_{Eth}= 3 %, x_{H2O}= 36 %, N_2 as balance.*

while the yield of CO increased indicating that the WGS shifted towards CO and H_2O. The yield of H_2 increased with temperature from 5 % at 400 °C to 80 % at 700 °C.

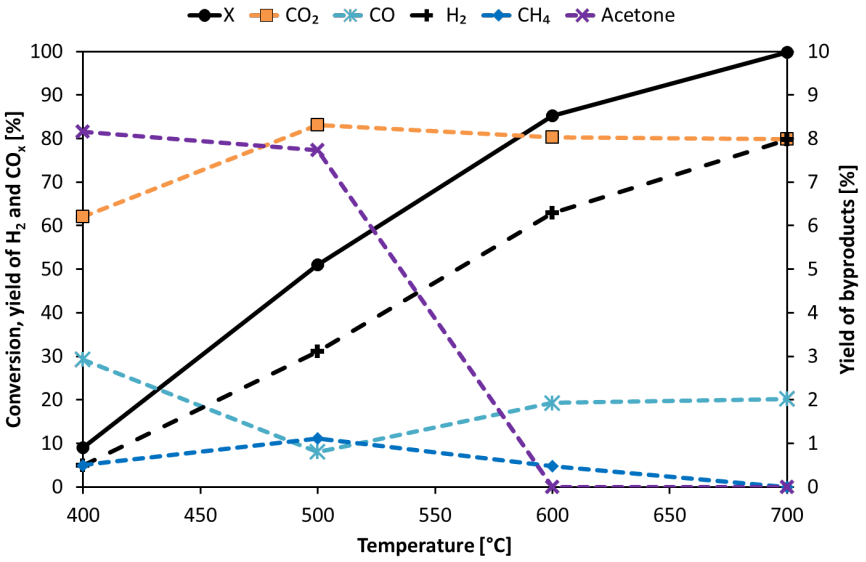

Fig. 5.3: *Conversion and yield of CO, CO_2, H_2, CH_4, and acetone as functions of temperature in SR of acetic acid. 8.0 wt% $Ni/MgAl_2O_4$, S/C= 6.0, m_{Cat} = 50 mg, Flow= 210 NmL/min, y_{AA}= 3 vol%, y_{H2O}= 36 vol%, N_2 as balance.*

Ketonization of acetic acid to acetone occurred at 400 and 500 °C and the yield of acetone was roughly 8 %. The yield of CH_4 was less than 1 % for all the temperatures and decreased with temperature and was thus much lower in the SR of acetic acid compared to the SR of ethanol. It might have been expected that the yield would be similar to yield of CH_4 in SR of ethanol as breaking the C-C bond in both cases would form a CH_3 and CH_xO_y-species, where especially the CH_3-species are likely to react with H forming CH_4 at low temperatures. Ketonization of acetic acid is shown by DFT and experiments to occur through the β-keto

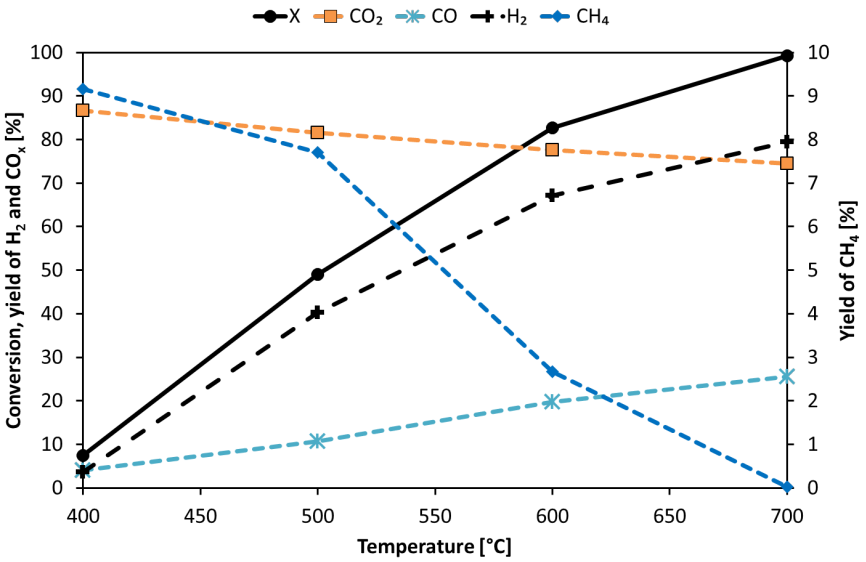

Fig. 5.4: *Conversion and yield of CO, CO_2, H_2, and CH_4 as functions of temperature in SR of acetone. 8.0 wt% $Ni/MgAl_2O_4$, S/C= 6.0, m_{Cat} = 50 mg, Flow= 210 NmL/min, y_{Ace}= 2 vol%, y_{H2O}= 36 vol%, N_2 as balance.*

acid route on ZrO_2 [237]. The lower yield of CH_4 could be due to ketonization, which form CO_2 and acetone and hereby remove two potential CH_3-species, which could be converted to CH_4. Furthermore the oxygen containing part of ethanol might also be easier to convert to methane as only one C-O bond needs to be broken before a CH_x-fraction is formed. For acetic acid two C-O bonds needs to be broken.

It appears that acetic acid can follow two reaction pathways after adsorption; it can either undergo ketonization to acetone or cleaving of the C-C-bond leading to C_1-species. The carbon precursor, ethene, was not observed. DFT-calculations on SR of acetic acid over Co show that the most favorable reaction pathway is adsorption through the carbonyl group, followed by removal of one oxygen atom and subsequent C-C-bond scission [78].

5.5 Steam reforming of acetone

The conversion of acetone and the product yields of CO, CO_2, H_2, and CH_4 as functions of temperature in the SR of acetone can be seen in fig. 5.4. There was mainly observed CO, CO_2, and CH_4 as the carbon containing products. However, small amounts of self-condensation products like 4-methyl 4-penten-2-one were observed at 400 °C. The yield of CO increased with temperature, while the yield of CO_2 and CH_4 decreased with temperature. The formation of methane and carbon oxides as the only products suggests that the acetone adsorbs through the carbonyl and then cleaves both of the C-C bonds. C_2-compounds like ethanol, acetaldehyde, or ethene might be expected in the product gas, but these compounds were not observed. This indicates that CH_3CO* formed when removing one of the methyl groups undergoes rapid transformation into $CO*$ and CH_3*.

5.6 Steam reforming of propanal

The conversion of propanal and the product yields of CO, CO_2, H_2, CH_4, and C_2-species as functions of temperature in the SR of propanal can be seen in fig. 5.5. There was observed

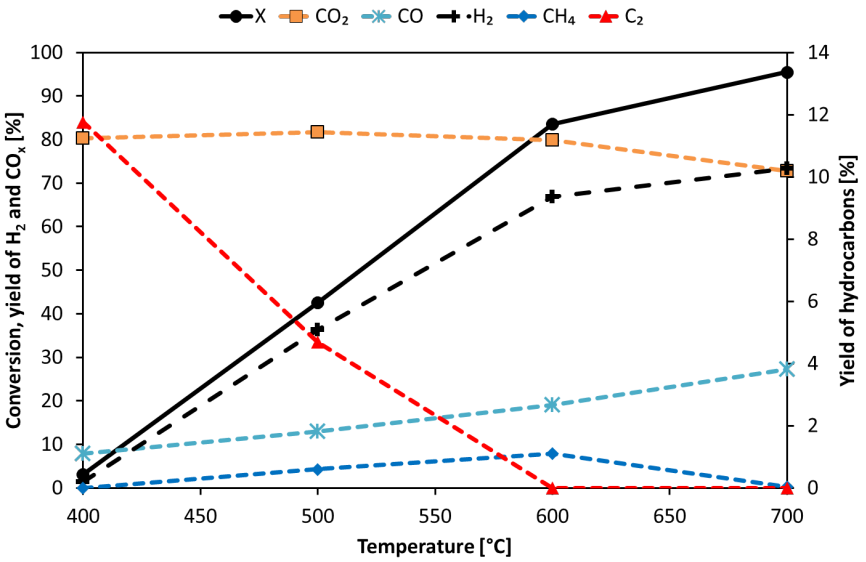

Fig. 5.5: *Conversion and yield of CO, CO_2, H_2, CH_4, and C_2H_4 as functions of temperature in SR of propanal. 8.0 wt% $Ni/MgAl_2O_4$, S/C= 6.0, m_{Cat} = 50 mg, Flow= 210 NmL/min, y_{PA}= 2 vol%, y_{H2O}= 36 vol%, N_2 as balance.*

ethene, ethane, methane, and carbon oxides as products. The C_2-fraction consisted of roughly 2/3 ethene and 1/3 ethane and the relative amounts of these species were not significantly influenced by temperature. At 400 ℃ there was a high yield of C_2-species and no formation of CH_4. Methane was observed in the SR of acetone, ethanol, and acetic acid at 400 ℃ and the difference could be that more C-C-bonds needs to be broken to convert propanal to methane compared with the model compounds discussed so far. The yield of C_2-species decreased with temperature while the yield of CH_4 increased with temperature until 600 ℃ and decreased hereafter. The formation of C_2-compounds could come from breaking the C-C bond closest to the carbonyl group in propanal and methane might be produced from breaking the C-C-bond in the C_2-species on the surface. This would also explain the increasing level of methane in the offgas, while the yield of C_2-species decreased.

The results suggest that the propanal is converted by sequential breaking of carbon backbone from the carbonyl end as no oxygen containing by-products were formed.

5.7 Steam reforming of 1-propanol

The conversion of 1-propanol and the product yields of CO, CO_2, H_2, CH_4, C_2-species, propene, and propanal as functions of temperature in the SR of 1-propanol are summarized in fig. 5.6. There was observed the same products as in SR of propanal with the addition of propene and propanal, which can be formed through dehydration and dehydrogenation of 1-propanol. The C_2 product fraction consisted of 75-85 % ethene and 15-25 % ethane. The major products were propene, CO_2, propanal, and C_2-species at 400 ℃. The yield of propene, C_2-species, and propanal all decreased with temperature and reached 0 % at 600 ℃. The yield of CH_4 increased with temperature until 600 ℃ and then decreased. This behavior was similar to what was observed in the SR of propanal and suggest that methane might be formed from further reaction of C_3- and C_2-species and is not a primary product.

The reaction path for conversion of 1-propanol appears to be a sequential scission of the carbon backbone similarly to what was observed in the SR of propanal. No methanol and ethanol was observed in SR of 1-propanol, indicating that the C-C-bond scission starts from the

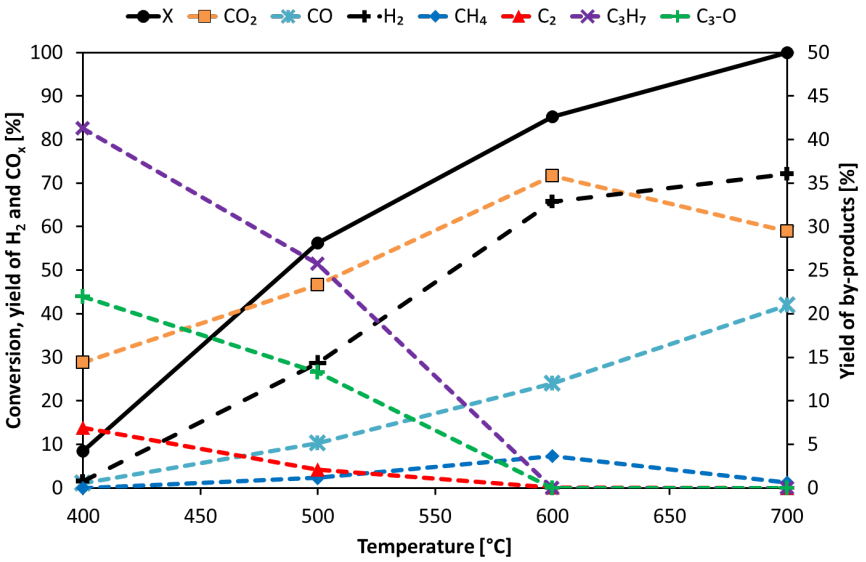

Fig. 5.6: *Conversion and yield of CO, CO_2, H_2, CH_4, and C_2H_4, C_3H_7, and propanal as functions of temperature in SR of 1-propanol. 8.0 wt% $Ni/MgAl_2O_4$, S/C= 6.0, m_{Cat} = 50 mg, Flow= 210 NmL/min, y_{PO}= 2 vol%, y_{H2O}= 36 vol%, N_2 as balance.*

hydroxyl end. Furthermore, it appears that dehydration is favored over this catalyst as a large fraction of ethene and propene was observed in SR of ethanol and 1-propanol, respectively.

5.8 Steam reforming of acetol

The conversion of acetol and the product yields of CO, CO_2, H_2, CH_4, and other products as functions of temperature in the SR of acetol can be seen in fig. 5.7. The products from SR of acetol was different from the other oxygenates investigated, especially at 400 and 500 ℃. Here a large fraction of products were formed through different condensation reactions forming butanediol, 2,5-hexanedione, substituted cyclopentanedione, furandiones, and furanones (Others in fig. 5.7) and constituted the major product group at both 400 and 500 ℃. Furthermore, there was observed small amounts of ethanol and acetaldehyde as products as well, which can be formed by breaking of one of the C-C-bonds in acetol. The yield of CH_4 had a maximum at 500 ℃ and then decreased to 0 % at 700 ℃, while the yield of H_2 increased from 0 at 400 ℃ to 76 % at 700 ℃. Acetol has two oxygen functionalities and this seems to induce a high formation of condensation products especially at low temperatures. This might be explained by a free oxygen end, when acetol is adsorbed on the catalyst, which can react with other compounds on the surface and oligomerize.

Two main types of reaction pathways can take place in the SR of acetol, either condensation reactions leading to larger compounds or C-C-bond breaking leading to smaller compounds like CO_x, H_2, and CH_4.

5.9 Comparison

The conversion of the investigated model compounds as function of temperature is summarized in fig. 5.8. There was mainly a difference in conversion at 500 ℃, while the conversions were similar at all other temperatures. The higher conversion of acetol at 400 ℃ and 500 ℃

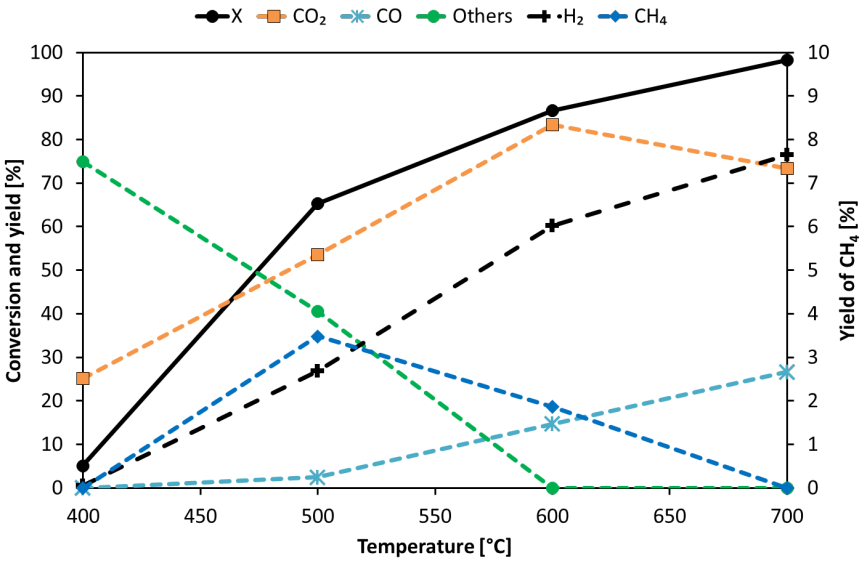

Fig. 5.7: *Conversion and yield of CO, CO_2, H_2, CH_4, and condensation products (others) as functions of temperature in SR of acetol. 8.0 wt% $Ni/MgAl_2O_4$, S/C= 6.0, m_{Cat} = 50 mg, Flow= 210 NmL/min, y_{AT}= 2 vol%, y_{H2O}= 37 vol%, N_2 as balance.*

compared with the other compounds was mainly as condensation products and included a wide range of different oxygenates, as discussed above. The conversion of ethanol was similar to the conversion of 1-propanol at all temperatures, which indicates that the chain length of oxygenate did not influence the total conversion in the SR of alcohols. Similar results were obtained by Palmeri et al. [131] for SR of alcohols. Furthermore the conversion of acetone was higher compared to the conversion of propanal indicating that the position of the oxygen functionality in the molecule influences the reactivity. In this case, it might be explained by a more favorable conversion of CH_3CO* formed when breaking the first C-C-bond in acetone. These species are probably more readily converted compared with ethene or C_2-species formed by breaking the first C-C-bond in propanal. DFT-calculations on the conversion of acetic acid shows that conversion of CH_3CO* to CH_3* and $CO*$ is favorable with a decrease in energy of 38 $kJ/mole$ and an activation energy of 78 $kJ/mole$ [78].

Many by-products were produced at 400 and 500 ℃ and a comparison of the yield of oxygenates as function of temperature can be seen in fig. 5.9(a), while a comparison of yield of hydrocarbons as function of temperature can be seen in fig. 5.9(b). The yield of both types of by-products decreased with temperature and were close to zero above 600 ℃. For the alcohols it can be seen that relatively high amounts of hydrocarbons were formed and a fraction of those were olefins, ethene and propene, which might cause problems with carbon deposition as indicated in the previous chapters as well in refs. [30, 32, 100]. The yield of hydrocarbons and oxygenates were higher for 1-propanol compared ethanol, which indicates that the reactivity decreased slightly with increasing chain length. Similar results has been reported by Palmeri et al. [131]. Acetic acid, 1-propanol, and acetol produced oxygen containing compounds as well as hydrocarbons. Acetol had the highest yield of oxygenates of all the compounds.

From fig. 5.9 it appears that temperatures above 600 ℃ are needed to avoid by-products in the offgas. However this might be due to either a higher degree of conversion or a changed reaction path at higher temperature. To investigate this, an experiment at a higher space velocity at 600 ℃ was carried out while keeping the overall conversion close to that at 500 ℃ and the lower space velocity. A comparison of the yield of by-products at the two conditions

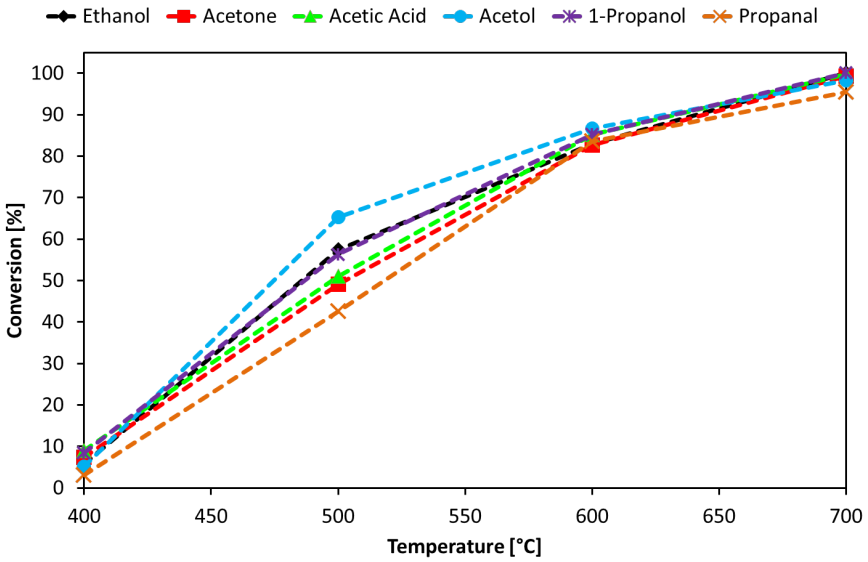

Fig. 5.8: *Conversion as function of temperature in SR of ethanol, acetic acid, acetone, 1-propanol, and propanal. 8.0 wt% $Ni/MgAl_2O_4$, S/C= 6.0, m_{Cat} = 50 mg, Flow= 210 NmL/min, y_{Oxy}= 2-3 vol%, y_{H2O}= 37 vol%, N_2 as balance.*

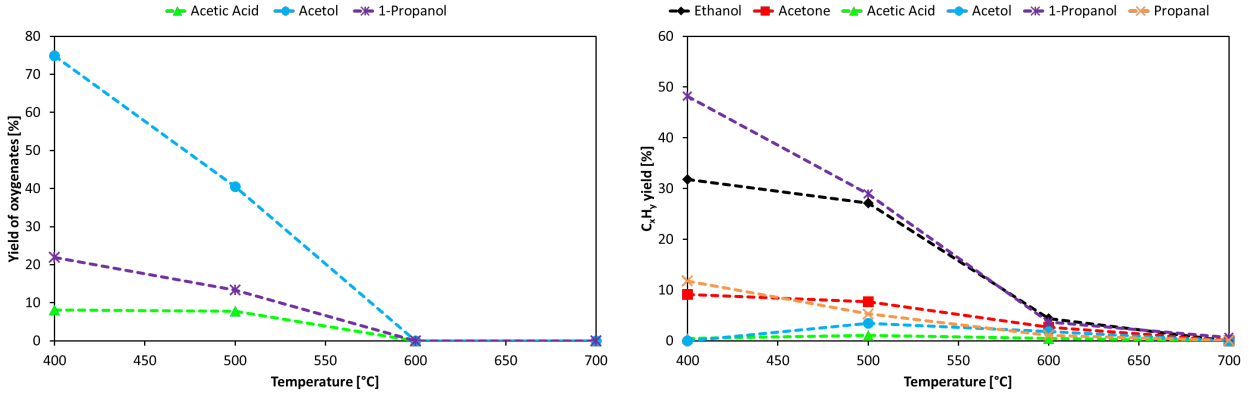

(a) Yield of oxygen containing hydrocarbons

(b) Yield of hydrocarbons

Fig. 5.9: *Yield of by-products as function of temperature in SR of light oxygenates. 8.0 wt% $Ni/MgAl_2O_4$, S/C= 6.0, m_{Cat} = 50 mg, Flow= 230 NmL/min, y_{Oxy}= 2-3 vol%, y_{H2O}= 36 vol%, N_2 as balance.*

can be seen in table 5.2. For most of the experiments at 600 ℃ the yield of hydrocarbons and oxygenates were lower compared to the experiment at 500 ℃. It was especially pronounced for acetol, where a decrease in yield of oxygenates from 51 to 5 % was observed at similar conversion but different temperatures. Furthermore the by-products were mainly acetone, ethanol, and acetaldehyde at 600 ℃ and not condensation products as observed at 500 ℃. Therefore it appears that operation at 600 ℃ or higher minimized the formation of by-products and especially condensation products.

The desired compounds in SR are carbon oxides and H_2 and the conversion to carbon oxides (CO_x) can be seen in fig. 5.10. Here it can be seen that the conversion of C_2 oxygenates was slightly higher compared with C_3 oxygenates. This indicates that the reactivity decreased with chain length. The one exception was acetone, which might be because breaking of the C-C

Tab. 5.2: *Comparison of conversion, yield of hydrocarbons, and yield of oxygenates at different temperatures and similar conversions. 8.0 wt% $Ni/MgAl_2O_4$, S/C= 6.0, m_{Cat} = 25 – 50 mg, Flow= 210 NmL/min, y_{Oxy}= 2-3 vol%, y_{H2O}= 36 vol%, N_2 as balance.*

Compound	Temp [°C]	X [%]	$Y_{C_xH_y}$ [%]	$Y_{C_xH_yO_z}$ [%]
Ethanol	500	57	27	0
Ethanol	600	68	12	0
Acetone	500	49	11	0
Acetone	600	60	2	0
Acetic Acid	500	51	1	8
Acetic Acid	600	62	0	8
Acetol	500	65	3	51
Acetol	600	58	2	5
1-Propanol	500	59	33	13
1-Propanol	600	65	27	5
Propanal	500	43	5	0
Propanal	600	61	6	0

bond closest to carbonyl group would lead to CH_3-species, which might be easier to convert as discussed previously.

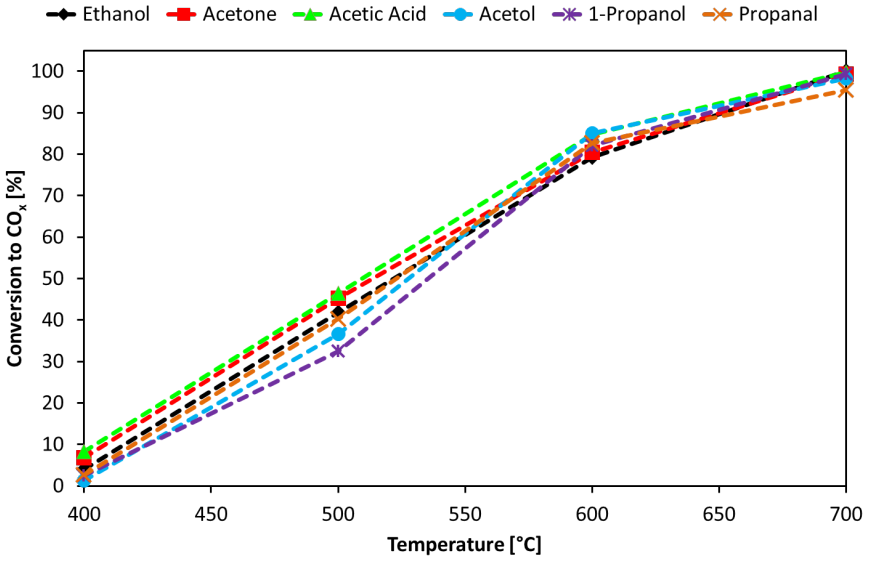

Fig. 5.10: *Conversion to carbon oxides as function of temperature in SR of light oxygenates. 8.0 wt% $Ni/MgAl_2O_4$, S/C= 6.0, m_{Cat} = 50 mg, Flow= 210 NmL/min, y_{Oxy}= 2-3 vol%, y_{H2O}= 37 vol%, N_2 as balance.*

5.9.1 Reaction pathway

Steam reforming of light oxygenates over $Ni/MgAl_2O_4$ at low temperatures produced a large fraction of byproducts with similar or shorter chain length than the parent model compounds. For alcohols dehydration to olefins or dehydrogenation to aldehydes with the same chain length were observed, while for the carbonyls only decarbonylation products were observed.

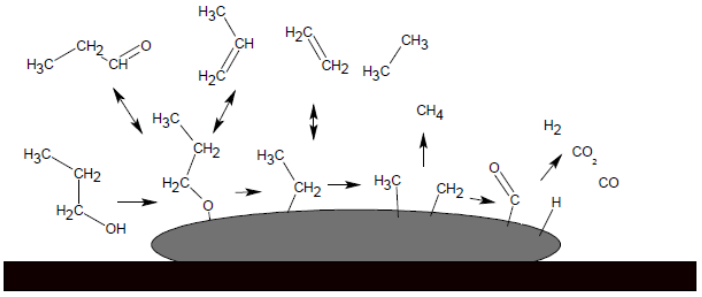

Fig. 5.11: *Proposed reaction pathway in SR of 1-propanol.*

This indicates that the first step in the reaction is adsorption to the catalyst site through the oxygen functionality. Adsorption through oxygen is shown to be preferred by DFT-studies on adsorption of oxygenates on transition metal surfaces [78, 233, 241, 242]. The products shifted from C_3 and C_2-species towards C_1-species with increasing conversion and temperature and furthermore a build-up of CH_4 was observed as C_3 and C_2-species was converted. This indicates that the conversion occurs through sequential breaking of the C-C-bonds in the oxygenate. Furthermore, in the SR of acetone, only C_1-products were formed, which also fits the proposed pathway of adsorption through the oxygen and breaking of the C-C-bonds closest to the oxygen. The proposed reaction pathway is shown for SR of 1-propanol in fig. 5.11.

The formation of condensation products at 500 °C was significantly higher for acetol which has two oxygen containing functional groups. This could be due to a free oxygen functionality, which can react with other surface species forming larger chains.

Carbon deposits can be formed through the Boudouard reaction, CO decomposition, polymerization of acetone, methane decomposition, as well as through polymerization of ethene and propene depending on the temperature and S/C-ratio.

5.9.2 Deactivation

Steam reforming of the different model compounds was investigated for 4 hours at 600 °C, S/C-ratio of 6, and with a conversion between 60-80 %. The influence of time-on-stream on the conversion can be seen in fig. 5.12. The conversion for all of the compounds decreased with time and the decrease was most pronounced for acetol and acetic acid, where the conversion decreased by 15-20 %-points, while for ethanol, 1-propanol, and propanal the decrease in conversion was roughly 10 %-points. The conversion of acetone was most stable with a 7 %-points decrease in conversion over time.

The final conversion (initial conversion can be seen in fig. 5.12), yield of by-products, and carbon deposition for a 4 hour experiment can be seen in table 5.3. The two model compounds which led to the highest carbon deposition were the two alcohols, ethanol and 1-propanol. This was due to the relatively high formation of ethene and propene, which are likely to polymerize as carbon deposits on the catalyst [31, 32, 100]. Acetic acid also had a high carbon deposition, while the other three model compound showed a 25 % lower carbon deposition. A higher carbon deposition in SR of alcohols compared to ketones and aldehydes over Ni/Al_2O_3 at 700 °C and S/C-ratio of 4 was also reported by Palmeri et al. [131]. However, the differences was more pronounced in the study by Palmeri et al. [131] as SR of ethanol resulted in 33 % higher carbon deposition compared with SR of acetaldehyde, while SR of 2-butanol produced 6 times

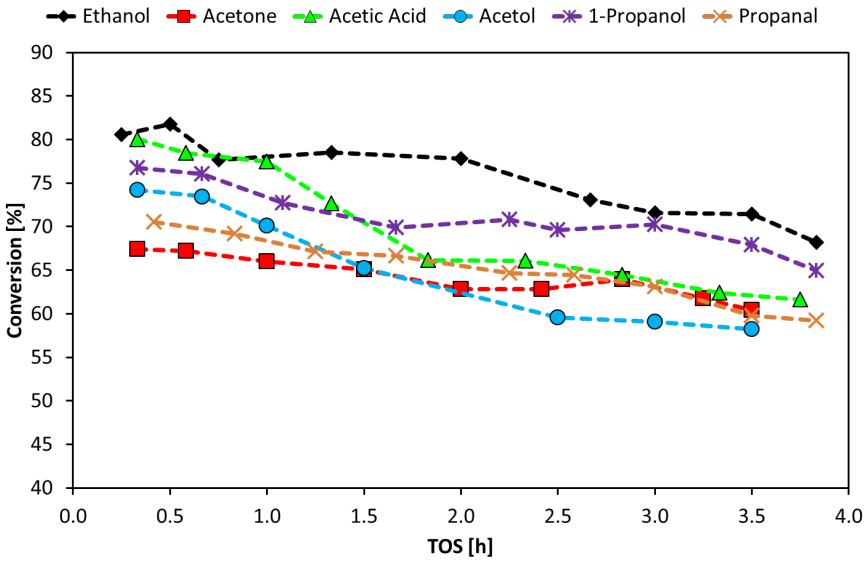

Fig. 5.12: *Conversion as function of time in SR of light oxygenates at 600 ℃. 8.0 wt% $Ni/MgAl_2O_4$, S/C= 6.0, m_{Cat} = 25 mg, Flow= 210 NmL/min, y_{Oxy}= 2-3 vol%, y_{H2O}= 37 vol%, N_2 as balance.*

Tab. 5.3: *Conversion, product yields, and carbon depositions in SR of light oxygenates at 600 ℃ after 4 h on stream. 8.0 wt% $Ni/MgAl_2O_4$, S/C= 6.0, m_{Cat} = 25 mg, Flow= 210 NmL/min, y_{Oxy}= 2-3 vol%, y_{H2O}= 37 vol%, N_2 as balance.*

Compound	X [%]	$Y_{C_xH_y}$ [%]	$Y_{C_xH_yO_z}$ [%]	Carbon deposition $[\frac{mg}{g_{Cat} \cdot h}]$	$[\frac{mmole_C}{mole_{C\ feed}}]$
Ethanol	68	12	0	41	2.5
Acetic acid	62	0.4	8	40	2.4
Acetone	60	2	0	32	1.9
Acetol	58	7	2	33	2.0
1-Propanol	65	28	5	42	2.5
Propanal	61	6	0	29	1.7

as much carbon as SR of 2-butanone. Hu and Lu [59] reported a higher carbon deposition in SR of acetone compared with acetic acid over Ni/Al_2O_3 at 600 ℃ and stoichiometric S/C-ratio. However, the opposite trend was observed in this study.

The carbon release during TPO of the spent catalysts is shown in fig. 5.13. Ethanol, 1-propanol, and acetone all show carbon oxidation in a single peak with a maximum at roughly 600-615 ℃. Acetol, acetic acid, and propanal had two carbon oxidation peaks, a main peak at roughly the same temperatures as the other model compounds, and a smaller peak at lower temperatures, 500-525 ℃. The low-temperature peak might indicate that encapsulating carbon was formed with these oxygen containing model compounds, as it would have close contact with Ni and therefore oxidize at a lower temperature. Furthermore acetol, acetic acid, and propanal also showed a rather steep deactivation with time on stream, which also could point to coverage of the Ni-particles by carbon, while whisker formation would not significantly deactivate the catalyst [30, 42].

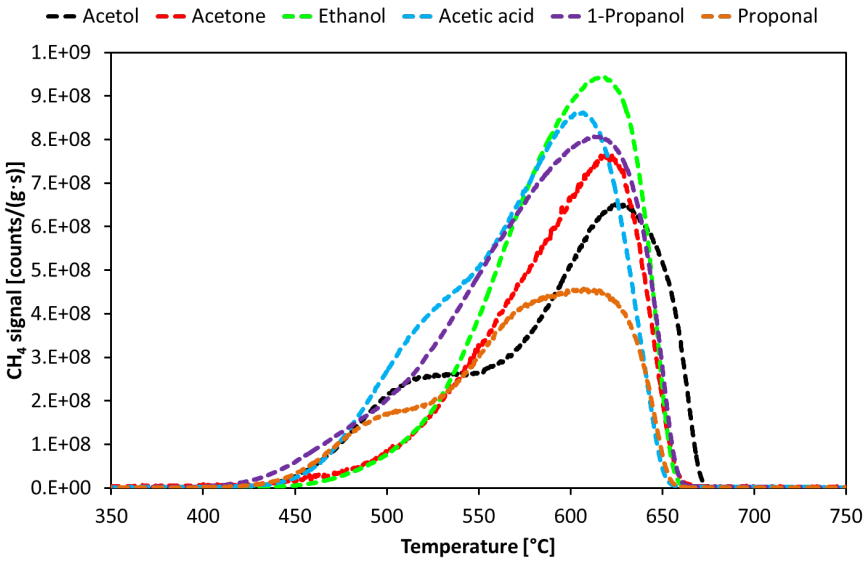

Fig. 5.13: *Formation of methane as function temperature during TPO of spent catalysts. $m_{Sample} = 2 - 5\ mg$, $\Delta\ T$: 10 °C/min, y_{O_2}= 5 vol%, He as balance. Methanation catalyst operated at 400 °C.*

5.10 Conclusions

Steam reforming of ethanol, acetic acid, acetone, acetol, 1-propanol, and propanal has been investigated on $Ni/MgAl_2O_4$ at temperatures between 400 and 700 °C at S/C-ratio of 6. In all the cases full conversion were achieved at 700 °C at the applied space velocity and the yield of H_2 varied between 70 and 80 %. The conversion as function of temperature did not vary significantly between the different model compounds. However, the yield of by-products was higher for C_3-oxygenates compared to C_2-oxygenates, which shows a decrease in reactivity with chain length.

The product gas consisted mainly of H_2, CO, CO_2, and CH_4 in various proportions and a fraction of by-products, which was most pronounced at temperature of 500 °C and below. Olefins and aldehydes were by-products in the SR of alcohols, while SR of propanal and acetone led to olefins and hydrocarbons as byproducts. Ketonization to acetone was observed in the SR of acetic acid at 500 °C and below. These results indicate that the SR of oxygenates proceeds through adsorption by the oxygen containing part followed by sequential breakage of the C-C-bonds.

Deactivation with time-on-stream was observed for all of model compounds and was most pronounced for acetol and acetic acid. However, the carbon deposition was roughly 30 % higher in the SR of alcohols and acetic acid compared with the SR of the remaining model compounds. The carbon deposition in the SR of alcohols was due to a high formation of olefins which are severe precursors for carbon deposition. The results further indicate that stable operation would require high S/C-ratios or oxidative reforming.

6. STEAM REFORMING OF CYCLIC OXYGENATES

Bio-oil contains many different compounds of varying size and little is known on the SR of other oxygen containing compounds other than ethanol and acetic acid. Furthermore are cyclic and aromatic compounds known to cause problems in SR and therefore the aim of this chapter is to investigate the SR of furfural, guaiacol, and 2-methyl furan. The focus will be on the product distribution as function temperature as well as function of time to investigate catalyst deactivation. Furthermore oxidative conditions will be investigated to clarify what levels of O_2 are needed for stable operation.

Steam reforming of bio-oil has been investigated with the entire oil fraction [67, 141, 146, 148, 150, 158, 163, 164, 243, 244] or the aqueous fraction of bio-oil, formed by water addition to the bio-oil [58, 142–144, 245, 246]. However there is a lack of studies with cyclic oxygenates as model compounds of bio-oil, which are present in the bio-oil and may be responsible for a high fraction of the carbon deposition. Recently Xu et al. [247] studied the SR of several model compounds of bio-oil, including furfural and *m*-cresol, over Ni/MgO at 600 ℃, S/C-ratio of 6, and liquid hourly space velocity (LHSV) of 5 h^{-1}. This study focused on the type of by-products formed, however the stability of system as well as the effect of temperature on product distribution was not investigated. Another study of SR of cyclic oxygenates was conducted Lan et al. [243], who investigated the SR of furfural and *m*-cresol at a S/C-ratio of 5 as function of temperature over several Ni/Al_2O_3 based catalysts and found that CO and CO_2 were the main products in the SR of furfural. Conversions above 90 % was achieved at temperatures above 700 ℃ and LHSV of 2.5 h^{-1}. A stability test over 10 h showed a slight deactivation, but the source of deactivation was not investigated [243]. To the authors knowledge, there are no other results on SR of furfural, guaiacol, and 2-methyl furan, which are all present in the bio-oil and may lead to severe deactivation.

Ni/CeO_2-$K/MgAl_2O_4$ have in chapter 3 showed high activity and low rate of carbon deposition in the SR of ethanol and therefore was it chosen as catalyst in this chapter.

6.1 Characterization

The surface areas and particle sizes of NiO and CeO_2 for the fresh catalysts used in this study can be seen in table 6.1. The surface area of Ni/CeO_2-$K/MgAl_2O_4$ was 78 m^2/g, while the NiO and CeO_2 particles had diameters of 7 nm and 6 nm, respectively. This was slightly higher compared with the NiO-particles on $MgAl_2O_4$, which was 5 nm in diameter. EDX-analysis of the catalyst showed that the loading of K, Ni, and CeO_2 was 3.2 $wt\%$, 7.8 $wt\%$, and 4.7 $wt\%$, respectively, which was closed to the nominal loading.

The XRD patterns of Ni/CeO_2-$K/MgAl_2O_4$ and $Ni/MgAl_2O_4$ are compared with the standard peaks for NiO, $MgAl_2O_4$, and CeO_2 in fig. 6.1. Here it can be seen that NiO and $MgAl_2O_4$ accounts for the peaks in the XRD pattern of $Ni/MgAl_2O_4$, while the additional peaks in the XRD pattern of Ni/CeO_2-$K/MgAl_2O_4$ corresponds to CeO_2. K was not observed on the XRD-pattern indicating that K is present as a layer, small crystallites, or amorphous K.

Tab. 6.1: *Characterization results of the fresh catalysts (Ni as NiO) prepared by calcination in stagnant air at 800 °C. Particles size of NiO and CeO_2 are determined based on the XRD patterns.*

Catalyst	Promoter	Ni loading [$wt\%$]	Surface area [m^2/g]	$d_{p,\ NiO}$ [nm]	$d_{p,\ CeO_2}$ [nm]
$MgAl_2O_4$	-		143	-	-
$Ni/MgAl_2O_4$	-	8.2	104	5	-
Ni/CeO_2-K/ $MgAl_2O_4$	5 $wt\%$ CeO_2 5 $wt\%$ K	8.2	78	7	6

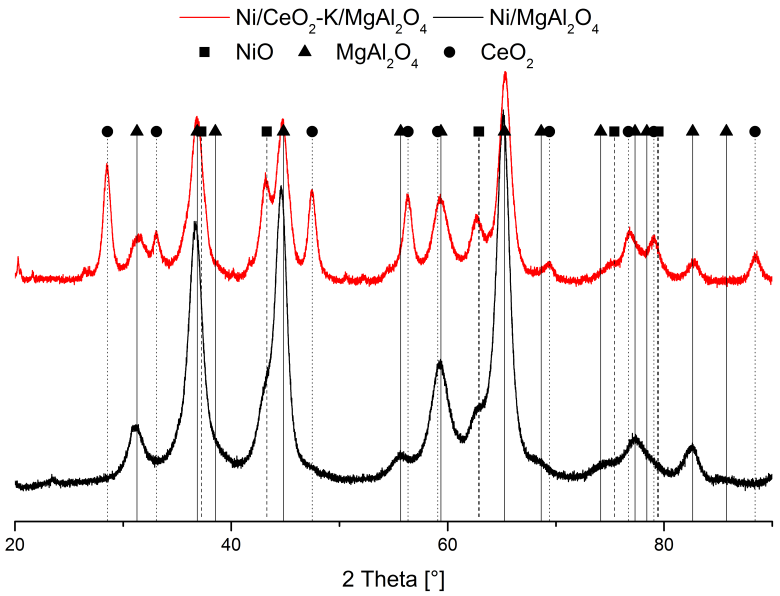

Fig. 6.1: *XRD patterns for unreduced catalysts, $NiO/MgAl_2O_4$ and Ni/CeO_2-$K/MgAl_2O_4$.*

6.2 Steam reforming of 2-methylfuran

Steam reforming of 2-methylfuran at S/C-ratio of 5 was carried out in an empty reactor to examine the extent of the homogenous decomposition of 2-methylfuran. The conversion to gasous products, CO, CO_2, CH_4, C_2-and C_3-hydrocarbons, was 3 % at 700 °C and increased to 66 % at 860 °C. Therefore homogeneous reactions seem to be insignificant at the investigated temperatures. It should be noted that carbon deposition was observed in reactor indicating that the thermal decomposition of 2-methylfuran also occurred.

Steam reforming of 2-methylfuran was investigated at temperatures between 400 and 700 °C over Ni/CeO_2-$K/MgAl_2O_4$ at a S/C-ratio of 5. The product yields and conversion of 2-methylfuran as function of temperature can be seen in fig. 6.2. The main products at all temperatures were CO, CO_2, CH_4, and H_2 and as expected from thermodynamics, the yield of CO increased with increasing temperature, while the yield of CO_2 and CH_4 decreased with temperature. The yield of H_2 had a maximum of 76 % at 600 °C (note our definition of yield, which is based on the fraction of converted reactant, eq. 2.6), while the conversion increased with increasing temperature, reaching full conversion at 700 °C. The product fraction called Others in fig. 6.2 covers various compounds like ethanol, acetone, acetaldehyde, 2-butanone, hydrofuranes, and furanes, which all are fragments of 2-methylfuran. This fraction decreased

with temperature from 7 % at 400 °C to 0 % at 600 °C. Ethanol and acetone were the major constituents of this fraction and reached maximum yields of 0.8 and 1.5 % respectively at 400 °C. However, the conversion was 20 % at 400 °C and therefore the production of these compounds were quite low.

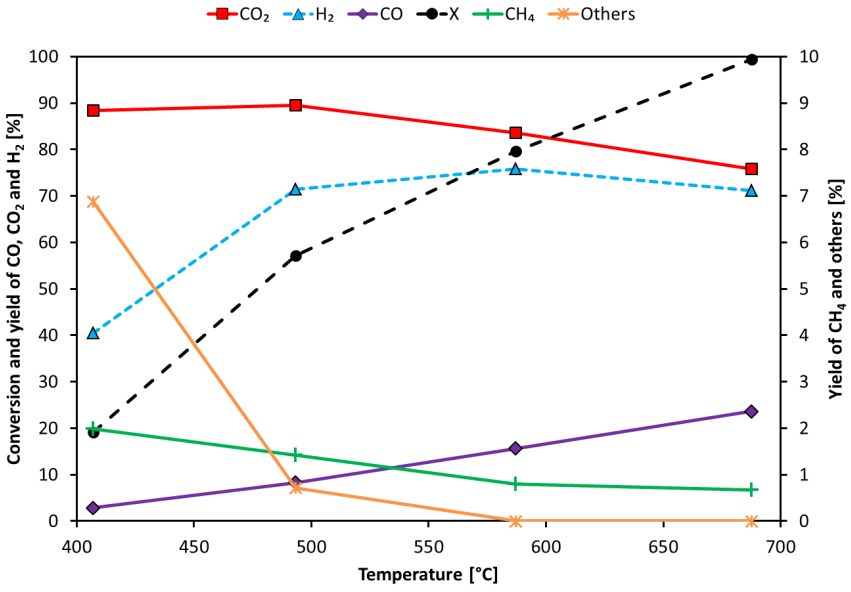

Fig. 6.2: *Yield of CO, CO_2, CH_4, H_2, Others, and conversion as function of temperature over Ni/CeO_2-$K/MgAl_2O_4$ in the SR of 2-methylfuran. Experimental conditions: S/C: 5, m_{Cat} = 0.50 g, Ni loading: 8.2 wt%, F_T = 1.6 NL/min, y_{2MF} = 1.4 vol%, y_{H_2O} = 38.0 vol%, N_2 as balance.*

The conversion of 2-methylfuran and the product yields of CO, CO_2, CH_4, and H_2 as function of time at 600 °C and S/C=5 can be seen in fig. 6.3. The yield of H_2 was 77 %, while the conversion was 86 % and both the product yields and conversion remained quite stable with time-on-stream. Nevertheless, carbon deposition at a rate of 8 $\frac{mg\ C}{g_{Cat} \cdot h}$ was observed (see table 6.2). The low degree of deactivation indicates that the carbon may be deposited as whiskers [40–42].

Steam reforming of 2-methylfuran was conducted for 24 *h* to further investigate the stability with time. A comparison of final conversion and carbon deposition at 600 °C and S/C=5 for different times on stream and over both $Ni/MgAl_2O_4$ or Ni/CeO_2-$K/MgAl_2O_4$ can be seen in table 6.2. The conversion of 2-methylfuran was 12 %-points lower and the carbon deposition was 7 times higher over $Ni/MgAl_2O_4$ compared with Ni/CeO_2-$K/MgAl_2O_4$, which shows the beneficial effect of adding both CeO_2 and K to the catalyst. This was also shown in chapter 4 for the SR of ethanol [240].

A comparison of the conversion over Ni/CeO_2-$K/MgAl_2O_4$ after 4 *h* and 24 *h* on stream shows that the catalyst deactivated with time, see table 6.2. This was probably due to carbon deposition which increased with a constant rate. This was different from the SR of ethanol over the same and similar Ni-based catalysts, where the rate of carbon deposition decreased with time on stream, see table 3.8 in chapter 3.

The release of carbon oxides as function of temperature during TPO of spent Ni/CeO_2-$K/MgAl_2O_4$-catalysts used in the SR of 2-methylfuran at SR- and oxidative SR-conditions can be seen in fig. 6.4. The carbon oxides release over a catalyst used in the SR at S/C=5 had a maximum at 410-420 °C, which was similar to the observations from the TPO of spent catalyst used in the SR of ethanol, see fig. 3.15 in chapter 3 [240]. A much smaller carbon

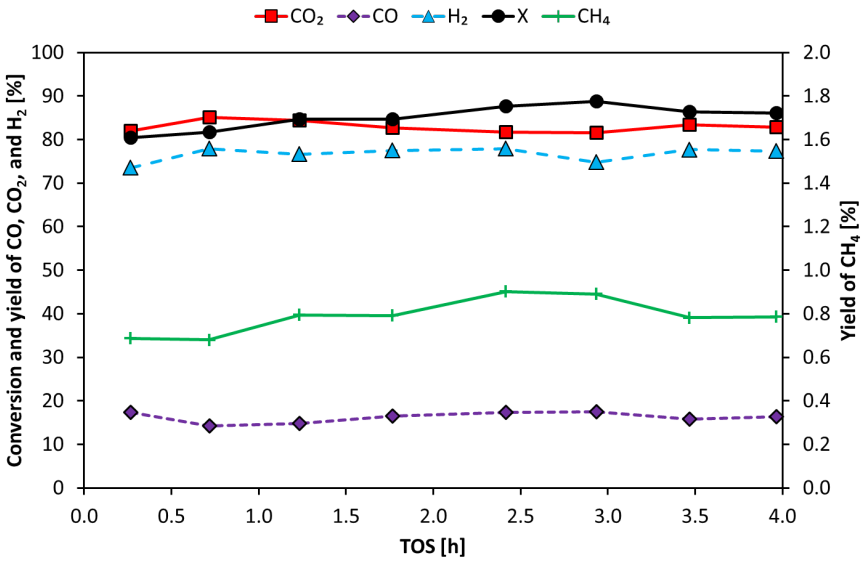

Fig. 6.3: *Yield of CO, CO_2, CH_4, H_2, and conversion as function of time in SR of 2-methylfuran over Ni/CeO_2-$K/MgAl_2O_4$. Experimental conditions: S/C: 5.1, m_{Cat} = 0.50 g, Ni loading: 8.2 wt%, Temp.: 584 °C, F_T = 1.6 NL/min, y_{2MF} = 1.4 vol%, y_{H_2O} = 38.0 vol%, N_2 as balance.*

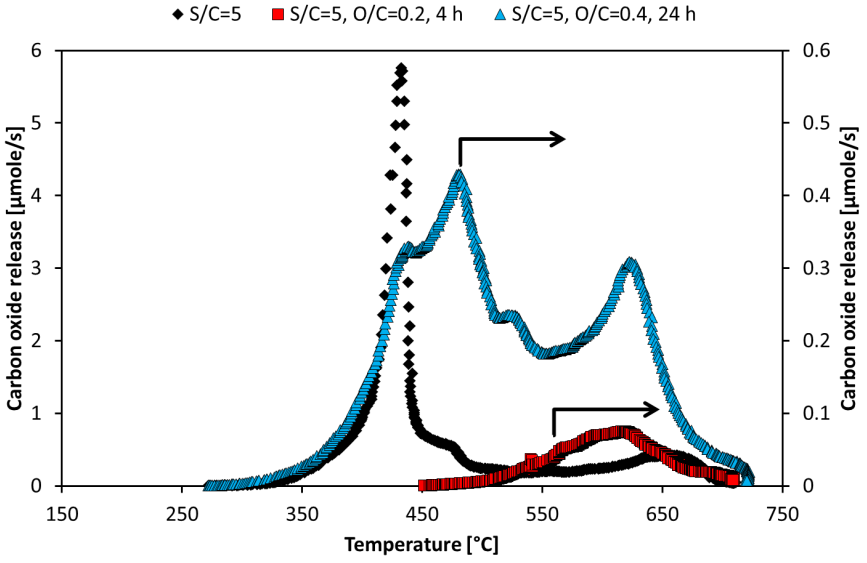

Fig. 6.4: *Carbon oxides release as function of temperature over Ni/CeO_2-$K/MgAl_2O_4$ after 4 h at SR and OSR conditions with 2-methylfuran as reactant. Experimental conditions: Δ T= 10 °C/min, $F_T = 1$ NL/min, $y_{O_2} = 2-3$ vol%, N_2 as balance.*

oxides release was observed at 650 °C, which was not seen in the SR of ethanol and could correspond to carbon deposition on the reactor walls. This was observed visually on the reactor used in the SR of 2-methylfuran, but not in the SR of ethanol. Carbon whiskers was observed in the SR of ethanol over Ni/CeO_2-$K/MgAl_2O_4$ [240] and together with the stable behavior with time and the similar TPO-profiles this suggests that the carbon deposition was as carbon whiskers in the SR of 2-methylfuran.

Tab. 6.2: *Final conversion and carbon deposition over $Ni/MgAl_2O_4$ and Ni/CeO_2-$K/MgAl_2O_4$ in the SR of 2-methylfuran. Experimental conditions: S/C: 5.1, m_{Cat} = 0.50 g, Ni loading: 8.2 wt%, Temp.: 584 °C, F_T = 1.6 NL/min, y_{2MF} = 1.4 vol%, y_{H_2O} = 38.0 vol%, N_2 as balance.*

Catalyst	TOS	X	Carbon deposition		
	[h]	[%]	$\left[\frac{mmole\ C}{mole\ C_{Feed}}\right]$	$\left[\frac{mg\ C}{g_{Cat} \cdot h}\right]$	[mg]
$Ni/MgAl_2O_4$	4	74	7.7	60	121
Ni/CeO_2-$K/MgAl_2O_4$	4	86	1.1	8	16
Ni/CeO_2-$K/MgAl_2O_4$	24	80	1.1	8	99

Oxidative SR of ethanol can minimize carbon deposition [248] and therefore the SR of 2-methylfuran was investigated under oxidative conditions at O/C-ratio of 0.2. The conversion of 2-methylfuran and the products yields of CO, CO_2, CH_4, and H_2 as function of time in the SR of 2-methylfuran at 600 °C, S/C=5, and O/C=0.2 can be seen in fig. 6.5. The conversion remained at 100 % during the 4 *h* experiment, while the yield of CH_4 and H_2 was stable at roughly 0.4 % and 68 %, respectively, which was lowered compared with yields at SR-conditions. The product yields of CO and CO_2 were also stable with time. No formation of other compounds was observed.

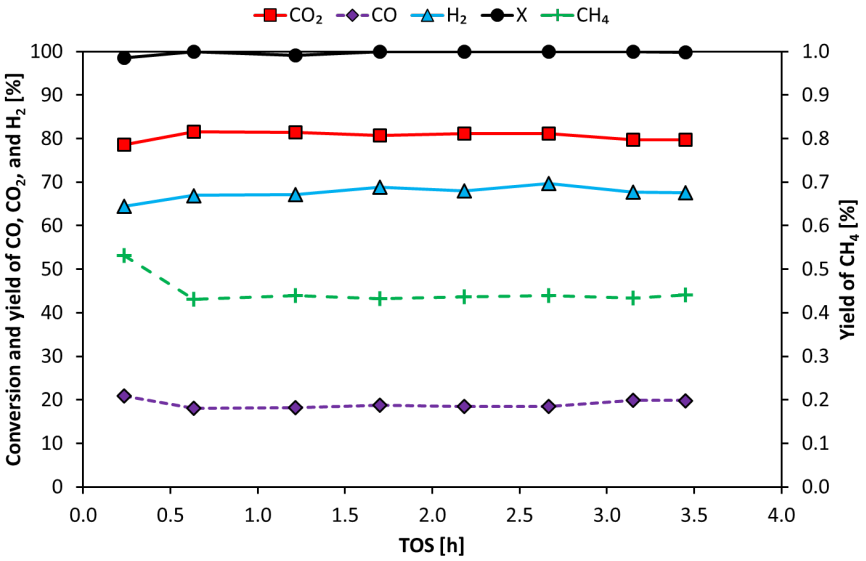

Fig. 6.5: *Yield of CO, CO_2, CH_4, H_2, and conversion as function of time in OSR of 2-methylfuran over Ni/CeO_2-$K/MgAl_2O_4$. Experimental conditions: S/C: 5.1, m_{Cat} = 0.50 g, Ni loading: 8.2 wt%, Temp.: 600 °C, F_T = 1.6 NL/min, y_{2MF} = 1.5 vol%, y_{H_2O} = 37.5 vol%, y_{O_2} = 1.5 vol%, N_2 as balance.*

A comparison of conversion, carbon deposition, yield of H_2 and CH_4 after 4 *h* and 24 *h* on stream in the OSR and 24 *h* in the SR can be seen in table 6.3. The addition of O_2 to the feed increased the conversion and therefore the mass of catalyst was lowered from 0.5 *g* to 0.39 *g* in the 24 *h* OSR experiment to see if less than full conversion could be achieved. However, full conversion was still reached, while the carbon deposition and yield of H_2 still were lower compared with SR at S/C=5. The fraction of feed being converted to carbon

deposits decreased by a factor of 18 from 1.1 $\frac{mmole\ C}{mole\ C_{Feed}}$ to 0.06 $\frac{mmole\ C}{mole\ C_{Feed}}$, showing that oxygen addition is effective in minimizing carbon deposition in SR of oxygenates.

The product yields were stable in the 24 h experiment, but the yield of CH_4 was slightly higher compared with the 4 h experiment. This was probably due to the lower mass of catalysts, which did not allow for the same degree of conversion of CH_4. The rate of carbon deposition was similar after 4 h and 24 h, when comparing the fraction of the feed converted to carbon deposition, $\frac{mmole\ C}{mole\ C_{Feed}}$.

Tab. 6.3: *Final conversion, yield of H_2 and CH_4, and carbon deposition after 24 h on stream in SR of 2-methylfuran and after 4 and 24 h in the OSR of 2-methylfuran over Ni/CeO_2-$K/MgAl_2O_4$. Experimental conditions: S/C: 5.1, $m_{Cat} = 0.39 - 0.50$ g, Ni loading: 8.2 wt%, Temp.: 584 °C, $F_T = 1.6$ NL/min, $y_{2MF} = 1.4 - 1.5$ vol%, $y_{H_2O} = 37.5 - 38.0$ vol%, $y_{O_2} = 0 - 1.5$ vol%, N_2 as balance.*

Type	TOS	X	Y_{H_2}	Y_{CH_4}	Carbon deposition	
	[h]	[%]	[%]	[%]	$\left[\frac{mmole\ C}{mole\ C_{Feed}}\right]$	$\left[\frac{mg\ C}{g_{Cat} \cdot h}\right]$
SR	24	82	81	0.7	1.1	8.2
OSR	4	100	68	0.4	0.05	0.35
OSR (High SV)	24	100	66	0.7	0.06	0.6

The release of carbon oxides during TPO of the catalysts used in the oxidative SR of 2-methylfuran for 4 and 24 h are shown in fig. 6.4. The rate of carbon oxidation had a maximum at roughly 610 °C after 4 h on stream, indicating that the carbon was not deposited on CeO_2, K, or Ni which catalyzes the oxidation leading to oxidation at lower temperatures [202, 215, 216, 240]. The carbon oxides release over 500 °C in SR was roughly 4 times as high as the carbon oxides release observed in OSR of 2-methylfuran after 4 h. This indicates that the oxygen addition decreases both the carbon deposition on the catalyst and on the reactor wall.

After 24 h the carbon oxidation occurred over a broader temperature range and with several peaks at 430 °C, 480 °C, 520 °C, and 620 °C, which indicates that carbon was deposited on the catalytic particles as well as surfaces with little or no catalytic activity. This shows that it is not only the amount of carbon deposits which changes with time; it is also the type and/or placement of the carbon.

6.3 Steam reforming of furfural

The product yields of CO, CO_2, CH_4, H_2, Others, and conversion of furfural as function of temperature in the SR of furfural at S/C=5 are summarized in fig. 6.6. The conversion increased with temperature and reached 96 % at 700 °C. The yield of CO increased with temperature while the yield of CO_2 had a maximum at 500 °C. The trends in the yield of CO and CO_2 at 500 °C and above are as expected based on thermodynamics. The yield of H_2 had a maximum of 85 % at 600 °C, however only slightly higher compared to yields at 500 and 700 °C. The yield of Others was 19 % at 400 °C and decreased to less 0.1 % at 500 °C. The fraction called Others contained 90 % of ethanol and 2-propanol in a ratio of 10:1, but small amounts of acetic acid, butanoic acid, furanes, and hydrofuranes were also detected in the effluent. Similar products were observed by Xu et al. [247]. Hydrofuranes are formed by oxidation of the furan-ring, while ethanol and 2-propanol are fragments of furfural. The yield of CH_4 had a maximum of 0.2 % at 500 °C, which was significantly lower compared with the

yield of CH_4 in the SR of 2-methylfuran. 2-methylfuran has a methyl group in the 2-position on the furan ring, where furfural has a carbonyl group. The higher yield of CH_4 in the SR of 2-methylfuran is probably related to the methyl-group, which easily can be converted to methane by reaction with $H*$.

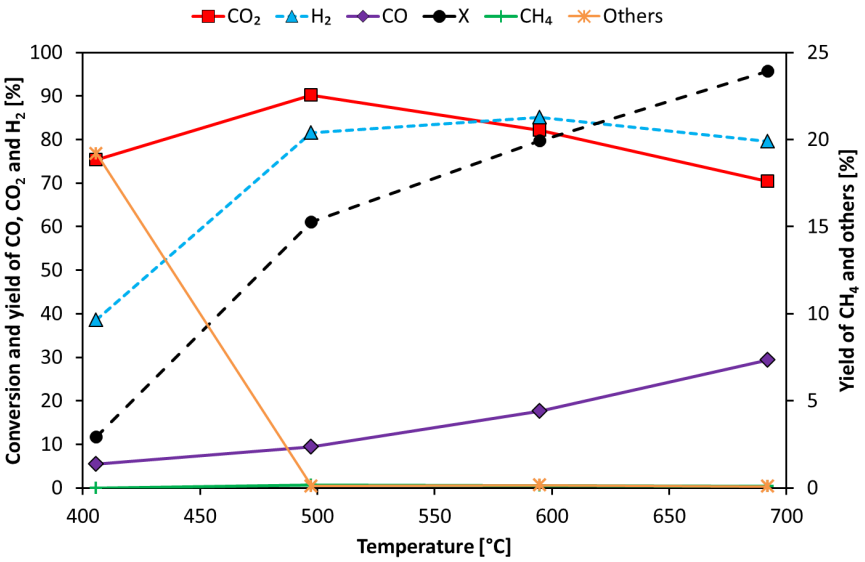

Fig. 6.6: *Yield of CO, CO_2, CH_4, H_2, Others, and conversion as function of temperature in the SR of furfural over Ni/CeO_2-$K/MgAl_2O_4$. Experimental conditions: S/C: 5, m_{Cat} = 0.50 g, Ni loading: 8.2 wt%, $F_T = 1.6$ NL/min, $y_{FF} = 1.5$ vol%, $y_{H_2O} = 38.7$ vol%, N_2 as balance.*

The conversion of furfural and the product yields of CO, CO_2, CH_4, and H_2 as function of time in the SR of furfural at 600 ℃ and S/C=5 can be seen in fig. 6.3. The product distribution was quite stable with time-on-stream although a slight decrease in the yield of H_2 from 61 % to 57 % was observed. However, the conversion decreased significantly from 82 % to 53 % during 4 h on stream. The much faster rate of deactivation compared with SR of 2-methylfuran was apparent in the rate of carbon deposition, which was 66 $\frac{mg\ C}{g_{Cat} \cdot h}$ compared to 8 $\frac{mg\ C}{g_{Cat} \cdot h}$ in the SR of 2-methylfuran at similar conditions.

Oxidative SR of furfural was investigated at two different O/C-ratios. The O/C-ratio of 0.4 used in the SR of 2-methylfuran was not high enough to induce a high and stable conversion and therefore a higher O/C-ratio of 1.2 was investigated as well. The conversion as function of time-on-stream at the different O/C-ratios can be seen in fig. 6.8. The conversion increased and became stable at the high O/C-ratio. Full conversion was achieved at O/C-ratio of 1.2 and it remained stable for 4 h.

The yield of H_2 and hydrocarbons as well as conversion and carbon deposition after 4 h on stream as function of O/C-ratio can be seen in fig. 6.9. Similar to the observations in the SR of 2-methylfuran under oxidative conditions the yield of H_2 and carbon deposition decreased while the conversion increased. The yield of hydrocarbons shown in fig. 6.8 includes methane, ethene, ethane, and propene, and increased with increasing O/C-ratio, which is unexpected. Generally a higher conversion leads to lower yields of hydrocarbons, as they are intermediates in the SR reactions. This trend could be due to partial oxidation of the Ni-particles as high amounts of H_2O and O_2 are fed to the reactor along with a low production of H_2, which may not be enough to keep the catalyst reduced. An unreduced Ni/CeO_2-$K/MgAl_2O_4$ produced a

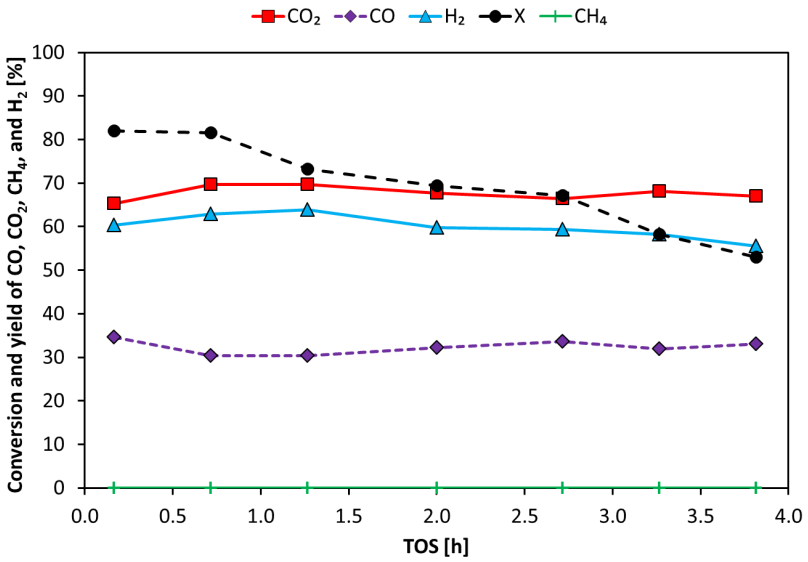

Fig. 6.7: *Yield of CO, CO_2, CH_4, H_2, and conversion as function of time in SR of furfural over Ni/CeO_2-$K/MgAl_2O_4$. Experimental conditions: S/C: 5.1, $m_{Cat} = 0.50$ g, Ni loading: 8.2 wt%, Temp.: 584 °C, $F_T = 1.6$ NL/min, $y_{FF} = 1.4$ vol%, $y_{H_2O} = 38.0$ vol%, N_2 as balance.*

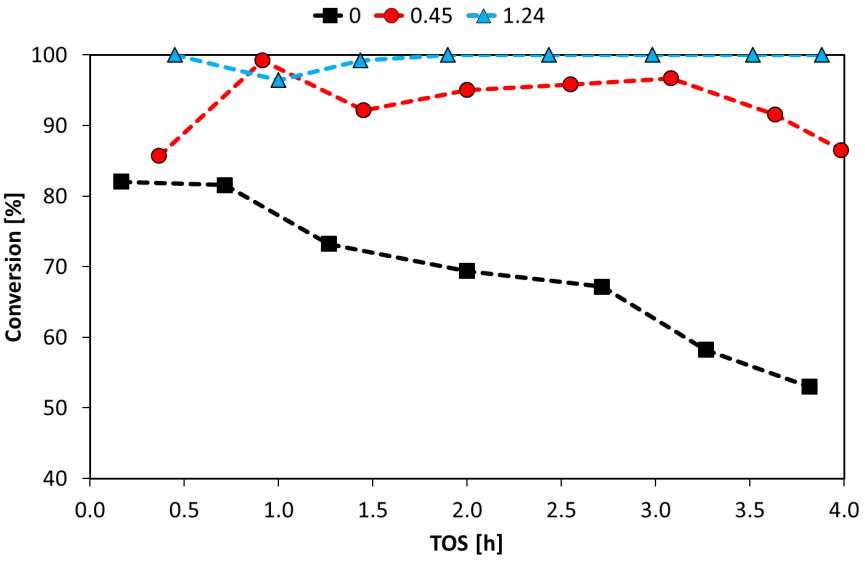

Fig. 6.8: *Conversion as function of time in SR of furfural over Ni/CeO_2-$K/MgAl_2O_4$ at different O/C-ratios. Experimental conditions: S/C: 5.0-5.3, $m_{Cat} = 0.50$ g, Ni loading: 8.2 wt%, Temp.: 584-616 °C, $F_T = 1.6$ NL/min, $y_{FF} = 1.4 - 1.5$ vol%, $y_{H_2O} = 38.0 - 38.4$ vol%, $y_{O_2} = 0 - 4.8$ vol%, N_2 as balance.*

high fraction of decomposition products like hydrocarbons. This can be seen in fig. 6.10, which shows the product yields and conversion as function of time on stream in the SR of furfural over an unreduced Ni/CeO_2-$K/MgAl_2O_4$. The total yield of hydrocarbons was initially 20 % and then decreased to zero % after 1 *h*. This decrease is likely due to reduction of NiO leading to an increase in the SR activity. It may be noticed that an unreduced $Ni/MgAl_2O_4$ is not able to catalyzes any reactions, which shows that K and CeO_2 either increases the reducibility of NiO or has enough SR activity to produce H_2 to initiate the reduction of NiO.

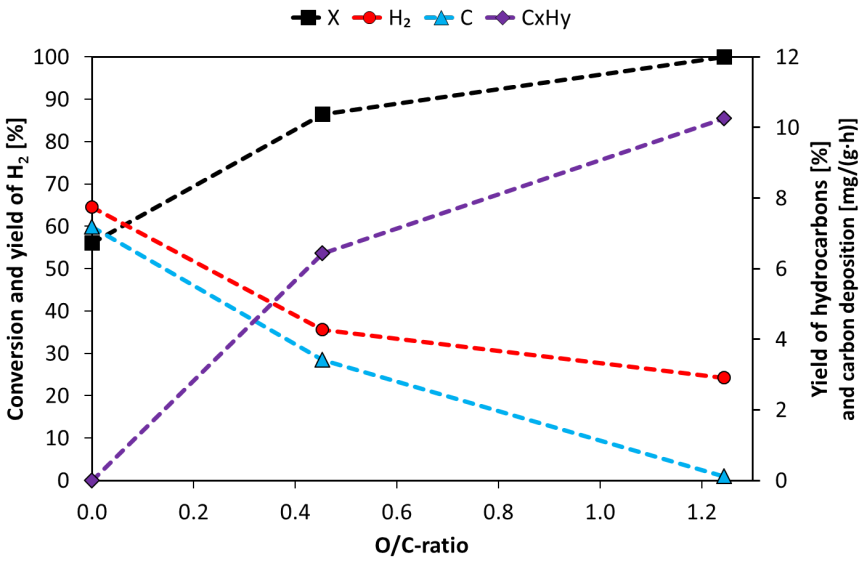

Fig. 6.9: *Conversion, carbon deposition, yield of H_2 and hydrocarbons as function of O/C-ratio in the SR of furfural over Ni/CeO_2-$K/MgAl_2O_4$. Experimental conditions: S/C: 5.0-5.3, $m_{Cat} = 0.50$ g, Ni loading: 8.2 wt%, Temp.: 584-616 °C, $F_T = 1.6$ NL/min, $y_{2MF} = 1.4 - 1.5$ vol%, $y_{H_2O} = 38.0 - 38.4$ vol%, $y_{O_2} = 0 - 4.8$ vol%, N_2 as balance.*

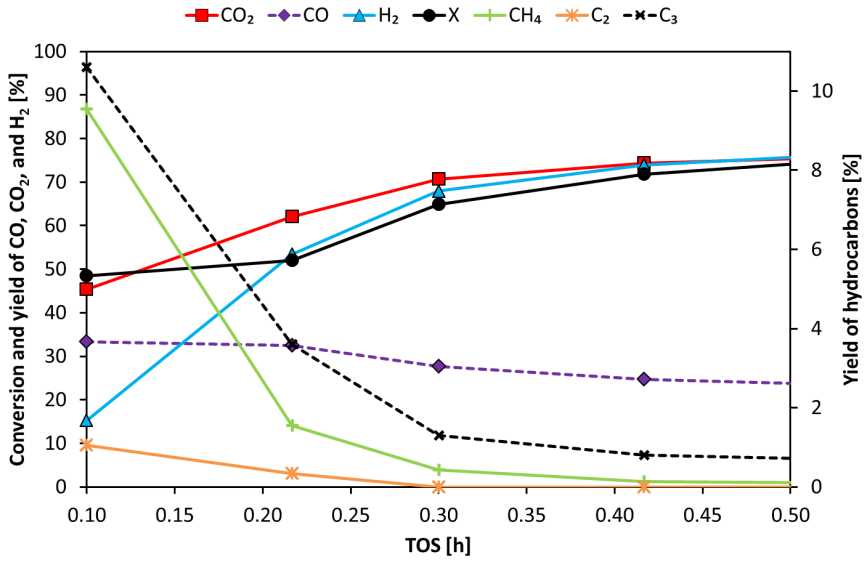

Fig. 6.10: *Product yields and conversion as function of time in the SR of furfural over unreduced Ni/CeO_2-$K/MgAl_2O_4$. Experimental conditions: S/C: 5.1, $m_{Cat} = 0.50$ g, Ni loading: 8.2 wt%, Temp.: 584 °C, $F_T = 1.6$ NL/min, $y_{FF} = 1.4$ vol%, $y_{H_2O} = 38.0$ vol%, N_2 as balance.*

Steam reforming of furfural at O/C=1.2, S/C=5.2, and 600 °C was conducted for 24 *h* and a comparison of product yields, conversion, and carbon deposition after 4 *h* and 24 *h* on stream can be seen in table 6.4. The conversion was 100 % both after 4 and 24 *h*, but the yield of hydrocarbons increased, while the yield of H_2 decreased showing deactivation of the catalyst. Furthermore, the CO_2/CO-ratio decreased with time indicating a loss in WGS activity. The deactivation was also apparent in the rate of carbon deposition, which increased drastically from 0.11 $\frac{mmole\ C}{mole\ C_{Feed}}$ after 4 *h* to 18.9 $\frac{mmole\ C}{mole\ C_{Feed}}$ after 24 *h*, which almost was a factor of 200.

Tab. 6.4: *Product yields, conversion, and carbon deposition after 4 and 24 h in OSR of furfural. Experimental conditions: S/C: 5.0-5.3, $m_{Cat} = 0.50$ g, Ni loading: 8.2 wt%, Temp.: 584-616 ℃, $F_T = 1.6$ NL/min, $y_{FF} = 1.4 - 1.5$ vol%, $y_{H_2O} = 38.0 - 38.4$ vol%, $y_{O_2} = 0 - 4.8$ vol%, N_2 as balance.*

TOS	[h]	4	24
Yield			
CO	[%]	23	34
CO_2	[%]	67	56
CH_4	[%]	5	2
C_2H_4	[%]	4	7
C_3H_7	[%]	1	1
H_2	[%]	24	14
X	[%]	100	100
C_{Dep}	$\left[\frac{mmole\ C}{mole\ C_{Feed}}\right]$	0.3	18.9
C_{Dep}	$\left[\frac{mg\ C}{g_{Cat} \cdot h}\right]$	0.1	6.2

The release of carbon oxides as function of temperature during TPO of the catalyst after 4 *h* at SR conditions and after 4 and 24 *h* at OSR conditions can be seen in fig. 6.11. The carbon release after 4 *h* at SR conditions showed one distinct oxidation peak at 410 ℃, which probably is due to oxidation of carbon in contact with K, Ni, or CeO_2. Carbon oxidation was also observed in the range of 600-700 ℃, which could be due to oxidation of carbon deposits on material with little or no catalytic activity like the reactor walls, $MgAl_2O_4$, and on top of the catalyst bed [249]. The release of carbon oxides in TPO of two empty reactors used in the SR of furfural are shown in fig. 6.12. This figure shows carbon oxidation at 400-450 ℃ and at 500-650 ℃, where the oxidation at high temperatures could correspond to carbon on reactor wall, while the oxidation at the low temperatures indicates that a more reactive carbon form also was deposited. However, it could also be catalyst particles or catalytic material deposited on the reactor walls. It should be noted that the majority of the carbon deposition is on the catalysts as carbon oxides release from the empty reactors only corresponds to 1 % of the total carbon deposition on the catalyst and reactor.

The carbon oxides release at 600-700 ℃ were observed in the SR and OSR after 4 hours, but was lower in OSR indicating that the oxygen decreases carbon deposition on both catalytic and uncatalytic materials. Similar to the observations in the SR and OSR of 2-methylfuran. The carbon oxides release after 24 *h* at OSR conditions showed one broad peak from 300 to 750 ℃ with a maximum at 415 ℃, indicating carbon deposits on both materials with and without catalytic activity. The large increase in rate of carbon deposition from 4 to 24 *h* as well as the change in oxidation profile could indicate an induction period and hereafter the rate of carbon deposition might reach a constant rate, similar to the observations in SR of 2-methylfuran.

6.4 Steam reforming of guaiacol

Steam reforming of guaiacol was investigated at S/C=5 and the conversion and product yields as function of temperature are summarized in fig. 6.13. The conversion, yield of H_2, and yield of CO all increased with increasing temperature, while the yield of CO_2 remained at a value

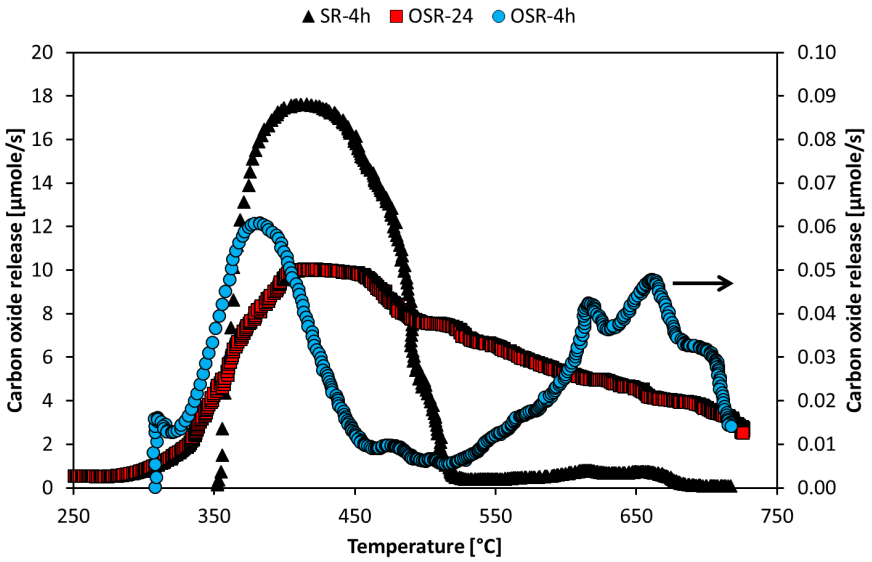

Fig. 6.11: *Carbon oxides release as function of temperature over Ni/CeO_2-$K/MgAl_2O_4$ after 4 h at SR and OSR conditions and 24 h at OSR conditions. Experimental conditions: δ T= 10 °C/min, $F_T = 1\ NL/min$, $y_{O_2} = 2-3\ vol\%$, N_2 as balance.*

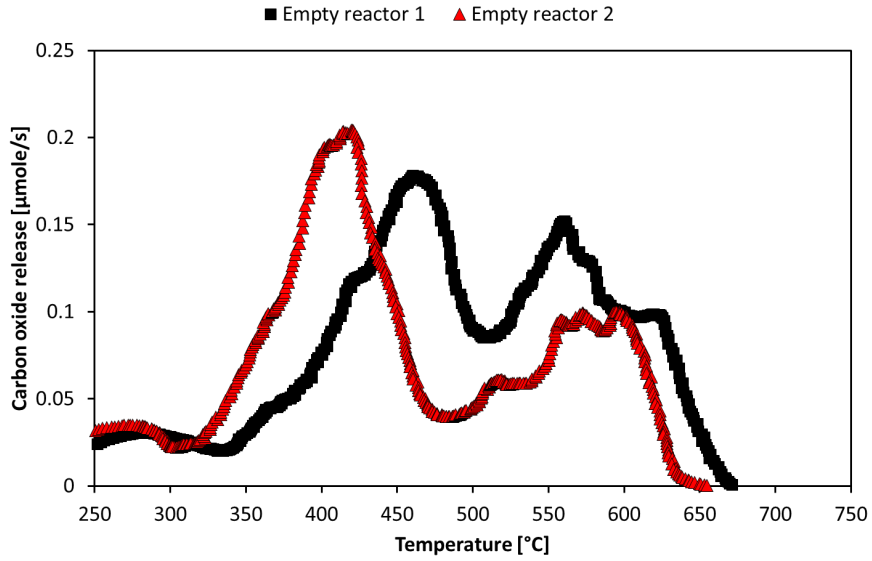

Fig. 6.12: *Carbon oxides release as function of temperature over empty reactors after 4 h at SR conditions with furfural as reactant. Experimental conditions: Δ T= 10 °C/min, $F_T = 1\ NL/min$, $y_{O_2} = 2-3\ vol\%$, N_2 as balance.*

of 60-70 % at all temperatures. The yield of H_2 had a maximum of 88 % at 780 °C, while full conversion was reached at 700 °C and above. Besides the expected products, CO, CO_2, CH_4, and H_2, ethene and ethane was produced in a ratio of 1:10 at all temperatures. The high formation of ethane was unlike any of the other compounds investigated. Benzenediols and phenol were produced in quite high yields and constituted the major part (70-80 %) of the product fraction Others shown in fig. 6.13. The high yield of benzenediols and phenols indicates that the removal of the methyl group from guaiacol is facile. The yield of Others, methane, ethane, and ethene all decreased with increasing temperature. The yield of Others was quite high even at 700 °C, which indicates that the activation and conversion of aromatic

compounds requires high temperature. Full conversion with yield of Others below 0.5 % was achieved at 780 ℃, which was significantly higher compared with furfural and 2-methylfuran.

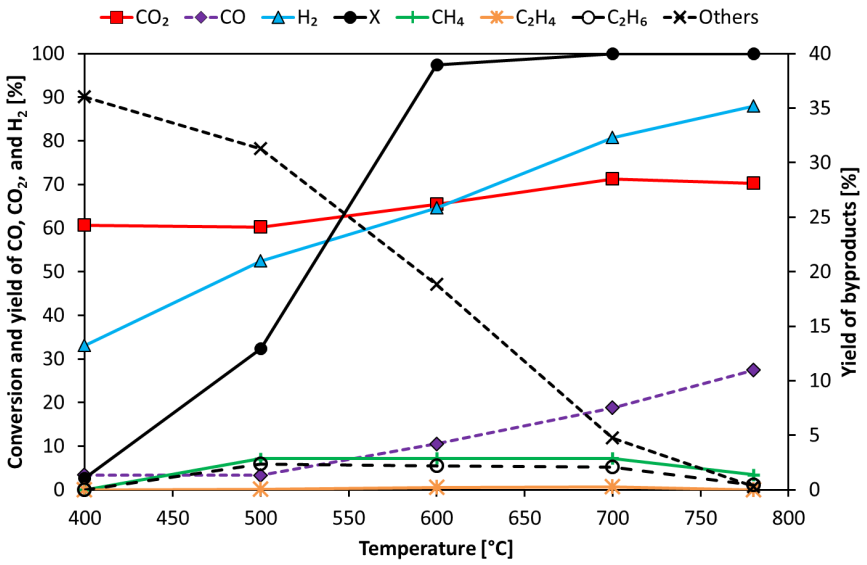

Fig. 6.13: *Yield of CO, CO_2, CH_4, C_2H_4, C_2H_6, H_2, Others, and conversion as function of temperature in the SR of guaiacol over Ni/CeO_2-$K/MgAl_2O_4$. Experimental conditions: S/C: 5.2, $m_{Cat} = 0.50\ g$, Ni loading: 8.2 wt%, $F_T = 1.6\ NL/min$, $y_{GUA} = 1.1\ vol\%$, $y_{H_2O} = 38.1\ vol\%$, N_2 as balance.*

The conversion and product yields as function of time-on-stream in the SR of guaiacol at 600 ℃ and S/C=5 can be seen in fig. 6.14. The yield of H_2 and conversion remained stable at 61 % and 90 %, respectively, for the entire experiment. Despite the stable behavior, there was still observed significant carbon deposition at a rate of 73.5 $\frac{mg\ C}{g_{Cat} \cdot h}$. This indicates that the carbon deposition was as whiskers.

Oxidative SR of guaiacol at S/C=5 and O/C=0.8 was tested for 4 *h* and 24 *h*, and the conversion and the products yields at the end of each experiment can be seen in table 6.5. The beneficial effect of adding O_2 is seen for SR of guaiacol as the conversion increased, while the carbon deposition was decreased significantly, again at the expense of the yield of H_2.

Full conversion was achieved both after 4 and 24 *h* on stream at OSR. However, the catalyst showed signs of deactivation in the product distribution as the yield of H_2 decreased while the yield of by-products increased. Furthermore the rate of carbon deposition increased with time.

The carbon oxides release as function of temperature after 4 *h* at SR conditions and 4 *h* and 24 *h* at OSR conditions can be seen in fig. 6.16. The carbon oxides release after 4 *h* at SR-conditions occurred in single peak at 410 ℃ with a shoulder at 580 ℃ similar to the other investigated compounds. The carbon oxides release during TPO of an empty reactor used in the SR of guaiacol is compared with the TPO-profile from a reactor with catalysts in fig. 6.15. The empty reactor showed carbon oxides release at 560 ℃ indicating that the shoulder is related to carbon deposited on the reactor walls. Furthermore the amount carbon deposited in the empty reactor was 10 % of total carbon deposition. This was higher compared to the SR of furfural, which indicates that the thermal decomposition of guaiacol is higher.

The TPO profiles of the spent catalysts used in OSR of guaiacol suggest that the main part of carbon deposition was on the reactor walls or other materials with little or no catalytic

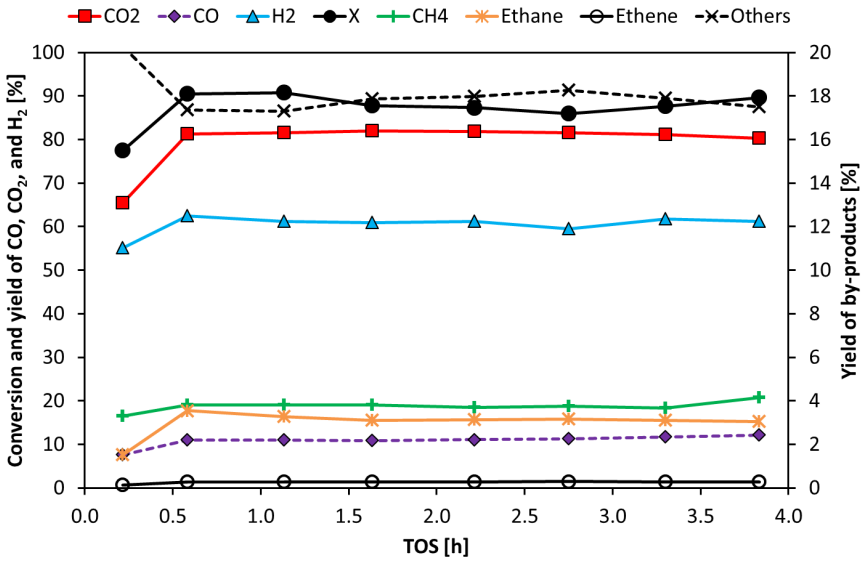

Fig. 6.14: *Product yields and conversion as function of time in SR of guaiacol over Ni/CeO_2-$K/MgAl_2O_4$. Experimental conditions: S/C: 5.1, m_{Cat} = 0.50 g, Ni loading: 8.2 wt%, Temp.: 584 ℃, $F_T = 1.6\ NL/min$, $y_{2MF} = 1.4\ vol\%$, $y_{H_2O} = 38.0\ vol\%$, N_2 as balance.*

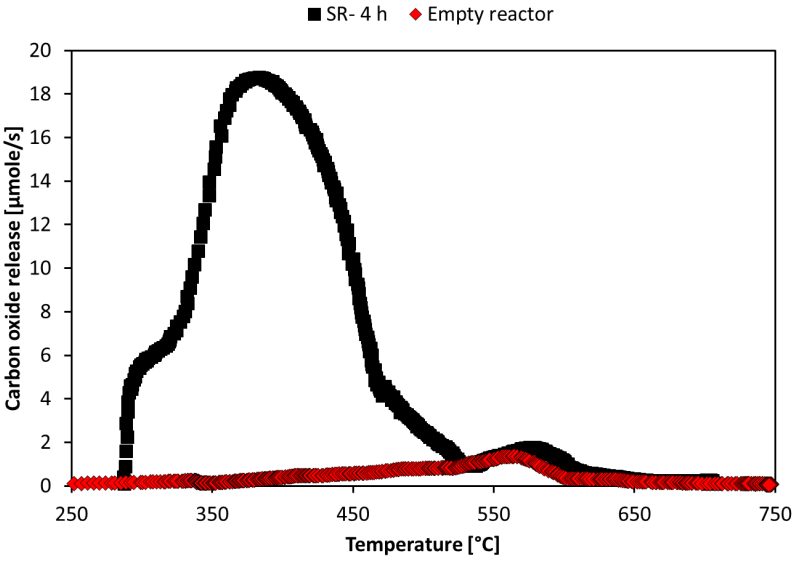

Fig. 6.15: *Comparison of carbon oxides release as function of temperature over Ni/CeO_2-$K/MgAl_2O_4$ after 4 h at SR conditions and an empty reactor used in the SR of guaiacol. Experimental conditions: Δ T= 10 ℃/min, $F_T = 1\ NL/min$, $y_{O_2} = 2-3\ vol\%$, N_2 as balance.*

activity as the carbon oxides release was mainly at 600 ℃ and above and not at 410-420 ℃ as expected for catalyzed carbon oxidation. The carbon oxides release after 24 *h* in OSR was higher and moved toward lower temperatures indicating covering of catalytic particles by carbon with time-on-stream, which also could explain the increase in the rate of carbon deposition.

Further increments of the O/C-ratio is probably needed to obtain a stable product distribution and suppress carbon deposition in the SR of guaiacol and furfural at 600 ℃.

Tab. 6.5: *Product yields, conversion, and carbon deposition after 4 and 24 h in OSR of furfural. Experimental conditions: S/C: 5.2-5.4, O/C: 0.80-0.83, m_{Cat} = 0.50 g, Ni loading: 8.2 wt%, Temp.: 584-616 °C, F_T = 1.6 NL/min, y_{GUA} = 1.0 − 1.1 vol%, y_{H_2O} = 38.2 − 39 vol%, y_{O_2} = 0 − 3.1 vol%, N_2 as balance.*

Type		SR	OSR	OSR
TOS	[h]	4	4	24
Yield				
CO	[%]	12.2	16.1	19.6
CO_2	[%]	80.4	80.5	76.3
CH_4	[%]	4.2	2.2	1.9
C_2H_4	[%]	0.3	0.2	0.2
C_2H_6	[%]	3.0	1.0	1.0
Others	[%]	13.7	0.9	5.1
H_2	[%]	64	54	48
X	[%]	86	100	100
C_{Dep}	$\left[\frac{mmole\ C}{mole\ C_{Feed}}\right]$	9.9	0.2	0.6
C_{Dep}	$\left[\frac{mg\ C}{g_{Cat} \cdot h}\right]$	73.5	1.3	4.5

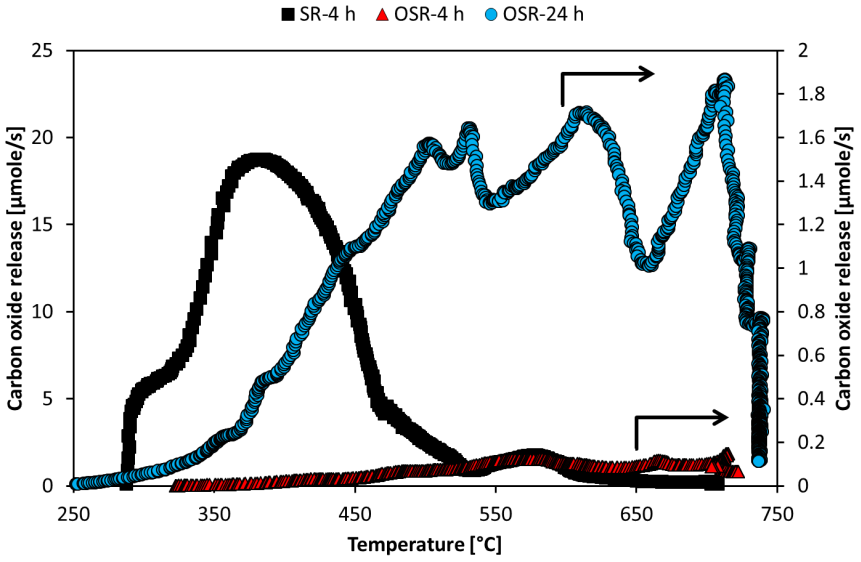

Fig. 6.16: *Carbon oxides release as function of temperature over Ni/CeO_2-$K/MgAl_2O_4$ after 4 h at SR and OSR conditions and 24 h at OSR conditions with guaiacol as reactant. Experimental conditions: Δ T= 10 °C/min, F_T = 1 NL/min, y_{O_2} = 2 − 3 vol%, N_2 as balance.*

6.5 Postreaction characterization

Catalysts, which have been used in the SR of furfural at S/C=5, SR of guaiacol at S/C=5, or SR of guaiacol at S/C=5 and O/C=1.2 for 4 h, were characterized by XRD and TEM. The XRD patterns of the spent catalysts used in the SR of furfural and guaiacol at S/C=5 can be seen in fig. 6.17. XRD analysis of the spent catalysts from SR of furfural and guaiacol showed an additional peak at 52° compared with the XRD pattern of the fresh catalyst. The peak is

Tab. 6.6: *Particle size of NiO and CeO_2 crystals on fresh and spent Ni/CeO_2-$K/MgAl_2O_4$-catalysts used in the SR of furfural and guaiacol at SR and oxidative SR conditions for 4 h and 24 h.*

	NiO [nm]	CeO_2 [nm]
Fresh	7	6
SR of furfural, S/C=5	6	7
SR of guaiacol, S/C=5	6	8
SR of guaiacol, S/C=5, O/C=1.2	17	6
SR of guaiacol, S/C=5, O/C=0.8, 24 h	17	6

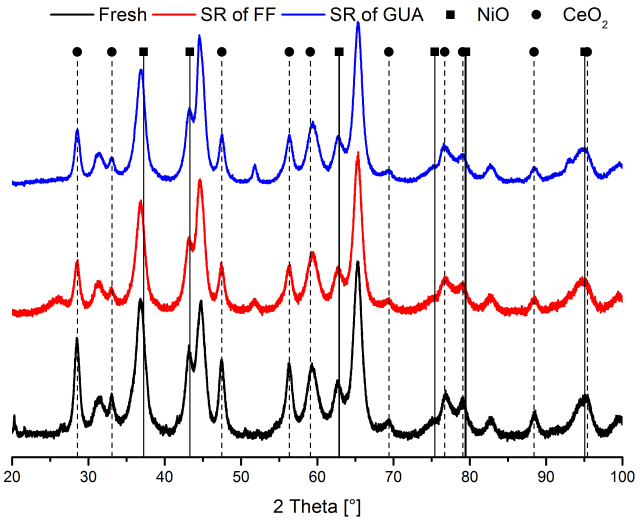

Fig. 6.17: *XRD patterns for spent Ni/CeO_2-$K/MgAl_2O_4$ catalysts used in the SR of furfural and guaiacol*

probably from metallic Ni.

The NiO and CeO_2 particle size of the fresh and spent catalyst, estimated by XRD, can be seen in table 6.6. Sintering was not significant in SR at S/C=5 as the Ni particles were estimated to be 6 *nm* in diameter.

The XRD patterns of spent catalyst used in the SR of guaiacol at S/C=5 and O/C=1.2 for 4 *h* and 24 *h* are shown in fig. 6.18. The peaks from NiO were higher for these catalysts, which indicate that the NiO particles sintered and the particle sizes were estimated to be roughly 17 *nm*. Sintering was more pronounced in oxidative SR, which also has been shown in the SR and oxidative SR of ethanol, see chapter 4. The sintering of the particles in oxidative SR did not significantly increase with time-on-stream as XRD analysis of spent catalysts, which had been operated for 24 *h* in the SR of guaiacol had a similar NiO particle diameter, see table 6.6.

Sintering of the CeO_2 was not observed neither under SR conditions nor oxidative SR conditions, as shown in table 6.6.

The sintering observed in OSR may explain the accelerated rate of carbon deposition with time, as the larger particles may be more susceptible to carbon deposition compared with smaller particles. Therefore the carbon deposition might accelerate, once the particles reach a critical size.

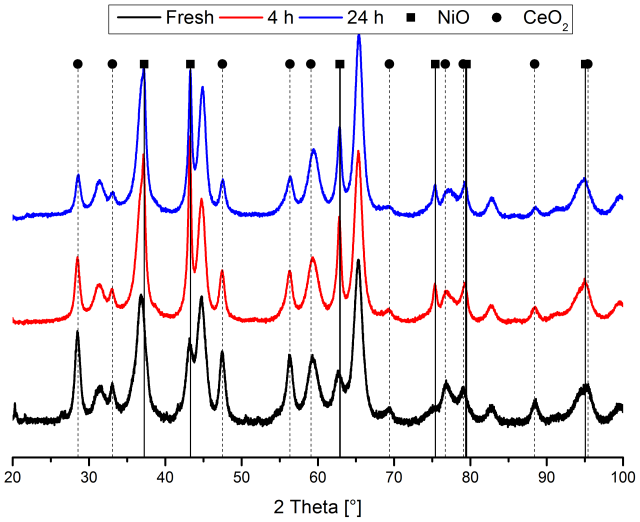

Fig. 6.18: *XRD patterns for spent Ni/CeO_2-$K/MgAl_2O_4$ catalysts used in the OSR of guaiacol*

TEM images of the spent catalysts can be seen in fig. 3.17. Carbon whiskers were formed in quite large amounts in the SR of furfural and guaiacol at S/C=5 as shown in fig. 3.17(a) and 3.17(c). This implies that the carbon oxidation at 400-430 ℃ is related to the carbon whisker. Carbon deposition as encapsulating gum was observed in the SR of guaiacol, which can be seen in fig. 3.17(d) as a layer on the surface of the metal particles, and in fig. 3.17(c) as large dark areas [122]. The encapsulating carbon was present is lower amounts and it could correspond to the carbon oxidized at temperatures above 500 ℃.

No formation of carbon whiskers was observed on the catalyst, which had been used in the oxidative SR of guaiacol, as indicated in fig. 3.17(e) and 3.17(f). However, indications of carbon deposition as encapsulation gum were still observed in fig. 3.17(f). This also implies that the high temperature carbon oxidation is encapsulating carbon as carbon oxidation was mainly observed at temperatures above 550 ℃ in oxidative SR of guaiacol after 4 *h* on stream

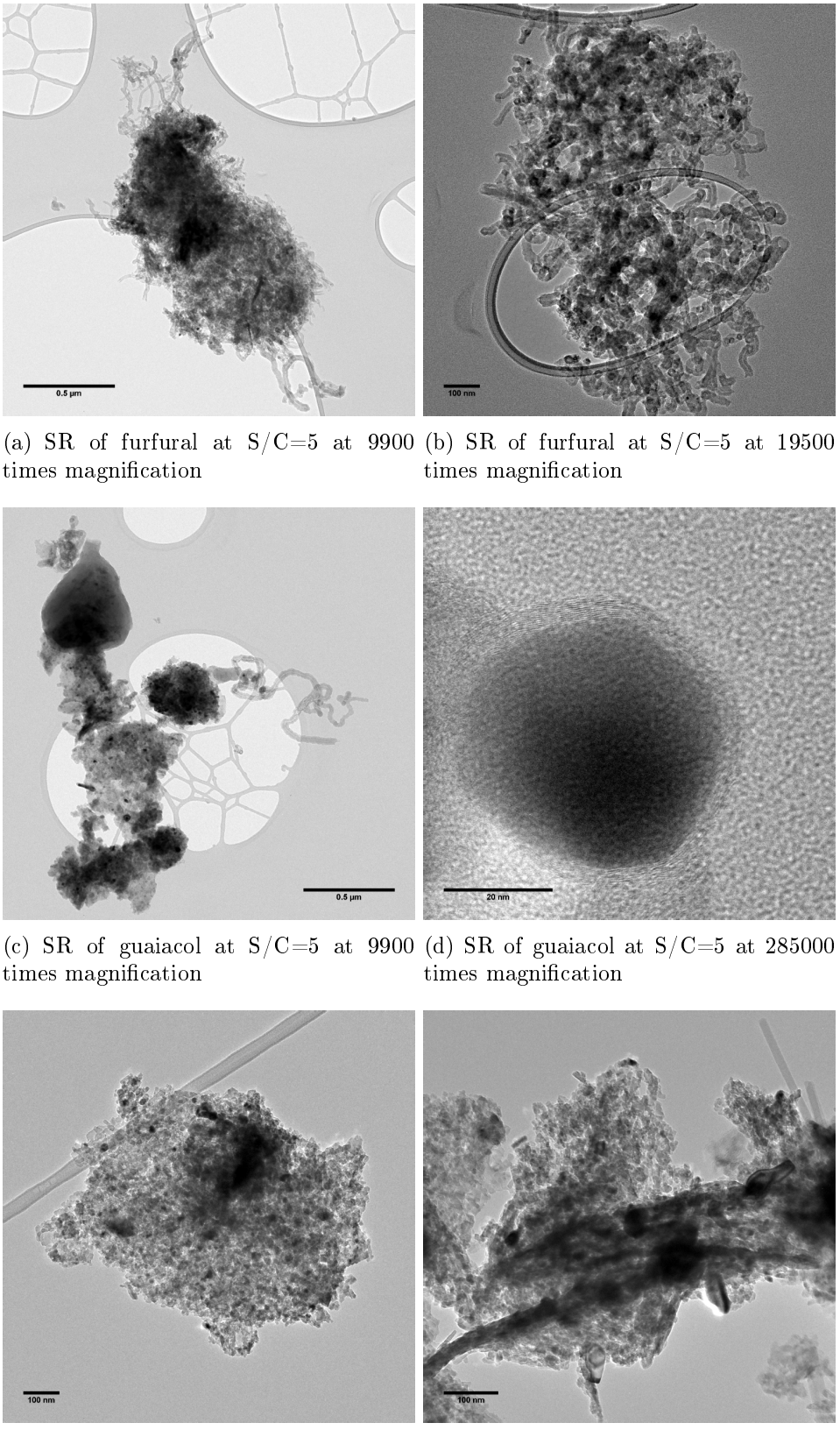

(a) SR of furfural at S/C=5 at 9900 times magnification

(b) SR of furfural at S/C=5 at 19500 times magnification

(c) SR of guaiacol at S/C=5 at 9900 times magnification

(d) SR of guaiacol at S/C=5 at 285000 times magnification

(e) SR of guaiacol at S/C=5 and O/C=1.2 at 19500 times magnification

(f) SR of guaiacol at S/C=5 and O/C=1.2 at 19500 times magnification

Fig. 6.19: *TEM images of spent Ni/CeO_2-$K/MgAl_2O_4$-catalysts used in the SR of furfural and guaiacol at SR- and oxidative conditions.*

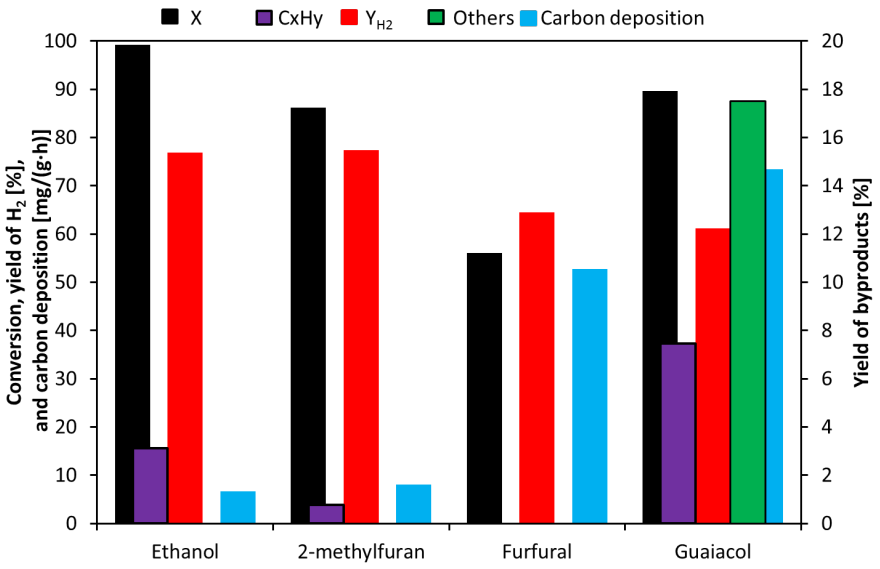

Fig. 6.20: *Conversion, carbon deposition, yield of H_2, by-products, and hydrocarbons after 4 h on stream for the ethanol, 2-methylfuran, furfural, and guaiacol in SR over Ni/CeO_2-$K/MgAl_2O_4$ at 600 °C and S/C-ratio of 5-6 . Experimental conditions: S/C: 5.2, $m_{Cat} = 0.50$ g, Ni loading: 8.2 wt%, $F_T = 1.6$ NL/min, $y_{Oxy} = 1.1 - 3.0$ vol%, $y_{H_2O} = 36.5 - 38.1$ vol%, N_2 as balance.*

6.6 Comparison of SR of different oxygenates

Steam reforming of different cyclic model compounds of bio-oil has been investigated in this study and a comparison of conversion, carbon deposition, yield of H_2, by-products, and hydrocarbons after 4 *h* on stream for the SR of ethanol (data from chapter 4), 2-methylfuran, furfural, and guaiacol at 600 °C and S/C-ratio of 5-6 can be seen in fig. 6.20. The conversion was lower for all the cyclic compounds compared to ethanol. The carbon deposition was highest for guaiacol followed by furfural, while 2-methylfuran and ethanol had similar rates of carbon deposition. The larger cyclic compounds were less reactive and had a higher tendency to form carbon deposits compared with the SR of ethanol. Similar results have been reported by Hu and Lu [59] for the SR of glucose, *m*-xylene, ethyl acetate, acetone, ethylene glycol, acetic acid.

The only structural difference between furfural and 2-methylfuran is that furfural has a carbonyl group in the 2-position on the furan-ring, while 2-methylfuran has a methyl group. This indicates that the increased rate of carbon deposition in the SR of furfural compared to the SR of 2-methylfuran is related to the carbonyl group. A possible explanation could be self-condensation reactions by furfural leading to carbon deposition and catalyst deactivation. Another explanation for the differences in carbon deposition could be differences in the formation of olefins, like ethene or propene, but this was not observed.

The aromatic nature of guaiacol is probably responsible for the high rate of carbon deposition observed in the SR of guaiacol compared to furfural and especially ethanol and 2-methylfuran. The yield of H_2 was similar in the SR of ethanol and 2-methylfuran and higher compared to the yield obtained in the SR of guaiacol and furfural. Significant amounts of by-products were mainly observed in the SR of guaiacol and ethanol, and was mainly methane in the SR of ethanol and large fractions of both CH_4, C_2H_6, and aromatic compounds in the SR of guaiacol.

The conversion and total yield of byproducts as function of temperature for the cyclic model compounds can be seen in fig. 6.21. The conversion as function of temperature was similar for 2-methylfuran and furfural which is expected as the two model compounds have similar structure. The conversion of guaiacol was lower compared to the other model compounds at 400 and 500 ℃ indicating that high temperatures are needed to activate the aromatic ring. At 600 ℃ the conversion was higher for guaiacol, but the yield of by-products was still high (24 %), so the conversion to the desired produced was lower compared with furfural and 2-methyl furan. Overall the results show that the conversion of guaiacol requires higher temperature and furthermore the carbon deposition in the SR of guaiacol is the highest of all showing that guaiacol is more difficult to steam reform.

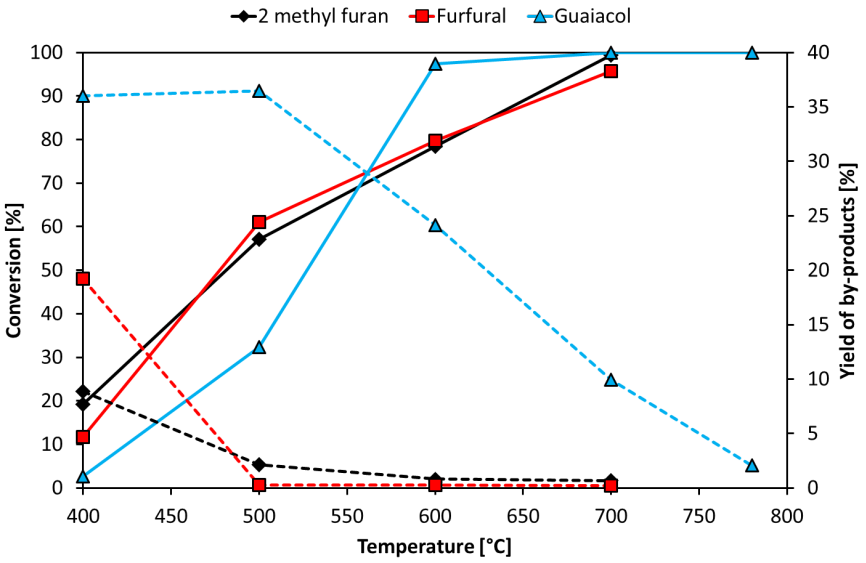

Fig. 6.21: *Conversion and yield of by-products as function of temperature in the SR of 2-methylfuran, furfural, and guaiacol in SR over Ni/CeO_2-$K/MgAl_2O_4$ at S/C-ratio of 5. Solid lines are conversion while dotted lines are yield of by-products. Experimental conditions: S/C: 5.0-5.2, $m_{Cat} = 0.50$ g, Ni loading: 8.2 wt%, $F_T = 1.6$ NL/min, $y_{Oxy} = 1.1 - 1.5$ vol%, $y_{H_2O} = 38.1$ vol%, N_2 as balance.*

6.7 Conclusions

Steam reforming of three different model compounds of the cyclic oxygenates in bio-oil, 2-methylfuran, furfural, and guaiacol, have been investigated at S/C-ratio of 5 and temperatures between 400-800 ℃ over Ni/CeO_2-$K/MgAl_2O_4$. The conversion, yield of H_2, and CO increased with increasing temperature, while the yield of CO_2 and by-products decreased with increasing temperature for all the model compounds. The major products at all temperatures were carbon oxides (CO and CO_2) and H_2, but small hydrocarbons, like methane and ethene, as well as of fragments of the model compounds, like acetone, ethanol, phenol, were also observed in the effluent. This was most pronounced for guaiacol, where a yield of aromatic by-products of 17 % at 97 % conversion was observed at 600 ℃. Temperatures of 700 ℃ were needed to fully convert 2-methylfuran and furfural to carbon oxides and H_2, while temperatures above 780 ℃ were required in the SR of guaiacol.

Significant carbon deposition was observed for all the model compounds and it was highest for guaiacol followed by furfural and 2-methylfuran. TEM-images showed that the carbon

deposited as carbon whiskers at SR conditions. Sintering of Ni or CeO_2 was not observed at SR-conditions.

The carbon deposition could be significantly decreased by adding oxygen to feed at a O/C-ratio between 0.4 and 1.2. The oxygen addition increased the conversion and full conversion, with low yields of by-products, could be achieved at 600 ℃. The beneficial effects of oxygen addition were at the expense of significant decrease in the yield of H_2. The actual decrease in the yield of H_2 depended on the model compound and the applied O/C-ratio. Furthermore significant sintering of the Ni-particles was observed in oxidative SR as well as an increase in the rate of carbon deposition with time on stream. Stable behavior was not achieved over 24 h in the oxidative SR of furfural and guaiacol.

Overall, the results indicate that the SR of oxygenates is very challenging and is even more so for aromatic compounds. The results indicate that the only path to stable operation with no carbon deposition is through oxidative SR although here sintering may be a challenge.

7. CONCLUSIONS

Flash pyrolysis of biomass can be used to produce bio-oil, which has the key feature that the energy density is higher compared with untreated biomass making the transportation less expensive. Conversion of biomass to bio-oil is expected to improve the economics in the energy production from biomass but the oil is not well suited for direct use. Therefore upgrading of bio-oil through steam reforming is an interesting and sustainable route to hydrogen and synthesis gas and can be incorporated into existing processes or it can be used as part of biorefinery, which upgrades bio-oil to transportation fuels. However, several problems arise from SR of bio-oil, with carbon deposition and catalysts deactivation as the most severe. Furthermore there is a lack of understanding of the surface reactions and the influence of process parameters, like O/C-, H/C-, and S/C-ratios, on product distribution, activity, and deactivation. Steam reforming of model compounds other than ethanol and acetone has not been investigated thoroughly. These points have been addressed in this thesis to get a deeper understanding of the SR of oxygen containing hydrocarbons.

Steam reforming of ethanol was investigated on Ni-based catalysts at a S/C-ratio of roughly 6 to elucidate the effect of support, additives, and selective poisoning as well the influence of process parameters. The product distribution as function of temperature did not vary much depending on the support and resembled the thermodynamic equilibrium at temperatures of 500 ℃ and above. CO, CO_2, and H_2 were the major products, while methane, ethene, acetaldehyde, acetone, and acetic acid were formed in low yields, which decreased with increasing temperature. The production of ethene was highest at 500 ℃, which coincided with the highest carbon deposition rate, showing that ethene is one of the main sources of carbon deposition in the SR of ethanol.

$Ni/Ce_{0.6}Zr_{0.4}O_2$ was the most active catalyst, but also suffered from severe carbon deposition as whiskers. $Ni/CeZrO_4/MgAl_2O_4$ showed both high conversion and low carbon deposition and therefore was more interesting. The high activity of both $Ni/Ce_{0.6}Zr_{0.4}O_2$ and $Ni/CeZrO_4/MgAl_2O_4$ is probably related to the $CeZrO_4$, which can decrease the water dissociation and supply oxygen to surface reactions.

Additives to $Ni/MgAl_2O_4$ could decrease the carbon deposition and increase the activity, but did not influence the product distribution significantly. CeO_2 induced the lowest carbon deposition and, in combination with K, increased the activity significantly as well. The effect of CeO_2 and K is probably due to an increased rate of carbon oxidation and facilitation of surface reactions with OH- or O-species. Despite stable activity over the first hours on stream, both $Ni\text{-}K/MgAl_2O_4$ and $Ni/CeO_2\text{-}K/MgAl_2O_4$, showed deactivation over longer periods on stream and detrimental carbon deposition as whiskers was observed.

Sulfur addition in small amounts to the catalyst had a beneficial effect on carbon deposition but a slight deactivating effect on the overall rate of reaction. The lowest rate carbon deposition in the SR of ethanol, without oxygen addition, was achieved with a sulfur poisoned $Ni\text{-}CeO_2/MgAl_2O_4$ catalyst and it was 1.2 $\frac{mg\ C}{g_{Cat} \cdot h}$.

Hydrogen addition to the feed in the SR of ethanol had little effect on the carbon deposition and conversion, while increasing the S/C-ratio from 1.6 to 8.2 or the O/C-ratio from 0 to 1.1 increased conversion and decreased carbon deposition. The yield of H_2 increased with increasing S/C-ratio, while it decreased with increasing O/C-ratio. Oxidative SR at O/C-ratios of 0.8 or above over $Ni/MgAl_2O_4$ could inhibit the carbon deposition and long term experiments did not show deactivation. However the yield of H_2 decreased by 1-2 moles of H_2 pr. mole of ethanol converted. Therefore oxidative SR seems as the most promising process for conversion of oxygen containing compounds.

Steam reforming of acetol, acetic acid, acetone, ethanol, 1-propanol, and proponal was investigated to elucidate differences in reactivity and catalysts deactivation between the different model compounds. The product distribution approached the thermodynamical equilibrium with increasing temperature. Meaning that the yield of H_2 and CO increased, while the yield of CO_2 and byproducts decreased with temperature. The conversion of the model compounds increased with increasing temperature, but did not vary significant between the model compounds. The formation of by-products was most pronounced at 500 ℃ and below. Dehydration and dehydrogenation as well as coupling reactions, e.g. ketonization of acetic acid or condensation reactions, could account for the observed by-products. Based on the product distribution as function of temperature it was found that the reaction pathway is a sequential breaking of C-C-bonds in the carbon backbone of the molecule initiated from the oxygen containing part of the molecule.

Deactivation occurred for all of the tested model compounds and the carbon deposition was most severe for alcohols, which can be related to the higher fraction of olefins in the offgas.

Steam reforming of 2-methylfuran, furfural, and guaiacol was investigated as function of temperature and time at S/C-ratio of 5 over $Ni/K\text{-}CeO_2/MgAl_2O_4$. The product distributions as function of temperature all showed an increase in the yield of H_2 and CO and a decrease in the yield of CO_2 and by-products with increasing temperature. The by-products were both small hydrocarbons, like methane, ethene, and propene, as well as fragments of the model compounds. Guaiacol was the most difficult compound to convert as the aromatic ring required high temperatures to open and convert and furthermore the carbon deposition was highest in the SR of guaiacol compared to the SR of furfural, 2-methylfuran, and ethanol. This shows that the reactivity decreases and the carbon deposition increases with increasing size of the model compounds.

Oxygen addition could increase conversion and significantly lower the carbon deposition, but also the yield of H_2. The level of O_2 needed to stabilize the conversion with time-on-stream depended on which compound was converted. Stable behavior over 24 *h* could not be achieved in the SR of furfural and guaiacol despite high levels of O_2 in the feed. Under these conditions catalyst sintering appeared to be more significant than carbon deposition.

7.1 Outlook

The results from this thesis shows that the SR of oxygen containing hydrocarbons is a difficult process as deactivation due to carbon deposition occurs. However, there are several approaches which can minimize the carbon deposition. Additives, like CeO_2 or K, which catalyzes oxidation reactions can increase the activity and lower the carbon deposition. Further lowering of the carbon deposition can be achieved by increasing the temperature or adding O_2 to the feed. However, the oxygen addition will lower the yield of the most interesting product, H_2,

and should therefore be kept at minimum level. A possible scheme could be to run the SR at 700 ℃ compared to 600 ℃ used in this study, where the carbon deposition is lower and the level of oxygen addition needed to minimize the carbon deposition probably would be lower and subsequently the yield of H_2 higher.

The catalysts used in this thesis have not been fully optimized and improvements of catalyst performance could be achieved. The levels of additives have not been varied and more optimal loadings of CeO_2 and K may be found. Furthermore, the preparation of the catalysts may also be optimized, as studies have shown that it is possible to lower the metal particle size by doing a combined calcination and reduction, where the catalyst is heated in a flow of H_2 in N_2. Smaller metal particles will probably give a higher activity and lower carbon deposition. Another route to small particles could be flame spray pyrolysis synthesis of the catalysts, which further has the advantage of being a one-step production method.

The active metal could also be changed to a noble metal, which are less prone to carbon deposition and have high activity. Another possibility is a $La_{0.9}Ce_{0.1}NiO_3$-perovskite catalyst, which have shown promising results in OSR of ethanol and could be interesting to investigate further. However, both types of catalysts are expensive and may only be interesting in smaller scale.

Scaling up of the SR of bio-oil to pilot or industrial scale might give additional problems besides catalyst deactivation and carbon deposition. Bio-oil is thermally unstable, and conventional heating of the feed through heat exchangers may lead to clogging of pipes as the bio-oil can polymerize forming gum or carbon deposits. A possible solution could be to spray the cold bio-oil into the reactor, however, this require a high input of energy to the reactor as the bio-oil needs to be heated and energy for the endothermic SR reactions should be provided. Oxygen addition could lower the energy demand as the reaction would be exothermic and deliver energy to the system. The addition of oxygen in industrial scale is quite expensive, due to the air separation unit, and mainly economical feasible in large scale.

There are still areas in the SR of bio-oil, which can be investigated further. The reaction mechanisms as well reaction kinetics for many compounds or compound groups are still undetermined and these are needed for sizing of industrial reactors and plants. The bio-oil can also contain S, P, and other inorganic elements, which can lead to deactivation, and the effects of these compounds should be elucidated as cleaning of the bio-oil may be expensive and difficult.

The investigated catalysts could also be characterized by other techniques e.g. it could be interesting to use in-situ XRD or EXAFS to determine if the Ni is partially oxidized under oxidative conditions. Furthermore, elemental mapping of Ni and additives on $MgAl_2O_4$ could be conducted as it may provide clues to the exact reason for the increased conversion and decreased carbon deposition.

BIBLIOGRAPHY

[1] I. S. Nashawi, A. Malallah, and M. Al-Bisharah. Forecasting world crude oil production using multicyclic hubbert model. *Energy Fuels*, 24:1788–1800, 2010.

[2] S. Sorrell, J. Speirs, R. Bentley, A. Brandt, and R. Miller. Global oil depletion: A review of the evidence. *Energy Policy*, 38:5290–5295, 2010.

[3] M. Hoogwijk, A. Faaij, R. van den Broek, G. Berndes, D. Gielen, and W. Turkenburg. Exploration of the ranges of the global potential of biomass for energy. *Biomass Bioenergy*, 25: 119–133, 2003.

[4] M. Hoogwijk, A. Faaij, B. Eickhout, B. de Vries, and W. Turkenburg. Potential of biomass energy out to 2100, for four IPCC SRES land-use scenarios. *Biomass Bioenergy*, 29:225–257, 2005.

[5] G. Fischer and L. Schrattenholzer. Global bioenergy potentials through 2050. *Biomass Bioenergy*, 20:151–159, 2001.

[6] H. Yamamoto, J. Fujino, and K. Yamaji. Evaluation of bioenergy potential with a multi-regional global-land-use-and-energy model. *Biomass Bioenergy*, 21:185–203, 2001.

[7] N. Nakicenovic. *World energy assessment: Energy and the challenge of sustainability*, chapter Energy Scenarios, pages 334–366. Published on-line, 2000. `http://www.undp.org/energy/activities/wea/drafts-frame.html`.

[8] G. W. Huber, S. Iborra, and A. Corma. Synthesis of transportation fuels from biomass: Chemistry, catalysts, and engineering. *Chem. Rev.*, 106:4044–4098, 2006.

[9] P. Gallezot and A. Kiennemann. *Handbook of Heterogeneous Catalysis*, chapter Conversion of Biomass on Solid Catalysts, pages 2447–2476. Wiley-VCH, 2010.

[10] J. M. Christensen, P. M. Mortensen, R. Trane, P. A. Jensen, and A. D. Jensen. Effects of H_2S and process conditions in the synthesis of mixed alcohols from syngas over alkali promoted cobalt-molybdenum sulfide. *Appl. Catal., A. Gen.*, 366:29–43, 2009.

[11] D. L. Klass. *Biomass for Renewable Energy, Fuels, and Chemicals*. Elsevier, 1998.

[12] D. Wang, S. Czernik, D. Montane, M. Mann, and E. Chornet. Biomass to hydrogen via fast pyrolysis and catalytic steam reforming of the pyrolysis oil or its fractions. *Ind. Eng. Chem. Res.*, 36:1507–1518, 1997.

[13] R. H. Venderbosch and W. Prins. Fast pyrolysis technology development. *Biofuel. Bioprod. Bioref.*, 4:178–208, 2010.

[14] T. N. Trinh, P. A. Jensen, K. Dam-Johansen, N. O. Knudsen, H. R. Sørensen, and S. Hvilsted. Comparison of lignin, macroalgae, wood, and straw fast pyrolysis. *Energy Fuels*, 27:1399–1409, 2013.

[15] K. Raffelt, E. Henrich, A. Koegel, R. Stahl, J. Steinhardt, and F. Weirich. The BTL2 process of biomass utilization entrained-flow gasification of pyrolyzed biomass slurries. *Appl. Biochem. Biotechnol.*, 129:153–164, 2006.

[16] W. Kwapinski, C. M. P. Byrne, E. Kryachko, P. Wolfram, C. Adley, J. J. Leahy, and et al. Biochar from biomass and waste. *Waste Biomass Valor*, 1:177–189, 2010.

[17] J. Lehman and S. Joseph, editors. *Bio-Char for Environmental Management: Science and Technology*, chapter Biochar for environmental management: an introduction., pages 1–12. Earthscan Publishers Ltd., 2009.

[18] C. A. Mullen, A. A. Boateng, K. B. Hicks, N. M. Goldberg, and R. A. Moreau. Analysis and comparison of bio-oil produced by fast pyrolysis from three barley biomass/byproduct streams. *Energy Fuels*, 24:699–706, 2010.

[19] A. Oasmaa, Y. Solantausta, V. Arpiainen, E. Kuoppala, and K. Sipilä. Fast pyrolysis bio-oils from wood and agricultural residues. *Energy Fuels*, 24:1380–1388, 2010.

[20] A. Oasmaa and D. Meier. Norms and standards for fast pyrolysis liquids 1. Round robin test. *J. Anal. Appl. Pyrolysis*, 73:323–334, 2005.

[21] A. Demirbas. Competitive liquid biofuels from biomass. *Appl. Energy*, 88:17–28, 2011.

[22] Z. Qi, C. Jie, W. Tiejun, and X. Ying. Review of biomass pyrolysis oil properties and upgrading research. *Energy Conv. Manage.*, 48:87–92, 2007.

[23] A. Oasmaa and S. Czernik. Fuel oil quality of biomass pyrolysis oils- State of the art for the end users. *Energy Fuels*, 13:914–921, 1999.

[24] P. M. Mortensen, J.-D. Grunwaldt, P. A. Jensen, K. G. Knudsen, and A. D. Jensen. A review of catalytic upgrading of bio-oil to engine fuel. *Appl. Catal., A. Gen.*, 407:1–19, 2011.

[25] E. Heracleous. Well-to-wheels analysis of hydrogen production from bio-oil reforming for use in internal combustion engines. *Int. J. Hydrogen Energy*, 36:11501–11511, 2011.

[26] B. H. Gebreslassie, M. Slivinsky, B. Wang, and F. You. Life cycle optimization for sustainable design and operations of hydrocarbon biorefinery via fast pyrolysis, hydrotreating and hydrocracking. *Comput. Chem. Eng.*, 50:71–91, 2013.

[27] J. Han, A. Elgowainy, J. B. Dunn, and M. Q. Wang. Life cycle analysis of fuel production from fast pyrolysis of biomass. *Bioresour. Technol.*, 133:421–428, 2013.

[28] J. G. Rogers and J. G. Brammer. Estimation of the production cost of fast pyrolysis bio-oil. *Biomass Bioenergy*, 36:208–213, 2012.

[29] G. Hochgesand, editor. *Ullmann's Encyclopedia of Industrial Chemistry*, chapter Gas Production, pages 1–169. Wiley-VCH, 2007.

[30] J. R. Rostrup-Nielsen, J. Sehested, and J. K. Nørskov. Hydrogen and synthesis gas by steam- and CO_2 reforming. *Adv. Catal.*, 47:65–139, 2002.

[31] J. R. Rostrup-Nielsen. *Handbook of Heterogeneous Catalysis*, chapter Steam Reforming, pages 2882–2905. Wiley-VCH, 2010.

[32] J. R. Rostrup-Nielsen. *Steam Reforming Catalysts*. Teknisk Forlag, 1975.

[33] K. Aasberg-Petersen, I. Dybkjaer, C. V. Ovesen, N. C. Skjøth, J. Sehested, and S. G. Thomsen. Natural gas to synthesis gas- Catalysts and catalytic processes. *J. Nat. Gas Sci. Eng.*, 3: 423–459, 2011.

[34] W. F. Baade, U. N. Parekh, and V. S. Raman. *Kirk-Othmer Encyclopedia of Chemical Technology*, volume 13, chapter Hydrogen, pages 759–807. Viley-VCH, 2000.

[35] K. Aasberg-Petersen, T. S. Christensen, I. Dybkjaer, J. Sehested, M. Østberg, R. M. Coertzen, M. J. Keyser, and A. P. Steynberg. *Fischer-Tropsch Technology*, chapter Synthesis gas production for FT synthesis, pages 258–406. Elsevier, 2004.

[36] C. Bartholomew. *Kirk-Othmer Encyclopedia of Chemical Technology*, volume 5, chapter Catalyst deactivation and regeneration, pages 255–322. Viley-VCH, 2000.

[37] J. R. Rostrup-Nielsen. Activity of nickel catalysts for the steam reforming of hydrocarbons. *J. Catal.*, 31:173–199, 1973.

[38] H. S. Bengaard, J. K. Nørskov, J. Sehested, B. S. Clausen, L. P. Nielsen, A. M. Molenbroek, and J. R. Rostrup-Nielsen. Steam reforming and graphite formation on Ni catalysts. *J. Catal.*, 209:365–384, 2002.

[39] I. Chorkendorff and J. W. Niemantsverdriet. *Concepts of Modern Catalysis and Kinetics*. Wiley, 2nd edition, 2007.

[40] D. L. Trimm. Coke formation and minimisation during steam reforming reactions. *Catal. Today*, 37:233–238, 1997.

[41] D. L. Trimm. Catalysts for the control of coking during steam reforming. *Catal. Today*, 49: 3–10, 1999.

[42] J. R. Rostrup-Nielsen and L. J. Christiansen. *Concepts in Syngas Manufacture*. Imperial College Press, 2011.

[43] J. R. Rostrup-Nielsen. Sulfur-passivated nickel catalysts for carbon-free steam reforming of methane. *J. Catal.*, 85:31–43, 1984.

[44] H. C. Dibbern, P. Olesen, J. R. Rostrup-Nielsen, P. Tottrup, and N. R. Udengaard. Make low H_2/CO syngas using sulphur passivated reforming. *Hydrocarb. Process.*, 65:71–74, 1986.

[45] J. Sehested, J. A. P. Gelten, and S. Helveg. Sintering of nickel catalysts: Effects of time, atmosphere, temperature, nickel-carrier interactions, and dopants. *Appl. Catal., A. Gen.*, 309: 237–246, 2006.

[46] J. A. Moulijn, A. E. van Diepen, and F. Kapteijn. *Handbook of Heterogeneous Catalysis*, chapter Deactivation and Regeneration, pages 1–17. Wiley-VCH, 2010.

[47] J. R. Rostrup-Nielsen and J.-H. B. Hansen. CO_2-reforming of methane over transition metals. *J. Catal.*, 144:38–49, 1993.

[48] A. C. Basagiannis and X. E. Verykios. Catalytic steam reforming of acetic acid for hydrogen production. *Int. J. Hydrogen Energy*, 32:3343–3355, 2007.

[49] M. Ni, D. Leung, and M. Leung. A review on reforming bio-ethanol for hydrogen production. *Int. J. Hydrogen Energy*, 32:3238–3247, 2007.

[50] A. Haryanto, S. Fernando, N. Murali, and S. Adhikari. Current status of hydrogen production techniques by steam reforming of ethanol: A review. *Energy Fuels*, 19:2098–2106, 2005.

[51] D. Wang, D. Montane, and E. Chornet. Catalytic steam reforming of biomass-derived oxygenates: acetic acid and hydroxyacetaldehyde. *Appl. Catal., A. Gen.*, 143:245–270, 1996.

[52] A. C. Basagiannis and X. E. Verykios. Influence of the carrier on steam reforming of acetic acid over Ru-based catalysts. *Appl. Catal., B. Environ.*, 82:77–88, 2008.

[53] E. C. Vagia and A. A. Lemonidou. Thermodynamic analysis of hydrogen production via steam reforming of selected components of aqueous bio-oil fraction. *Int. J. Hydrogen Energy*, 32: 212–223, 2007.

[54] E. C. Vagia and A. A. Lemonidou. Thermodynamic analysis of hydrogen production via autothermal steam reforming of selected components of aqueous bio-oil fraction. *Int. J. Hydrogen Energy*, 33:2489–2500, 2008.

[55] S. Aktas, M. Karakaya, and A. K. Avcim. Thermodynamic analysis of steam assisted conversions of bio-oil components to synthesis gas. *Int. J. Hydrogen Energy*, 34:1752–1759, 2009.

[56] G. A. Nahar and S. S. Madhani. Thermodynamics of hydrogen production by the steam reforming of butanol: Analysis of inorganic gases and light hydrocarbons. *Int. J. Hydrogen Energy*, 35:98–109, 2010.

[57] L. Barattini, G. Ramis, C: Resini, G. Busca, M. Sisani, and U. Constantino. Reaction path of ethanol and acetic acid steam reforming over Ni−Zn−Al catalysts. Flow reactor studies. *Chem. Eng. J.*, 153:43–49, 2009.

[58] A. C. Basagiannis and X. E. Verykios. Steam reforming of the aqueous fraction of bio-oil over structured $Ru/MgO/Al_2O_3$ catalysts. *Catal. Today*, 127:256–264, 2007.

[59] X. Hu and G. Lu. Investigation of the steam reforming of a series of model compounds derived from bio-oil for hydrogen production. *Appl. Catal., B. Environ.*, 88:376–385, 2009.

[60] F. Bimbela, M. Oliva, L. Garcia, J. Ruiz, and J. Arauzo. Hydrogen production by catalytic steam reforming of acetic acid, a model compound of biomass pyrolysis liquids. *J. Anal. Appl. Pyrolysis*, 79:112–120, 2007.

[61] F. Bimbela, M. Oliva, J. Ruiz, and J. Arauzo. Catalytic steam reforming of model compounds of biomass pyrolysis liquids in fixed bed: Acetol and *n*-butanol. *J. Anal. Appl. Pyrolysis*, 85: 204–213, 2009.

[62] P. Ciambelli, V. Palma, and A. Ruggeiro. Low temperature catalytic steam reforming of ethanol. 2. Preliminary kinetic investigation of Pt/CeO_2 catalysts. *Appl. Catal., B. Environ.*, 96:190–197, 2010.

[63] S. Cavallaro, V. Chiodo, S. Freni, N. Mondello, and F. Frusteri. Performance of Rh/Al_2O_3 catalyst in the steam reforming of ethanol: H_2 production for MCFC. *Appl. Catal., A. Gen.*, 249:119–128, 2003.

[64] E. C. Vagia and A. A. Lemonidou. Hydrogen production via steam reforming of bio-oil components over calcium aluminate supported nickel and noble metal catalysts. *Appl. Catal., A. Gen.*, 351:111–121, 2008.

[65] K. Takanabe, K. Aika, K. Seshan, and L. Lefferts. Catalyst deactivation during steam reforming of acetic acid over Pt/ZrO_2. *Chem. Eng. J.*, 120:133–137, 2006.

[66] K. Takanabe, K. Aika, K. Seshan, and L. Lefferts. Sustainable hydrogen from bio-oil-Steam reforming of acetic acid as a model oxygenate. *J. Catal.*, 227:101–108, 2004.

[67] R. Rioche, S. Kulkarni, F. C. Meunier, J. P. Breen, and R. Burch. Steam reforming of model compounds and fast pyrolysis bio-oil on supported noble metal catalysts. *Appl. Catal., B. Environ.*, 61:130–139, 2005.

[68] B. M. Güell, I. Babich, K. P. Nichols, J. G. E. Gardeniers, L. Lefferts, and K. Seshan. Design of a stable steam reforming catalyst-A promising route to sustainable hydrogen from biomass oxygenates. *Appl. Catal., B. Environ.*, 90:38–44, 2009.

[69] X. Hu and G. Lu. Investigation of steam reforming of acetic acid to hydrogen over Ni-Co metal catalyst. *J. Mol. Catal. A: Chem.*, 261:41–48, 2007.

[70] X. Hu and G. Lu. Comparative study of alumina supported transition metal catalysts for hydrogen generation by steam reforming of acetic acid. *Appl. Catal., B. Environ.*, 99:289–297, 2010.

[71] F. Bimbela, D. Chen, L. Garcìa, and J. Arauzo. Ni/Al coprecipitated catalysts modified with magnesium and copper for the catalytic steam reforming of model compounds from biomass pyrolysis liquids. *Appl. Catal., B. Environ.*, 119-120:1–12, 2012.

[72] Z. Li, X. Hu, L. Zhang, and G. Lu. Renewable hydrogen production by a mild-temperature steam reforming of the model compound acetic acid derived from bio-oil. *J. Mol. Catal. A: Chem.*, 355:123–133, 2012.

[73] Z. Li, X. Hu, L. Zhang, S. Liu, and G. Lu. Steam reforming of acetic acid over Ni/ZrO_2 catalysts: Effects of nickel loading and particle size on product distribution and coke formation. *Appl. Catal., A. Gen.*, 417-418:281–289, 2012.

[74] A. C. Basagiannis and X. E. Verykios. Reforming reactions of acetic acid on nickel catalysts over a wide temperature range. *Appl. Catal., A. Gen.*, 308:182–193, 2006.

[75] K. Takanabe, K. Aika, K. Inazu, T. Baba, K. Seshan, and L. Lefferts. Steam reforming of acetic acid as a biomass derived oxygenate: Bifunctional pathway for hydrogen formation over Pt/ZrO_2 catalysts. *J. Catal.*, 243:263–269, 2006.

[76] K. I. Gursahani, R. Alcala, R. D. Cortright, and J. A. Dumesic. Reaction kinetics measurements and analysis of reaction pathways for conversions of acetic acid, ethanol, and ethyl acetate over silica-supported Pt. *Appl. Catal., A. Gen.*, 222:369–392, 2001.

[77] B. M. Güell, I. Babich, K. Seshan, and L. Lefferts. Steam reforming of biomass based oxygenates-Mechanism of acetic acid activation on supported platinum catalysts. *J. Catal.*, 257:229–231, 2008.

[78] S. Wang, X. Li, L. Guo, and Z. Luo. Experimental research on acetic acid steam reforming over Co-Fe catalysts and subsequent density functional theory studies. *Int. J. Hydrogen Energy*, 37: 11122–11131, 2012.

[79] K. Takanabe, K. Aika, K. Seshan, and L. Lefferts. Mechanistic aspects of catalytic steam reforming of biomass-related oxygenates. *Top. Catal.*, 49:68–72, 2008.

[80] L. An, C. Dong, Y. Yang, J. Zhang, and L. He. The infuence of Ni loading on coke formation in steam reforming of acetic acid. *Renew. Energy*, 36:930–935, 2011.

[81] J. R. Galdamez, L. Garcia, and R. Bilbao. Hydrogen production by steam reforming of bio-oil using coprecipitated Ni-Al catalysts. Acetic acid as a model compound. *Energy Fuels*, 19: 1133–1142, 2005.

[82] X. Hu and G. Lu. Inhibition of methane formation in steam reforming reactions through modification of Ni catalyst and the reactants. *Green Chem.*, 11:724–732, 2009.

[83] X. Hu and G. Lu. Acetic acid steam reforming to hydrogen over Co-Ce/Al_2O_3 and Co-La/Al_2O_3 catalysts-The promotion effect of Ce and La addition. *Catal. Commun.*, 12:50–53, 2010.

[84] N. Iwasa, T. Yamane, M. Takei, J. Ozaki, and M. Arai. Hydrogen production by steam reforming of acetic acid: Comparison of conventional supported metal catalysts and metal-incorporated mesoporous smectite-like catalysts. *Int. J. Hydrogen Energy*, 35:110–117, 2010.

[85] C N. de Ávila, C. E. Hori, and A. J. de Assis. Thermodynamic assessment of hydrogen production and cobalt oxidation susceptibility under ethanol reforming conditions. *Energy*, 36: 4385–4395, 2011.

[86] E. C. Vagia and A. A. Lemonidou. Investigations on the properties of ceria-zirconia-supported Ni and Rh catalysts and their performance in acetic acid steam reforming. *J. Catal.*, 269: 388–396, 2010.

[87] T. Davidian, N. Guilhaume, E. E. Iojoiu, H. Provendier, and C. Mirodatos. Hydrogen production from crude pyrolysis oil by a sequential catalytic process. *Appl. Catal., B. Environ.*, 73: 116–127, 2007.

[88] W. Xu, S. L. Suib, and C. L. O'Young. Studies of acidic sites on boralites by temperature-programmed desorption (TPD) of NH_3, C_2H_4, and 1-C_4H_8. *J. Catal.*, 144:285–295, 1993.

[89] A. N. Fatsikostas and X. E. Verykios. Reaction network of steam reforming of ethanol over Ni-based catalysts. *J. Catal.*, 225:439–452, 2004.

[90] S. M. de Lima, A. M. Silva, I. O. da Cruz, G. Jacobs, B. H. Davis, L. V. Mattos, and F. B. Noronha. H_2 production through steam reforming of ethanol over Pt/ZrO_2, Pt/CeO_2 and Pt/$CeZrO_2$ catalysts. *Catal. Today*, 138:162–168, 2008.

[91] C-. F. Yan, F-. F. Cheng, and R-. R. Hu. Hydrogen production from catalytic steam reforming of bio-oil aqueous fraction over Ni/CeO_2-ZrO_2 catalysts. *Int. J. Hydrogen Energy*, 35:11693–11699, 2010.

[92] F. Aupretre, C. Descorme, and D. Duprez. Bio-ethanol catalytic steam reforming over supported metal catalysts. *Catal. Commun.*, 3:263–267, 2002.

[93] B. Zhang, X. Tang, Y. Li, W. Cai, Y. Xu, and W. Shen. Steam reforming of bio-ethanol for the production of hydrogen over ceria-supported Co, Ir and Ni catalysts. *Catal. Commun.*, 7: 367–372, 2006.

[94] C. Diagne, H. Idriss, K. Pearson, M. A. Gomez-Garcia, and A. Kiennemann. Efficient hydrogen production by ethanol reforming over Rh catalysts. Effect of addition of Zr on CeO_2 for the oxidation of CO to CO_2. *C. R. Chim.*, 7:617–622, 2004.

[95] D. K. Liguras, D. I. Kondarides, and X. E. Verykios. Production of hydrogen for fuel cells by steam reforming of ethanol over supported noble metal catalysts. *Appl. Catal., B. Environ.*, 43: 345–354, 2003.

[96] Y. Chen, L. Yuan, T. Ye, S. Qiu, X. Zhu, Y. Torimoto, M.. Yamamoto, and Q. Li. Effects of current upon hydrogen production from electrochemical catalytic reforming of acetic acid. *Int. J. Hydrogen Energy*, 34:1760–1770, 2009.

[97] A. C. Basagiannis, P. Panagiotopoulou, and X. E. Verykios. Low temperature steam reforming of ethanol over supported noble metal catalysts. *Top. Catal.*, 51:2–12, 2008.

[98] P. D. Vaidya and A. E. Rodrigues. Insight into steam reforming of ethanol to produce hydrogen for fuel cells. *Chem. Eng. J.*, 117:39–49, 2006.

[99] V. Subramani and C. Song. Advances in catalysis and processes for hydrogen production from ethanol reforming. *Catal.*, 20:65–106, 2007.

[100] J. R. Rostrup-Nielsen. Coking of nickel catalysts for steam reforming of hydrocarbons. *J. Catal.*, 33:184–201, 1974.

[101] M. Benito, R. Padilla, A. Serrano-Lotina, L. Rodriguez, J. J. Brey, and L. Daza. The role of surface reactions on the active and selective catalyst design for bioethanol steam reforming. *J. Power Sources*, 192:158–164, 2009.

[102] J. Comas, F. Marino, M. Laborde, and N. Amadeo. Bio-ethanol steam reforming on Ni/Al_2O_3 catalyst. *Chem. Eng. J.*, 98:61–68, 2004.

[103] S. M. de Lima, A. M. Silva, U. M. Graham, G. Jacobs, B. H. Davis, L. V. Mattos, and F. B. Noronha. Ethanol decomposition and steam reforming of ethanol over $CeZrO_2$ and $Pt/CeZrO_2$ catalyst: Reaction mechanism and deactivation. *Appl. Catal., A. Gen.*, 352:95–113, 2009.

[104] D. R. Sahoo, S. Vajpai, S. Patel, and K. K. Pant. Kinetic modeling of steam reforming of ethanol for the production of hydrogen over Co/Al_2O_3 catalyst. *Chem. Eng. J.*, 125:139–147, 2007.

[105] G. Busca, T. Montanari, C. Resini, G. Ramis, and U. Constantino. Hydrogen from alcohols: IR and flow reactor studies. *Catal. Today*, 143:2–8, 2009.

[106] M. Mavrikakis, P. Ferrin, D. Simonetti, S. Kandoi, E. Kunkes, J. A. Dumesic, and J. K. Nø rskov. Modelling ethanol decomposition on transition metals: A combined application of scaling and Brønsted-Evans-Polanyi relations. *J. Am. Chem. Soc.*, 131:5809–5815, 2009.

[107] K.-O. Hinrichsen, K. Kochloefl, and M. Muhler. *Handbook of Heterogeneous Catalysis*, chapter Water Gas Shift and COS Removal, pages 2905–2920. Wiley-VCH, 2010.

[108] I. Llerca, V. Mas, M. L. Bergamini, M. Laborde, and N. Amadeo. Bio-ethanol steam reforming on ni based catalysts. Kinetic study. *Chem. Eng. Sci.*, 71:356–366, 2012.

[109] C: Graschinsky, M. Laborde, N. Amadeo, A. Le Valant, N. Bion, F. Epron, and D. Duprez. Ethanol steam reforming over $Rh(1\%)MgAl_2O_4/Al_2O_3$: A kinetic study. *Ind. Eng. Chem. Res.*, 49:12383–12389, 2010.

[110] J. E. Sutton, P. Panagiotopoulou, X. E. Verykios, and D. G. Vlachos. Combined DFT, microkinetic, and experimental study of ethanol steam reforming on Pt. *J. Phys. Chem. C.*, 117: 4691–4706, 2013.

[111] G. Jacobs, R. A. Keogh, and B. H. Davis. Steam reforming of ethanol over Pt/ceria with co-fed hydrogen. *J. Catal.*, 245:326–337, 2007.

[112] V. Mas, M. L. Bergamini, G. Baronetti, N. Amadeo, and M. Laborde. A kinetic study of ethanol steam reforming using a nickel based catalyst. *Top. Catal.*, 51:39–48, 2008.

[113] O. Görke, P. Pfeifer, and K. Schubert. Kinetic study of ethanol reforming in a microreactor. *Appl. Catal., A. Gen.*, 360:232–241, 2009.

[114] A. Akande, A. Aboudheir, R. Idem, and A. Dalai. Kinetic modeling of hydrogen production by the catalytic reforming of crude ethanol over a co-precipitated $Ni\text{-}Al_2O_3$ catalyst in a packed bed tubular reactor. *Int. J. Hydrogen Energy*, 31:1707–1715, 2006.

[115] F. Soyal-Baltacioglu, A. E. Aksoylu, and Z. I. Önsan. Steam reforming of ethanol over Pt-Ni catalysts. *Catal. Today*, 138:183–186, 2008.

[116] V. Mas, G. Baronetti, N. Amadeo, and M. Laborde. Ethanol steam reforming using Ni(II)-Al(III) layered double hydroxide as catalyst precursor: Kinetic study. *Chem. Eng. J.*, 138: 602–607, 2008.

[117] S. Freni, S. Cavallaro, N. Mondello, L. Spadaro, and F. Frusteri. Production of hydrogen for MC fuel cell by steam reforming of ethanol over MgO supported Ni and Co catalysts. *Catal. Commun.*, 4:259–268, 2003.

[118] J. P. Breen, R. Burch, and H. M. Coleman. Metal-catalysed steam reforming of ethanol in the production of hydrogen for fuel cell applications. *Appl. Catal., B. Environ.*, 39:65–74, 2002.

[119] R. Padilla, M. Benito, L. Rodrigues, G. Muñoz, and L. Daza. Nickel and cobalt as active phase on supported zirconia catalysts for bio-ethanol reforming: Influence of the reaction mechanism on catalysts performance. *Int. J. Hydrogen Energy*, 35:8921–8928, 2010.

[120] A. M. da Silva, K. R. de Souza, G. Jacobs, U. M. Graham, B. H. Davis, L. V. Mattos, and F. B. Noronha. Steam and CO_2 reforming of ethanol over Rh/CeO_2 catalyst. *Appl. Catal., B. Environ.*, 102:94–109, 2011.

[121] J. Rass-Hansen, R. Johansson, M. Møller, and C. H. Christensen. Steam reforming of technical bioethanol for hydrogen production. *Int. J. Hydrogen Energy*, 33:4547–4554, 2008.

[122] J. Rass-Hansen, C. H. Christensen, J. Sehested, S. Helveg, J. R. Rostrup-Nielsen, and S. Dahl. Renewable hydrogen: carbon formation on Ni and Ru catalysts during ethanol steam-reforming. *Green Chem.*, 9:1016–1021, 2007.

[123] A. Le Valant, F. Can, N. Bion, D. Duprez, and F. Epron. Hydrogen production from raw bioethanol steam reforming: Optimization of catalyst composition with improved stability against various impurities. *Int. J. Hydrogen Energy*, 35:5015–5020, 2010.

[124] J. Sun, X-. P. Qiu, F. Wu, and W-. T. Zhu. H_2 from steam reforming of ethanol at low temperature over Ni/Y_2O_3, Ni/La_2O_3 and Ni/Al_2O_3 catalysts for fuel-cell application. *Int. J. Hydrogen Energy*, 30:437–445, 2005.

[125] F. Aupretre, C. Descorme, D. Duprez, D. Casanave, and D. Uzio. Ethanol steam reforming over $Mg_xNi_{1-x}Al_2O_3$ spinel oxide-supported Rh catalysts. *J. Catal.*, 233:464–477, 2005.

[126] T. Hirai, N. Ikenaga, T. Miyake, and T. Suzuki. Production of hydrogen by steam reforming of glycerin on ruthenium catalyst. *Energy Fuels*, 19:1761–1762, 2005.

[127] J. Llorca, P. R. Piscina, J-.A. Dalmon, J. Sales, and N. Homs. CO-free hydrogen from steam-reforming of bioethanol over ZnO-supported cobalt catalysts effect of the metallic precursor. *Appl. Catal., B. Environ.*, 43:355–369, 2003.

[128] Y. Yang, J. Ma, and F. Wu. Production of hydrogen by steam reforming of ethanol over a Ni/ZnO catalyst. *Int. J. Hydrogen Energy*, 31:877–882, 2006.

[129] C. Wu and R. Liu. Hydrogen production from steam reforming of *m*-cresol, a model compound derived from bio-oil: Green process evaluation based on liquid condensate recycling. *Energy Fuels*, 24:5139–5147, 2010.

[130] C. Wu and R. Liu. Carbon deposition behavior in steam reforming of bio-oil model compound for hydrogen production. *Int. J. Hydrogen Energy*, 35:7386–7398, 2010.

[131] N. Palmeri, V. Chiodo, S. Freni, F. Frusteri, J. C. J. Bart, and S. Cavallaro. Hydrogen from oxygenated solvents by steam reforming on Ni/Al_2O_3 catalyst. *Int. J. Hydrogen Energy*, 33: 6627–6634, 2008.

[132] M. Marquevich, S. Czernik, E. Chornet, and D. Montane. Hydrogen from biomass: Steam reforming of model compounds of fast-pyrolysis oil. *Energy Fuels*, 13:1160–1166, 1999.

[133] P. J. Dauenhauer, J. R. Salge, and L. D. Schmidt. Renewable hydrogen by auto-thermal steam reforming of volatile carbohydrates. *J. Catal.*, 244:238–247, 2006.

[134] K. Polychronopoulou, J. L. G. Fierro, and A. M. Efstathiou. The phenol steam reforming reaction over MgO-based supported Rh catalysts. *J. Catal.*, 228:417–432, 2004.

[135] K. Polychronopoulou, C. N. Costa, and A. M. Efstathiou. The steam reforming of phenol reaction over supported-Rh catalysts. *Appl. Catal., A. Gen.*, 272:37–52, 2004.

[136] D. A. Constantinou, J. L. G. Fierro, and A. M. Efstathiou. The phenol steam reforming reaction towards H_2 production on natural calcite. *Appl. Catal., B. Environ.*, 90:347–359, 2009.

[137] D. A. Constantinou, J. L. G. Fierro, and A. M. Efstathiou. A comparative study of the steam reforming of phenol towards H_2 production over natural calcite, dolomite and olivine materials. *Appl. Catal., B. Environ.*, 95:255–269, 2010.

[138] K. Polychronopoulou, A. Bakandritsos, V. Tzitzios, J. L. G. Fierro, and A. M. Efstathiou. Absorption-enhanced reforming of phenol by steam over supported Fe catalysts. *J. Catal.*, 241: 132–148, 2006.

[139] D. A. Constantinou and A. M. Efstathiou. Low-temperature purification of gas streams from phenol by steam reforming over novel supported-Rh catalysts. *Appl. Catal., B. Environ.*, 96: 276–289, 2010.

[140] S. Zhang, Y. Yan, T. Li, and Z. Ren. Upgrading of liquid fuel from the pyrolysis of biomass. *Bioresour. Technol.*, 96:545–550, 2005.

[141] D. Wang, S. Czernik, and E. Chornet. Production of hydrogen from biomass by catalytic steam reforming of fast pyrolysis oils. *Energy Fuels*, 12:19–24, 1998.

[142] H. Li, Q. Xu, H. Xue, and Y. Yan. Catalytic reforming of the aqueous phase derived from fast-pyrolysis of biomass. *Renew. Energy*, 34:2872–2877, 2009.

[143] P. N. Kechagiopoulos, S. S. Voutetakis, A. A. Lemonidou, and I. A. Vasalos. Hydrogen production via steam reforming of the aqueous phase of bio-oil in a fixed bed reactor. *Energy Fuels*, 20:2155–2163, 2006.

[144] J. A. Medrano, M. Oliva, J. Ruiz, and L. Garcìa. Hydrogen from aqueous fraction of biomass pyrolysis liquids by catalytic steam reforming in fluidized bed. *Energy*, 36:2215–2224, 2011.

[145] M. Sakaguchi, A. P. Watkinson, and N. Ellis. Steam gasification of bio-oil and bio-oil/char slurry in a fluidized bed reactor. *Energy Fuels*, 24:5181–5189, 2010.

[146] S. Czernik, R. Evans, and R. French. Hydrogen from biomass-production by steam reforming of biomass pyrolysis oil. *Catal. Today*, 129:265–268, 2007.

[147] C. Wu, Q. Huang, M. Sui, Y. Yan, and F. Wang. Hydrogen production via catalytic steam reforming of fast pyrolysis bio-oil in a two-stage fixed bed reactor system. *Fuel Process. Technol.*, 89:1306–1316, 2008.

[148] L. Garcìa, R. French, S. Czernik, and E. Chornet. Catalytic steam reforming of bio-oils for the production of hydrogen: effects of catalyst composition. *Appl. Catal., A. Gen.*, 201:225–239, 2000.

[149] C-. F. Yan, E-. Y. Hu, and C-.L. Cai. Hydrogen production from bio-oil aqueous fraction with in-situ carbon dioxide capture. *Int. J. Hydrogen Energy*, 35:2612–2616, 2010.

[150] S. Czernik, R. French, C. Feik, and E. Chornet. Hydrogen by catalytic steam reforming of liquid byproducts from biomass thermoconversion processes. *Ind. Eng. Chem. Res.*, 41:4209–4215, 2002.

[151] T. Hou, L. Yuan, T. Ye, L. Gong, J. Tu, M. Yamamoto, Y. Torimoto, and Q. Li. Hydrogen production by low-temperature reforming of organic compounds in bio-oil over a CNT-promoting Ni catalyst. *Int. J. Hydrogen Energy*, 34:9095–9107, 2009.

[152] M. E. Domine, E. E. Iojoiu, T. Davidian, N. Guilhaume, and C. Mirodatos. Hydrogen production from biomass-derived oil over monolithic Pt- and Rh-based catalysts using steam reforming and sequential cracking processes. *Catal. Today*, 133-135:265–573, 2008.

[153] A-M. Azad and M. J. Duran. Development of ceria-supported sulfur tolerant nanocatalysts: Rh-based formulations. *Appl. Catal., A. Gen.*, 330:77–88, 2007.

[154] A-M. Azad and M. J. Duran. Development of ceria-supported sulfur tolerant nanocatalysts: Pd-based formulations. *Appl. Catal., A. Gen.*, 332:225–236, 2007.

[155] K. Sato and K. Fujimoto. Development of new nickel based catalyst for tar reforming with superior resistance to sulfur poisoning and coking in biomass gasification. *Catal. Commun.*, 8: 1697–1701, 2007.

[156] Y. Lu, J. Chen, Y. Liu, Q. Xue, and M. He. Highly sulfur-tolerant $Pt/Ce_{0.8}Gd_{0.2}O_{1.9}$ catalyst for steam reforming of liquid hydrocarbons in fuel cell applications. *J. Catal.*, 254:39–48, 2008.

[157] G. A. Deluga, J. R. Salge, L. D. Schmidt, and X. E. Verykios. Renewable hydrogen from ethanol by autothermal reforming. *Science*, 303:993–997, 2004.

[158] L. Schmidt, R. French, S. Czernik, T. Josephson, and D. Rennard. Production of synthesis gas by partial oxidation and steam reforming of biomass pyrolysis oils. *Int. J. Hydrogen Energy*, 35:4048–1059, 2010.

[159] S. Freni, N. Mondello, S. Cavallaro, G. Cacciola, V. N. Parmon, and V. A. Sobyanin. Hydrogen production by steam reforming of ethanol: A two step process. *React. Kinet. Catal. Lett.*, 71: 143–152, 2000.

[160] J. A. Medrano, M. Oliva, L. Garcia, J. Ruiz, and J. Arauzo. Catalytic steam reforming of model compounds of biomass pyrolysis liquids in fluidized bed reactor with modified Ni/Al catalysts. *J. Anal. Appl. Pyrolysis*, 85:214–225, 2009.

[161] G. Rabenstein and V. Hacker. Hydrogen for fuel cells from ethanol by steam-reforming, partial-oxidation and combined auto-thermal reforming: A thermodynamic analysis. *J. Power Sources*, 185:1293–1304, 2008.

[162] G. van Rossum, S. R. A. Kersten, and W. P. M. van Swaaij. Catalytic and noncatalytic gasification of pyrolysis oil. *Ind. Eng. Chem. Res.*, 46:3559–3697, 2007.

[163] P. Lan, Q. Xu, M. Zhou, L. Lan, S. Zhang, and S. Yan. Catalytic steam reforming of fast pyrolysis bio-oil in fixed bed and fluidized bed reactorscatalytic. *Chem. Eng. Technol.*, 33: 2021–2028, 2010.

[164] Q. Xu, P. Lan, B. Zhang, Z. Ren, and Y. Yan. Hydrogen production via catalytic steam reforming of fast pyrolysis bio-oil in a fluidized-bed reactor. *Energy Fuels*, 24:6456–6462, 2010. doi: 10.1021/ef1010995.

[165] G. van Rossum, S. R. A. Kersten, and W. P. M. van Swaaij. Staged catalytic gasification/steam reforming of pyrolysis oil. *Ind. Eng. Chem. Res.*, 48:5857–5866, 2009.

[166] S. Cavallaro, V. Chiodo, A. Vita, and S. Freni. Hydrogen production by auto-thermal reforming of ethanol on Rh/Al_2O_3 catalyst. *J. Power Sources*, 123:10–16, 2003.

[167] A. Platon, H-. S. Roh, D. L. King, and Y. Wang. Deactivation studies of $Rh/Ce_{0.8}Zr_{0.2}O_2$ catalysts in low temperature ethanol steam reforming. *Top. Catal.*, 46:374–379, 2007.

[168] J. A. Medrano, M. Oliva, J. Ruiz, L. Garcìa, and J. Arauzo. Catalytic steam reforming of acetic acid in a fluidized bed reactor with oxygen addition. *Int. J. Hydrogen Energy*, 33:4387–4396, 2008.

[169] N. Laosiripojana, S. Assabumrungrat, and S. Charojrochkul. Steam reforming of ethanol with co-fed oxygen and hydrogen over Ni on high surface area ceria support. *Appl. Catal., A. Gen.*, 327:180–188, 2007.

[170] T. Kan, J. Xiong, X. Li, T. Ye, L. Yuan, Y. Torimoto, M. Yamamoto, and Q. Li. High efficient production of hydrogen from crude bio-oil via an integrative process between gasification and current-enhanced catalytic steam reforming. *Int. J. Hydrogen Energy*, 35:518–532, 2010.

[171] A. Iulianelli, T. Longo, and A. Basile. CO-free hydrogen production by steam reforming of acetic acid carried out in a Pd-Ag membrane reactor: The effect of co-current and counter-current mode. *Int. J. Hydrogen Energy*, 33:4091–4096, 2008.

[172] A. Basile, F. Gallucci, A. Iulianelli, F. Borgognoni, and S. Tosti. Acetic acid steam reforming in a Pd-Ag membrane reactor: The effect of the catalytic bed pattern. *J. Membr. Sci.*, 311: 46–52, 2008.

[173] X. Hu and G. Lu. Bio-oil steam reforming, partial oxidation or oxidative steam reforming coupled with bio-oil dry reforming to eliminate CO_2 emission. *Int. J. Hydrogen Energy*, 35: 7169–7176, 2010.

[174] T. S. Christensen. Adiabatic prereforming of hydrocarbons - an important step in syngas production. *Appl. Catal., A. Gen.*, 138:285–309, 1996.

[175] E. E. Iojoiu, M. E. Domine, T. Davidian, N. Guilhaume, and C. Mirodatos. Hydrogen production by sequential cracking of biomass-derived pyrolysis oil over noble metal catalysts supported on ceria-zirconia. *Appl. Catal., A. Gen.*, 323:147–161, 2007.

[176] T. Davidian, N. Guilhaume, C. Daniel, and C. Mirodatos. Continuous hydrogen production by sequential catalytic cracking of acetic acid Part I. Investigation of reaction conditions and application to two parallel reactors operated cyclically. *Appl. Catal., A. Gen.*, 335:64–73, 2008.

[177] T. Davidian, N. Guilhaume, H. Provendier, and C. Mirodatos. Continuous hydrogen production by sequential catalytic cracking of acetic acid Part II. Mechanistic features and characterisation of catalysts under redox cycling. *Appl. Catal., A. Gen.*, 337:111–120, 2008.

[178] R. R. Davda, J. W. Shabaker, G. W. Huber, R. D. Cortright, and J. A. Dumesic. A review of catalytic issues and process conditions for renewable hydrogen and alkanes by aqueous-phase reforming of oxygenated hydrocarbons over supported metal catalysts. *Appl. Catal., B. Environ.*, 56:171–186, 2005.

[179] J. A. Dumesic and G. W. Huber. An overview of aqueous-phase catalytic processes for production of hydrogen and alkanes in a biorefinery. *Catal. Today*, 111:119–132, 2006.

[180] A. V. Tokarev, A. V. Kirilin, E. V. Murzina, K. Eranen, L. M. Kustov, D. Y. Murzin, and et al. The role of bio-ethanol in aqueous phase reforming to sustainable hydrogen. *Int. J. Hydrogen Energy*, 35:12642–12649, 2010.

[181] Z. Tang, J. Monroe, J. Dong, T. Nenoff, and D. Weinkauf. Platinum-loaded NaY zeolite for aqueous-phase reforming of methanol and ethanol to hydrogen. *Ind. Eng. Chem. Res.*, 48: 2728–2733, 2009.

[182] J. W. Shabaker, G. W. Huber, R. D. Cortright, and J. A. Dumesic. Aqueous-phase reforming of ethylene glycol over supported platinum catalysts. *Catal. Lett.*, 88:1–8, 2003.

[183] R. R. Davda, J. W. Shabaker, G. W. Huber, R. D. Cortright, and J. A. Dumesic. Aqueous-phase reforming of ethylene glycol on silica-supported metal catalysts. *Appl. Catal., B. Environ.*, 43: 13–26, 2003.

[184] I. O. Cruz, N. F. P. Ribeiro, D. A. G. Aranda, and Souza M. M. V. M. Hydrogen production by aqueous-phase reforming of ethanol over nickel catalysts prepared from hydrotalcite precursors. *Catal. Commun.*, 9:2606–2611, 2008.

[185] G. Wen, Y. Xu, Z. Xu, and Z. Tian. Direct conversion of cellulose into hydrogen by aqueous-phase reforming process. *Catal. Commun.*, 11:522–526, 2010.

[186] A. V. Kirilin, A. V. Tokarev, E. V. Murzina, L. M. Kustov, J.-P. Mikkola, and D. Y. Murzin. Reaction products and transformations of intermediates in the aqueous-phase reforming of sorbitol. *Chem. Sus.*, 3:708–718, 2010.

[187] J. W. Shabaker, D. A. Simonetti, R. D. Cortright, and J. A. Dumesic. Sn-modified Ni catalysts for aqueous-phase reforming: Characterization and deactivation studies. *J. Catal.*, 231:67–76, 2005.

[188] P. Gallezot and G. Bergeret. *Handbook of Heterogeneous Catalysis*, chapter Particle size and dispersion measurements, pages 738–765. Wiley-VCH, 2010.

[189] H. S. Fogler. *Elements of chemical reaction engineering*. Prentice Hall, 4th edition, 2006.

[190] A. E. Galletti, M. F. Gomez, L. A. Arrúa, and M. C. Abello. Ni catalysts supported on modified $ZnAl_2O_4$ for ethanol steam reforming. *Appl. Catal., A. Gen.*, 380:40–47, 2010.

[191] M. Benito, J. L. Sanz, R. Isabel, R. Padilla, R. Arjona, and L. Daza. Bio-ethanol steam reforming: Insights on the mechanism for hydrogen production. *J. Power Sources*, 151:11–17, 2005.

[192] J. R. Rostrup-Nielsen. Hydrogen via steam reforming of naphtha. *Chem. Eng. Prog.*, 73:87–92, 1977.

[193] L. De Rogatis, T. Montini, B. Lorenzut, and P. Fornasiero. Ni_xCu_y/Al_2O_3 based catalysts for hydrogen production. *Energy Environ. Sci.*, 1:501–509, 2008.

[194] C.-C. Hung, S.-L. Chen, Y.-K. Liao, C.-H. Chen, and J.-H. Wang. Oxidative steam reforming of ethanol for hydrogen production on M/Al_2O_3. *Int. J. Hydrogen Energy*, 37:4955–4966, 2012.

[195] J. S. Moura, Souza M. O. G., J. D. A. Bellido, E. M. Assaf, M. Opportus, and M. C. Rangel. Ethanol steam reforming over rhodium and cobalt-based catalysts: Effect of the support. *Int. J. Hydrogen Energy*, 37:3213–3224, 2012.

[196] W. Cai, F. Wang, C. Daniel, A. C. van Veen, H. Provendier, and C. Mirodatos. Oxidative steam reforming of ethanol over Ir/CeO_2 catalysts: A structure sensitivity analysis. *J. Catal.*, 286:137–152, 2012.

[197] N. R. Peela, A. Mubayi, and D. Kunzru. Steam reforming of ethanol over $Rh/CeO_2/Al_2O_3$ catalysts in a microchannel reactor. *Chem. Eng. J.*, 167:578–587, 2011.

[198] L. Jalowiecki-Duhamel, C. Pirez, M. Capron, F. Dumeignil, and E. Payen. Hydrogen production from ethanol steam reforming over cerium and nickel based oxyhydrides. *Int. J. Hydrogen Energy*, 35:12741–12750, 2010.

[199] G. Zhou, L. Barrio, S. Agnoli, S. D. Senanayake, J. Evans, A. Kubacka, M. Estralla, J. C. Hanson, A. Martinez-Arias, M. Fernandez-Garcia, and J. A. Rodriguez. High activity of $Ce_{1-x}Ni_xO_{2-y}$ for H_2 production through ethanol steam reforming: Tuning catalytic performance through metal-oxide interactions. *Angew. Chem., Int. Ed.*, 49:9680–9684, 2010.

[200] S. M. de Lima, A. M. da Silva, L. O. O. de Costa, J. M. Assaf, L. V. Mattos, L. V. Mattos, R. Sarkari, A. Venugopal, and F. B. Noronha. Hydrogen production through oxidative steam reforming of ethanol over ni-based catalysts derived from $La_{1-x}Ce_xNiO_3$ perovskite-type oxides. *Appl. Catal., B. Environ.*, 121:1–9, 2012.

[201] B. M. Güell, I. Babich, L. Lefferts, and K. Seshan. Steam reforming of phenol over Ni-based catalysts-A comparative study. *Appl. Catal., B. Environ.*, 106:280–286, 2011.

[202] R. J. Gorte. Ceria in catalysis: From automotive applications to the water-gas shift reaction. *React. Kinet. Catal.*, 56:1126–1135, 2010.

[203] A. Ranjbar and M. Rezaei. Preparation of nickel catalysts supported on $Ca_{O.2}Al_2O_3$ for methane reforming with carbon dioxide. *Int. J. Hydrogen Energy*, 37:6356–6363, 2012.

[204] H. Eltejaei, H. R. Bozorgzadeh, J. Towfighi, M. R. Omidkhah, M. Rezaei, R. Zangeneh, A. Zamaniyan, and A. Z. Ghalam. Methane dry reforming on $cfNi/Ce_{0.75}Zr_{0.25}O_2$-$MgAl_2O_4$ and $Ni/Ce_{0.75}Zr_{0.25}O_2$-γ-alumina: Effects of support composition and water addition. *Int. J. Hydrogen Energy*, 37:4107–4118, 2012.

[205] J. Guo, H. Lou, H. Zhao, D. Chai, and X. Zheng. Dry reforming of methane over nickel catalysts supported on magnesium aluminate spinels. *Appl. Catal., A. Gen.*, 273:75–82, 2004.

[206] W. Shan, M. Luo, P. Ying, W. Shen, and C. Li. Reduction property and catalytic activity of $Ce_{1-X}Ni_XO_2$ mixed oxide catalysts for CH_4 oxidation. *Appl. Catal., A. Gen.*, 246:1–9, 2003.

[207] R. Pérez-Hernández, A. Gutiérrez-Martínez, J. Palacios, M. Vega-Hernández, and V. Rodríguez-Lugo. Hydrogen production by oxidative steam reforming of methanol over Ni/CeO_2-ZrO_2 catalysts. *Int. J. Hydrogen Energy*, 36:6601–6608, 2011.

[208] P. Djinovic, J. Batista, and A. Pintar. Efficient catalytic abatement of greenhouse gases: Methane reforming with CO_2 using a novel and thermally stable $Rh\text{-}CeO_2$ catalyst. *Int. J. Hydrogen Energy*, 37:2699–2707, 2012.

[209] C. Zhang, S. Li, M. Li, S. Wang, X. Ma, and J. Gong. Enhanced oxygen mobility and reactivity for ethanol steam reforming. *AIChE J.*, 58:517–525, 2012.

[210] H. Wang, Y. Liu, L. Wang, and Y. N. Qin. Study of carbon deposition in steam reforming of ethanol over Co/CeO_2 catalyst. *Chem. Eng. J.*, 145:25–31, 2008.

[211] L. Zhang, W. Li, J. Liu, C. Guo, Y. Wang, and J. Zhang. Ethanol steam reforming reactions over Al_2O_3-SiO_2-supported Ni-La catalysts. *Fuel*, 88:511–518, 2009.

[212] P. Wang, E. Tanabe, K. Ito, J. Jia, H. Morioka, T. Shishido, and K. Takehira. Filamentous carbon prepared by the catalytic pyrolysis of CH_4 on Ni/SiO_2. *Appl. Catal., A. Gen.*, 231: 35–44, 2002.

[213] J. Li, H. Yu, G. Yang, F. Peng, D. Xie, H. Wang, and J. Yang. Steam reforming of oxygenate fuels for hydrogen production: A thermodynamic study. *Energy Fuels*, 25:2643–2650, 2011.

[214] P. Sengupta, A. Khan, M. A. Zahid, H. Ibrahim, and R. Idem. Evaluation of the catalytic activity of various $5Ni/Ce_{0.5}Zr_{0.33}M_{0.17}O_{2-\delta}$ catalysts for hydrogen production by the steam reforming of a mixture of oxygenated hydrocarbons. *Energy Fuels*, 26:816–828, 2012.

[215] C. F. Oliveira, F. A. C. Garcia, D. R. Araujo, J. L. Macedo, J. L. Dias, and S. C. L. Dias. Effects of preparation and structure of cerium-zirconium mixed oxides on diesel soot catalytic combustion. *Appl. Catal., A. Gen.*, 413-414:292–300, 2012.

[216] C. A. Neyertz, E. E. Miro, and C. A. Querini. K/CeO_2 catalysts supported on cordierite monoliths: Diesel soot combustion study. *Chem. Eng. J.*, 181-182:93–102, 2012.

[217] C. H. Bartholomew. Mechanisms of catalyst deactivation. *Appl. Catal., A. Gen.*, 212:17–60, 2001.

[218] J. R. Salge, G. A. Deluga, and L. D. Schmidt. Catalytic partial oxidation of ethanol over noble metal catalysts. *J. Catal.*, 235:69–78, 2005.

[219] N. Laosiripojana, W. Sangtongkitcharoen, and S. Assabumrungrat. Catalytic steam reforming of ethane and propane over CeO_2-doped Ni/Al_2O_3 at SOFC temperature: Improvement of resistance toward carbon formation by the redox property of doping CeO_2. *Fuel*, 85:323–332, 2006.

[220] G. P. Szijjarto, Z. Paszti, I. Sajo, A. Erdohelyi, G. Radnoczi, and A. Tompos. Nature of the active sites in $Ni/MgAl_2O_4$-based catalysts designed for steam reforming of ethanol. *J. Catal.*, 305:290–306, 2013.

[221] G. Jones, J. G. Jakobsen, S. S. Shim, J. Kleis, M. P. Andersson, J. Rossmeisl, F. Abild-Petersen, T. Bligaard, S. Helveg, B. Hinnemann, J. R. Rostrup-Nielsen, I. Chorkendorff, J. Sehested, and J. K. Nørskov. First principles calculations and experimental insight into methane steam reforming over transition metal catalysts. *J. Catal.*, 259:14–7160, 2008.

[222] R. Trane, A. D. Jensen, and S. Dahl. Catalytic steam reforming of bio-oil. *Int. J. Hydrogen Energy*, 37:6447–6472, 2012.

[223] M. C. Ramos, A. I. Navascues, L. Garcìa, and R. Bilbao. Hydrogen production by catalytic steam reforming of acetol, a model compound of bio-oil. *Ind. Eng. Chem. Res.*, 46:2399–2406, 2007.

[224] X. Hu and G. Lu. Investigation of the effects of molecular structure on oxygenated hydrocarbon steam reforming. *Energy Fuels*, 23:926–833, 2009.

[225] T. Mizuno and T. Nakajima. TPR studies on steam reforming of 2-propanol on Rh/Al_2O_3, Ru/Al_2O_3 and Pd/Al_2O_3. *React. Kinet. Catal. Lett.*, 78:315–324, 2003.

[226] T. Mizuno, Y. Matsumura, T. Nakajima, and S. Mishima. Effect of support on catalytic properties of Rh catalysts for steam reforming of 2-propanol. *Int. J. Hydrogen Energy*, 28: 1393–1399, 2003.

[227] R. R. Davda and J. A. Dumesic. Renewable hydrogen by aqueous-phase reforming of glucose. *Chem. Comm.*, pages 36–37, 2004.

[228] B. T. Schädel, M. Duisberg, and O. Deutschmann. Steam reforming of methane, ethane, propane, butane, and natural gas over a rhodium-based catalyst. *Catal. Today*, 142:42–51, 2009.

[229] J. R. Rostrup-Nielsen. *Catalytic steam reforming*. Springer, 1984.

[230] P. O. Graf, B. L. Mojet, van Ommen J. G., and L. Lefferts. Comparative study of steam reforming of methane, ethane and ethylene on Pt, Rh and Pd supported on yttrium-stabilized zirconia. *Appl. Catal., A. Gen.*, 332:310–317, 2007.

[231] H. Jeong and M. Kang. Hydrogen production from butane steam reforming over Ni/Ag loaded $MgAl_2O_4$ catalyst. *Appl. Catal., B. Environ.*, 95:446–455, 2010.

[232] I. Aartun, B. Silberova, H. Venvik, P. Pfeifer, O. Görke, K. Schubert, and A. Holmen. Hydrogen production from propane in Rh-impregnated metallic microchannel reactors and alumina foams. *Catal. Today*, 105:469–478, 2005.

[233] J. L. F. Da Silva and P. Tereshchuk. Ethanol and water adsorption on close-packed 3d, 4d, and 5d transition-metal surfaces: A density functional theory investigation with van der waals correction. *J. Phys. Chem. C*, 116:24695–24705, 2012.

[234] C. Resini, L. Arrighi, M. C. H. Delgado, M. A. L. Vargas, L. J. Alemany, P. Riani, S. Berardinelli, R. Marazza, and G. Busca. Production of hydrogen by steam reforming of c3 organics over Pd-Cu/γ-Al_2O_3 catalyst. *Int. J. Hydrogen Energy*, 31:13–19, 2006.

[235] P. Bichon, G. Haugom, H. J. Venvik, A. Holmen, and E. A. Blekkan. Steam reforming of ethanol over supported CO and Ni catalysts. *Top. Catal.*, 49:38–45, 2008.

[236] A. Birot, F. Epron, C. Descorme, and D. Duprez. Ethanol steam reforming over $Rh/Ce_xZr_{1-x}O_2$ catalysts: Impact of the CO-CO_2-CH_4 interconversion reactions on the H_2 production. *Appl. Catal., B. Environ.*, 79:17–25, 2008.

[237] A. Pulido, B. Oliver-Tomas, M. Renz, M. Boronat, and A. Corma. Ketonic decarboxylation reaction mechanism: A combined experimental and DFT study. *Chem. Sus.*, 6:141–151, 2013.

[238] R. W. Snell and B. H. Shanks. Ceria calcination temperature influence on acetic acid ketonization: Mechanistic insights. *Appl. Catal., A. Gen.*, 451:86–93, 2013.

[239] A. Gangadharan, M. Shen, T. Sooknoi, D. E. Resasco, and R. G. Mallinson. Condensation reactions of propanal over $Ce_xZr_{1-x}O_2$ mixed oxide catalysts. *Appl. Catal., A. Gen.*, 1:80–91, 2010.

[240] R. Trane-Restrup, S. Dahl, and A. D. Jensen. Steam reforming of ethanol: Effects of support and additives on ni-based catalystsNi-based catalysts. *Int. J. Hydrogen Energy*, Accepted:X–X, 2013.

[241] M. Mavrikakis and M. A. Barteau. Oxygenate reaction pathways on transition metal surfaces. *J. Mol. Catal. A: Chem.*, 131:135–147, 1998.

[242] S. Y. Wu, Y. R. Lia, J. J. Ho, and H. M. Hsieh. Density functional studies of ethanol dehydrogenation on a $2Rh/\gamma$-$Al_2O_3(110)$ surface. *J. Phys. Chem. C*, 113:16181–16187, 2009.

[243] P. Lan, Q.-L. Xu, L.-H. Lan, D. Xie, S.-P. Zhang, and Y.-J. Yan. Steam reforming of model compounds and fast pyrolysis bio-oil on supported nickle metal catalysts for hydrogen production. *Energy Sources, Part A: Recovery, Utilization, and Environmental Effects*, 34:2004–2015, 2012.

[244] J. Remon, J. A. Medrano, F. Bimbela, L. Garcìa, and J. Arauzo. Ni/Al-Mg-O solids modified with Co or Cu for the catalytic steam reforming of bio-oil. *Appl. Catal., B. Environ.*, 132-133: 433–444, 2013.

[245] S. Liu, M. Chen, L. Chu, Z. Yang, C. Zhu, J. Wang, and M. Chen. Catalytic steam reforming of bio-oil aqueous fraction for hydrogen production over Ni-Mo supported on modified sepiolite catalysts. *Int. J. Hydrogen Energy*, 38:3948–3955, 2013.

[246] B. Valle, A. Remiro, A. T. Aguayo, J. Bilbao, and A. G. Gayobo. Catalysts of Ni/α-Al_2O_3 and Ni/La_2O_3-α-Al_2O_3 for hydrogen production by steam reforming of bio-oil aqueous fraction with pyrolytic lignin retention. *Int. J. Hydrogen Energy*, 38:1307–1318, 2013.

[247] Q. Xu, D. Xie, F. Wang, and Y. Yan. Mechanism of hydrogen production by the catalytic steam reforming of bio-oil. *Energy Sources, Part A: Recovery, Utilization, and Environmental Effects*, 35:1028–1038, 2013.

[248] R. Trane-Restrup, S. Dahl, and A. D. Jensen. Steam reforming of ethanol over Ni-based catalysts: Effect of feed composition on catalyst stability. *Appl. Catal., A. Gen.*, Submitted:X–X, 2013.

[249] A. Remiro, B. Valle, A. T. Aguayo, J. Bilbao, and Gayubo. Operating conditions for attenuating Ni/La_2O_3-αAl_2O_3 catalyst deactivation in the steam reforming of bio-oil aqueous fraction. *Fuel Process. Technol.*, 115:222–232, 2013.

[250] R. C. Reid, J. M. Prausnitz, and T. K. Sherwood. *The Properties of Liquids and Gases.* Mcgraw-Hill, 3rd edition, 1987.

[251] R. B. Bird, W. E. Stewart, and E. N. Lightfoot. *Transport phenomena.* John Wiley And Sons Ltd., 2007.

[252] F. A. L. Dullien. *Porous Media. Fluid Transport and Pore Structure.* Academic Press Inc., 1992.

[253] N. Wakao and S. Kaguei. *Heat and mass transfer in packed beds.* Gordon and Breach Science Publishers, 1982.

[254] I. Barin. *Thermochemical Data of Pure Substances Vol. 1.* VCH, 1995.

[255] F. Kapteijn and J. A. Moulijn. *Handbook of Heterogeneous Catalysis*, chapter Laboratory testing of solid catalysts, pages 2019–2045. Wiley-VCH, 2008.

Appendices

Appendix A

DIFFUSION LIMITATIONS

In experimental work it is important to know as much as possible about the system, which is being studied. For example the transport of reactants or products to and from the active site might be hindered and therefore slow down the entire reaction. The data from such experiments cannot be used for measurements of intrinsic kinetics and might give a wrong picture of the product distribution and conversion. In the following it will therefore be examined if diffusion from the bulk gas to the catalyst particles or diffusion of reactants within the particles is rate limiting for the overall reaction. This will be estimated by using Mears and Weisz-Prater criteria, which can be used to examine if internal or external diffusion is rate limiting based on the physical parameters of the system. The reactor is a gas phase reactor operated at atmospheric pressure and diffusion limitations can cause concentrations gradients across the boundary layer between gas and pellets or inside the catalyst pellets. The overall SR of ethanol reaction is:

$$CH_3CH_2OH + H_2O \quad \rightarrow \quad 2CO + 4H_2 \tag{A.1}$$

However the water gas shift, reaction A.2, and the methanation reaction, reaction A.3, will influence the off gas composition as well:

$$CO + H_2O \quad \rightleftharpoons \quad CO_2 + H_2 \tag{A.2}$$

$$CO + 3H_2 \quad \rightleftharpoons \quad CH_4 + H_2O \tag{A.3}$$

A.1 Mears criterion

To evaluate the effect of the external diffusion Mears criterion for external diffusion will be used. This criterion states that external diffusion can be neglected if [189]:

$$\frac{-r'_a(obs) \cdot \rho_b \cdot d_p \cdot n}{2 \cdot k_c \cdot C_{Ab}} < 0.15 \tag{A.4}$$

Where $-r'_a$ is the measured reaction rate in $mol/(kg \cdot s)$, ρ_b is the bulk density of the catalyst bed in kg/m^3, d_p is the diameter of the catalyst particles in m, n is the reaction order, k_c is the mass transfer coefficient in m/s, and C_{Ab} is the concentration of reactant A in the bulk in mol/m^3.

Mears criterion is an evaluation of the external diffusion of one compound and this investigation will focus on the diffusion of ethanol or water in N_2.

In order to calculate Mears criterion (eq. A.4) many parameters have to be determined and how this is done will be explained in the following.

The observed reaction rate is calculated based on experimental data as the number of moles of ethanol converted to gaseous species pr. time divided by the mass of catalyst:

$$-r'_a(obs) = \frac{F_{Eth,\ in} \cdot X}{m_{cat}} \tag{A.5}$$

Where $F_{Eth,\ in}$ is the molar flow of ethanol to the reactor and m_{cat} is the mass catalyst used in the experiment. The observed rate is taken as the maximum rate observed in the experiments, which at temperatures above 600 °C, where full conversion is observed:

$$-r'_a(obs) = \frac{1.19 \cdot 10^{-5}\ mol/s}{5 \cdot 10^{-4}\ kg} = 0.024\ \frac{mole}{kg \cdot s} \tag{A.6}$$

The bed density, ρ_b, is calculated as the mass of the catalyst used in the given experiment divided by the volume of the bed:

$$\rho_b = \frac{m_{cat}}{V_{bed}} = \frac{2.1\ g}{4.4\ mL} = 482\ \frac{kg}{m^3} \tag{A.7}$$

Where V_{bed} is the volume of the catalyst, which is measured by pouring m_{cat} of catalyst into a measuring glass and measure the volume, V_{bed}.

To determine the mass transfer coefficient, k_c, the Frössling correlation will be used, which is valid for laminar flows [189]:

$$Sh = 2 + 0,6 \cdot Re^{1/2} \cdot Sc^{1/3} \tag{A.8}$$

Where Sh is Sherwoods number, Re is Reynolds number, and Sc is Schmidts number. The three dimensionless numbers are defined as:

$$Sh = \frac{k_c \cdot d_p}{D_{AB}} \qquad Sc = \frac{\nu}{D_{AB}} \qquad Re = \frac{U \cdot d_p}{\nu} \tag{A.9}$$

Where U is the free-stream velocity, D_{AB} is the diffusion coefficient and ν is the kinematic viscosity. There is no data available on neither D_{AB} nor ν. These two parameters therefore have to be estimated, which can be done by using the Lennard-Jones potentials for the relevant compounds and these are given in table A.1.

Tab. A.1: *The Lennard-Jones potentials for the relevant compounds, where σ is the hard-sphere diameter and $\frac{\epsilon}{k}$ is the characteristic energy divided by Boltzmann's constant. The data are obtained from [250]*

Compound	σ $[\mathring{A}]$	$\frac{\epsilon}{k}$ $[K]$
Nitrogen	3.789	71.4
Ethanol	4.53	362.6
Water	2.641	809.1

It is difficult to calculate D_{AB}, because the gas which surrounds the catalyst is a mixture of different compounds. To simplify the system, it is assumed that the surrounding gas is nitrogen, as it constitutes 58 $vol\%$ of the feed gas. To estimate the value of the diffusion

coefficient of one of the products (A) into the surrounding gas (B) the Chapman and Enskog equation is used [250]:

$$D_{AB} = \frac{0.00266 \cdot T^{3/2}}{P \cdot M_{AB}^{1/2} \cdot \sigma_{AB}^2 \cdot \Omega_D} \quad [cm^2/s] \tag{A.10}$$

Where T is the temperature, P is the pressure, and M_{AB}, σ_{AB}, and Ω_D are given by:

$$M_{AB} = 2 \cdot \left(\frac{1}{M_A} + \frac{1}{M_B}\right)^{-1} \tag{A.11}$$

$$\sigma_{AB} = \frac{\sigma_A + \sigma_B}{2} \tag{A.12}$$

$$\Omega_D = \frac{1.06036}{\left(\frac{k \cdot T}{\epsilon_{AB}}\right)^{0.156}} + \frac{0.193}{\exp\left(0.4764 \frac{k \cdot T}{\epsilon_{AB}}\right)} + \frac{1.03587}{\exp\left(1.530 \frac{k \cdot T}{\epsilon_{AB}}\right)} + \frac{1.76474}{\exp\left(3.8941 \frac{k \cdot T}{\epsilon_{AB}}\right)} \tag{A.13}$$

$$\frac{\epsilon_{AB}}{k} = \frac{(\epsilon_A \cdot \epsilon_B)^{1/2}}{k} \tag{A.14}$$

Where M is the molar mass. Equation A.10 is valid for binary gas systems at low pressure.

To estimate the kinematic viscosity, ν, of the gas in the reactor, it is assumed that the stream consist of nitrogen. ν can be calculated as:

$$\nu = \frac{\eta}{\rho} \tag{A.15}$$

The viscosity can, in analogy to the diffusion coefficient, be determined by the Chapman-Enskog equation [250]:

$$\eta = \frac{26.69 \cdot M_A \cdot T}{\sigma_A^2 \cdot \Omega_v} \tag{A.16}$$

Where Ω_v is:

$$\Omega_v = \frac{1.16145}{\left(\frac{k \cdot T}{\epsilon_A}\right)^{0.1561}} + \frac{0.14874}{\exp\left(0.7732 \frac{k \cdot T}{\epsilon_A}\right)} + \frac{2.16178}{\exp\left(2.43787 \frac{k \cdot T}{\epsilon_A}\right)} \tag{A.17}$$

This equation is only valid for low pressures.

The density of nitrogen is calculated by the ideal gas law:

$$\rho = \frac{P \cdot M_{Avg}}{R \cdot T} = \frac{101325\ Pa \cdot 0.024\ kg/mol}{8.314\ \frac{m^3 \cdot Pa}{mol \cdot K} \cdot 873\ K} = 0.34\ kg/m^3 \tag{A.18}$$

A viscosity for nitrogen of 0.036 cP at 600 °C and a kinematic viscosity of 0.0011 m^2/s has been estimated based on eq. A.15 to A.18.

The velocity, U, is calculated from the flow measurements conducted during the experiment through the following equation:

$$U = \frac{F_v \cdot \frac{T}{T_0} \cdot \frac{P_0}{P}}{A_{tube}} = \frac{1600\ Nml/min \cdot \frac{873\ K}{273\ K} \frac{101325\ Pa}{101325\ Pa}}{(8.5\ mm)^2 \cdot \pi} = 0.375\ m/s \tag{A.19}$$

Where F_v is the volumetric inlet flow.

Re can now be determined:

$$Re = \frac{U \cdot d_p}{\nu} = \frac{0.375\ m/s \cdot 710 \cdot 10^{-6}\ m}{0.0011\ m^2/s} = 2.5 \tag{A.20}$$

It is hereby seen, that the flow is laminar, because Re is below 20 [251] and therefore is the Frössling correlation valid. Equation A.8 can then be used to find k_c from Sh as:

$$k_c = \frac{Sh \cdot D_{AB}}{d_p} = \frac{2.80 \cdot 8.14 \cdot 10^{-5}\ m^2/s}{710\ \mu m} = 0.35\ m/s \tag{A.21}$$

The last parameter we have to determine is the concentration of A in the bulk. This is determined as the concentration of ethanol or H_2O in the feed, which can be calculated by the ideal gas law using a molar fraction of 0.030 for ethanol and 0.36 for H_2O:

$$C_{Eth} = \frac{y_{Eth} \cdot P}{R \cdot T} = \frac{0.03 \cdot 101325\ Pa}{8.314\ \frac{J}{mol \cdot K} \cdot 873\ K} = 0.42\ mol/m^3 \tag{A.22}$$

$$C_{H_2O} = \frac{y_{H_2O} \cdot P}{R \cdot T} = \frac{0.36 \cdot 101325\ Pa}{8.314\ \frac{J}{mol \cdot K} \cdot 873\ K} = 5.0\ mol/m^3 \tag{A.23}$$

In table A.2 all the values for each of the calculations steps can be seen, and also the value of the left hand side of eq. A.4. It can here be seen that the criterion is met for the investigated compounds, which means that there is probably not exterior diffusion limitations.

Tab. A.2: *Different values calculated to estimate Mears criterion*

		Ethanol	H_2O
y_i		0.030	0.36
d_p	$[\mu m]$	710	710
M_{ab}	$[g/mol]$	34.81	21.92
F_i	$[mol/s]$	$0.8{\cdot}10^{-5}$	$1.0{\cdot}10^{-4}$
$-r'_a(obs)$	$[mol/(kg \cdot s)]$	0.022	0.27
n		1	1
ϵ_{AB}	$[K]$	160.9	240.4
σ_{AB}		4.16	3.22
Ω_D		0.81	0.87
D_{AB}	$[m^2/s]$	$8.2{\cdot}10^{-5}$	$1.6{\cdot}10^{-4}$
Sc		1.33	0.67
Sh		3.03	2.82
k_c	$[m/s]$	0.35	0.64
Mears		0.03	0.01

A.2 Weisz-Prater criterion

The reaction is not limited by external diffusion, but it can still be limited by diffusion within the pore structure of the catalyst, also called internal diffusion. In order to investigate if this is the case the Weisz-Prater criterion [189] is used. The Weisz-Prater criterion is:

$$C_{wp} = \frac{-r'_a(obs) \cdot \rho_c \cdot \left(\frac{d_p}{2}\right)^2}{D_e \cdot C_{As}} \tag{A.24}$$

Where ρ_c is the density of the catalyst in kg/m^3, D_e is the pore diffusion coefficient, and C_{As} is the concentration of the investigated compound upon the surface of the catalyst. The Weisz-Prater criterion says, that if $C_{wp} \gg 1$ there is interior diffusion problems, and if $C_{wp} \ll 1$

there is not interior diffusion problems. To evaluate eq. A.24 the different parameters has to be determined like it was done for Mears criterion.

$-r'_a(obs)$ is determined analogously eq. A.5, and d_p is the catalyst particle diameter. These parameters have been determined already in the previous calculations. C_{As} can be assumed to be equal to the concentration in the bulk, because it was concluded that there was not any external diffusion limitation. C_{As} is therefore found from eq. A.22 or A.23.

ρ_c is the density of the solid catalyst and it is calculated by:

$$\rho_c = \frac{m_{Cat}}{V_{Bed} - \phi_{bed} \cdot V_{Bed}} = 778\ kg/m^3 \tag{A.25}$$

Where ϕ_{Bed} is the porosity of the bed which is assumed to be 0.38, which an average value for spheres poured into bed [252].

To determine the pore volume diffusion, the procedures described in [253] will be used, where it is calculated on the basis of two diffusion coefficients: D_K and D_{AB}. Where D_{AB} is the same diffusion coefficient as the one calculated from eq. A.10 and listed in table A.2.

The Knudsen diffusivity, D_K, is an estimation of how large the resistance the molecules meet inside the catalyst pores, and it is given by:

$$D_K = 3.068 \cdot a \cdot \left(\frac{T}{M}\right)^{1/2} \quad [m/s] \tag{A.26}$$

Where a $[m]$ is the radius of the pores inside the catalyst. The exact pore size have not been determined but it is assumed to 44 nm, which is estimated based on a pore volume (1.0 mL/g), surface area (90 m^2/g), and assuming that the pores are tubes.

The effective diffusion coefficient can now be calculated as:

$$D_{ABe} = \left(\frac{1}{D_K} + \frac{1}{D_{AB}}\right)^{-1} \tag{A.27}$$

$$D_e = \frac{D_{ABe} \cdot \phi_p \cdot \sigma_c}{\tau} \tag{A.28}$$

Where ϕ_p is the porosity of the catalyst, σ_c is the constriction factor, and τ is the tortuosity [1]. Equation A.28 is introduced to correct the diffusion coefficient calculated from eq. A.27, because the diffusion is taking place inside a pellet. This is done with ϕ_p, σ_c and τ, which have the respective values of 0.77, 0.8, and 2.5. The porosity is calculated as:

$$\phi_p = \frac{V_{Pore}}{V_{Cat}} = \frac{V_{Pore}}{V_{Bed} - V_{Void}} = -\frac{2.1\ cm^3}{4.4 - 1.73\ cm^3} = 0.77 \tag{A.29}$$

All the parameters needed to calculate C_{wp} from eq. A.24 are now determined. In table A.3 all the calculated coefficients needed for the calculations can be seen. The Weisz-Prater criterion is around one for ethanol and particles between 425 and 710 μm indicated that there might not be internal diffusion problems for ethanol, while for water C_{wp} is well below one and diffusion of water should not cause problems.

The particle diameter can be decreased in order to minimize diffusion problems and in table A.4 C_{wp} can be seen for several different particle diameters. As expected the Weisz-Prater decreases with decreasing particle sizes. A catalyst fraction consisting of 125-250 μm or 250-425 μm particles should have little or no internal diffusion limitations.

[1] Equation A.27 is obtained from [253] and A.28 is obtained from [189]

Tab. A.3: *Different values calculated to estimate the Weisz-Prater criterion.*

		Ethanol	H_2O
D_k	$[m^2/s]$	$3.9{\cdot}10^{-5}$	$4.9{\cdot}10^{-5}$
D_e	$[m^2/s]$	$6.5{\cdot}10^{-6}$	$9.3{\cdot}10^{-6}$
C_{wp} (710 μm)		1.25	0.15
C_{wp} (425 μm)		0.45	0.05

Tab. A.4: *Values of Weisz-Prater criterion at different particle sizes.*

Particle diameter $[\mu m]$	C_{wp}
710	1.25
425	0.45
250	0.16
125	0.04

Two size fractions, 250-425 μm and 425-710 μm, were tested in a standard experiment at 600 ℃ for 4 h to determine if diffusion was limiting for performance of the catalyst. The average conversion, yield of methane, and carbon deposition are shown in table A.5. Here it can be seen that there only are small differences between the different fractions and therefore diffusion do not seem to be limiting.

A.3 Temperature gradients

Steam reforming reactions are highly endothermic and temperature gradients between the surrounding gas and the particles might occur. Mear has also proposed a criterion for whether or not there is a significant temperature difference particle and gas [189]. The criterion is:

$$\left|\frac{-r'_a(obs)\cdot\rho_b\cdot d_p\cdot(-\Delta H_R)}{h\cdot T^2\cdot R}\right| < 0.15 \tag{A.30}$$

Where $-\Delta H_r$ is the reaction enthalpy, which is 210 $kJ/mole$, E is the activation energy, which is assumed to be 82.7 $kJ/mole$, and h is the heat transfer coefficient. $-\Delta H_r$ is calculated for reaction 1.4 from the formation enthalpies found in ref. [254]. The activation energy is found in ref. [104].

Tab. A.5: *Conversion, yield of methane, and carbon deposition in SR of ethanol at 600 ℃ for two size fractions of $Ni/MgAl_2O_4$.*

Fraction $[\mu m]$	Conversion [%]	CH_4-sel. [%]	Carbon deposition [*mole*% of feed]
250-425	79.5	5.2	0.44
425-710	79.1	6.3	0.53

The heat transfer coefficient, h, can be estimated from Nusselts number, which is given by:

$$Nu = \frac{h \cdot d_p}{k_t} \tag{A.31}$$

Where k_t is the thermal conductivity of the gas, which is estimated to be 0.061 $W/(K \cdot m)$.

Nusselts number, Nu, can be estimated by the following correlation [189]:

$$Nu = 2 + 0.6 \cdot Re^{1/2} \cdot Pr^{1/3} \tag{A.32}$$

Prandtl number, Pr, is defined as:

$$Pr = \frac{\nu \cdot C_p}{k_t} \tag{A.33}$$

The kinematic viscosity, ν, is estimated by eq. A.16.

The values for Mears criteria for temperature gradients along with selected calculated values are shown in table A.6. Here it can be that temperature difference is negligible as the values are well below 0.15.

Tab. A.6: *Different values calculated to estimate Mears criterion for temperature gradients.*

		Ethanol
Pr		0.062
Nu		2.56
h	$[kJ/(m^2 \cdot s \cdot K)]$	0.20
Mears		$1.9 \cdot 10^{-4}$

Another way to estimate the temperature gradients between particles and the surrounding gas is by a simple energy balance:

$$q = h \cdot A \cdot \Delta T \tag{A.34}$$

Where A is the surface area of the particle. The energy needed can be calculated as:

$$q = \Delta H_r \cdot r'_a \cdot V_p \tag{A.35}$$

Where V_p is the particle volume. Eq. A.34 and A.35 can be combined to:

$$\begin{aligned} \Delta T &= \frac{\Delta H_r \cdot r'_a \cdot V_p}{A \cdot h} \\ &= \frac{210\ kJ/mole \cdot 9.70\ mole/(m^3 \cdot s) \cdot 1.87 \cdot 10^{-10}\ m^3}{1.58 \cdot 10^{-6}\ m^2 \cdot 0.222\ kJ/(m^2 \cdot s \cdot K)} = 1.08\ K \end{aligned} \tag{A.36}$$

Based on the energy balance is also appears the temperature differences between gas and particles should be small. A drop of up to 5-15 K in temperature is observed when the SR reactions is initiated, depending on catalyst and temperature. However, the temperature remains constant after the initial temperature drop and it is this value which is reported.

Tab. A.7: *Right hand side of eq. A.37 at different degrees of conversion for particles with a diameter of 425 μm. First order reaction assumed.*

Conversion [%]	0.1	0.5	0.9	0.95	0.99
$\frac{8 \cdot n}{Pe} \cdot \ln\left(\frac{1}{1-X}\right)$	4	26	87	113	173

A.4 Reactor geometry

The reactor was a quartz tube with an inner diameter of 17 mm and the bed was roughly 4 mm high. The catalysts were crushed to 425-710 μm or 250-425 μm fractions. The ratio of bed diameter to particle diameter is recommended to be over 10 to achieve plug flow and it is 24 for 710 μm particles and 40 for 425 μm particles [255]. The ratio between height of the bed and particle diameter (H/d_p) is also determining for the possibility to obtain plug flow. It has been shown that [255]:

$$\frac{H}{d_p} > \frac{8 \cdot n}{Pe_p} \cdot \ln\left(\frac{1}{1-X}\right) \tag{A.37}$$

in order to obtain plug flow. Where H is the height of the bed, n is the reaction order, and Pe_p is the particle Peclet number, defined as:

$$Pe_p = \frac{d_p \cdot Pe}{L_b} \tag{A.38}$$

Where d_p is the particle size and L_b is the bed length. Pe is assumed be 2 (see further below). The right hand side of eq. A.37 at different degrees of conversion can be seen in table A.7. $\frac{H}{d_p}$ is 7.0 for a particle size of 567 μm (average of 710 and 425 μm) and 11.8 for 338 μm particles (average of 250 and 425 μm). It can be seen that the criteria for plug flow is not met. Therefore it appears that plug flow is not fully achieved for this reactor geometry.

A.5 Dispersion

The effective dispersion coefficient, D_a, can estimated from figure 14-12 in Fogler [189]. This figure shows $\frac{D_a \cdot \epsilon}{U \cdot d_p}$ as function of Reynolds number. $\frac{D_a \cdot \epsilon}{U \cdot d_p}$ at $Re = 1.5$ is approx. 0.5 and based on this $D_a = 1 \cdot 10^{-4}\ m^2/s$. The Peclet number, which describes the ratio between transport by convection and transport by diffusion or dispersion, can then be calculated by:

$$Pe = \frac{U \cdot d_p}{\epsilon \cdot D_a} = 2 \tag{A.39}$$

This shows transport by convection is more important than transport by diffusion or dispersion.

The dispersion model, first published by Danckwerts, can be used to predict the rate constant, k, if the Peclet number is known. The conversion as function of Pe_r for the dispersion is:

$$X = \frac{4 \cdot q \cdot \exp(Pe_r/2)}{(1+q)^2 \cdot \exp(Pe_r \cdot q/2) - (1-q)^2 \cdot \exp(-Pe_r \cdot q/2)} \tag{A.40}$$

$$\text{where} \quad q = \sqrt{1 + 4 \cdot Da/Pe_r} \quad \text{and} \quad Da = \tau \cdot k \tag{A.41}$$

Tab. A.8: *Rate constants calculated from the dispersion model (eq. A.40) at different temperatures and degrees of conversion.*

Temperature	Conversion [%]	Rate constant $[s^{-1}]$
398	9	4.7
500	35	22.0
593	85	120.1
697	95	230.4

The Peclet number, Pe_r, used in eq. A.40 is calculated by:

$$Pe_r = \frac{U \cdot L}{D_a} = 14.5 \tag{A.42}$$

Where L is the height of catalytic bed. The inverse of Pe_r can be used to predict the amount of dispersion in the reactor and based on fig. 14-13 in ref. [189], it seems that the dispersion in the reactor is low.

Based on eq. A.40 values for of k were calculated using the measured conversion in the temperature dependence experiment. The values of k, X, and the corresponding temperature are shown in tab. A.8.

The reaction rate for steam reforming of ethanol can be calculated by:

$$-r_{Eth} = k \cdot C_{eth} \quad \left[\frac{mole}{m^3 \cdot s}\right] \tag{A.43}$$

It is assumed that the reaction is first order with respect to ethanol.

It is possible to calculate the conversion based on a CSTR or a PFR design equation and the rate constants estimated from eq. A.40 and then compared these values with the measured values to see if the reactor behaves either as a PFR or a CSTR. The design equations used are:

$$\text{CSTR:} \qquad V = \frac{F_{A0} \cdot X}{-r_A} \tag{A.44}$$

$$\text{PFR:} \qquad \frac{dX}{dW} = \frac{-r'_A}{F_{A0}} \tag{A.45}$$

The conversion for a CSTR can be calculated from:

$$X_{CSTR} = \frac{\tau \cdot k}{1 + \tau \cdot k} \tag{A.46}$$

For a PFR, the conversion is calculated by:

$$X_{PFR} = 1 - \exp(-\tau \cdot k) \tag{A.47}$$

A constant volume is assumed in the derivation of eq. A.47. The conversion has also been calculated assuming an increase in volume as more molecules are formed than consumed and it is denoted X_{PFRm}. The general design equation for a PFR has been used along with the following expression for the reaction rate:

$$r = k \cdot C \cdot \frac{1 - X}{1 + X} \tag{A.48}$$

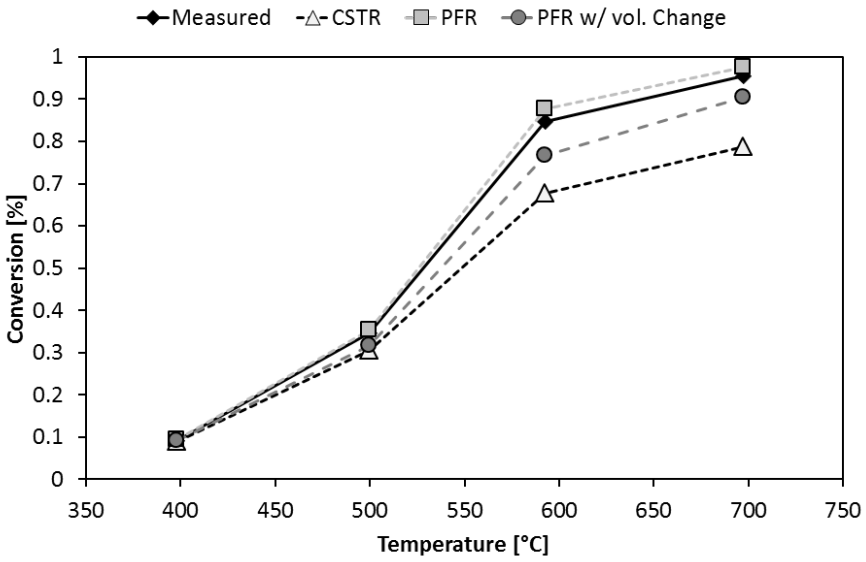

Fig. A.1: *Comparison of the conversion as function of temperature for the measured and calculated values. X_{PFRm} is the conversion calculated assuming $\epsilon = 1$.*

The design equation is solved numerically using Maple 17.

The conversion as function of temperature for the measured and the calculated conversion are shown in fig. A.1. Here it can be seen that both a CSTR and PFR model describes the measured conversion quite well. However, it appears that PFR model has a better fit as the deviation from the measured values is quite low at all temperatures.

A.6 Conclusions

The calculations of Mears and Weisz-Prater criteria shown that external and internal diffusion were negligible and that temperature gradients between gas and particles are negligible as well. The reactor geometry did not meet the criteria for achieving plug flow but, based on dispersion, but it appears that the reactor can be modeled as plug flow reactor.

Appendix B

ESTIMATION OF AFFINITY FOR CARBON DEPOSITION

Carbon deposition in the SR of CH_4 can occur through methane decomposition, CO decomposition, or the Boudouard reaction and the two latter are mainly a problem at low temperatures, while the former occurs at high temperatures. Based on the equilibrium constants for these reactions as well as a gas composition it is possible to estimate if there is a risk of forming carbon deposits from any of three reactions. The theory behind the estimation is described in ref. [42] and it is called the principle of equilibrated gas or the principle of actual gas, depending on whether it is the equilibrium or the actual gas phase composition, which is used in the calculations. The affinity, ΔG_C, is calculated and if ΔG_C is negative then there is no affinity for carbon formation through the investigated reaction. The method is developed for SR of methane, and not well suited for the SR of higher hydrocarbons as the decomposition of these compounds are irreversible and not taken into account. The affinity calculations will be used to estimate the affinity for carbon formation through methane decomposition, CO decomposition, or the Boudouard reaction, and determine if these can contribute to the observed carbon formation.

The three carbon forming reactions are:

$$\text{Boudouard:} \quad 2CO \rightleftharpoons C_s + CO_2 \tag{B.1}$$

$$\text{CO decomposition:} \quad CO + H_2 \rightleftharpoons C_s + H_2O \tag{B.2}$$

$$\text{CH}_4\text{ decomposition:} \quad CH_4 \rightleftharpoons C_s + 2H_2 \tag{B.3}$$

$$\tag{B.4}$$

ΔG_C for methane decomposition is calculated by:

$$\Delta G_C = R \cdot T \ln \left[\frac{K_{eq}}{Q} \right] \tag{B.5}$$

Where K is the equilibrium constant and Q is reaction quotient, which can be calculated from the actual or equilibrated gas. For the methane decomposition eq. B.5 translates to:

$$\Delta G_C = R \cdot T \ln \left[K_{eq} \cdot \frac{p_{CH_4}}{p_{H_2}^2} \right] \tag{B.6}$$

The equilibrium constants for methane decomposition, CO decomposition, and the Boudouard reaction used for estimations of affinity for carbon formation is calculated by:

$$\ln(K_{eq}) = C_1 \cdot \ln(T) + \frac{C_2}{T} + C_3 + C_4 \cdot T + C_5 \cdot T^2 + C_6 \cdot T^3 \tag{B.7}$$

The coefficients, $C_1 - C_6$, for the different reactions are listed in table B.1. The are two equilibrium constants for methane decomposition, where one reaction assumes carbon formation as graphite and one assuming carbon formation as whisker, C_W. The equilibrium constant for carbon formation as whiskers compared to graphite is higher, because it is more energy demanding to form whiskers compared with graphite [42].

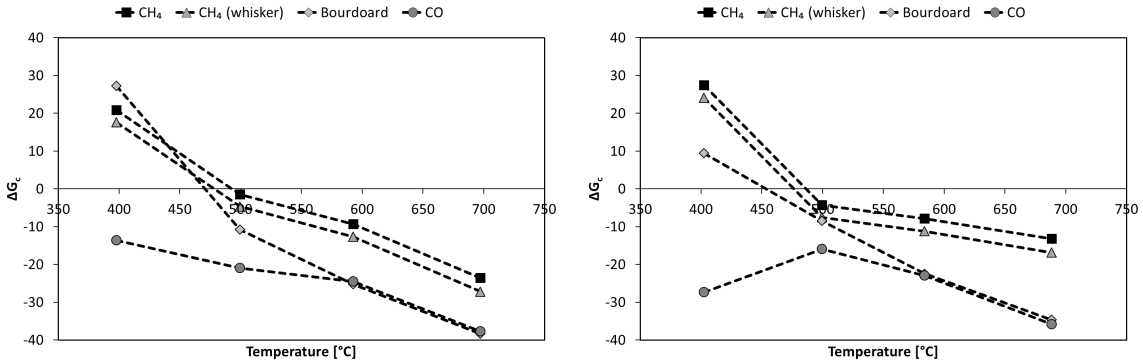

(a) SR of ethanol over $Ni/MgAl_2O_4$ (b) SR of ethanol over $Ni/Ni/Ce_{0.6}Zr_{0.4}O_2$

Fig. B.1: *Affinity to form carbon from a actual gas composition in SR of ethanol at S/C-ratio of 6.*

Tab. B.1: *Coefficients used in the calculations of equilibrium constant by eq. B.7 [42]. C_W refers carbon deposition as whiskers.*

	$CH_4 \leftrightarrow C + 2H_2$	$CH_4 \leftrightarrow C_W + 2H_2$	$2CO \leftrightarrow C + CO_2$	$CO + H_2 \leftrightarrow C + H_2O$
C_1	5.291666	0	-3.635623	-3.319458
C_2	-7610.846	-10779	20053.61	15037.16
C_3	-24.48443	12.68	0.3674049	4.471772
C_4	-0.002023153		0.005096533	0.00295691
C_5	$-1.59352 \cdot 10^{-7}$		$-1.16153 \cdot 10^{-6}$	$-5.57093 \cdot 10^{-7}$
C_6	$7.79721 \cdot 10^{-11}$		$1.33663 \cdot 10^{-10}$	$5.78377 \cdot 10^{-11}$

The affinity to form carbon as function of temperature is estimated for a real and equilibrium gas in the SR of ethanol at S/C-ratio of 6. The equilibrium gas does not show affinity for forming carbon through the investigated reactions, but as indicated in fig. B.1 the actual gas composition does show affinity to form carbon through methane decomposition and the Boudouard reaction at 400 ℃.

There was no affinity to form carbon from an equilibrium gas phase composition in SR of ethanol at S/C-ratios between 1.5 and 8, O/C-ratios between 0 and 1.2 at S/C=6, or H/C-ratios between 0 and 2.4 at S/C=6 by methane decomposition, CO decomposition, or the Boudouard reaction. The carbon affinity for the actual gas phase composition in the experiments where the S/C-, O/C-, and H/C-ratios are varied can be seen in fig. B.2. There is only an affinity to form carbon through methane decomposition at a S/C-ratio of 1.6.

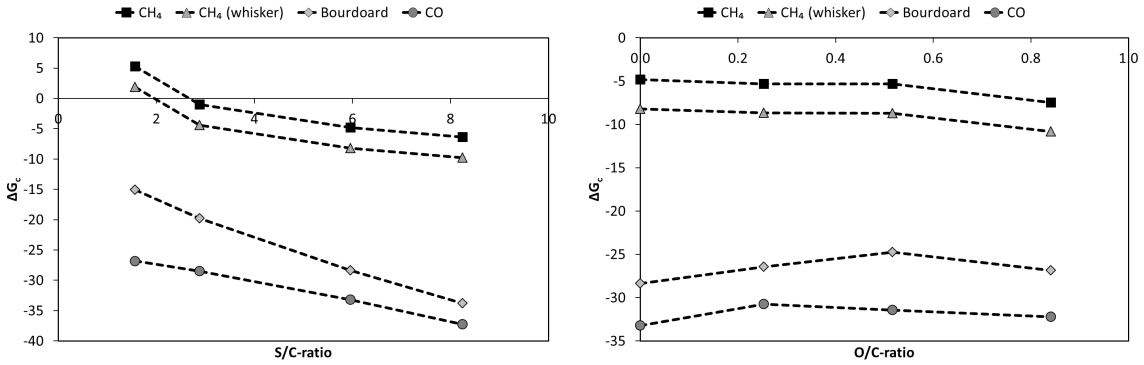

(a) S/C-ratio varied

(b) O/C-ratio varied

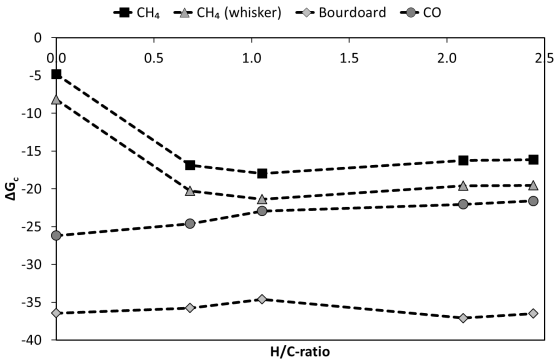

(c) H/C-ratio varied

Fig. B.2: *Affinity to form carbon from the actual gas compositions in SR of ethanol over* $Ni/MgAl_2O_4$ *at 600 ℃.*